Controlling the risk of cross-contamination from the building drainage system using the reflected wave technique to identify depleted water trap seals

David A Kelly

Submitted for the degree of Doctor of Philosophy

Heriot-Watt University

School of the Built Environment

March 2009

ABSTRACT

The appliance trap seal remains the primary defence against cross-contamination from the foul air present within the building drainage system. As an identified vector in the spread of severe acute respiratory syndrome (SARS) in Hong Kong in 2003, trap seal failure has been confirmed as a significant, and potentially fatal, risk to public health. Prevention of trap seal failure depends upon both good design, to limit the air pressure transients propagated within the system, and good maintenance. However, current maintenance regimes rely solely on visual inspections which is time consuming and often impractical to implement in large complex buildings.

This thesis documents the development of a novel approach to system maintenance whereby the threat of cross-contamination of disease is minimised by the remote monitoring of trap seal status. This was approached through the application and development of the *reflected wave technique* which is fundamentally based upon the characteristic reflection coefficients of system boundary conditions.

An extensive programme of laboratory experiments and field trials were carried out to collect transient pressure data which, together with results from an existing mathematical model (AIRNET), developed by the Drainage Research Group at Heriot-Watt University, have been used to validate the proposed technique and to formulate a practical methodology which may be applied to any building drainage system.

Automatic system diagnosis, which would in the future allow the proposed technique to be integrated as an automated system test, was provided by the development of the **tra**p **c**ondition **e**valuato**r** (TRACER) program by this author. Incorporating a time series change detection algorithm, the TRACER program accurately detects and locates a depleted trap seal by automatically identifying the return time of the trap's reflection.

The *reflected wave technique* has been demonstrated as a successful approach to depleted trap identification provided that the wave propagation speed is known and the dampening influence of the *junction effect* (which can delay the observed reflection return time) are taken into account. The *reflected wave technique* offers a remote and non-invasive approach to maintaining the building drainage system and provides, for the first time, a diagnostic tool to help prevent cross-contamination.

ACKNOWLEDGEMENTS

The author would like to express his deepest gratitude to Professor John Swaffield for his expert guidance and support throughout this research. Sincere acknowledgements are also expressed to the members of the Drainage Research Group for their involvement in this work. Very special thanks to Dr. Michael Gormley for his invaluable support and input throughout this project.

Acknowledgements are also due to the staff of the School of the Built Environment at Heriot-Watt University for their assistance. Special gratitude is expressed to Mr David Walker for his skilful resourcefulness, attention to detail and unwavering enthusiasm during the experimental programme.

This research project was financially supported by the Engineering and Physical Sciences Research Council (EPSRC), whose funding is greatly acknowledged. In addition, the author would like to thank Studor Ltd for their collaboration and financial input during this project.

Deepest and sincere gratitude are expressed to the author's parents for their immeasurable support and constant encouragement.

Finally, a very special thank you to David for his everlasting patience, support and understanding during this endeavour.

ACADEMIC REGISTRY
Research Thesis Submission

Name*:*	David A Kelly		
School/PGI:	School of the Built Environment		
Version: *(i.e. First, Resubmission, Final)*	Final	Degree Sought : (Award **and** Subject area)	Doctor of Philosophy (Construction)

Declaration

In accordance with the appropriate regulations I hereby submit my thesis and I declare that:

1) the thesis embodies the results of my own work and has been composed by myself
2) where appropriate, I have made acknowledgement of the work of others and have made reference to work carried out in collaboration with other persons
3) the thesis is the correct version of the thesis for submission and is the same version as any electronic versions submitted*.
4) my thesis for the award referred to, deposited in the Heriot-Watt University Library, should be made available for loan or photocopying and be available via the Institutional Repository, subject to such conditions as the Librarian may require
5) I understand that as a student of the University I am required to abide by the Regulations of the University and to conform to its discipline.

* *Please note that it is the responsibility of the candidate to ensure that the correct version of the thesis is submitted.*

Signature of Candidate*:*		Date:	

Submission

Submitted By *(name in capitals):*	
Signature of Individual Submitting:	
Date Submitted:	

For Completion in Academic Registry

Received in the Academic Registry by *(name in capitals):*			
1.1 Method of Submission *(Handed in to Academic Registry; posted through internal/external mail):*			
1.2 E-thesis Submitted (mandatory from January 2009)			
Signature:		Date:	

TABLE OF CONTENTS

LIST OF FIGURES

LIST OF TABLES

NOTATION

A	Flow cross-sectional area	(m^2)
c	Wave propagation speed	(m/s)
c_{base}	Base value wave propagation speed	(m/s)
C_R	Boundary reflection coefficient	
C_T	Boundary transmission coefficient	
D	Pipe diameter	(m)
D_t	Absolute difference	
f	Friction factor	
$F(), f()$	Pressure waves	
g	Gravity	(m/s)
H	Trap fluid height	(mm)
h	Threshold level	(mm water gauge)
k	Loss coefficient	
L	Pipe length	(m)
N, n	Number of pipes, nodes or defect	
P	Wetted perimeter	(m)
p	Pressure	(N/m^2) or (mm water gauge)
P_j^{DF}	Defect free baseline	(mm water gauge)
P_j^M	Measured test system response	(mm water gauge)
Q	Volumetric flow rate	(m^3/s)
R	Radius	(m)
S_N	Signal noise	(mm water gauge)
t	Time	(s)
t_a	transient wave arrival time	(s)
t_D	Pipe period of depleted trap	(s)
t_p	Pipe period	(s)
t_R	Actual reflection arrival time	(s)
U_w	Liquid column velocity	(m/s)
u	Mean airflow velocity	(m/s)
V	Mean water velocity	(m/s)
X_D	Distance to depleted trap seal	(m)

Δt	Time increment	(s)
Δx	Distance increment	(m)
ε	Trap location error	(%)
ε_j	Individual junction error	(%)
ϕ	Peak amplitude noise multiplier	
γ	Ratio of specific heat	
μ	Poisson's ratio	
θ	Peak angular noise deviation	(radians)
ρ	Density	(kg/m^3)
σ	Surface tension	(N/m)
τ	Shear stress	(N/m^2)
ψ	random noise phase	(radians)

Subscripts

atm	atmospheric conditions
D	defect
j	measurement point
P, R, S	nodes in MoC calculation
t + Δt, t	conditions at node at a time
1, 2, N	nodes

Other terms

C^+, C^-	Characteristic slopes
K1-K4	constant in characteristic equations based on known parameters

LIST OF PUBLICATIONS

A number of papers have been presented and published during the development of this work. These papers are listed by author and chronological order as follows:

Kelly D.A., Swaffield J.A., Jack L.B., Campbell D.P. and Gormley M. (2006). "Transient defect identification in building drainage and vent systems – an application of pressure transient theory and practice." *Proceedings from the CIBW62 32nd International Symposium on Water Supply and Drainage for Buildings*, Taipei, Taiwan, 17-20 September 2006.

Kelly D.A. (2007). "Identification of depleted appliance trap seals within the building drainage and ventilation system – A transient based technique." *Proceedings from the CIBW62 33rd International Symposium on Water Supply and Drainage for Buildings*, Brno, Czech Republic, 19-21 September 2007.

Kelly D.A., Swaffield J.A., Campbell D.P., Gormley M. and Jack L.B. (2008). "A transient-based technique to locate depleted appliance trap seals within the building drainage system", *10th International Conference on Pressure Surges*, BHR Group Ltd., Edinburgh, UK, 14-16 May 2008.

Kelly D.A. (2008). "Reducing the risk of infection spread from the building drainage system through identification of depleted appliance trap seals using the reflected wave technique." *Proceedings from the CIBW62 34th International Symposium on Water Supply and Drainage for Buildings*, Hong Kong, China, 8-10 September 2008.

Kelly D.A., Swaffield J.A., Jack L.B., Campbell D.P. and Gormley M. (2008). "Pressure transient identification of depleted appliance trap seals: A pressure pulse technique." *Building Services Engineering Research & Technology*, **29** (2), 165-181.

Kelly D.A., Swaffield J.A., Jack L.B., Campbell D.P. and Gormley M. (2008). "Pressure transient identification of depleted appliance trap seals: A sinusoidal wave technique." *Building Services Engineering Research & Technology*, **29** (3), 219-232.

Chapter 1
Introduction and background

1.1 Background and motivation

The fundamental purpose of a building drainage system is to rapidly remove appliance discharge while simultaneously ensuring that foul sewer gases from the drainage network are prevented from entering the building. The primary defence against cross-contamination is provided by the water trap seal which, provided the water seal is retained, prevents the ingress of sewer gases, and other airborne contamination, by forming a physical barrier between the drainage network and the occupied space. Retention of the water trap seal has dominated the development of the building drainage system since the end of the 19th century when it was first acknowledged that air pressure transient propagation - generated during appliance discharge – could compromise the integrity of the water trap seal and ultimately lead to trap depletion. Subsequent research, aimed at understanding and controlling these air pressure transients, prompted the development and inclusion of ventilation pipes and active pressure control devices including, since the 1980s, the air admittance valve (AAV) and the positive air pressure attenuator (PAPA) - to alleviate the effects of air pressure transient propagation, and thus protect the integrity of the water trap seal.

The protection provided by these control measures cannot, however, be guaranteed due to the inherently unsteady flow regime that exists within the building drainage system as a result of the normal, yet random, appliance discharge. When coupled with additional extraneous influences such as improper system design and construction, excessive pressure excursions due to sewer surcharge, pressure fluctuations due to wind shear, and evaporation due to lack of use; the unsteady nature of the conditions existing within the building drainage system ensures that trap seal depletion remains a major concern.

The consequence of trap seal depletion gained international attention in 2003 following the outbreak of severe acute respiratory syndrome (SARS) – a highly contagious viral disease capable of airborne transmission. The large community outbreak at Amoy

Gardens, Hong Kong has since been attributed, in part, to depleted water trap seals which facilitated the transmission of virus-laden aerosols, which had been introduced into the drainage system following faecal virus shedding by an infected resident (WHO, 2003; Hong Kong SAR Government – SARS Expert Committee, 2003). Had there been an adequate maintenance regime in place at Amoy Gardens, which allowed depleted trap seals to be quickly identified and replenished, then it is reasonable to assume that the severity of the outbreak would have been significantly reduced and many lives may have been saved. This urgent requirement for a robust and reliable method for monitoring and maintaining the building drainage system provides the motivation for the following research.

1.2 Identification of depleted trap seals

The severity of the SARS outbreak at Amoy Gardens highlights the importance of adequate system maintenance so that, when trap seal depletion does occur, it can be quickly identified and rectified to ensure that cross-contamination is minimised.

1.2.1 Current method

Maintenance methods currently available to building operators and facilities managers are inadequate, relying solely on visual inspection of the trap seal which is not only labour-intensive but impractical and effectively impossible to sustain in large buildings. There is, therefore, a continuing and urgent need to develop a novel technique whereby the conditions of all the trap seals can be determined quickly and easily. This has led the author to investigate a transient-based method, described as the *reflected wave technique*, to provide a means whereby depleted trap seals can, for the first time, be detected and located using a remote and non-invasive methodology.

1.2.2 Proposed approach

Pressure transients occur within the drainage system following rapid changes in flow conditions as a result of appliance discharge and are normally considered a problem because they are a potential cause of trap seal depletion. However, since transient pressure waves propagate back and forth in the system at the appropriate wave propagation speed and, at the same time, are affected by the presence of each component in the system, such transients carry important information about the features of the network boundaries - each of which display a characteristic transient reflection

coefficient (Swaffield and Galowin, 1992; Covas, 2003). The reflection coefficients of common system boundaries will be discussed in more detail in Chapter 2, however, some examples include:

i. a closed-end pipe, such as one terminated with an air admittance valve (AAV) or fully primed trap seal, generates a positive reflection (equal in magnitude and sign to the incident wave), demonstrating a +1 reflection coefficient;

ii. an open-end pipe, such as an open stack termination or a depleted trap seal, generates a negative reflection (equal in magnitude but opposite in sign to the incident wave), demonstrating a -1 reflection coefficient;

iii. a junction both reflects and transmits the incident wave, the proportion of which is dependant upon the area ratio of the various pipes connecting at the junction (Swaffield and Galowin, 1992).

Recognition of these features and their effect on the resultant pressure response allows their identification within the system – provided the wave propagation speed is known – thus providing a potential tool for the detection and location of depleted trap seals.

The application of the reflected wave technique for the detection and location of depleted trap seals requires the comparison of the system response to an applied low-amplitude pressure transient with a predetermined “defect free” system response in order to determine the arrival time of the first reflected wave returned by the changed boundary condition. This approach relies on: (i) the ability of the reflected wave, induced by the depleted trap, to sufficiently alter the system response in order to identify its location within the system, and (ii) the accurate determination of the wave propagation speed.

Previous applications of the reflected wave technique include leak detection in water supply systems (Jonsson, 1995; Covas and Ramos, 1999; Brunone and Ferrante, 2001, 2004); valve status determination in water supply networks (Stephens *et al.*., 2004; Arbon *et al.*, 2008); and blockage detection in natural gas supply pipes (Adewumi *et al.*, 2000; Adewumi *et al.* 2003). This research aims to develop this method further for the detection and location of depleted trap seals in a building drainage system.

1.3 Historical developments

The natural abhorrence of foul odours emitted from human waste – together with the belief that they were responsible for causing an array of diseases – has been the main driver responsible for the evolution of what we know today as the building drainage system. Although today our understanding of disease transmission is somewhat more advanced, this early connection between dirt and disease encouraged public health reforms and cleanliness. The preoccupation of protecting building occupants from these noxious fumes heralded the development of more efficient sanitary systems and improved domestic hygiene.

1.3.1 Pre 1800

The problem of tackling odour ingress can be traced as far back as medieval times when it was, quite surprisingly, a matter of concern for reigning monarchs. Johnson (1978) in his depiction of the sanitary systems at Castel del Monte (built around 1240), shows evidence that Henry III had attempted to alleviate the problem by ordering that:

> *"the privy was placed as far away as possible, on account of the smell, at the end of a passage in the thickness of the wall, with access to the chamber by means of a right-hand turn. Sometimes, as at Woodstock, Henry III ordered double doors to reduce the smell further." (Johnson, 1978)*

Although positioning the sanitary system away from the main rooms did provide some alleviation from the foul odours, it did nothing to address the unpleasant and unavoidable smell suffered by those using the system.

It was centuries later, in 1596, that Sir John Harington, an Elizabethan poet, first addressed this problem by designing the first true water closet (wc) – so called as it used water not only to clean the bowl and to help in removing the waste, but also to suppress the foul odours. Described in his book *The Metamorphosis of Ajax* (1596) as an odourless toilet, Harington's wc incorporated all the main features that we expect to see in a wc today; a cistern with lever and overflow, a bowl, a flushing pipe, a plug outlet valve, and a seat, see **Figure 1.1**.

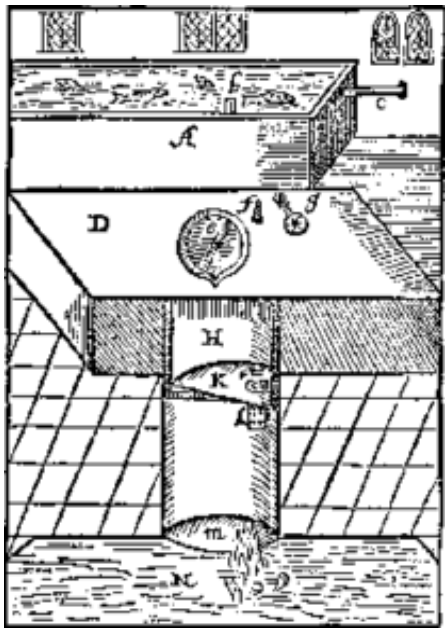

Figure 1.1 Sir John Harington's 16th Century water closet the 'Ajax' (Billington and Roberts, 1982)

A plate at the base of the bowl held six inches of water which acted as a barrier between the room and the drain and this prevented the foul odours from entering the room – instead keeping them contained within the drain. After use, the content of the bowl was deposited to the drain by removing the plate. Harington installed one wc at his home in Bath and another in Richmond Palace for his godmother, Queen Elizabeth I. Unfortunately, however, Harington's water closet was never really taken seriously, partly because there were few drains or sewers and also because water supplies were limited and over the next two centuries the invention was virtually ignored and forgotten. Preference instead turned to the chamber pot (Billington and Roberts, 1982; Stoke-on-Trent Council, 2006).

In 1775, however, a patent was taken out by a Bond Street watchmaker, Alexander Cummings, for an improved version of Harington's invention which incorporated one very significant development – the use of a water trap seal to isolate the bowl from the drain, providing improved protection from the invasion of foul odour, **Figure 1.2**. Further developments were made by Joseph Bramah, a cabinet maker, who registered his patent in 1778 incorporating a hinged outlet valve, and a connection directly to a cesspool in the basement or under the garden (Wright, 1980).

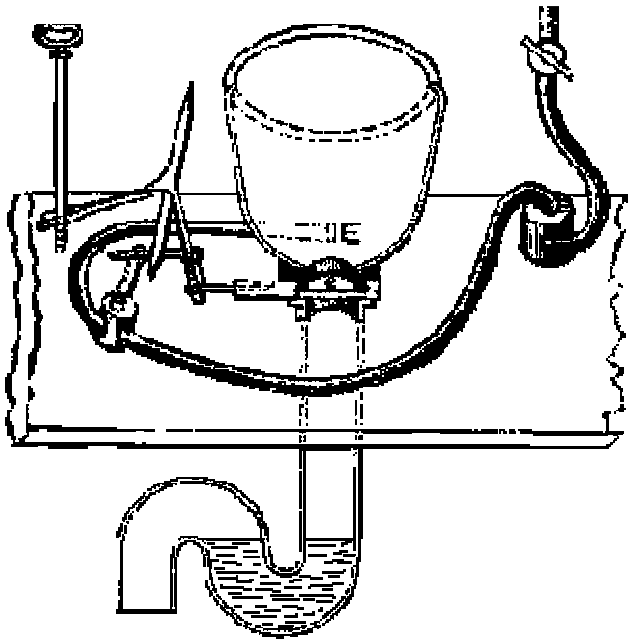

Figure 1.2 Alexander Cummings' patented water closet of 1775 incorporating a water trap seal

1.3.2 1800 to 1899

By the beginning of the nineteenth century the popularity of the wc was on the rise. However, when coupled with an ever-increasing population, this created new problems regarding the issue of waste disposal. Cesspools were considered the proper receptacle for domestic waste (Cook, 2001), however, the increasing volumes of discharging waste would often cause the cesspools to overflow (Halliday, 1999) and the accumulating quantities of stagnant waste would often give off an offensive foul odour and, it was believed, disease (Allen, 2002).

Until the mid-nineteenth century it was generally accepted that disease was caused by *miasma* – a noxious mist containing particles of decomposing matter capable of causing illness and which could be identified by a nasty foul smell. Sanitary reformers, such as Sir Edwin Chadwick, were avid supporters of the miasmic theory of disease transmission as it explained why disease were epidemic in the undrained, filthy and stinking areas inhabited by the poor. Quoted in 1846 giving evidence to a Parliamentary Committee considering the problem of London's waste, Chadwick suggests:

> *"All smell is, if it be intense, immediate acute disease." (Parliamentary Papers*, 1846, vol. 10, p. 651*)*

In 1847, a contemporary of Chadwick and fellow campaigner for sanitary reform, William Farr, the chief statistician for the Office of the Registrar-General, estimated in his Tenth Annual Report, that at least 38 people died every day in London as a result of poor living conditions believing the cause to be, in part, due the miasma emanating from the sewage system:

> *"This disease mist, arising from…cesspools…is continually kept up and undergoing changes; in one season it was pervaded by Cholera, in another by Influenza; at one time it bears Smallpox, Measles, Scarlatina and Whooping Cough among your children; at another it carried fever on its wings. Like an angel of death it has hovered for centuries over London". (Tenth Annual Report of the Registrar-General, 1847, p. xvii.).*

Chadwick's activism, through the publication of his 1842 *Report on the Sanitary Condition of the Labouring Population of Great Britain*, helped shape the important body of sanitary legislation passed in 1848, including the Public Health Act, the Nuisances Removal and Disease Prevention Act, and the Metropolitan and City Sewers Act, which brought revolutionary changes in the sanitary practice of London's inhabitants who, for the first time, were legally obliged to discharge domestic waste into the city's rapidly expanding network of sewers (Allen, 2002). Within a few years more than 30,000 cesspools were systematically abolished in preference for the sewer system (Cook, 2001).

However, the fear of emanations produced by stagnant waste was not eradicated by the connection to the sewer system. Instead, the sewer created a new foe: sewer gas. Built only to accommodate surface water, the city's pre-existing sewers were unable to cope with the increased flow of household waste and the accumulation of waste was a common occurrence. The noxious vapours generated by these deposits tended to escape through any available outlet, usually into houses with connecting drains (Allen, 2002). The anxiety surrounding the emanating sewer gases is shown clearly in a text by Booth opposing a plan for a main sewer development by the Metropolitan Board of Works in the early 1850s:

> *"It therefore becomes a point of the utmost importance that the seeds of disease should at once be arrested: that they should not be carried from house to house, from street to street, from unhealthy parts to salubrious districts, by the*

construction of monster sewers, impregnating with the feculent matter of each locality." Booth (1853)

The literal connection that the sewer created between every household was seen as a path for disease transmission; allowing foul smelling and disease-conveying sewer gases to escape into houses through connecting drains. In addition to the health anxieties surrounding sewer gas, the sewer system also created social anxieties. Such sewer systems, in effect, permitted the movement of noxious emanations from "*house to house*" or, more specifically, from disease-infested homes of the poor to clean homes of the wealthy (An, 2005). In a time when social barriers were fastidiously enforced, the sewer began to erode the class divide and threaten the integrity of the bourgeoisie. This realisation heightened the fear of sewer gas as it now "*threatened the health and stability of the social order it was designed to uphold*" (Allen, 2002)

The threat of epidemic diseases in the nineteenth century also increased the perceived danger of sewer gas. Cholera epidemics raged in London in 1831-32, 1848-49 and 1853-54. During the last of these Farr served as a member of the *Committee for Scientific Enquiry into the Recent Cholera Epidemic* who undertook a detailed study of an outbreak of the disease on Broad Street. Despite recent evidence, published in 1849, by Dr John Snow in his paper *On the Mode of Communication of Cholera* in which he suggested that drinking water contaminated with sewage might be the method by which cholera was transmitted, the Committee concluded:

"We cannot help thinking that the outbreak arose from the multitude of untrapped and imperfectly trapped gullies and ventilation shafts constantly emitting an immense amount of noxious, health-destroying, life-destroying exhalations". (Parliamentary Papers, 1854-5).

Despite the compelling evidence, the conclusions of the Committee clearly demonstrate the strength of the miasmic theory and the inherent fear of sewer gas at the time. In her classic text *Notes on Nursing*, published in 1860, Florence Nightingale (herself a miasmatist) stated:

"No house with any untrapped unventilated drain pipe communicating immediately with an unventilated sewer, whether it be from a water closet, sink, or gully-grate, can ever be healthy. An untrapped sink may at any time spread fever or pyaemia among the inmates of a palace." (Nightingale, 1860)

She went further to criticise the practice of laying drains beneath houses, suggesting that sewer gas would escape from them, penetrate the dwelling and cause epidemics of scarlet fever, measles and smallpox.

The anxiety surrounding sewer gases focused public attention not only on the dangers, but also on the prevention of sewer gas emanations. A number of publications appeared at the end of the nineteenth century, including *Sewer Gas, and how to keep it out of houses* by Osborne Reynolds (1872), *Hints on drains, traps, closets, sewer gases and sewage* by Peter Bird (1877) and *Dangers to health: A pictorial guide to domestic sanitary defects* by Teale (1881). Teale provides an effective illustration showing the perceived threat of the emanating sewer gases into the home, **Figure 1.3**. The drawing provides a cutaway view of a house showing a number of "*the most common sanitary faults of ordinary houses.*" These include untrapped appliances and drain pipes laid under the house and shows the conditions that existed even towards the end of the 19th century. The spread of the sewer gas is indicated by a series of arrows and is shown to contaminate every room.

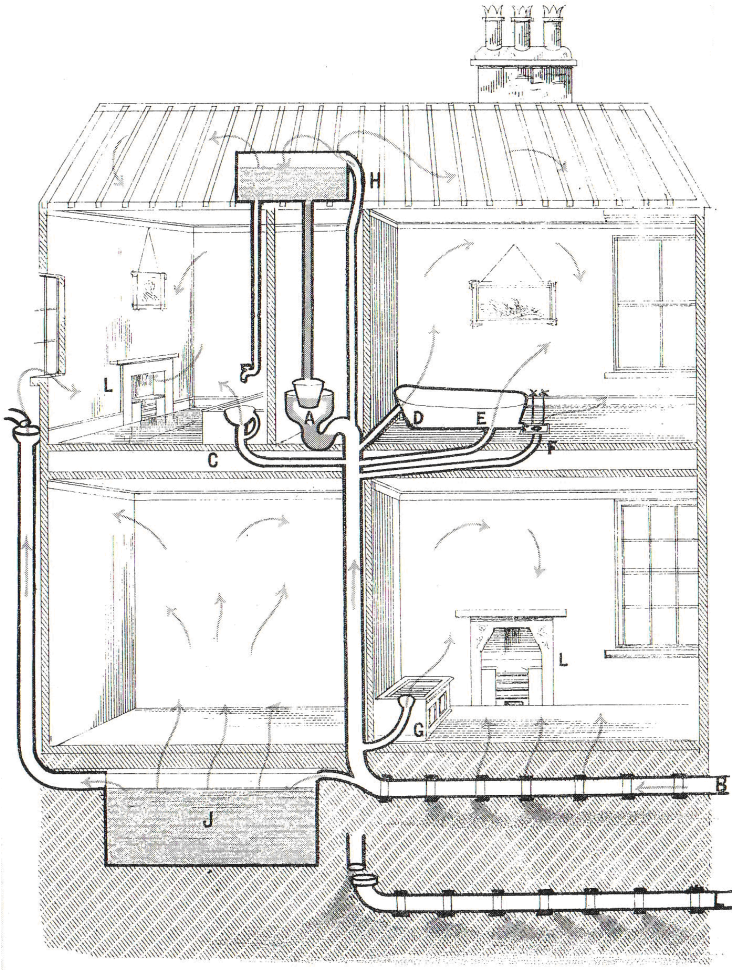

Figure 1.3 House with every sanitary arrangement faulty (Teale, 1881)

Two modes of action were promoted by these publications to help combat the emanation of sewer gases and communicable diseases: (i) drain trapping - Reynolds assures his reader that "*an efficient trap…will completely cut off the house from the sewer*."; (ii) system surveillance and monitoring - Reynolds advises: "*the first thing for the anxious householder to do is to get clear conception of what the drains in his house are for, and whereabouts he may expect to find them.*" Teale (1881) hopes that his pictorial guide will serve the householder with this very task: "*aided by the diagrams, he may test every sanitary point, one by one, and as he goes round book in hand, may catechise his plumber, his mason, or his joiner.*"

By the end of the 19th century, sanitation techniques and designs were generally recognisable against modern practice. The importance of the water trap seal, and its role in preventing the ingress of foul sewer gases into buildings, was well understood, as was the necessity for regular system maintenance.

1.3.3 1900 to present

The rise of microbiology at the end of the nineteenth century provided a new understanding of disease. The germ theory of disease transmission was becoming more generally accepted (Cook, 2001). In addition, the exploration of the nature of sewer gas reached new standards and bacteriological investigations by prominent scientists, such as Jacobi (1894) and Winslow (1909), claimed that the air from sewers contained fewer numbers of pathogenic microorganisms than ambient air – claiming that the putrefaction process in the sewers destroyed specific germs – and also that the two were similar in composition[1]. These findings began to debunk the earlier anxieties over sewer gas and there became a rapid shift towards the belief that sewer gas was in fact harmless.

This change in attitude continued throughout the middle of the twentieth century and is evident from an extract from a report by the American Public Health Association (1951) which states *"…the air of a properly constructed sewer or house drain differs from outdoor air only in having a musty odour…"* and in a prominent text of drainage system design by Wise who writes *"…evidence shows that the purpose of the [trap] seal is to exclude smell, as distinct from the lethal gas which was once thought to occupy the pipework…"* (Wise, 1957).

[1] The chemical composition of sewer gas is now better understood and is known to contain hydrogen sulphide (H_2S) – a by-product of the bacterial breakdown of organic waste material – which can cause sudden death at levels > 600ppm (Yalamanchili and Smith, 2008)

Further advances in microbiology, however, offered new techniques to analyse the modes of disease transmission. Scientists such as Hutchison (1956), Darlow and Bale (1959) and Gebra *et al.* (1975) conducted experiments that revealed that pathogenic microorganisms could be transmitted in airborne aerosols. These important findings revealed that instead of being the perpetrator of disease, sewer gas could, in fact, facilitate the spread of disease by mediating the movement of pathogen-rich aerosols.

A great number of viruses (i.e. adenoviruses, astrovirus, enteroviruses, hepatovirus, norovirus, reoviruses and rotavirus) and bacteria (i.e. Escherichia coli (*E. coli*), Legionella pneumophila, Salmonella and Shigella) passed in the excreta of infected individuals have been found not only to exist within the building drainage system but are also amenable to airborne transmission within aerosolised water particles (Feachem *et al.* 1983). Aside from coughing and sneezing, aerosols generated during toilet flushing have been identified as the most likely source of potentially disease-causing aerosols (Hutchinson, 1956; Darlow and Bale, 1959; Gebra *et al.*, 1975).

Once aerosolised, these infective pathogens may either be deposited on surfaces, leading to self-inoculation through hand-to-mouth contact (Hendley *et al.*, 1973), or remain airborne (Couch *et al.*, 1966) and thus spread the disease further a field through ingestion or inhalation by uninfected victims. Airborne transmission, through the transfer of infectious droplets and aerosols, remains the most important mechanism of uncontrollable dissemination of disease and studies have shown that aerosolized pathogens can travel up to 1.5 km from source (Parker *et al.*, 1977; Cronholm, 1980)

The risk of infection by inhaling aerosolized pathogens depends on factors such as the quantity inhaled, infective load and the aerosol particle size (Feachem *et al.*, 1983). Research has shown that aerosols generated during toilet flushing are particularly hazardous in this regard. Such aerosols contain much greater concentrations of pathogens than the water from which they came. The presence of the pathogen reduces the surface tension at the air to water interface and so when the water is agitated the aerosols are created where the surface tension is weakest (i.e. where the greatest concentration of pathogens are present) and so the aerosols contain concentrated quantities of the pathogen. Studies by Baylor (1977) and Baylor *et al.* (1977) found the pathogen concentration in aerosols was between 50 and 250 times higher than the water from which they were generated.

Additionally, the risk of infection is dependant, in part, upon the ability of the aerosol to penetrate deep into the lungs. Lung penetration is especially important in the establishment of respiratory infections. Aerosols that penetrate best are those which are less than 5 or 6 microns in diameter (Druett *et al.* 1953; May and Druett, 1953; Druett *et al.*, 1956). Although only small aerosols are likely to penetrate to the lower respiratory tract, it is probable that bacteria and viruses in larger aerosols caught in the upper respiratory tract may subsequently be swallowed. Reported aerosol sizes from sewage sources vary considerably but, in general, smaller aerosols predominate as distance from the source increases because larger particles have settled. Darlow and Bale (1959) found that a toilet flush produces aerosols with a mean diameter of 2.3 microns, 87% of them being less than 4 microns and capable of reaching the lower respiratory tract.

Despite evidence to the contrary, the popular view throughout the twentieth century continued to consider sewer gas as harmless. Care to avoid the ingress of sewer gas was generally only a concern to avoid its offensive odour. However, the true consequences of the cross-contamination of this foul air was realised at the beginning of the twenty-first century when it was identified as a vector for the transmission of the SARS virus at Amoy Gardens which will be discussed in more detail in Section 2.4.

1.4 Current design code

In the UK, the building drainage system must be designed, installed and maintained in accordance with the current British Standard, BS EN 12056: 2000. This document recognises the importance of trap seal retention and sets out strict system performance requirements giving guidelines for the selection of pipe diameters, trap diameters, trap seal depths, branch to stack connections, pipe lengths, pipe material and vent sizing; all aimed at limiting the maximum allowable pressure variation to ± 38 mm water gauge; this limit being the pressure that would retain an appliance trap seal of 25 mm, the generally accepted minimum retention to avoid the danger of evaporative trap seal loss. This limit is aimed at maintaining the minimum retention level of the wc trap whose non-uniform shape makes it more susceptible to incoming pressure transients, corresponding typically to a loss of approximately two-thirds of the applied water gauge pressure. Acting on a trap seal depth of 50 mm this would leave only the minimum accepted retention level. In uniform bore traps, such a maximum pressure fluctuation would give a trap seal loss of 19 mm (half of the water gauge pressure) and with a

normal depth of 50 mm and 75 mm, these traps would retain a minimum seal of 31 mm and 56 mm respectively (Swaffield and Galowin, 1992; Jack, 1997).

The code goes further to detail how pressure transients (both positive and negative) are generated within the system, and describes the various methods by which an appliance trap seal can be depleted and thereby provides the designer with an insight into the operation of the system.

Little guidance is given in the Standard for system maintenance; instead the onus is firmly on the system designers to ensure adequate capacity. The little advice that is provided focuses on the cleaning of the pipework, and in particular, the removal of grease, lime scale and soap residues, which could impede the efficiency of the system. Very little information is provided on the necessity for monitoring trap seal status; only going as far to advise periodic system inspection.

1.5 Aims and objectives of this research

The aim of this research focuses mainly on the development and validation of a systematic method of remotely monitoring trap seal status as a regular and routine preventative tool against the transmission of infection and disease from the building drainage system. Provision of such a methodology would thereby provide an automatic and periodic system maintenance regime.

The primary objective of the research is to determine the potential application of a transient-based defect identification method - namely the reflected wave technique – for the detection and location of depleted trap seals in building drainage systems and to provide guidance to allow its implementation in support of complex building Facilities Management. To evaluate the concept and to provide operational guidance, the research combines laboratory transient measurements with a detailed consideration of network simulation as well as extensive site testing to evaluate the practical operation of the methodology. A further objective will be to generate confidence in the proposed methodology, which for the first time introduces the use of automatically imposed low amplitude air pressure transient propagation as a means of identifying depleted trap seals as part of the reflected wave technique.

The research objectives were:

i. Identify by laboratory testing a suitable transient generator to deliver an appropriate low amplitude transient into the network and utilise this to develop the proposed transient-based method within a test facility designed to represent a multi-storey building drainage system. Defective trap seals were introduced and the monitored system response evaluated to confirm the ability to locate changed boundary conditions.

ii. The numerical model (AIRNET) developed at Heriot-Watt University under previous EPSRC awards, was enhanced in order to allow predicted system responses to be compared with those measured during the laboratory tests and field trials. The software was extended to include the addition of a new boundary condition to represent the pressure transient generator.

iii. Site testing followed from the laboratory confirmation of the practicality of this transient-based method. To minimise the effects of ambient system noise these site tests took place either in an unoccupied building or during quiescent periods - typically during the night. Full cooperation was obtained and suitable buildings made available by the Sanctuary Housing Association in Dundee, Heriot-Watt Univeristy in Edinburgh, and the Royal Bank of Scotland Facilities Management Group.

iv. Develop the test methodology in a form readily accessible to facility managers and building users and identify suitable monitoring equipment capable of withstanding field conditions over a prolonged period.

1.6 This thesis

This thesis documents the developmental process of the application of the reflected wave technique for the remote and non-invasive identification of depleted appliance trap seals within the building drainage system.

Chapter 1 has introduced the scope and background of the project, as well as the proposed depleted trap detection method. The main aims and objectives of this research have also been summarised.

Chapter 2 provides the main principles governing the propagation of low amplitude pressure transients within the building drainage system and relates these to the main causes of trap seal depletion which continue to be a problem for system designers. The risks of trap seal depletion will be considered by reviewing both the mechanisms contributing and the consequences arising from the outbreak of the SARS virus at Amoy Gardens.

Chapter 3 covers the development of the modelling of low amplitude air pressure transient propagation within the building drainage system, giving a general summary of the method of characteristics and the Heriot-Watt University developed computer program, AIRNET. A new boundary condition to represent the pressure transient generator is given together with a summary of the previously developed boundary conditions.

Chapter 4 focuses on the description of the reflected wave technique. The numerous approaches available for defect detection in fluid transportation systems are reviewed. The principles behind the reflected wave technique and its application to the detection and location of depleted trap seals will be evaluated. A description of the automatic ***tra****p* ***c****ondition* ***e****valuato****r*** (TRACER) program developed by this author, which allows the detection and location of depleted traps to be determined automatically without relying on user interrogation, will also be presented.

Chapter 5 describes the experimental programme carried out to evaluate the reflected wave technique during a series of laboratory and field investigations. A description of the apparatus and the test methodology is provided together with the practical considerations required for the application of the technique to complex building drainage systems.

Chapter 6 presents the results from the laboratory and field investigations and evaluates the effect that a depleted trap seal has on the measured system response. The sensitivity of the proposed method will be evaluated with particular attention made to the effect of system junctions and trap diameter.

Chapter 7 contains the main conclusions of this research including a summary of the developed work followed by the main achievements and conclusions of the research. Finally, recommendations for future work are presented.

Chapter 2

Air pressure transients within the building drainage system

2.1 Introduction

Before air pressure transients can be utilised to identify depleted trap seals within the building drainage system it is important first to determine the mechanisms that govern transient generation and propagation and to understand the consequences that these transients may have within the system. This chapter provides the theoretical background and fundamental equations defining pressure transient propagation applicable to any fluid carrying system, including those expressions defining the influential effect of the most important system boundaries. With specific attention to the building drainage system, the mechanisms of transient generation and the effect that these transients may have on system integrity, particularly trap seal retention, will be discussed.

The harmful consequences of trap depletion and the dangers of cross-contamination of the foul air within the building drainage system will be explored by examining their role as a transmission vector in the spread of the SARS virus.

2.2 Fundamental relationships

Air pressure transients are generated within any fluid carrying system as a natural consequence of changes in flow conditions at some point within the system, and are effectively the means by which information regarding this change is communicated to all other points within the system (Swaffield and Boldy, 1993). Although normally of a much lower amplitude, the air pressure transients generated within the building drainage system obey the same mechanisms of propagation as pressure transients in all other full bore fluid carrying systems.

Pressure transient analysis, or "waterhammer" as it was previously known, dates back to 1900 when Joukowsky, following an extensive programme of experimental work at the St Petersburg Water Works, first established an understanding of the phenomenon of transient propagation. Through his research, Joukowsky, established the fundamental relationship between pressure change and velocity change:

$$\Delta p = -\rho c \Delta V \tag{2.1}$$

where Δp, is pressure change, ΔV, is velocity change, ρ, is the fluid density, and c is the wave propagation speed. The significance of the negative sign means that pressure increases with a decrease of velocity, and vice versa. This expression establishes the importance of wave propagation speed in the analysis of transient propagation. The wave propagation speed for low amplitude pressure transients travelling along a pipe filled with air may be calculated by (Swaffield and Boldy, 1993):

$$c = \sqrt{\frac{p\gamma}{\rho}} \tag{2.2}$$

where p is the absolute pressure, γ is the ratio of specific heat and ρ is the fluid density. This expression assumes isentropic flow and ignores the effect of pipe-wall elasticity (an important factor in estimating the wave propagation speed in liquids such as water) which is acceptable due to the very small pressure fluctuations and insignificant temperature variations occurring during transient propagation within a pipe filled with air only. The pipe walls can, therefore, be regarded as rigid (Swaffield and Galowin, 1992; Massey and Ward-Smith, 1998). For air at 20^{o}C, Equation (2.2) gives a wave propagation speed of 343 m/s (p = 1.10913x10^{5} Pa, γ= 1.4 and ρ = 1.32 kg m^{-3}).

Therefore any change in system flow results in the generation of a pressure wave that propagates within the pipe at the appropriate wave propagation speed until, as Joukowsky discovered, it is reflected upon arrival at a system boundary, either internal or terminal. Realising the significance of wave reflections within the pipe system, Joukowsky introduced the concept of pipe period, t_p, which is the time taken for a generated wave to travel to a reflecting boundary and return to the source:

$$t_p = \frac{2L}{c} \tag{2.3}$$

where L is the pipe length and c is the wave propagation speed. The pipe period is used to assess the nature of the change in flow condition. For the application presented in this work, if the change in flow condition occurs in less than one pipe period then this is considered a "rapid" change, while those taking longer than one pipe period are considered a "slow" change. Equation (2.1) is only valid for rapid changes in flow condition. In the case of a slow change the peak pressure generated does not reach the maximum Joukowsky value, $\rho c V_0$, due to the interaction and superposition of boundary reflections which are returned prior to the completion of the change in flow condition.

2.2.1 Transient reflection and transmission

To explain the propagation of pressure transients and their interaction with system boundaries, Allievi (1903) applied a simplified version of the frictionless equations of continuity and motion:

Equation of Continuity

$$\frac{\partial p}{\partial t} + \rho c^2 \frac{\partial v}{\partial x} = 0 \tag{2.4}$$

Equation of Motion

$$\frac{\partial p}{\partial x} + \rho \frac{\partial v}{\partial t} = 0 \tag{2.5}$$

which have a general solution and may be expressed as (Swaffield and Boldy, 1993):

$$V - V_o = -\frac{1}{\rho c}\left[F\left(t + \frac{x}{c}\right) - f\left(t - \frac{x}{c}\right)\right] \tag{2.6}$$

$$p - p_0 = F\left(t + \frac{x}{c}\right) + f\left(t - \frac{x}{c}\right) \tag{2.7}$$

The *F()* and *f()* functions are used to represent a pair of pressure wave transients propagated in the $-x$ and $+x$ directions, respectively, as a result of a change in boundary condition (when x is measured in the initial flow direction). These two functions follow the principle of superposition of pressure waves such that the pressure at a point in the system at a time t, following the generation of a pressure transient, will be given by the summation of all the *F()* and *f()* that have propagated past that point up to that time.

2.2.2 Transient reflection at a closed-end pipe

In the case of a closed-end pipe, **Figure 2.1(a)**, the fluid in contact with the dead end must remain at rest, i.e. zero flow velocity. To achieve this, the incoming pressure transient must be reflected with the same magnitude and sign – with the effect that the local pressure at the dead end is doubled - thus returning the fluid in the pipe to its original flow condition. If *F()* is the incoming pressure transient and *f()* is the reflected transient, then assigning $(V\text{-}V_0)$ to zero in Equation (2.6) confirms the appropriate reflection coefficient at a closed-end pipe as:

$$C_R^{closed} = +1 \tag{2.8}$$

2.2.3 Transient reflection at an open-end pipe

In the case of an open-end pipe, **Figure 2.1(b)**, the pressure at the boundary must remain constant and, therefore, the incoming transient must be reflected with the same magnitude but a sign reversal. This reflected pressure transient then propagates back along the system, returning the fluid pressure in the pipe to its original condition. Assigning $(p\text{-}p_0)$ to zero in Equation (2.7) provides the appropriate reflection coefficient at an open-end pipe as:

$$C_R^{open} = -1 \tag{2.9}$$

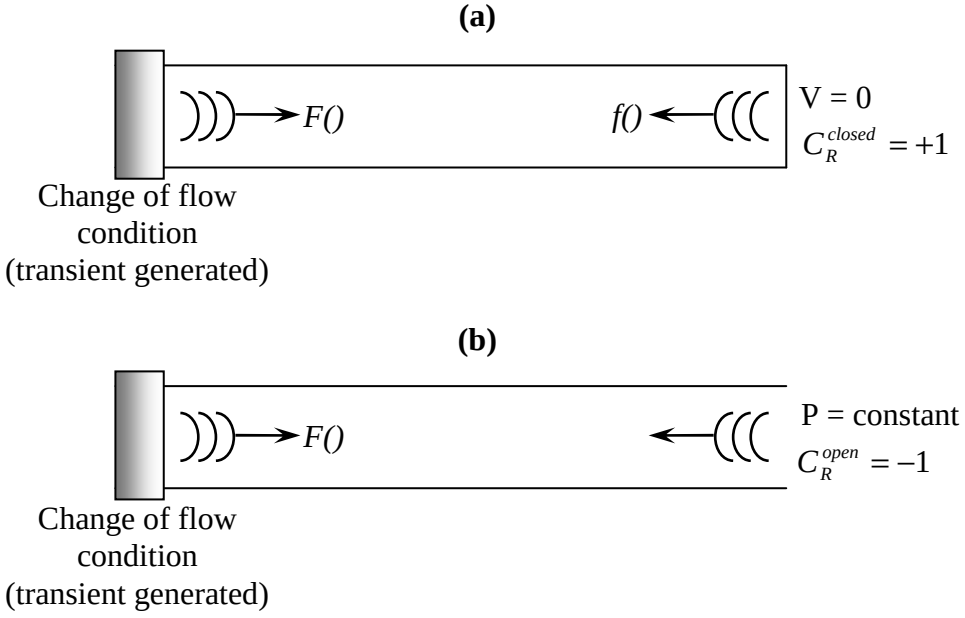

Figure 2.1 Pressure transient propagation, illustrating the concept of transient reflection at system boundaries for a pipe terminated with (a) a closed end; (b) an open end

2.2.4 Transient reflection at a junction

Transients arriving at a junction, **Figure 2.2**, are both transmitted and reflected. Equations (2.6) and (2.7) may be solved together with the continuity of flow and pressure to determine the reflection and transmission coefficients at a junction of *n* number of pipes, where it is assumed that there are no separate losses at the junction:

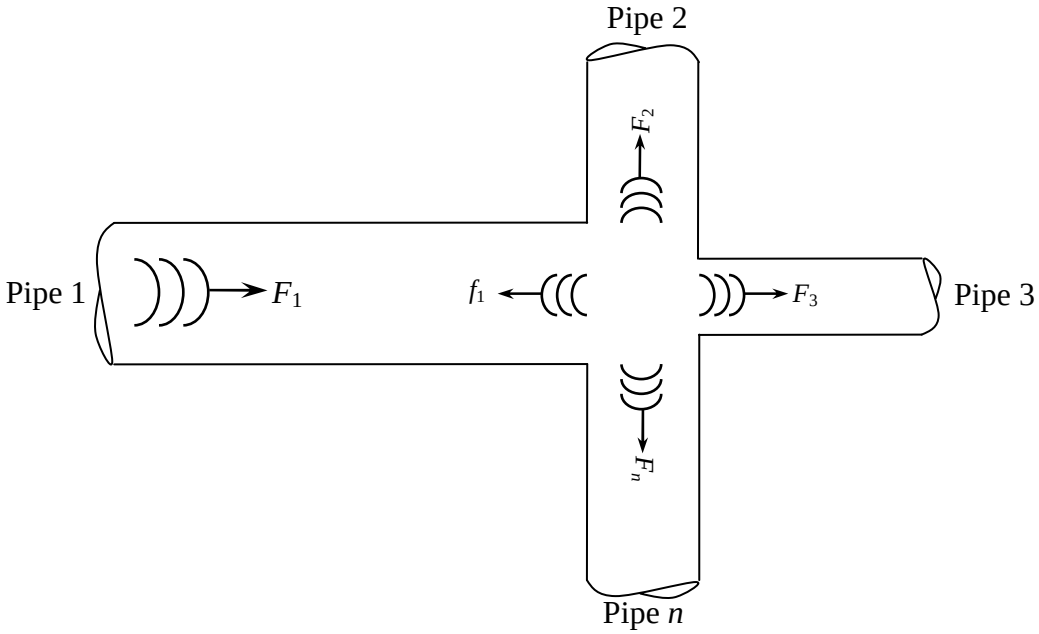

Figure 2.2 Pressure transient propagation, illustrating concept of wave reflection and transmission at a general pipe junction of n number pipes

Continuity of flow

$$Q_1 = Q_2 + Q_3 + ... + Q_n \tag{2.10}$$

and

$$\Delta Q_1 = \Delta Q_2 + \Delta Q_3 + ... + \Delta Q_n$$

Commonality of pressure

$$p_1 = p_2 = p_3 = ... = p_n \tag{2.11}$$

and

$$\Delta p_1 = \Delta p_2 = \Delta p_3 = ... = \Delta p_n$$

Solution of Equations (2.6) and (2.7) with (2.10) and (2.11) for an incoming pressure transient, F_1, in pipe 1, and transmitted waves $F_{2\text{-}n}$ in pipes 2-n and a reflected wave f_1 in pipe 1 provide a general expression for the reflection and transmission coefficients respectively for the junction (Swaffield and Boldy, 1993):

$$C_R^{junction} = \frac{\frac{A_1}{c_1} - \frac{A_2}{c_2} - \frac{A_3}{c_3} - \ldots - \frac{A_n}{c_n}}{\frac{A_1}{c_1} + \frac{A_2}{c_2} + \frac{A_3}{c_3} + \ldots + \frac{A_n}{c_n}} \tag{2.12}$$

and

$$C_T^{junction} = \frac{\frac{2A_1}{c_1}}{\frac{A_1}{c_1} + \frac{A_2}{c_2} + \frac{A_3}{c_3} + \ldots + \frac{A_n}{c_n}} \tag{2.13}$$

Note that $f_{2\text{-}n}$ may be put to zero in this solution as reflections are assumed not to have arrived back at the junction. The coefficients given above in Equations (2.12) and (2.13) demonstrate several important points:

i. The reflection and transmission coefficients are dependant upon both the area of each pipe and the wave propagation speed within them. Therefore, factors affecting wave propagation speed, such as pipe material and pipe-wall thickness, and changes in pipe area due to a change in diameter, will also generate reflected and transmitted transients.

ii. In systems where the wave propagation speed can be assumed constant, such as building drainage systems where only low amplitude pressure transients are considered and the system pipework may be assumed rigid, Equations (2.12) and (2.13) can be reduced to area ratios by excluding the wave propagation speed.

iii. The transmission coefficient is identical for all the receiving pipes, however, this value does depend upon which pipe carries the incoming pressure transient (i.e. the index pipe).

2.3 Air pressure transients within the building drainage system

The air pressure transients generated during the operation of the building drainage system conform to the transient propagation theory presented. This section reviews the mechanisms involved in the generation of air pressure transients within the building drainage system and what effect these transients may have on the integrity of the trap seal. Common methods employed within the building drainage system to provide transient suppression and control will also be reviewed.

2.3.1 Traditionally accepted stack pressure profile

To understand the mechanisms leading to the generation of air pressure transients it is first necessary to review the mechanisms that lead to the accepted air pressure profile within the building drainage system.

On entering the vertical stack from a horizontal branch connection, the wastewater travels across the diameter of the stack where it impinges onto the opposite pipe wall before establishing a downward annular water flow around a central air core. Due to the principal of "no slip" at the water/air interface the descending annular water flow entrains an airflow from the upper stack termination. Instead of falling exclusively as an annulus, Campbell and MacLeod (1999) and MacLeod (2000) have demonstrated that a proportion of the water is actually distributed as droplets across the diameter of the stack. As a result, the shear force acting on the air is a sum of the shear force at the water/air interface and the shear force of the droplets. At the base of the stack, the transition from vertical annual water flow to horizontal free surface flow forms a periodic water curtain through which the entrained airflow must pass.

In response to these flow conditions, the air pressure within the stack is altered from atmospheric at its upper termination and the pressure distribution follows a characteristic variation down the stack. **Figure 2.3** shows the well-recognised pressure response diagram for a simple single-stack system operating under steady state conditions with an open termination. The top of the stack, *A*, is at atmospheric pressure. The pressure within the upper "dry" stack, *AB*, falls due to pipe friction loss as the air flow is drawn down the stack. A concentrated pressure loss occurs at *B* due to the effect of drawing air through the water curtain formed at the discharging branch junction with a further concentrated loss at *C* due to the second discharging branch in this example. Within the lower "wet" stack, *CD*, the air pressure recovers to above atmospheric due to the traction effect of the water annulus on the entrained airflow before it is forced

through the water curtain at the base of the stack. The entrained airflow is a function of the total annular water downflow. The "no-slip" condition provides the traction in *CD* and the pressure recovery. In *BC*, the pressure may continue to fall or display recovery dependant upon the water flow in this stack section. A low water flow in *BC* will display a pressure fall as the entrained airflow, dependant on a higher water flow in *CD*, is drawn over the water film.

The distribution and magnitude of the pressures that occur are important in relation to water trap seal displacement. Pressures below atmospheric tend to draw the water trap seal toward the system side so that water can be lost into the branch; pressures above atmospheric tend to push the water into the appliance and may force potentially contaminated sewer gas into the building, **Figure 2.3**.

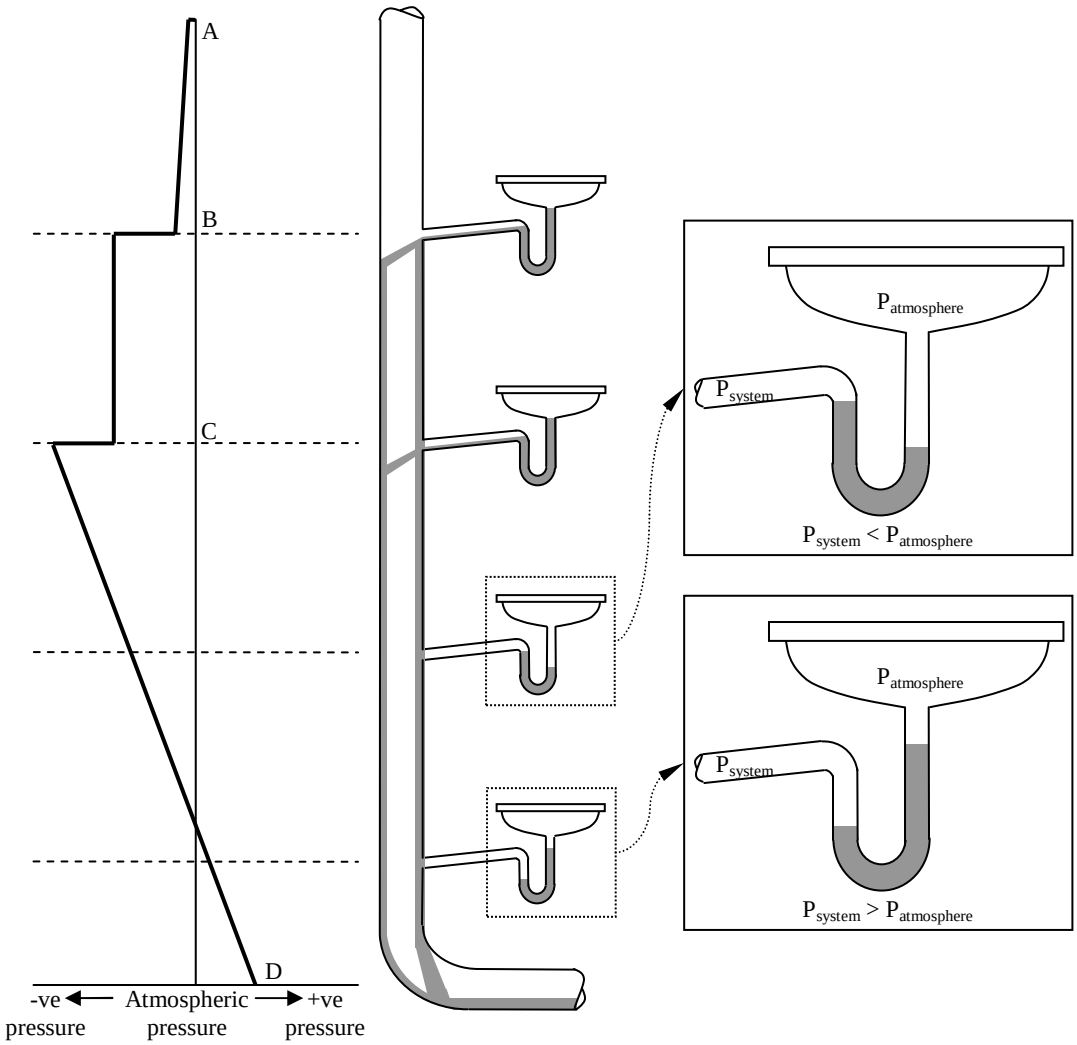

Figure 2.3 Pressure profile for a single stack system with two active branches

2.3.2 Causes of air pressure transients

This steady state description of the expected stack pressure profile was developed through international research undertaken in such centres as the National Bureau of Standards in the USA and the Building Research Establishment in the UK (Wyly and Eaton, 1961; Wise, 1973; Wise, 1979). However, the pressure regime within the building drainage system is, in reality, more accurately defined as unsteady. Appliance discharge to the system is inherently time dependant and random and, therefore, the water downflow and entrained airflows are both temporally and spatially varied, and thus the entrained airflows, and the resultant air pressure variations, are also unsteady.

Changes in annular water downflow, due to the random discharge of system appliances, and the corresponding changes in entrained airflow, are communicated throughout the building drainage system by the propagation of low-amplitude air pressure transients whose magnitude is determined by the Joukowsky expression, Equation (2.1). Increases in annular water flow lead to increased air entrainment which generates the transmission of negative pressure transients whilst local reductions in the entrained airflow generate positive pressure transients (Swaffield and Jack, 1998, 2004). These low-amplitude air pressure transients, which are dependant upon the rate of change of the system conditions, are transmitted and or reflected at all system boundaries including every connected water trap seal.

2.3.3 The effect of air pressure transients propagation

While the pressure transients generated within the building drainage system are of low amplitude, they are, however, capable of destroying the system protection provided by the water trap seal against the ingress of contaminated sewer gas. By the very nature of its simple design, the water column in the trap seal (similar to a U-tube manometer) moves in response to fluctuations in air pressure and is, therefore, vulnerable to any low-amplitude pressure transient that may be propagated throughout the system.

As mentioned in Section 1.5, the maximum allowable pressure excursions within the building drainage system, as stated in the British Standard, is ±38 mm water gauge. An instantaneous change in airflow velocity of only 1 m/s would be sufficient to generate low-amplitude pressure transients with a magnitude greater than this limit, Equation (2.1), thus precipitating a possibly catastrophic system failure due to trap seal depletion. Depletion of the water trap seal can occur in a number of different ways and these will be discussed in the following sections:

2.3.3.1 Induced siphonage

Negative pressure transients are capable of depleting the water trap seal by induced siphonage by creating a suction pressure within the pipe adjacent to the trap, **Figure 2.4**. This suction pressure may be caused either by the branch discharge pipe to which the trap is connected flowing at full bore, or, if the flow conditions in the vertical stack are sufficient to create a negative pressure, by the arrival of a negative transient.

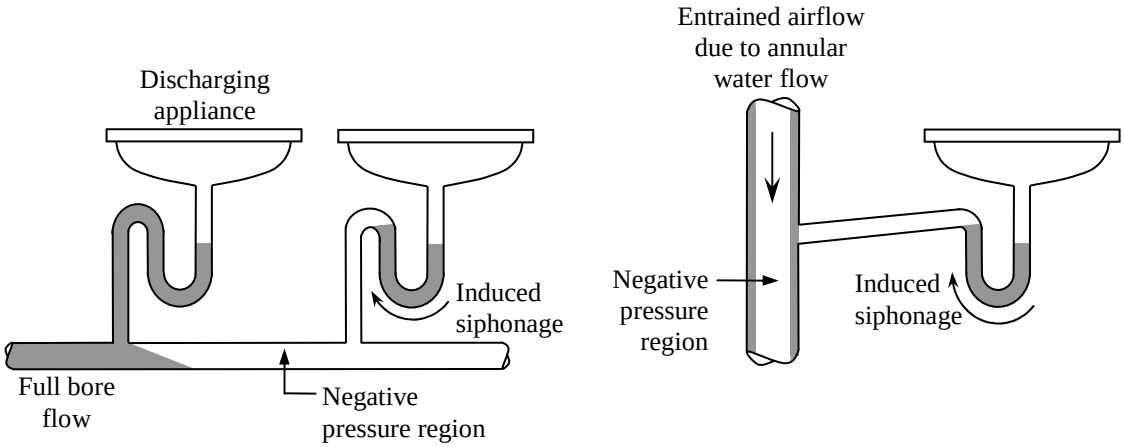

Figure 2.4 Trap depletion due to induced siphonage

2.3.3.2 Self siphonage

Trap seal depletion due to self siphonage may occur if the branch discharge pipe flows at full bore and the water velocity is sufficiently high to cause the water column in the branch to break, **Figure 2.5**. An air pocket forms which expands due to the continuing movement of the front plug of water which causes a drop in pressure and effectively sucks the water seal out of the trap.

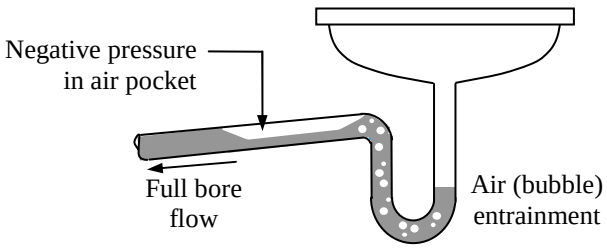

Figure 2.5 Trap depletion due to self siphonage

2.3.3.3 Back pressure

The term "back pressure" is used to describe any positive pressure transients generated within the system. Positive pressure transients are capable of displacing the water trap seal upwards towards the appliance, **Figure 2.6**. When the positive pressure transient is of sufficient magnitude it is possible for the water to be completely displaced into the appliance, leaving the trap either wholly or partially depleted. In some cases, even though the trap is not completely destroyed, air bubbles (containing contaminated sewer gas) can be forced through the water seal and into the appliance. Cessation of the positive pressure transient then causes the trap seal water column to fall back into the trap which may then be lost into the system due to self siphonage. If the trap seal survives this "bubble through" it may be impossible to detect a failure condition.

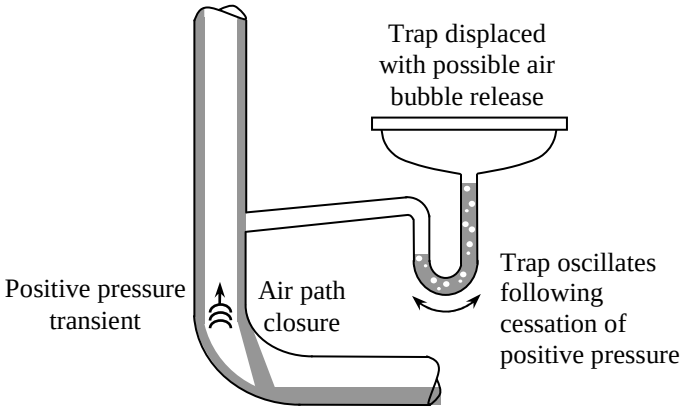

Figure 2.6 Trap depletion due to positive back pressure

2.3.3.4 External air pressures

Pressure fluctuations from external sources can also generate transients that propagate throughout the drainage network. These imposed air pressure fluctuations include wind shear over the stack termination at roof level, **Figure 2.7**, and remote sewer surcharges. These pressure fluctuations are capable of initiating oscillations in the water trap seal that can eventually lead to depletion of the trap.

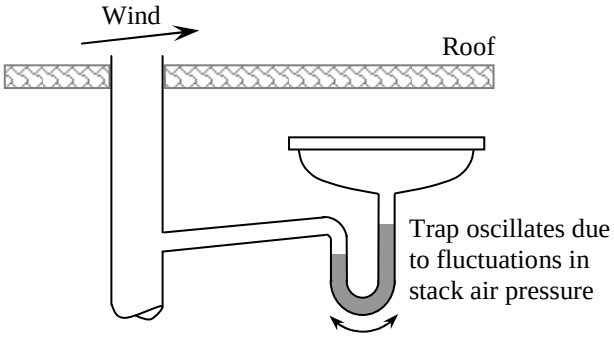

Figure 2.7 Trap depletion due to wind shear

2.3.3.5 Evaporation

If an appliance remains unused for some time or high temperatures exist within the space served, then trap depletion may occur due to evaporation of the water seal. In the UK, the rate of evaporation under normal ambient conditions has been found to be in the region of 3 mm per week (Wise, 1957; Wise and Swaffield, 1995). It follows that under these conditions, trap depletion would occur after 17 weeks of un-use for a 50 mm trap, and 25 weeks for a 75 mm trap. Considerably higher rates of evaporation will exist under higher temperatures. This was experienced during the field investigations described later when a 50 mm floor gulley trap located within a boiler room was found to completely evaporate over a 24 hour period.

2.3.4 Transient control and suppression

In order to avoid the occurrence of water trap seal depletion, research has concentrated on the provision of system venting so that pressure fluctuations at any trap seal are kept within the prescribed limits to ensure water trap seal retention. Traditionally, this protection was provided by the introduction of dedicated passive vent systems such as in the one-pipe, two-pipe and the single stack drainage systems (Wise, 1979), all terminating in open ended external vents.

More recently, active pressure transient suppression and control solutions have been developed to alleviate the effect of transient propagation by providing localised relief to protect trap seals from both positive and negative pressure excursions.

2.3.4.1 Control of negative transients

The air admittance valve (AAV), **Figure 2.8**, provides a localised *inwards* relief airflow that contributes to the control of negative pressure transients. The AAV opens on the arrival of a negative pressure transient allowing relief airflow to enter the system. To avoid the ingress of contaminated sewer gases the AAV is designed to remain closed when not in use or in response to positive pressure transients (Swaffield, Jack, Campbell, 2004). AAVs can be installed locally to the appliance trap seal or at the stack termination to avoid the need for a roof penetration.

2.3.4.2 Control of positive transients

The control and suppression of positive pressure transients cannot, however, be simply achieved by inclusion of an *outward* relief valve as this would allow cross-contamination of sewer gases into the building. Instead, positive pressure transient alleviation is provided by a positive air pressure attenuator (PAPA), **Figure 2.9**, –

consisting of a flexible containment vessel – which diverts and attenuates the propagating positive pressure transient by providing this alternative route and thus reducing the rate of change of the airflow (Swaffield, Campbell and Gormley, 2005a, 2005b).

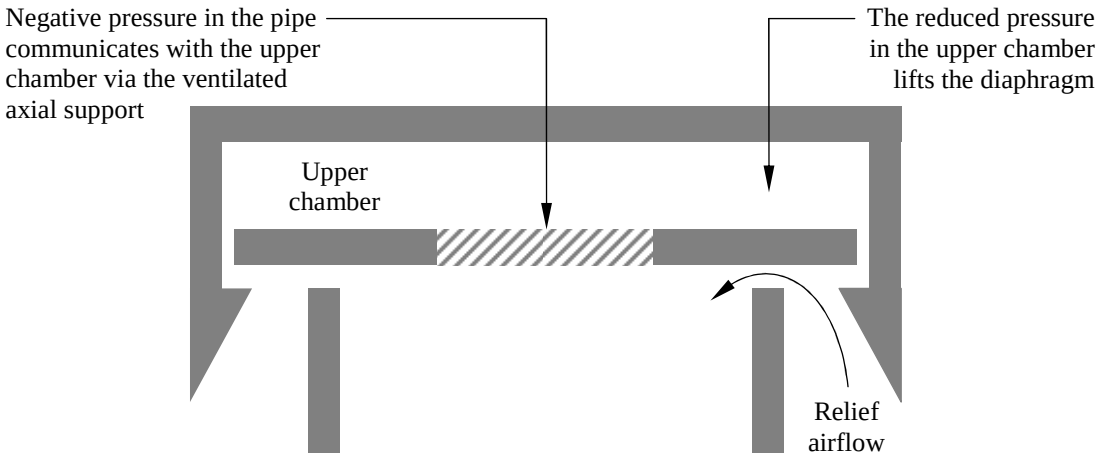

Figure 2.8 Method of operation of a typical air admittance valve

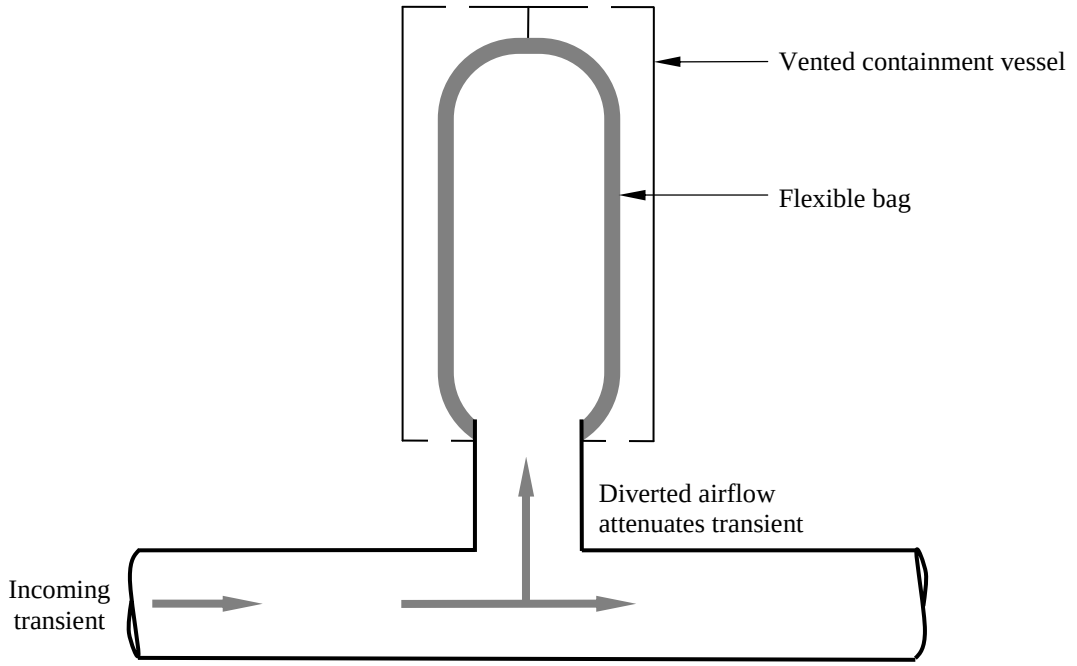

Figure 2.9 Method of operation of a typical positive air pressure attenuator

2.4 Consequences of depleted appliance trap seals

The integrity of the water trap seal is continuously tested due to the arrival of air pressure transients propagated as a result of system operation or external effects from wind shear, sewer surcharge and evaporation (Swaffield, 2005). A depleted trap seal permits airflow both into and out of the drainage system depending upon the local system air pressure. As discussed by Swaffield and Jack (2004), an open trap will not only act as a main vent, contributing to the entrained airflow following appliance discharge, but will also act as an outward relief valve to relieve the pressure by allowing the sewer gases to exit the system and enter the habitable space, see **Figure 2.10**.

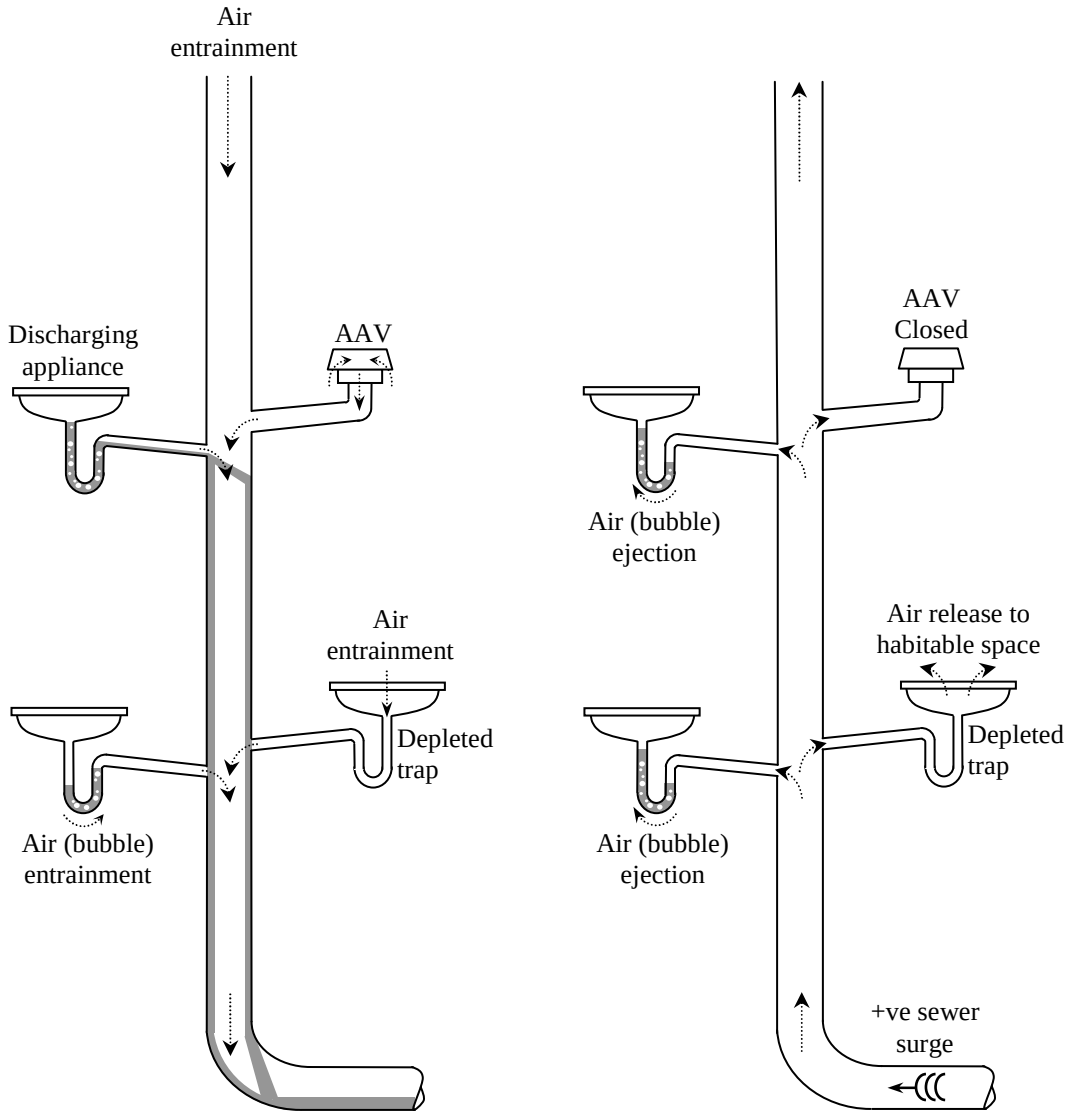

Figure 2.10 Illustration of air entrainment and air release through a depleted trap

Although engineers and researchers have endeavoured to safeguard the integrity of the trap seal through good design practice and by incorporating active pressure control devices to combat the detrimental effects of pressure transients, trap depletion remains a major concern. Although there has been much debate over the health risks from the foul air that is present within the building drainage system (Section 1.3), realisation of its harmful effects were finally confirmed in 2003 when, once again, public attention and anxiety were drawn to the building drainage system following its identification as the transmission route of a novel coronavirus in the Amoy Gardens private residential estate in the densely populated Kwun Tong District in Kowloon Bay, Hong Kong. This coronavirus, the causative agent of severe acute respiratory syndrome (SARS), quickly became the first newly emergent communicable disease epidemic of the 21st century (Leung et al. 2004).

2.4.1 Outbreak of the SARS virus at Amoy Gardens and the role that the building drainage system played in the transmission of the disease

The worldwide SARS epidemic reportedly infected 8098 individuals, 774 of whom died (WHO, 2003b). Hong Kong was the worst hit, with the highest incidence rate (1755 cases in a population of 6.7 million) and a high case fatality rate of 17% (302 deaths) (Leung et al. 2004). Throughout the epidemic, unusual clusters of cases were reported.

2.4.1.1 Amoy Gardens

Home to approximately 20,000 residents and consisting of 19 tower blocks, the outbreak of SARS at Amoy Gardens saw a total of 321 reported cases of infection (almost 20% of all cases in Hong Kong), resulting in 42 deaths (WHO, 2003b). The majority of cases were concentrated in Block E, accounting for 41% of all cases and home to the index patient. Further cases, appearing later, occurred in Block C (15%), Block B (13%) and Block D (13%). The remaining cases (18%) were spread throughout 11 other blocks (Hong Kong Dept. of Health Report, 2003).

Each block was 33 stories high with 8 apartments on each floor. Each neighbouring apartment was separated by a common utility channel 7 m in depth which served as a lightwell, a fresh air supply plenum for bathroom and master bedroom windows, an exhaust plenum for window mounted bathroom and kitchen extract fans, and a services riser housing the building drainage stacks, see **Figure 2.11**.

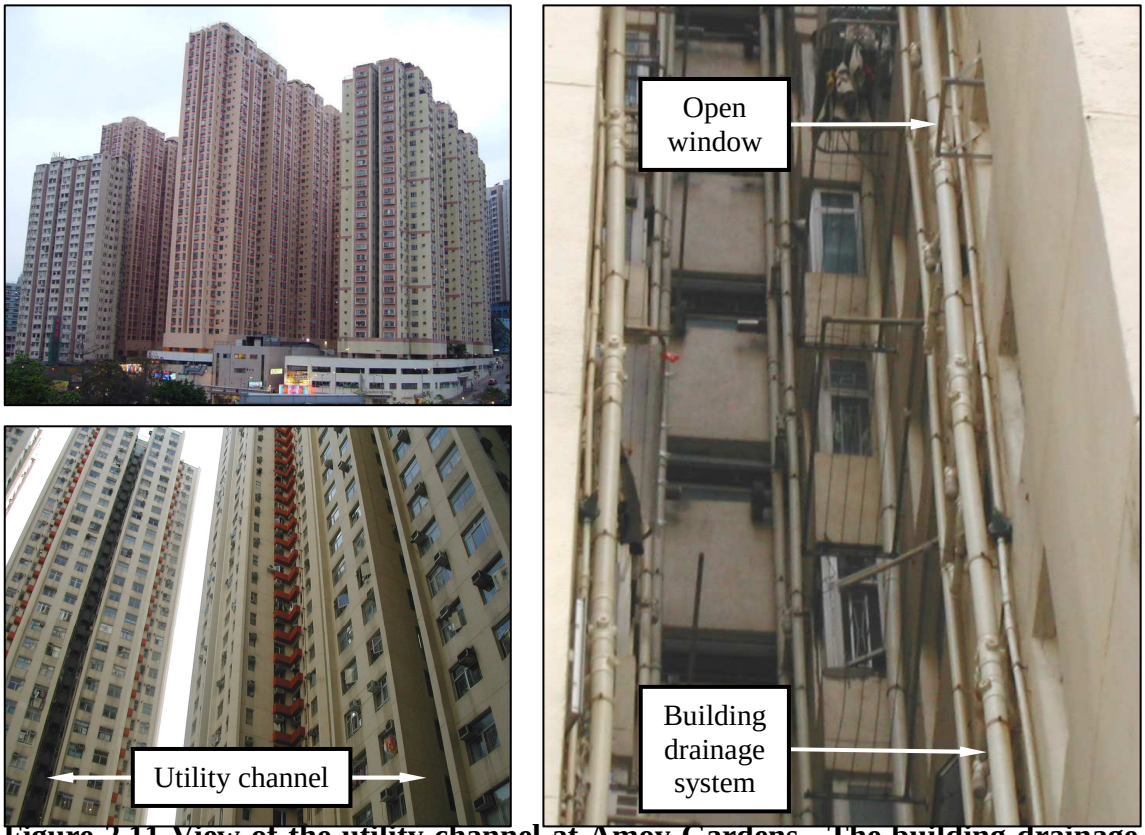

Figure 2.11 View of the utility channel at Amoy Gardens. The building drainage system is clearly visible as are the windows opening onto the channel. (image provided courtesy of Henry Hung, WPC Vice-Chairman)

2.4.1.2 Determining the cause of the outbreak

In response to the Amoy Gardens outbreak both the Hong Kong Government and an expert environmental team from the World Health Organisation (WHO) undertook independent investigations to determine the cause of this large cluster of SARS cases (Hong Kong Dept. of Health Report, 2003; WHO 2003a). Identification of a prominent vertical pattern of distribution in Block E and the lack of contact between affected apartments led the investigators away from their initial postulation that transmission was facilitated by direct contact with contaminated body secretions, and instead suggested the possibility of airborne aerosol transmission. To isolate the mode of transmission, investigators examined the range of environmental services provision to the building - including the mechanical, electrical and public health systems - and following further investigation identified the building drainage system, facilitated by the presence of depleted trap seals, as the conveyor of the virus. Both investigations identified a number of individual contributory factors, summarised in **Figure 2.12**, which culminated in the rapid spread of the virus:

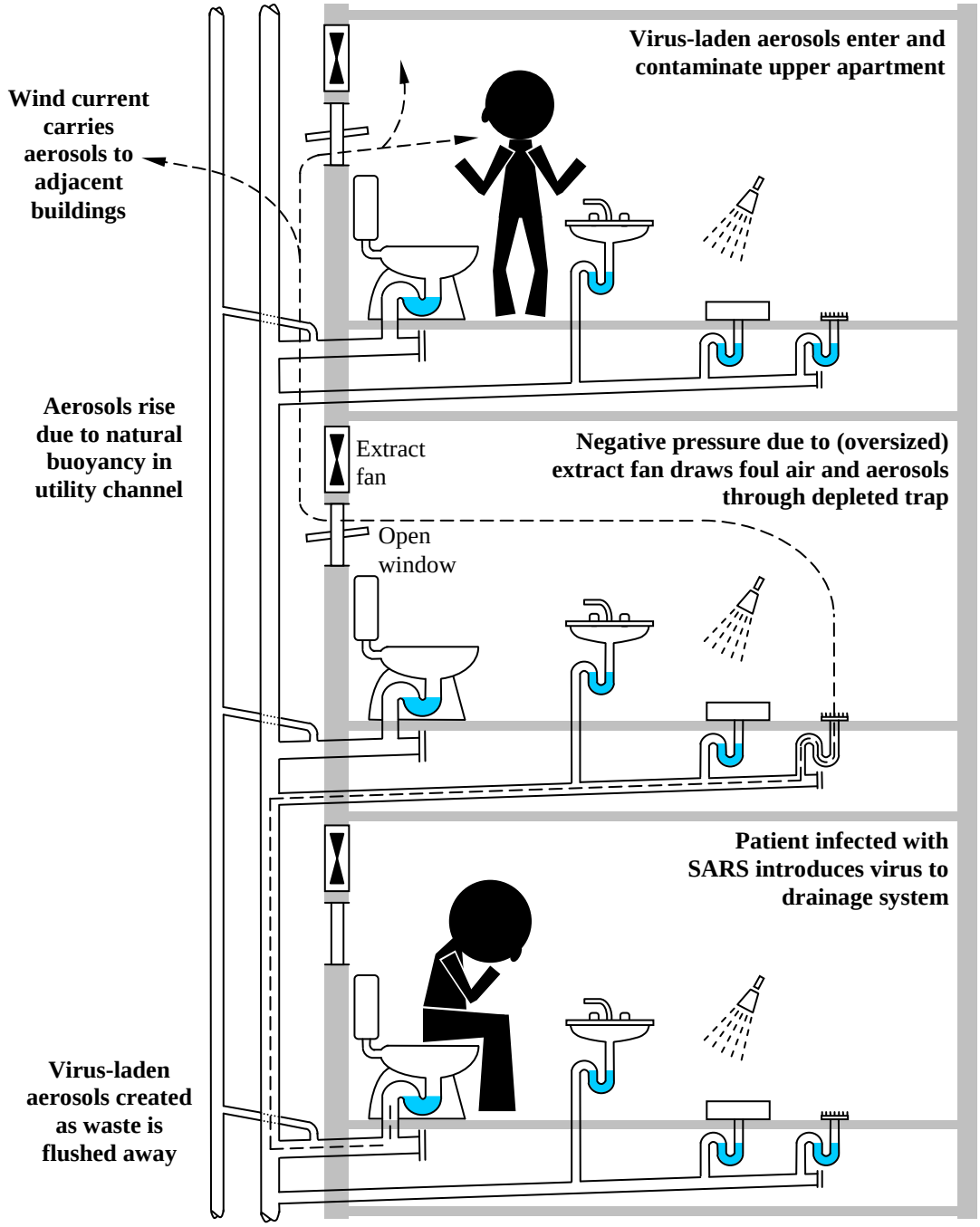

Figure 2.12 Route of transmission of the SARS virus at Amoy Gardens

i. *Vertical connection between apartments by a common building drainage system*: the normal approach to the provision of building drainage, with its "network-like" arrangement, provides a physical interconnection between adjacent apartments connected to the same system.

ii. *The presence of virus-laden aerosols*: patients infected with SARS were found to suffer severe and frequent diarrhoea which clinical studies found contained a high viral load (Cheng et al, 2004). It is likely that large quantities of the virus would have been discharged into the drainage system by infected patients. The

drainage system would have accumulated large volumes of contaminated faecal waste which would have been broken up into virus-laden aerosols as it passed through the drainage system.

iii. *Trap seal depletion*: The prevention against the free flow of contaminated air from the building drainage system into the occupied space had, in some instances, been compromised. The floor drain traps were found, in many of the apartments, not to have been regularly primed and had, therefore, become depleted through evaporation of the water seal, **Figure 2.13**; traps were found to have been removed completely from some appliances, **Figure 2.14**; and the build-up of foam in some vent pipes from discharging washing machines caused the unexpected depletion of the trap seal in even frequently used appliances such as showers. The loss of the water trap seal established a pathway through which virus-laden aerosols could enter and contaminate the indoor environment.

iv. *Generation of a prevailing negative pressure within the apartment*: the operation of an oversized bathroom extract fan, found to have a capacity 6 to 10 times higher than required, created a sub-atmospheric pressure within the bathroom which enhanced the transfer of contaminated air and virus-laden aerosols from the drainage system into the bathroom. This condition worsened when both the bathroom door and window were closed as the extract fan, deprived of make-up air from any other source, drew large quantities of contaminated air through the depleted trap seal. This transfer mechanism has been verified by post-event forensic analysis (WHO, 2003a) and by numerical simulation of the system operation (Jack, 2006). The ingress of contaminated air has also been shown to occur following positive pressure fluctuations generated within the system as a natural consequence of appliance discharge (Hung et al, 2006).

v. *Discharge of the contaminated air to atmosphere*: the extracted bathroom air, containing virus-laden aerosols, was subsequently exhausted to the external utility channels. The virus-laden aerosols were then carried upward by the natural buoyancy within the utility channel allowing potential contamination of other apartments several floors away by entering through an open window.

vi. *Dispersal to adjacent blocks by wind current effect*: the prevailing wind currents facilitated further contamination by exposing the virus-laden aerosols to neighboring apartment blocks (Yu et al., 2004).

Figure 2.13 Evaporation of the bathroom floor drain water seal provided an open path for cross-contamination (image supplied courtesy of M. Y. Chan, Hong Kong Polytechnic University)

Figure 2.14 Unapproved system adaptation including completely removing the water trap seal provided an open path for cross-contamination (image supplied courtesy of M. Y. Chan, Hong Kong Polytechnic University)

2.4.1.3 Maintenance of the building drainage system at Amoy Gardens

What is clear from these post-event investigations is that if a proper maintenance regime had been in place and the water trap seals were functioning normally and had not become depleted or, as in some cases, had not been completely removed and the virus-laden aerosols, as a result, had been contained within the drainage system, then the community outbreak of SARS at Amoy Gardens would not have occurred, or at least would have been considerably reduced.

The series of unfortunate events that lead to the outbreak of SARS at Amoy Gardens, and the regrettable morbidity and mortality rates that occurred as a result, provide a clear lesson: if the potential transmission of infection by the spread of aerosols through depleted trap seals is to be reduced, then an improved method of monitoring and maintaining the drainage system and, in particular, the water trap seal is urgently required to ensure that the unintentional transfer of infectious aerosols is minimized.

2.5 Chapter summary

This chapter has introduced some of the theory associated with pressure transients within fluid carrying systems to which the low amplitude air pressure transients experienced within the building drainage system belong. The mechanisms involved in the generation and propagation of transients in the building drainage system have been described and particular attention has been given to their effect at system boundaries, and in particularly at the trap seal where they have been shown to compromise seal retention.

Finally, the consequences of trap seal depletion and the harmful effects of the cross-contamination have been discussed by reviewing their role in the spread of the SARS virus at Amoy Gardens. These fatal consequences of trap depletion have provided further impetus for the development of an effective monitoring and maintenance system for the building drainage system.

Chapter 3

Air pressure transient modelling using the method of characteristics

3.1 Introduction

It is essential, for the successful application of the transient-based reflected wave technique, that the complex interaction between the system and fluid properties, effectively responsible for the generation and alleviation of pressure transients, be understood. This chapter details the theoretical background to the existing numerical model, AIRNET, which is capable of accurately simulating transient generation and propagation within general building drainage systems.

The AIRNET model, through the application of the method of characteristics solution to the St Venant equations of continuity and momentum, provides an understanding of the mechanisms by which transients propagate within any network and a means to "decipher" the sometimes complex system pressure response that follow the sequence of events at any location within the network. This ensures that the method developed for the reflected wave technique is non-destructive (i.e. it does not itself threaten the integrity of the water trap seals of which it was designed to protect) and also identifies the most efficient system monitoring point.

The general equations of continuity and momentum for unsteady flow in conduits will be developed, before they are applied to the case of low amplitude air pressure transient propagation in building drainage systems. The numerical methods available to solve the continuity and momentum equations will then be provided. The reasons for choosing the method of characteristics based numerical method will be discussed before detailing the main elements of the method of characteristics based AIRNET model.

3.2 Derivation of the St Venant equations

The St Venant equations of continuity and momentum form the basis of all methods of analysing unsteady flows in conduits. This section will show the development of the general St Venant equations applicable to the flow of any fluid in any type of conduit.

3.2.1 Continuity equation

The continuity equation is derived from the law of conservation of mass for an element of fluid flowing in a conduit, **Figure 3.1**, and can be expressed as:

Fluid inflow – Fluid outflow = Rate of change of mass in the control volume

$$\rho Au - (u + \delta u)(\rho + \delta\rho)A = \frac{\partial}{\partial t}(\rho A \delta x)$$

where A is the elemental cross-sectional area which can be assumed to be constant, since the transient events are insufficient to distort the pipe wall.

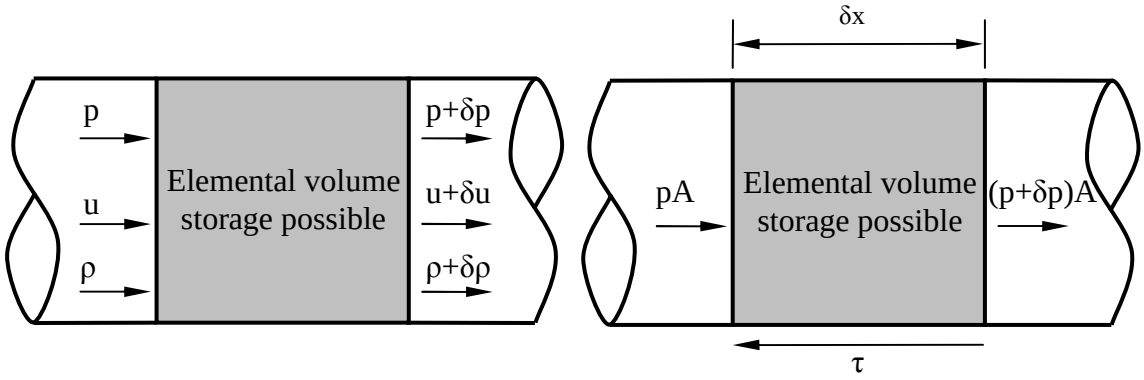

Figure 3.1 Development of the continuity and momentum equations demonstrated by elemental volume of flow (Swaffield and Galowin, 1992).

Neglecting second order terms gives:

$$\rho\delta u + u\delta\rho + \frac{\partial}{\partial t}\rho\delta x = 0$$

Rearranging, the final form of the continuity equation becomes:

$$\rho\frac{\partial u}{\partial x} + u\frac{\partial \rho}{\partial x} + \frac{\partial \rho}{\partial t} = 0 \qquad (3.1)$$

3.2.2 Momentum equation

The momentum equation is derived by considering the forces acting on a small element of fluid within the conduit, see **Figure 3.1**, and can be expressed as:

Force = mass x acceleration

$$pA-(p+\delta p)A-\tau P\delta x=\frac{d}{dt}(\rho A\cdot\delta x\cdot u)$$

where A is again the elemental cross sectional area and P the wetted perimeter and since:

$$\frac{d}{dt}(\rho A\cdot\delta x\cdot u)=\frac{\partial}{\partial t}(\rho A\cdot\delta x\cdot u)+\frac{\partial}{\partial x}(\rho A\cdot\delta x\cdot u^2)$$

becomes:

$$-\delta pA-\tau P\delta x=\frac{\partial}{\partial t}(\rho A\cdot\delta x\cdot u)+\frac{\partial}{\partial x}(\rho A\cdot\delta x\cdot u^2)$$

Dividing by $A\ \delta x$ gives:

$$-\frac{\partial p}{\partial x}-\tau\frac{P}{A}-\frac{\partial}{\partial t}(\rho u)-\frac{\partial}{\partial x}(\rho u^2)=0$$

which by expansion gives:

$$-\frac{\partial p}{\partial x}-\tau\frac{P}{A}-u\left[\frac{\partial\rho}{\partial t}+u\frac{\partial\rho}{\partial x}+\rho\frac{\partial u}{\partial x}\right]-\rho\frac{\partial u}{\partial t}-\rho u\frac{\partial u}{\partial x}=0$$

Incorporating Equation (3.1), it follows that:

$$-\frac{\partial p}{\partial x}-\tau\frac{P}{A}-\rho\frac{\partial u}{\partial t}-\rho u\frac{\partial u}{\partial x}=0$$

Substituting for the shear stress, τ, at the conduit wall and the wetted perimeter, P, where:

$$\tau=\frac{1}{2}f\rho u^2$$

and where (for full bore air flow or for a central air core induced by annular water flow):

$$\frac{A}{P} = \frac{D}{4}$$

which gives the final form of the momentum equation:

$$\frac{\partial p}{\partial x} + \rho u \frac{\partial u}{\partial x} + \rho \frac{\partial u}{\partial t} + \frac{4\rho f u|u|}{2D} = 0 \qquad (3.2)$$

where f is the appropriate friction factor. Note that $u|u|$ has been substituted for u^2 to ensure that the frictional forces always oppose the direction of fluid flow.

Equations (3.1) and (3.2) respectively form the general St Venant equations of continuity and momentum and provide the mathematical basis for the study of unsteady flow in conduits. This pair of quasi-linear hyperbolic partial differential equations can be solved by the finite difference solution once transformed via the method of characteristics into total differential equations.

3.3 Application of the general St Venant equations to the propagation of low amplitude air pressure transients in the building drainage system

The air within the building drainage system is considered to behave as a perfect gas, conforming to Boyle's Law whereby its internal energy is dependant upon temperature. Furthermore, any change in condition is assumed to be rapid and reversible with no heat transfer so that transient propagation may be reasonably assumed to be consistent with isentropic flow conditions. Therefore, air pressure and density are related by:

$$\frac{p}{\rho^{\gamma}} = K \qquad (3.3)$$

where K is a constant and γ is the ratio of specific heat of the fluid at constant pressure to that at constant volume.

The wave propagation speed, c, of a low-amplitude pressure transient can be determined by applying the continuity and momentum equations across the transient wave front shown in **Figure 3.2**.

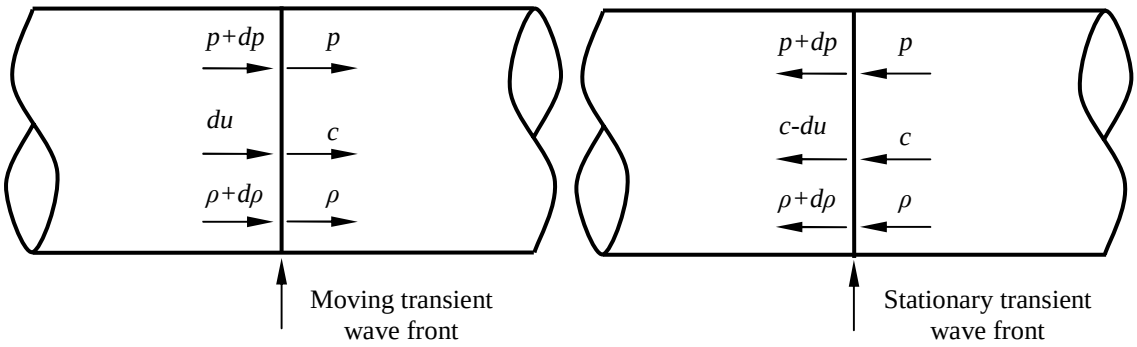

Figure 3.2 Representation of an air pressure transient wave brought to rest by superposition of an equal but opposite wave (Swaffield and Galowin, 1992).

From the momentum equation, when a transient wave front has been brought to rest by a wave front with an equal but opposite wave propagation speed, the following relationship can be derived:

$$(p+dp)A - pA = cA\rho(-(c-du)-(-c))$$

which, by rearranging and dividing by *A*, reduces to:

$$dp = \rho c du \tag{3.4}$$

Applying the continuity equation to the same, now stationary, transient wave front yields:

$$cA\rho = (c-du)A(\rho+d\rho)$$

which, when second order terms are neglected and *du* is substituted from equation (3.4), gives:

$$c^2 = \frac{dp}{d\rho} \tag{3.5}$$

Rearranging Equation (3.3) and differentiating the pressure term with respect to ρ gives:

$$\frac{dp}{d\rho} = \gamma\rho^{\gamma-1}K \tag{3.6}$$

Combining Equations (3.5) and (3.6) and substituting *K* from Equation (3.3) gives:

$$c = \sqrt{\frac{\gamma p}{\rho}} \tag{3.7}$$

This derivation of wave propagation speed is only applicable to inviscid flow. However, previous experimental investigations by Henson and Fox (1972) and Woodhead, Fox and Vardy (1976) have reported close agreement between measured values of pressure and wave propagation speed with those predicted using Equation (3.7). This approach is particularly applicable to conditions within the building drainage system as the ambient pressure is low (close to atmospheric) and transient pressure excursions are small (measured in mm water gauge). This simplification allows the characteristic equations, derived from the equations of continuity and momentum, to be solved directly by the following method.

The two equations of momentum and continuity are usually solved for velocity and pressure as density is taken as a constant. However, in dealing with air applications, density and pressure are linked through the wave propagation speed, Equation (3.7), so that the St Venant equations must be recast in terms of the two dependant variables, *c* and *u*, and the two independent variables, *x* and *t*. This requires a modification to Equations (3.1) and (3.2) and the introduction of a post solution equation to allow the calculation of pressure.

Rearranging Equation (3.7) and substituting into Equation (3.3) and differentiating *c* with respect to ρ gives:

$$2c\partial c = \gamma K(\gamma - 1)\rho^{\gamma-2}\partial\rho$$

Substituting for *K* gives:

$$\partial\rho = \left(\frac{2}{\gamma - 1}\right)\frac{\rho}{c}\partial c \tag{3.8}$$

By differentiating *p* with respect to ρ in Equation (3.3), it may be shown that:

$$\partial p = \gamma K\rho^{\gamma-1}\partial\rho$$

which, when $\partial\rho$ and *K* are substituted, gives:

$$\partial p = \left(\frac{2}{\gamma - 1} \right) \rho c \partial c \tag{3.9}$$

Substituting Equation (3.8) into Equation (3.1) allows the continuity equation to be expressed as:

$$\rho \frac{\partial u}{\partial x} + \left(\frac{2}{\gamma - 1} \right) \frac{\rho}{c} \left[u \frac{\partial c}{\partial x} + \frac{\partial c}{\partial t} \right] = 0 \tag{3.10}$$

While substituting Equation (3.9) into Equation (3.2) allows the momentum equation to be expressed as:

$$\left(\frac{2}{\gamma - 1} \right) \rho c \frac{\partial c}{\partial x} + \rho u \frac{\partial u}{\partial x} + \rho \frac{\partial u}{\partial t} + \frac{4 \rho f u |u|}{2D} = 0 \tag{3.11}$$

These equations are generally derived in terms of the flow velocity, *u*, at any point and the wave propagation speed, *c*, at that location. The choice of *u* and *c* results from the interdependence of air pressure and density. As a result, it is necessary to determine pressure by combining Equations (3.3) and (3.7) such that:

$$p = \left[\left(\frac{p_o}{\rho_o{}^{\gamma}} \right) \left(\frac{\gamma}{c^2} \right)^{\gamma} \right]^{\frac{1}{(1-\gamma)}} \tag{3.12}$$

where atmospheric pressure and density are expressed as p_o and ρ_o respectively. Equation (3.12) demonstrates the dependency of wave propagation speed on air pressure and density. However, Appendix A shows that, in the context of the low amplitude air pressure transient excursions experienced within the building drainage system, the variations of wave propagation speed are small. Pressure fluctuations of between -212.17 and +252.07 mm water gauge (which would be considered as extreme pressure events) would generate variations in *c* of less than 0.65%. Such insignificant variations permit the wave propagation speed to be empirically regarded as sensibly constant and allow pipe periods to be adequately represented by a constant atmospheric pressure wave propagation speed defined by the user.

3.4 Applicable numerical methods

As stated previously, all methods of analysing unsteady flow in conduits are based on the St Venant equations of continuity and momentum. Having no general mathematical solution, this pair of quasi-liner hyperbolic partial differential equations requires simplification and/or modification to allow solutions to be obtained. Wylie and Streeter (1978) provide a good summary of the applicable methods within the context of pressure surge which include the arithmetic method, graphical techniques, and the method of characteristics.

The arithmetic method (Allievi, 1903; Joukowsky, 1904) is based on simplified versions of the St Venant equations which neglect frictional resistance and is based on the principle of superposition of travelling pressure waves. However, even after simplification of the governing equations, this method is time consuming and only practical for the simplest systems.

Progress in the field during the first half of the twentieth century, most notably the development of the graphical techniques (Schnyder, 1929; Bergeron, 1935), led to vast improvements in analysis techniques. The graphical method continued to employ simplifying assumptions by neglecting frictional resistance in its theoretical development, but utilized means to take it into account by a correction. Although particularly suited to free surface flows and open channel fluid flow, this approach was laborious and suffered from cumulative graphical errors (Campbell, 1992). However, this method was the principle way of solving transient problems from the early 1930s to the early 1960s before the advent of digital computers. Again system complexity limited the application of the graphical method.

Since the 1960s a large number of methods of solving the St Venant equations have been developed (Wylie and Streeter, 1978). The most powerful of these, both in terms of accuracy and general applicability, are based on the computer supported numerical solution of the full St Venant equations using one of a variety of finite difference methods, such as the Lax-Wendroff explicit method, the leap frog method, Amein's four point implicit method, the Ligget and Woolhiser six point implicit method, and the method of characteristics. Fox (1977) provides an assessment of these methods and concludes that although some of these methods permit increases in Δt without significant increases in error or stability, the fixed mesh approach of the method of characteristics is preferred to all others for the waterhammer problem. Although some

of the other methods have been found to be equally reliable and convenient as the method of characteristics, they sometimes rely on the method of characteristics to deal with boundary conditions.

The method of characteristics is currently the most popular and extensively used technique for solving the St Venant equations using the finite difference approach. The method of characteristics can actually be traced as far back to 1900 when Massau utilised the technique in the study of open channel flow, while Lamoen (1947) followed by Gray (1953) were the first to apply the method to fluid transient problems.

The method of characteristics has numerous advantages: the simplicity of programming and efficiency of computations, even for complex systems with numerous boundary conditions; and its particular suitability to applications where the event to be simulated is of relatively short duration. Additionally, the method deals with networks in terms of internal nodes and boundaries which, when linked to a first order finite difference scheme, only involves the simultaneous solution of two equations at each internal pipe node and, at boundaries, the solution of one characteristic per pipe and an equation defining the boundary condition. This is a particular strength of the method as it allows the development and solution of complex boundary conditions in isolation form the calculation of all other boundaries and internal nodes. This is a major advantage over other numerical techniques based on, for example, the finite difference method where all conditions within the network are required to be known in order to proceed.

The method of characteristics transforms the St Venant equations (themselves a pair of quasi-linear hyperbolic partial differential equations) into a pair of total differential equations, termed the characteristic equations, which are then expressed in finite difference form and solved, i.e. the finite difference representations are based on the characteristic forms of the St Venant equations (Swaffield and Boldy, 1993).

A considerable number of authors, most notably in the USA, began to employ the method of characteristics, coupled with finite difference techniques, for the numerical modelling of unsteady fluid flows, in the majority of cases basing their approach on the significant work of Lister (1960) who detailed the finite difference schemes which were then utilised by Streeter and Lai (1962), Streeter and Wylie (1967) and Streeter (1969). In the UK and Europe interest in the use of the method of characteristics developed rapidly with papers from Fox (1968), Evangelisti (1969), Swaffield (1970) and Boldy (1976). By the 1970s this technique was established as the standard method for

transient analysis and the development of computing technology in the 1970s and 1980s improved the use and applicability of this technique and facilitated the development of large and complex network models.

Subsequently, the method of characteristics has become the standard technique for the analysis of pressure transient phenomena with many authors applying and modifying the basic method to allow previously difficult transient conditions to be treated and system designs to be modified to prevent potentially damaging transient propagation, including gas release (Kranenberg, 1974), column separation and vapour generation (Doyle and Swaffield, 1972; Swaffield, 1972), machine interface boundary problems (Boldy, 1976), and the application of the method to investigate related areas such as air pressure transients in high speed train tunnels (Henson and Fox, 1972; Vardy, 1976) and open channel and partially filled pipe flow transients (Price, 1974; Song, 1976; Galowin and Swaffield, 1989).

Since the method of characteristics approach is based around the equations of continuity and momentum, which are generally applicable, it can be used not only to examine waterhammer and partially filled unsteady liquid pipe flows but also the propagation of full bore low amplitude air pressure transients, such as those present in the building drainage system under consideration in this thesis.

3.5 Method of Characteristics

3.5.1 Conversion of partial to total derivative equations

The quasi-liner hyperbolic partial differential equations of continuity and momentum, shown in Equations (3.10) and (3.11) respectively, must first be transformed to total derivatives prior to solution by finite difference techniques by introducing limitations in terms of the rate of change of distance with time, *dx/dt*. If Equations (3.11) and (3.10) are equated to the terms L_1 and L_2 respectively, they may be linearly combined where:

$$L_1 = \left(\frac{2}{\gamma - 1}\right)\rho c\frac{\partial c}{\partial x} + \rho u\frac{\partial u}{\partial x} + \rho\frac{\partial u}{\partial t} + \frac{4\rho f u|u|}{2D} = 0 \qquad (3.13)$$

and

$$L_2 = \rho \frac{\partial u}{\partial x} + \left(\frac{2}{\gamma - 1} \right) \frac{\rho}{c} \left[u \frac{\partial c}{\partial x} + \frac{\partial c}{\partial t} \right] = 0 \tag{3.14}$$

then if:

$$L = L_1 + \lambda L_2 = 0$$

(where λ is a linear multiplying factor) gives:

$$L = \frac{\partial u}{\partial x}(\lambda + u) + \frac{\partial u}{\partial t} + \left(\frac{2}{\gamma - 1} \right) \left[\frac{\partial c}{\partial x} \left(\lambda \frac{u}{c} + c \right) + \frac{\lambda}{c} \frac{\partial c}{\partial t} \right] + \frac{4 f u |u|}{2D} = 0 \tag{3.15}$$

The partial derivatives in Equation (3.15) may be replaced by total derivatives using the following two equations:

$$\frac{dc}{dt} = \frac{\partial c}{\partial x} \frac{dx}{dt} + \frac{\partial c}{\partial t}$$

and

$$\frac{du}{dt} = \frac{\partial u}{\partial x} \frac{dx}{dt} + \frac{\partial u}{\partial t}$$

which limit the rates of change *x* with *t* to give:

$$\frac{du}{dt} \pm \frac{2}{\gamma - 1} \frac{dc}{dt} + \left(\frac{4 f u |u|}{2D} \right) = 0 \tag{3.16}$$

provided that:

$$\frac{dx}{dt} = u \pm c \tag{3.17}$$

In this total derivative form the combined equations of continuity and momentum describing the air pressure transients generated in the building drainage system may be solved by finite difference techniques.

3.5.2 Finite difference solution of fluid transient equations

Figure 3.3 shows the rectangular grid upon which the solution of the air pressure transient analysis by finite difference techniques is based. The grid is formed in two dimensions representing *t* and *x*. The conditions at any node one time step in the future

can be determined from the current conditions at adjacent upstream and downstream nodes and require definition of the conditional equations defining the "characteristic" slope, *dx/dt*. The time step depends on both the wave speed appropriate to the fluid-pipe combination and the length of the pipe section chosen as the internode distance.

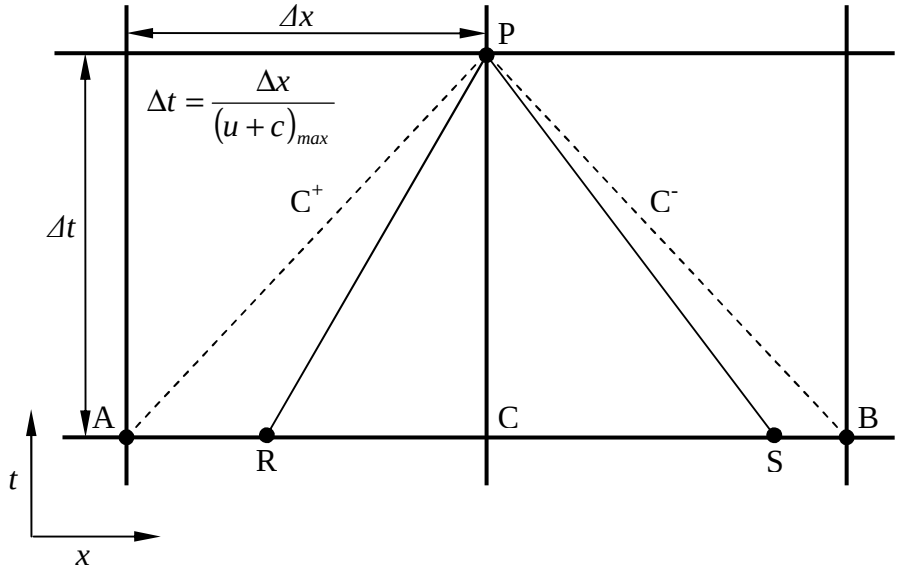

Note: If $c >> u$, then points R and S tend to A and B

.

Figure 3.3 Grid showing characteristic lines as utilised in the Method of Characteristics approach to air pressure transient modelling, (Swaffield and Galowin, 1992).

The choice of the internode distance depends on the number of locations at which a knowledge of the transient pressure would be useful, however, it cannot be greater than the actual length of the pipe being considered, setting an upper limit on time step equal to half the pipe period. As the characteristic slopes of these lines are dependant upon the flow conditions, which change with both *t* and *x*, they are not straight lines but are instead curved, however, the small time step utilised permits the straight line assumption to be made.

The solution of the St Venant equations is restricted as they must fall upon these lines. The line of communication formed by the "characteristic" slopes allows information regarding air velocity and wave speed (and therefore pressure) to be transmitted throughout the network and as demonstrated by Equation (3.17), the slope of these lines is directly related to the speed of propagation of the pressure wave. Thus the solution is therefore capable of communicating changes in conditions throughout the network. Using the notation shown in **Figure 3.3**, *R* and *S* represent points where the current

conditions are known by interpolation from known or previously calculated values at *A*, *B*, and *C*; and *P* represents the point one time step in the future at which conditions are unknown, but which may be determined utilising the characteristic equations.

It can be seen that the C^+ characteristic may be expressed as:

$$C^+ \begin{cases} u_P - u_R + \dfrac{2}{\gamma - 1}\left(c_P - c_R\right) + 4 f_R u_R \left|u_R\right| \dfrac{\Delta t}{2D} = 0 & (3.18) \\ \text{when} & \\ \dfrac{dx}{dt} = u_R + c_R & (3.19) \end{cases}$$

and the corresponding C^- characteristic may be expressed as:

$$C^- \begin{cases} u_P - u_S + \dfrac{2}{\gamma - 1}\left(c_P - c_S\right) + 4 f_S u_S \left|u_S\right| \dfrac{\Delta t}{2D} = 0 & (3.20) \\ \text{when} & \\ \dfrac{dx}{dt} = u_S - c_S & (3.21) \end{cases}$$

The sign convention of the characteristic lines, i.e. C^+ and C^-, serve merely to differentiate between the differences in sign of the gradient of the slopes. The definition of the C^+ and C^- characteristic equations may be respectively reduced to a pair of first order equations, linking flow velocity and wave propagation speed, to be solved simultaneously:

$$u_P = K1 - K2 \cdot c_P \tag{3.22}$$

and

$$u_P = K3 + K4 \cdot c_P \tag{3.23}$$

where:

$$K1 = u_R + \frac{2}{\gamma - 1} c_R - 4 f_R u_R \left|u_R\right| \frac{\Delta t}{2D} \tag{3.24}$$

$$K2 = K4 = \frac{2}{\gamma - 1} \tag{3.25}$$

and

$$K3 = u_S - \frac{2}{\gamma - 1} c_S - 4 f_S u_S |u_S| \frac{\Delta t}{2D} \tag{3.26}$$

As mentioned previously, the slope of the characteristic lines is directly related to both the wave propagation speed, *c*, and the fluid velocity, *u*, so that *R* and *S* may lie anywhere within one Δx either side of *P*. In such cases, linear interpolation (Lister, 1960) is necessary to evaluate the values of *R* and *S* at each time step. However, in the case of building drainage systems, where the typical local air velocity is only a fraction of the local wave propagation speed, such that $c >> u$, changes in the slope of the characteristics may be assumed as negligible such that the points *R* and *S* tend to the adjacent grid nodes *A* and *B*, **Figure 3.3**, and there appears no need for interpolation. However, as mentioned in Section 3.4, the value of the wave propagation speed is dependant upon air pressure and density and, hence, the value of $(u + c)$ and consequently, from Equation (3.27), the size of the time step will change during the passage of a transient.

For a rectangular grid, the length Δx may be fixed, however, as both *R* and *S* must lie within adjacent grid sections for a stable solution, the size of the time step Δt must not exceed that given by the Courant stability criterion (Courant and Fredrichs, 1948) which may be expressed as:

$$\Delta t = \frac{\Delta x}{(u + c)_{max}} \tag{3.27}$$

where the maximum values of *u* and *c* present in the whole network at time *t* are used to calculate the size of the time step at each successive time step. The smallest time step present in the whole network must therefore be used, resulting in the need for only minimum interpolation at certain nodes.

3.6 Boundary conditions for the method of characteristics

3.6.1 Requirement for boundary conditions

As shown previously in **Figure 3.3** the solution across each time step may be calculated by simultaneously solving the C^+ and C^- characteristics that intersect at that node. However, as illustrated in **Figure 3.4**, which shows a simple single pipe divided into *N* sections with *N+1* nodes, this technique cannot be applied to nodes located at element boundaries as only one characteristic can exist at entry and similarly only one at exit.

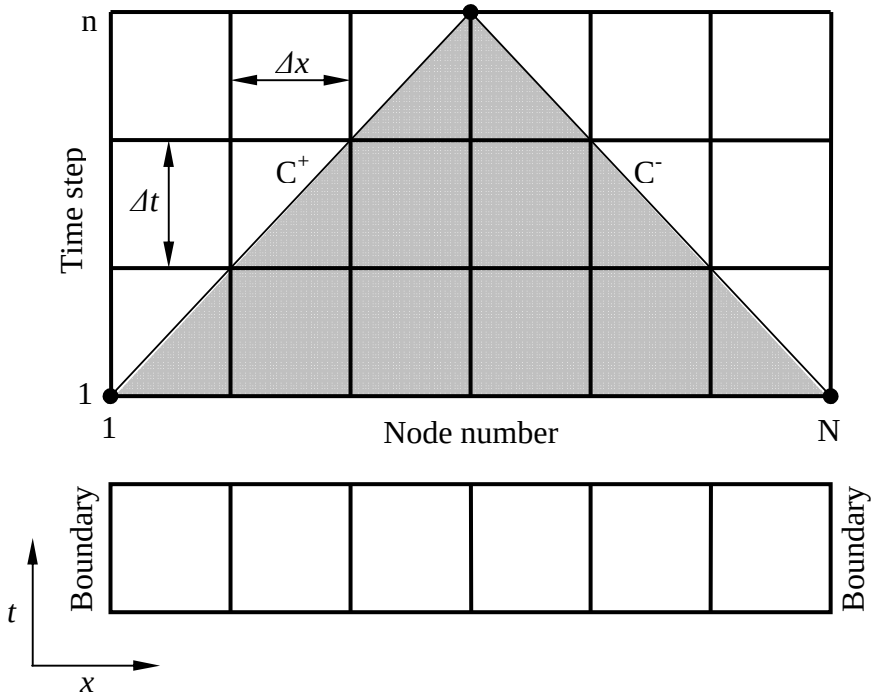

Figure 3.4 Shaded zone demonstrating area of calculation without definition of boundary conditions (Swaffield and Boldy, 1993).

The limit to the solution in this case is thus triangular in shape over *n* time steps, where $n = N/2$, after which the solution stalls. In order for the analysis to progress further, it is necessary to provide a second defining equation at each boundary location, to be solved simultaneously with the appropriate existing single C^+ or C^- characteristic. This is achieved by using theoretical or empirical relationships to describe the physical conditions at these terminations. Use of such equations, commonly referred to as boundary conditions, allows the continuation of the model into subsequent time steps. It should be noted that, in addition to network entries and exits, boundary conditions are also required for all internal boundaries whether stationary, e.g. pipe junctions; or capable of interface movement, e.g. displaced trap water columns or a piston interface.

In order for the analysis to begin, conditions throughout the network at time zero must be defined and for the analysis to progress, boundary condition definition for the network is required. It should be noted thereafter that the progression of a transient through the system and the simulation depends entirely on the changes introduced at a boundary – for example the forced interface motion of a piston.

3.6.2 Establishment of initial conditions

For a method of characteristics based solution to begin, it is necessary to know the conditions throughout the entire network at time zero. This may be achieved by assuming that steady state conditions, upon which the subsequent unsteady flow is superimposed, exist throughout the network. When considering the pressure transients generated within the building drainage system, the initial steady state conditions can be assumed to be representative of zero fluid flow at atmospheric pressure. This assumption provides the initial conditions, i.e. pressure, fluid velocity and wave speed, at all points in the network at time zero. Once the base conditions have been established, the model can then calculate the appropriate time step as discussed in Section 3.4.2 and the transient analysis may proceed provided all network boundary conditions have been defined.

3.6.3 Frictional representation

Normally, the modelling of low-amplitude air pressure transients in building drainage systems requires a representation of the shear between the applied appliance water discharge flows and the entrained air within the system vertical stack. Jack (2000) provides substitution equations for the friction factor terms, f_R and f_S, contained in Equations (3.15) and (3.17) respectively, which allow the simulation of the traction force exerted on the entrained air core by the falling annular water flow through the application of a "pseudo friction factor" term.

However, in the application presented here, modelling the appliance discharge water flows and the consequent shear that generates both the entrained airflow and its accompanying transients is unnecessary as it is envisaged that the reflected wave technique would be programmed to take place during a quiescent period and, therefore, the system response to the applied pressure transient would take place when there was no water flow in the network. This offers a considerable simplification to the model that effectively becomes an air pressure transient simulation that can be based on traditional surge prediction techniques. Therefore, the friction in the dry stack is fully

represented by the expected application of standard relationships e.g., the Colebrook-White friction formula.

When considering the prediction of trap seal oscillation, the rate of change of local pressure at the trap seal interface is normally sufficiently slow to allow the assumption of quasi-steady frictional representation of the forces acting on the water column (Swaffield, 2007). However, where there is a rapid rate of change in boundary conditions it may be necessary to consider the available body of work on unsteady friction. The application of unsteady friction representation of trap seal oscillation will be discussed in Section 3.6.6.3

3.6.4 Boundary Conditions in the building drainage system model

Only one characteristic is available at the termination of each constituent pipe and so in order for these nodes to be solved and the calculation to progress, boundary conditions compatible with a single C^+ and C^- characteristic are required. It should be noted that x is measured positive upwards from the base of the stack so that the entrained airflow has a negative sign in the simulation. This convention results in the base of the stack being regarded as the single entry (with a C^- characteristic available) and all other terminal boundaries are therefore exits (with a C^+ characteristic available).

The development of suitable boundary conditions relating to the network model is an important factor in determining the accuracy with which transient propagation can be modelled. It is the change in conditions at a boundary that initiates the transient to be analysed. There are two groups into which boundary conditions may be categorised:

i. *Passive boundary conditions* which represent the physical attributes of the system and in the case of a typical building drainage system include junctions of two or more pipes, open-ended pipes, closed-ended pipes, or changes in pipe cross section. These boundary conditions are independent of time and the local unsteady flow regime (Swaffield and Campbell, 1992a, 1992b).

ii. *Active boundary conditions* which represent equipment connected to the system and which have a direct influence on the response of the system include water trap seals, air admittance valves and positive air pressure attenuators or piston interfaces used to introduce pressure waves into the network. These boundary conditions are dependant on equipment operation or local system conditions.

Figure 3.5 shows a typical building drainage system and demonstrates some of the common boundary conditions requiring definition together with the additional boundary of the pressure transient generator used to apply the control pressure transient for the identification of depleted water trap seals. The definition of suitable boundary condition equations will normally link the flow rate or pressure within the system to time. In some cases, the required boundary condition equation will only be activated if certain pre-determined conditions are met, for example the representation of an opening air admittance valve.

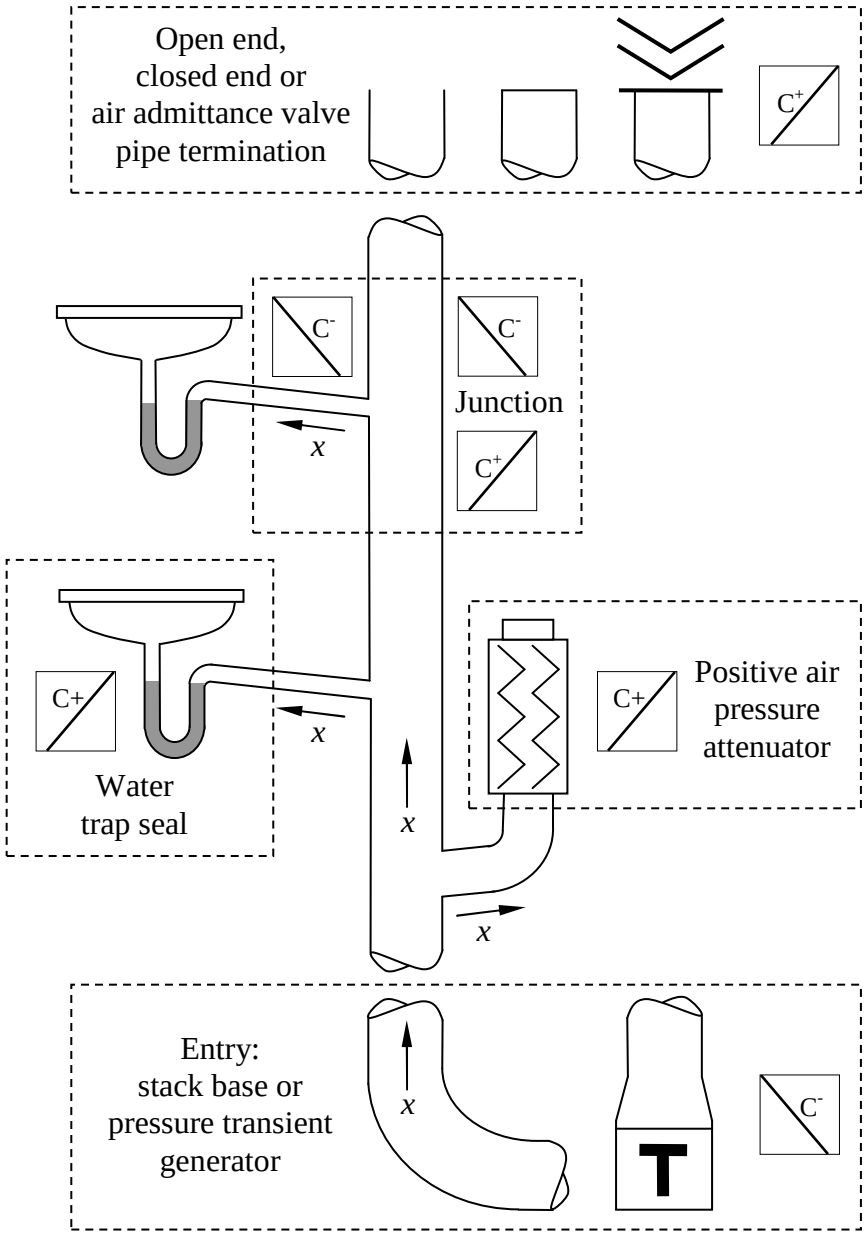

Figure 3.5 Boundary conditions and available characteristics for a typical building drainage system with pressure transient generator

The notation used in this discussion will assume that each pipe is divided into N sections therefore having *N+1* nodes. Pipe nodes will be identified from node 1 at pipe entry, defined at x = 0.0, to node *N+1* at pipe exit, defined at x = pipe length. The variables will be defined as occurring at pipe "*i*" and node "*j*", for example, *u(i,j)* denotes the fluid velocity at the *j*th node of the *i*th pipe.

3.6.5 Passive boundary conditions

3.6.5.1 Junction

Figure 3.5 demonstrates the number and sign convention of the characteristic slope equations required at a junction, i.e. one slope per pipe at the junction. Moving up from the base of the stack, each pipe terminating at a junction is represented by a C^+ characteristic while those originating at a junction are represented by a C^- characteristic. Since the pressure and the wave propagation speed is uniform at the junction, then based on the principle of flow continuity:

$$\sum Inflows + \sum Outflows = 0$$

as outflows are assumed to adopt a negative sign convention. When applied to a junction with "*m*" inflow pipes and "*n*" outflow pipes and where "*j*" represents the inflow pipe and "*i*" an outflow pipe then the flow continuity may be expressed as:

$$\sum_{j=1}^{m} u(j,N(j)+1)A(j,N(j)+1) + \sum_{i=1}^{n} u(i,1)A(i,1) = 0 \qquad (3.28)$$

where the inflow, based on the C^+ characteristic may be expressed as:

$$u(j,N(j)+1) = K1(j,N(j)+1) - K2(j,N(j)+1)c(j,N(j)+1) \qquad (3.29)$$

and the outflow, based on the C^- characteristic as:

$$u(i,1) = K3(i,1) + K4(i,1)c(i,1) \qquad (3.30)$$

With no loss coefficient, the pressure at the junction is common in all pipes where:

$$p(j,N(j)+1) = p(i,1) \qquad (3.31)$$

At any junction of (m+n) pipes, there are 2(m+n) unknowns so 2(m+n) equations are required which are represented by the flow continuity and (m+n-1) pressure equality

statements and ($m+n$) characteristics. Solving 2($m+n$) simultaneous equations yields values for u, c and then p.

3.6.5.2 Open-ended pipe

As shown in **Figure 3.5**, where a pipe is open to atmosphere or another zone of known pressure, whether it be a stack termination or a depleted water trap seal, the boundary expression may be referred to as the network exit condition where the C^+ equation is combined with the local loss equation:

$$u_{N+1} = K1_N - K2_N c_{N+1} \tag{3.32}$$

and

$$p_{N+1} = p_{ref} - K0.5\rho u_{N+1}|u|_{N+1} \tag{3.33}$$

where p_{ref} is the known pressure at the pipe exit, normally taken as atmospheric pressure, and K is a loss coefficient dependant on the degree of flow obstruction at the pipe termination and the suffix $N+1$ represents the pipe exit node. Note that during the numerical simulation of the SARS contamination route at Amoy Gardens (Jack, 2006) p_{ref} was set to the depressed bathroom pressure created by the operation of the oversized extract fan.

3.6.5.3 Closed-ended pipe

In the case of a closed-ended pipe, the velocity term in Equation (3.32) is zero and the boundary is therefore defined by the expression:

$$c_{N+1} = \frac{K1_N}{K2_N} \tag{3.34}$$

3.6.6 Active boundary conditions

3.6.6.1 Air admittance valve

Air admittance valves are installed in the building drainage system to relieve negative pressure transients where the use of open-ended terminations is not feasible, e.g. where roof penetrations are not possible. The valve diaphragm remains closed in response to positive pressures, or a small threshold negative pressure. When the pressure, however, falls below this threshold the diaphragm will lift. This allows air to enter the system to alleviate the pressure differential across the valve diaphragm. Once the valve diaphragm lifts it either rises to its maximum height (fully open) or hovers at some intermediate level (partially open), depending on the pressure within the system.

Thus the three possible boundary condition equations to be solved with the C^+ characteristic are:

Closed valve: $u_{N+1} = 0$ (3.35)

Partially open valve: $p_{atm} - p_{N+1} = K 0.5 \rho u_{N+1}^2$ (3.36)

Fully open: $p_{atm} - p_{N+1} = K_{min} 0.5 \rho u_{N+1}^2$ (3.37)

where K is the appropriate loss coefficient across the valve which decreases as the diaphragm lifts in response to greater negative pressures until the valve is fully open and thereafter having a constant value of K_{min} (Swaffield and Campbell 1992b).

The pressure is calculated as:

$$p_{atm} - p_{N+1} = K 0.5 \rho u_{N+1} |u_{N+1}| \quad (3.38)$$

where p_{N+1} is determined using Equations (3.12).

3.6.6.2 Positive air pressure attenuator

The positive air pressure attenuator is a recent development in building drainage system design and is used to alleviate positive pressure transients. The boundary equation (Swaffield *et al.*, 2005b) is formed by assuming that the bag is initially held deflated by the suction pressure in the stack and therefore has an inflow velocity of zero. Rising pressure due to the arrival of a positive transient causes the bag to open and partially inflate. Once the bag begins to open it remains at atmospheric pressure until the accumulated air inflow reaches its full capacity. Once fully inflated the bag acts as a pressurised boundary obeying the Gas Laws. Thus the possible boundary condition equations to be solved with the C^+ characteristic are:

Deflated bag: $u_{N+1} = 0$ (3.39)

Inflating bag: $p(bag) = p(atm)$ (3.40)

$$Vol(bag)_{t+\Delta t} = Vol(bag)_t + 0.5 A_{entry\ junction} (V_{t+\Delta t} + V_t) \quad (3.41)$$

Full bag: $$p(bag)_{t+\Delta t} = \frac{Vol(bag)_{t+\Delta t}\, p(atm)}{Vol(Full\ bag)} \quad (3.42)$$

3.6.6.3 Water trap seal

Any water trap seal connected to the network will be displaced in response to pressure fluctuations at the air to water interface. It may be shown that the response of the water trap seal may be analysed by application of Newton's Second Law of Motion to the liquid column (Swaffield and Galowin, 1992):

$$A\left(p\left(j,N\left(j\right)+1\right)-p\left(ref\right)\right)+\rho_w Ag\left(H_1-H_0\right)-\tau_0 LP=\rho_w LA\frac{dU_w}{dt} \tag{3.43}$$

where *A, L* and *P* represent the trap cross-sectional area, liquid column length, which may vary as the trap loses water, and the wetted perimeter respectively, see **Figure 3.6**.

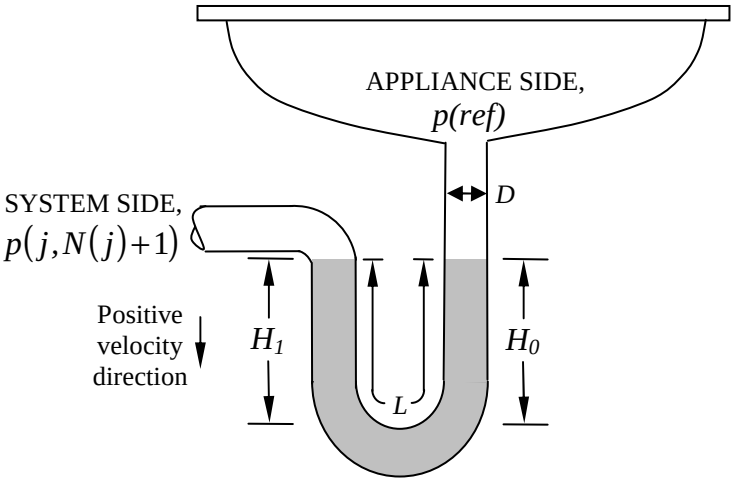

Figure 3.6 Definition of water trap seal termination. Note trap diameter, *D*, water column height, *H*, and trap seal water length, *L*.

H_1 and H_0 denote the water surface levels and $p\left(j,N\left(j\right)+1\right)$ is the air pressure exerted upon the trap fluid column at the system side and *p(ref)* is the air pressure exerted upon the fluid column at the appliance side, both of which may initially be taken as atmospheric.

Replacing the wall shear stress for the liquid flow in the oscillating trap with the Darcy equation for friction factor reduces Equation (3.43) to (Swaffield and Boldy, 1993):

$$p\left(j,N\left(j\right)+1\right)-p\left(ref\right)+\rho_w\left[\left(H_1-H_0\right)-L\left(\frac{4fU_w\left|U_w\right|}{2D}-A\frac{dU_w}{dt}\right)\right]=0 \tag{3.44}$$

where U_w is the liquid column velocity, f is the liquid column friction factor which is normally based on the Colebrook-White steady state friction expression, and D is the

trap diameter. However, the flow conditions within a water trap seal are not steady as the water column oscillates in response to system air pressure followed by a damped oscillation once the transient pressure propagation has cessed. A study of trap seal response by Swaffield (2007) found that steady state frictional representation severely underestimated the frictional forces acting on an oscillating liquid column due to the rapid reversal of flow direction inherent in seal oscillation in response to rapid system pressure excursions. Swaffield (2007) incorporated two unsteady frictional expressions to better represent the observed conditions. The first was based on earlier work by Carstens and Roller (1959) and was used to represent the frictional losses in the air flow within the network:

$$f_{unsteady} = f_{steady} + 0.449\frac{D}{U_w^{\,2}}\frac{\partial U_w}{\partial t} \tag{3.45}$$

The second was used to represent the liquid column friction in the trap and was based on earlier work by Zilke (1968):

$$\Delta p = \frac{f\rho L U_w^{\,2}}{2D} + \frac{16\rho L}{D^2}\sum_{1,3,5}^{M}\left[U_w(time - j\Delta t + \Delta t) - U_w(time - j\Delta t - \Delta t)\right] W\left(t^*(j\Delta t)\right) \tag{3.46}$$

where, $M = time/(\Delta t\text{-}1)$, "*time*" is the current calculation time, referred to as $t + \Delta t$ and W is a weighting factor. Both Equations (3.45) and (3.46) include the steady state frictional loss along with a term dependant on the flow local accelerations and the time history of the flow.

The pressure term in Equation (3.46) is determined using the C^+ characteristic term and the wave propagation speed, Equation (3.7), where:

$$u(j, N(j)+1) = K1(j, N(j)+1) - K2(j, N(j)+1)c(j, N(j)+1) \tag{3.47}$$

and

$$u(j, N(j)+1) = U_w \tag{3.48}$$

In addition to predicted water trap seal displacement, the developed boundary condition can, by subtracting the water overflowing into the system side, also predict the effect of air pressure transients on trap seal retention. As the air pressure falls in the network, the water column in the trap is displaced so that the appliance side water level falls. However, the system side level is governed by the level of the branch entry connection so that water is lost to the network.

If the transient event is severe then the trap may become totally depleted allowing a potential cross contamination route from the network to habitable space.

3.6.6.4 Pressure transient generator

The final boundary condition is that required to represent the action of the pressure transient generator used to create the incident transient for application with the reflected wave technique.

Preliminary evaluation of the reflected wave technique was carried out using a single positive pressure pulse transient generated by the forward movement of a flat plate piston using a pneumatic ram. However, as will be discussed later in Chapter 5, the use of a single positive pressure pulse transient raised concern over the protection of system integrity as a single pressure pulse with a magnitude of $\Delta p_{I(pulse)}$ will cause a corresponding trap displacement of ΔH such that $\Delta p_{I(pulse)} = \Delta H$, for a uniform diameter trap, see **Figure 3.7**.

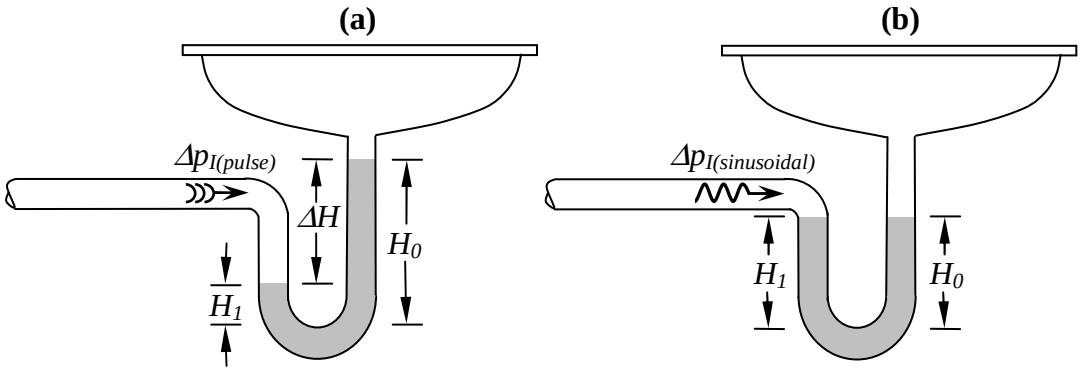

Figure 3.7 Trap response to a (a) single pressure pulse; and (b) sinusoidal waveform

For example, if a single pressure pulse of magnitude $\Delta p_{I(pulse)}$ = 100 mm water gauge arrived at the trap then this would instigate a trap displacement of 100 mm which would cause a catastrophic system failure due to trap depletion.

For the successful application of the reflected wave technique it was imperative that the incident transient would not itself pose a threat to system integrity. Kelly (2007) found that trap displacement could be avoided, and system integrity protected, by the application of a 10 Hz sinusoidal transient $\Delta p_{I(sinusoidal)}$. Beattie (2007) confirmed and quantified these findings by investigating the trap seal response to various sinusoidal

pressure frequencies for three trap depths (i.e. 38 mm, 50 mm and 80 mm), **Figure 3.8**. It can be seen that the ability for a transient to cause trap seal displacement is dependant upon both the magnitude and duration of the transient acting at the trap interface as well as the mass and frictional characteristics of the water column. For all three trap depths tested, the maximum observed trap displacement in response to a 10 Hz sinusoidal transient was only ± 1 mm.

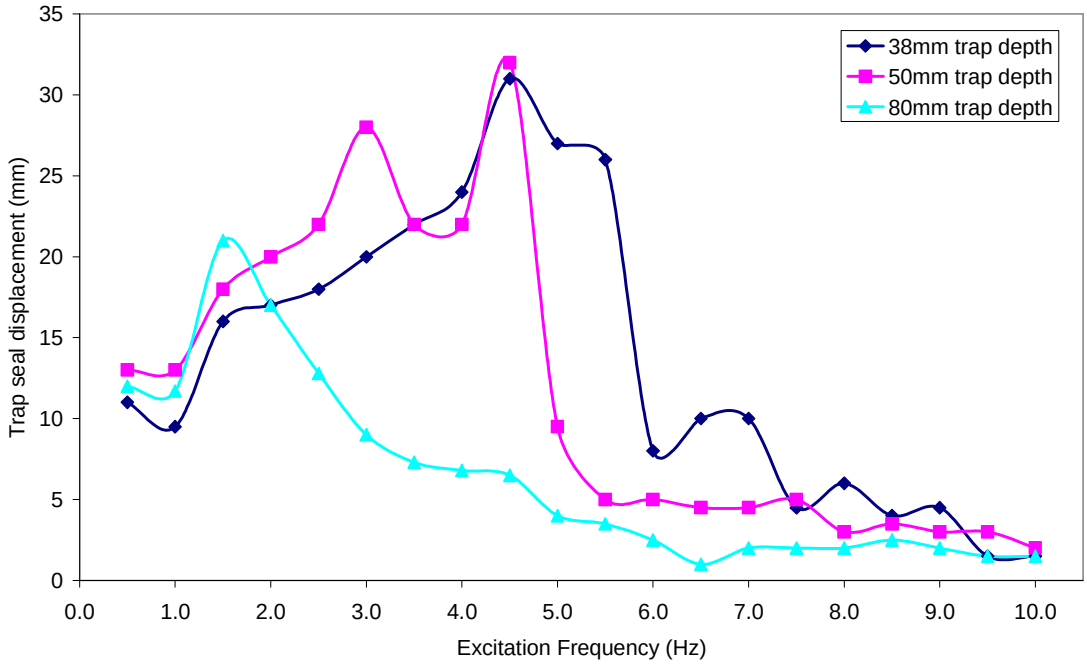

Figure 3.8 Recorded trap seal displacement in response to a range of imposed excitation frequencies (0.5 Hz to 10 Hz) adapted from Beattie (2007)

At this frequency the positive and negative transient waves, generated by the forwards and backward motion of the sinusoidal transient generator, arriving in rapid succession at the trap interface, were not capable of displacing the water column as the duration to which the water column is subject to these incoming transient waves is not sufficient to overcome the inertia of the water, thus opposing the change of direction and limiting the movement of the water seal. At lower frequencies, however, trap displacement of up to ± 15 mm (total displacement of around 30 mm) were observed. Swaffield (2007) confirmed the capability of AIRNET to model these effects of trap displacement in response to various applied sinusoidal transient frequencies.

A pressure transient generator consisting of a flat plate piston is used to generate both types of transient with the only difference being the method of driving the piston, see **Figure 3.9**.

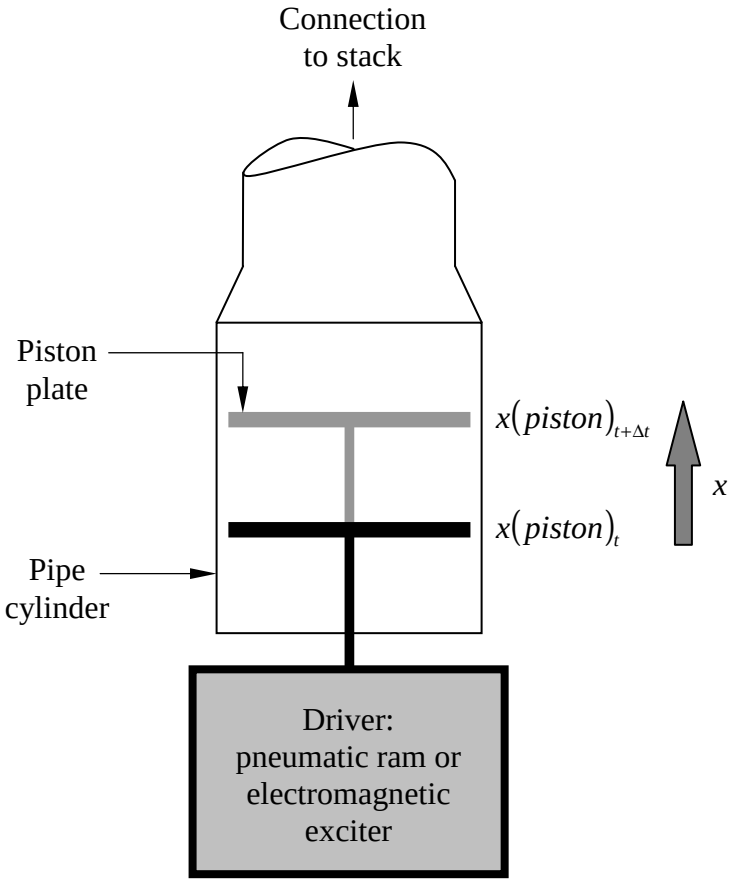

Figure 3.9 Definition of the pressure transient generator entry boundary condition

As mentioned earlier, the single pressure pulse was generated by the forward motion of the piston by a pneumatic ram, while the sinusoidal transient was driven by an electromagnetic exciter and frequency signal generator to move the piston forwards and backwards (at the control frequency) in order to produce a sinusoidal pressure wave. Both driving methods allow the motion of the piston to be defined by:

$$u = \frac{\left(x(piston)_{t+\Delta t} - x(piston)_t\right)}{\Delta t} \tag{3.49}$$

Setting the pressure transient generator as the single system entry allows it to be solved by the available C^- characteristic to yield the pressure at the piston face. If the pressure transient generator is not located at the base of the stack then distance is no longer measured from the bottom of the stack and the C^+ and C^- at each internal node must be altered to account for the new entry point, e.g. the base of the stack would become an exit termination.

3.7 Chapter summary

This chapter has presented the mathematical basis of the AIRNET numerical model (developed at Heriot-Watt University under previous EPSRC funded research) which employs the method of characteristics solution to the St Venant equations of continuity and momentum to allow air pressure transient propagation within the building drainage system to be modelled.

The general St Venant equations of continuity and momentum, applicable to the flow of any fluid in any type of conduit, were derived in terms of flow velocity, *u*, and wave propagation speed, *c*, allowing pressure to be defined due to the interdependence of air pressure and density. These general quasi-linear hyperbolic partial differential equations were then transformed via the method of characteristics into total differential relationships prior to solution by finite difference techniques.

The importance of accurate boundary conditions in the development of the model to provide complete network solutions was emphasised. The method of characteristics approach to the modelling of building drainage network boundaries was illustrated by describing the boundary conditions already incorporated into the existing AIRNET model. It was shown that by using a combination of theoretical and empirical relationships, in conjunction with the available characteristic, the air flow conditions at boundaries can be calculated, hence allowing complete network solutions to proceed. The existing AIRNET model was shown to incorporate boundary conditions to represent open-ended pipes, closed-ended pipes, junctions, air admittance valves, positive air pressure attenuators and water trap seals. The new boundary condition required to represent the pressure transient generator was developed as part of this current research.

Chapter 4
The reflected wave technique

4.1 Introduction

This chapter focuses on the development of the reflected wave technique for the detection and location of depleted trap seals within the building drainage system. The technique draws upon the pressure transient theory presented previously, particularly the reflection and transmission of pressure waves at system boundaries, which will be applied in the context of defect detection. First, a review of current pipe defect detection methods used at present in the water, oil and gas industries; as well as those conceptually developed will be undertaken.

A ***tra**p **c**ondition **e**valuato**r*** (TRACER) program, developed as part of this research to perform automatic identification of depleted trap seals, will be presented. A numerical example using perfect data will be performed to test the accuracy of the TRACER program and general conclusions will be drawn regarding parameter sensitivity.

4.2 Pipe defect detection and location

There are many different approaches available for the identification of defects within pipe systems. These methods have been developed through the need to identify leaks and blockages, within water, oil and gas supply pipes. Disruption to the operation of such pipelines can lead to excessive economic loss as well as both environmental and health hazards. These consequences have, therefore, spurred the development of methods for pipeline monitoring and defect detection (Emara-Shabaik *et al.*, 2002). This section will review the defect detection methods currently available as well as those theoretically developed. This list is not exhaustive as only those considered potentially applicable to depleted trap seal detection and location will be reviewed.

4.2.1 Direct - Non-acoustic techniques

Visual observation

The traditional and simplest method to detect pipe defects is by visual inspection of the pipe system. This method relies on experienced personnel making regular inspections of the system, looking, smelling and listening for anything unusual which may allude to the presence of a defect. The effectiveness of this technique depends on the individuals' experience and the inspection frequency as well as the physical layout and accessibility of the network. Currently this is the only method available for monitoring the building drainage system.

Video Inspection

This method involves inserting a remotely operated camera into the pipe, thus, providing an internal pipe inspection system. The camera can be combined with on-board ultrasonic equipment for both corrosion and leak detection and it can also be used to clean, monitor and, sometimes, repair cracked pipes within the system. This method is frequently used to determine the condition of sewage systems and relies on well-trained staff to operate and analyse the video footage. However, this method is intrusive and may require that the system is shut down prior to testing.

Ambient air monitoring or tracer injection

In this technique a tracer gas, such as helium or hydrogen, is injected into an isolated section of the pipe system. The gas will escape at a defect in the pipe and the defect is located by highly sensitive gas detectors which will either be at fixed locations along the pipe or which can be carried to effectively "scan" the surface of the pipe. It can often take some time to locate a defect and success is dependant on atmospheric conditions. The tracer gas must also be fully removed before the pipe system can again be used.

4.2.2 Direct - Acoustic techniques

Direct listening method

A common method used to detect defects in water supply pipes, this method uses an acoustic listening rod and ground microphone to locate leaks in underground pipes. This equipment incorporates signal amplifiers and noise filters to sense leak induced sound or vibration within the pipe. First, the listening rod is used to detect leak induced sound by placing the rod in direct contact with the pipe at convenient access sites (i.e.

fire hydrants, valves and stop-taps). Next, the ground microphone is used to locate leaks by listening directly above the pipe at ground level in order to pinpoint the leak location (Hunaidi and Chu, 1999; Hunaidi and Wang, 2006). The effectiveness of this method, which can be time consuming, depends on user experience, background noise, leak size and environmental conditions.

Acoustic correlator

This method uses the cross-correlation method to compare the leak induced sound signals measured at two locations on the pipe. The measured sound signals are analysed to determine the position of a leak based on the time delay of the signal arriving at two measurement points along the pipe, the wave propagation speed and the distance between the two measurement points. The time delay occurs as a result of one of the measurement points being closer to the leak than the other. If the leak is equally spaced between the two measurement points then the time delay is zero. The acoustic correlator method shows a better efficiency and accuracy and relies less on the experience of the user than the direct listening method (Hunaidi and Chu, 1999; Hunaidi and Wang, 2006).

4.2.3 Inference methods

The inference methods are based on the measurement of internal pipeline parameters (pressure, flow and temperature) and the use of a computer model that detects the defect based on the collected data. The accuracy of inference methods depends on the uncertainties associated with the system's characteristics, operating conditions, the mathematical model and the collected data. A defect can only be detected based on a particular measured parameter; if the defect can cause this parameter to change more than the uncertainties associated with the collected data it is possible to infer the presence of a defect and determine its location within the system through careful analysis of the measured parameter.

Hydrostatic testing

The method is used to test the integrity of steel pipelines and involves sealing and pressurising a section of the pipeline (Hough, 1988). It requires the measurement of pressure and temperature over a certain period. The pressure change is compared with temperature change and if there is a correlation between the two parameters within a predetermined threshold, then the system is normal; lack of correlation indicates a

defect. Similar methods are used to test against air leakage of new sewer pipe systems (Gokhale and Graham, 2003).

Mass or volume balance method

If a difference occurs between upstream and downstream flow measurements, and if the difference is greater than an established tolerance, then a leak can be assumed to have occurred within the pipe system. The leak flow rate is given by the mass-balance between the upstream and downstream flows (Butler, 1982; Liou, 1998; Fukushima *et al.*, 2000). This method requires flow measurements at both ends of the pipe system and is sensitive to measurement accuracy and transient events. The test can be based on flow difference alone which would generate a simple mass or volume balance scheme or on flow difference compensated by pressure/temperature changes and inventory fluctuations in a pipeline (Liou, 1993). The method automatically determines the defect location in real-time; however, a defect can only be detected when its size exceeds overall uncertainties (Liou, 1998).

Real-time transient model method

This method uses measured values of transient flow and pressure to simulate the real-time system operation using a transient model. In normal conditions, both the measured and computed data would be ideally matched. The occurrence of a defect will cause a discrepancy between the measured and computed data. Three types of transient model-based defect detection methods are used: *flow discrepancy* (Wade and Rachford, 1987), *pressure and flow discrepancy* (Kiuchi, 1993; Liou and Tian, 1995) and *dynamic volume balance* (Thompson and Skogman, 1983; Nicholas, 1987).

The success of these methods rely on the availability of a mathematical model capable of accurately simulating the transient behaviour of the pipe system together with reliable pressure and flow measurement data.

Frequency response method

This method involves applying sinusoidal excitations to the pipe system and analysing the system response in the frequency domain. The frequency response can be determined by either using a frequency sweeping technique (Chaudhry, 1987) where sinusoidal oscillations at various frequencies are used to excite the system and the response at every frequency determined, or by applying a sufficiently wide bandwidth input signal where the entire frequency response can be extracted from only a single system excitation (Lee *et al.*, 2005). The presence of a defect within the system will

cause the propagating sinusoidal transient signal to be partly reflected at a time specific to the defect location. As the process of reflection repeats, a series of travelling and standing waves are generated in the system. These waves can be used to detect and locate a defect by analysing the frequency response (Sattar and Chaudhry, 2008).

There are a number of methods used to interpret the frequency response to find the defect location. Lee *et al.* (2005) proposed two numerical methods for leak detection in simple pipelines based on the system frequency response using the relative sizes of resonance peaks at various harmonic frequencies: (i) an inverse resonance method, which matches the modelled frequency responses to those observed; and (ii) a peak-sequencing method to determine the region in which the leak is located by comparing the relative sizes between peaks in the frequency response diagram. Covas *et al.* (2005) proposed a method for leak detection based on the standing wave difference method which is often used for fault location in electrical cables and which uses the difference between two consecutive resonant frequencies to identify the location of the leak within the system. In addition to leak detection, the use of defect-dependant resonant frequencies has also been applied to blockage detection in pipelines (Antonopoulous-Domis, 1980; Qunli and Fricke, 1989, 1991; De Salis and Oldham, 1999, 2001).

Currently, this technique has only been applied to very simple pipe systems, often consisting only of a single laboratory pipe with defined boundary conditions at each end. Whilst it shows potential, many issues need to be addressed for the extension of the technique to field applications. In any real system, all physical singularities, such as dead-ends, junctions and changes in pipe diameter, would reflect the incident wave, generating multiple resonance frequencies within the system making it difficult to distinguish irrelevant resonance frequencies from those generated by a pipe defect.

Inverse transient analysis

The inverse transient analysis (ITA) method, first proposed by Liggett and Chen (1994), takes the system response recorded in a real system during a transient event and compares it with those generated by a numerical model of the same system experiencing the identical transient event. An optimisation algorithm is used to evaluate and adjust the system parameters (i.e. defect location and size, friction coefficient, wave propagation speed) to bring the predicted and measured responses into agreement.

The ITA method has been widely tested using artificial data (Ligget and Chen, 1994; Covas *et al.*, 1998, 1999; Nash and Karney, 1999; Vitkovsky *et al.*, 2000), and has been

validated, to some extent, using laboratory data (Karney *et al.*, 2000; Covas and Ramos, 2001; Covas *et al.*, 2003, Vitkovsky at al., 2007). Yet, only a few field trials have been conducted and these have been limited to only very simple systems (Covas, 2003; Covas *et al.*, 2004; Stephens *et al.*, 2005).

The efficiency of ITA is limited by the accuracy of the numerical model and, of course, the ability to fully define the boundary conditions and system properties of the real system. These issues partly limit ITA to numerical and laboratory experiments or, at the very least, to well-defined field systems (Jung and Karney, 2008).

Reflected wave technique

When a transient event is induced within a piped system, every physical feature induces a reflection which modifies the original profile of the incident wave. This method focuses on the time analysis of the first reflected wave from the defect in response to an applied control transient. The location of the defect is determined by the total time taken for the incident wave to travel to the defect and for the reflected wave to be returned to the source.

The advantage of this method is that it provides a visual confirmation of any defect in the form of a characteristic reflection which reveals both the identity and location of the defect (Maloney, 1973). However, it requires an accurate measurement of the arrival time of the reflected wave and knowledge of the wave propagation speed.

The reflected wave technique has been successfully applied to a wide range of defect detection applications including leak detection in water distribution systems (Jonsson, 1995; Covas, 1998, 2003; Covas and Ramos, 1999; Brunone and Ferrante, 2001, 2004) and wastewater outflow pipes (Brunone, 1999); blockage detection in natural gas supply pipes (Adewumi *et al.*, 2000; Adewumi et al 2003); valve status determination in water supply networks (Stephens *et al.*, 2004; Arbon *et al.*, 2008); and even fault detection in electrical cables (Maloney, 1973; Liu and Lu, 2003). Although showing excellent potential, all of these previous studies have been limited to simple systems consisting of only a small number of connected pipes and boundary conditions.

4.3 Selection of detection technique

The majority of defect detection techniques reviewed in the literature consider single pipelines and cannot be directly applied to multi-pipe systems (Misiunas *et al.* 2005). If a defect detection technique is to be successfully used to detect and locate depleted trap seals within building drainage systems (which often have a large and complex layout) and if this technique is to be easy to implement and simple to understand for facility managers and building users, then the method adopted must be flexible and robust, yet accurate and uncomplicated.

From the range of defect detection methods reviewed, the most straightforward and readily applicable technique to the identification of depleted trap seals is the reflected wave technique. Preliminary results have shown the technique to be an efficient and accurate method for the detection of defects in a number of different piping systems (Jonsson, 1995; Covas *et al.* 1998; Covas and Ramos, 1999; Covas, 2003; Brunone, 1999; Brunone and Ferrante, 2001, 2004; Adewumi *et al.*, 2000; Adewumi et al 2003; Stephens *et al.*, 2004; Arbon *et al.*, 2008). When compared to other methods, the reflected wave technique offers a fast and relatively simple method of defect detection which generally requires less system information than other more complex methods (Covas, 2003).

The application of the reflected wave technique to identify depleted trap seals in the building drainage system offers a simplification to the technique over its previous application for leak detection in fluid-carrying pipe systems for the reason that every trap seal has a fixed position within the system, providing every potential defect with a fixed and known pipe period. Leaks, on the other hand, are generally unexpected and can occur at any point within the system, thus presenting a more unpredictable challenge. Additionally, while leak investigators have the added complication of estimating leak magnitude in order to assess the severity of the pipe rupture (Covas, 2003), this is not necessary for the identification of depleted trap seals as it is important only to determine, firstly, *if* a depleted trap exists within the system and, secondly, *where* in the system this failure has occurred. Any size of depleted trap seal will provide a route for potential cross-contamination so, therefore, *detection* and *location* are the only two factors of concern. The reflected wave technique is, therefore, particularly amenable to this current application to identify and locate depleted trap seals and is therefore the method utilised in this research.

4.4 The reflected wave technique applied to the detection and location of depleted trap seals

The technique applied here is fundamentally based on the mechanisms of pressure transient propagation and, in particular, the reflection and transmission of pressure waves at system boundaries, which is common to all full bore piped systems as discussed in Section 2.2. As a pressure transient propagates through the building drainage system, every boundary condition (whether it be a junction, an air admittance valve or a trap seal) will induce a characteristic reflection which alters the normal shape of the transient. The detection of these reflections in the monitored system response allows their identification and reveals their location. The information carried in the system response can, therefore, be used to detect and locate depleted trap seals.

Consider, for simplicity, an instantaneous change in flow conditions, ΔV, which generates an instantaneously occurring pressure transient, Δp, given by the Joukowsky formula (Equation 2.1 restated here for clarity):

$$\Delta p = -\rho c \Delta V \tag{4.1}$$

As the incident pressure transient, Δp_I, propagates along the pipe, at every system boundary, it will be partly transmitted forward, Δp_T, while the remainder will be reflected backward, Δp_R. Neglecting energy losses along the pipeline and at the boundary, the transmitted wave added to the reflected wave equals the incident wave:

$$\Delta p_I = \Delta p_T + \Delta p_R$$

As discussed in Section 2.2, the reflection induced by a trap seal is dependant upon the status of the trap. A fully primed trap seal (acting generally as a closed end, $V = 0$) will generate a +1 reflection and a depleted trap seal (acting as an open end, p = constant) will generate a -1 reflection. The effect on the measured system response can be explained by considering the simple example shown in **Figure 4.1**. Responding to an incoming positive transient, the +1 reflection generated by a fully primed trap seal will appear as a *pressure rise* (having the same magnitude and sign as the incident wave) in the system response, whereas the -1 reflection generated by a depleted trap seal will appear as a *pressure drop* (having the same magnitude, but a reversal of sign, as the incident wave).

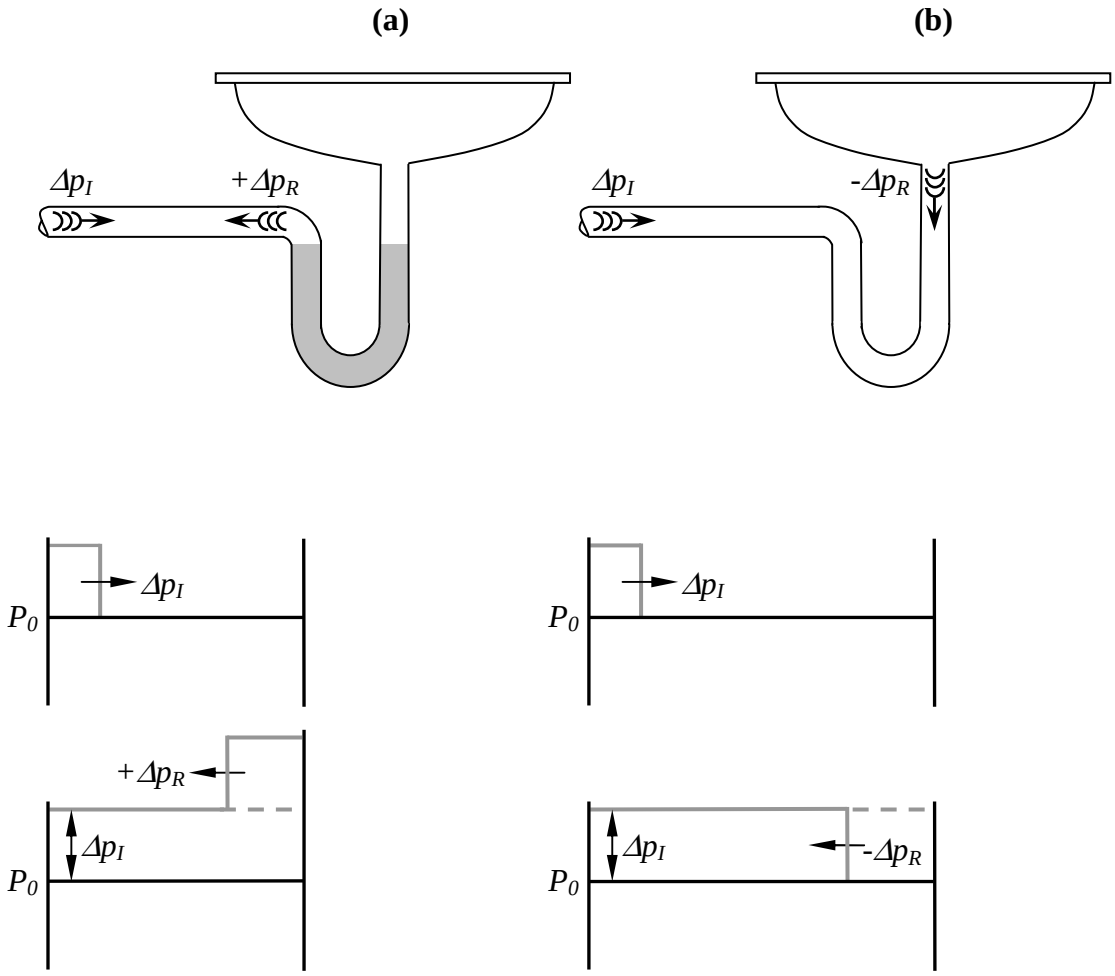

Figure 4.1 Pressure transient Δp_I generated by a change in flow conditions ΔV showing (a) reflection $+\Delta p_R$ from fully primed trap and (b) reflection $-\Delta p_R$ from depleted trap

The complete reversal in reflection coefficient between a fully primed and depleted trap seal is central to the detection technique outlined here. By analysing the system response to an applied positive pressure transient, the presence of a depleted trap seal is indicated by the arrival of a negative reflection which shows as a pressure drop in the system response.

Precision in locating the depleted trap seal strictly depends on the accuracy in evaluating the arrival times, at the measurement point, of both the incident transient wave and the subsequent trap induced reflection and also on having a knowledge of the wave propagation speed. Section 2.2 has already introduced the concept of pipe period which is the time taken for a pressure transient to travel to a reflecting boundary and

return to source. By rearranging Equation 2.3, the location of a depleted trap seal can be determined as:

$$X_D = \frac{c\ t_D}{2} \tag{4.2}$$

where X_D is the distance to the depleted trap seal from the measurement point, t_D is the pipe period of the depleted trap (i.e. the time taken for the pressure transient to travel from the monitoring point to the trap and for the induced reflection to be returned to the measurement point), and c is the wave propagation speed.

Due to the complexity of normal building drainage systems and the consequently large amount of different system boundaries contained within them, the number of reflections and re-reflections that occur within the system can be high. The successful operation of the reflected wave technique, therefore, relies on the ability to distinguish the reflection returned from a depleted trap seal from the normal features that exist within the system (e.g. junctions and open terminations).

By first obtaining a system response for the system under normal defect free conditions – which will include the effect of all reflections induced by normal system boundaries – and using this as a comparison for subsequent test system responses, any variation between the two system responses would be attributable to a change in the measured test pressure due to the arrival of a new reflection generated by an unexpected change in the system conditions, such as the depletion of a trap seal. The time at which the two system responses diverge provides t_D which can then be used to derive the location of the trap, X_D, from Equation 4.2, once c is known.

This approach of incorporating a defect free system response into the data analysis of the reflected wave technique is central to the proposed technique and avoids the problem of *misleading information* experienced by some authors when applying the technique to the identification of leaks in water supply pipes (Covas and Ramos, 1999; Covas *et al.* 2000) who found that the reflections generated by the normal system boundary conditions interfered with the success of the technique. In those investigations the authors found it necessary to determine exactly the geometry and layout of the system in order to reduce the number of unexpected reflections, thus increasing both the test set-up time and the complexity of the data analysis process.

4.5 Automatic detection and location of a single depleted trap seal

The success of the reflected wave technique in providing the necessary protection against potential cross-contamination from depleted trap seals requires the whole building drainage system to be systematically monitored. This requirement will be assured by providing automatic test scheduling and data analysis which is not reliant on user interrogation. This section presents the development of the TRACER program for the automatic detection and location of depleted trap seals which removes the dependence on user interrogation and which provides a fast and simple method for automated system monitoring.

The TRACER program is a time series change detection indicator which is used to identify a depleted trap seal from the arrival time of the trap-induced reflection. The reflection arrival time is detected by calculating the absolute difference between the defect free and measured test system responses.

4.5.1 Automatic determination of trap status

4.5.1.1 Test set-up

Before the TRACER program can be used for the automatic detection and location of depleted trap seals, some important system information is first required.

As discussed in Section 4.4, a defect free system response, to which all subsequent test system responses can be compared, must first be obtained. Ensuring that all trap seals are fully primed, the system response to the applied incident transient is recorded at one or more measurement points within the system. A total of N defect free system responses are recorded from which the average *defect free baseline,* P_j^{DF}, is calculated:

$$P_j^{DF} = \frac{1}{N}\sum_{i=1}^{N} P_{j,i} = \frac{P_{j,1} + P_{j,2} + ... + P_{j,N}}{N} \tag{4.3}$$

where j is the measurement point. To ensure that all system responses are exactly aligned before calculating P_j^{DF}, the transient wave arrival time, t_a, (taken as the time when the pressure first becomes greater than atmospheric), is set to time zero, t_0, see **Figure 4.2**. To allow direct comparison with the defect free baseline t_a is set to t_0 for all subsequent test system responses.

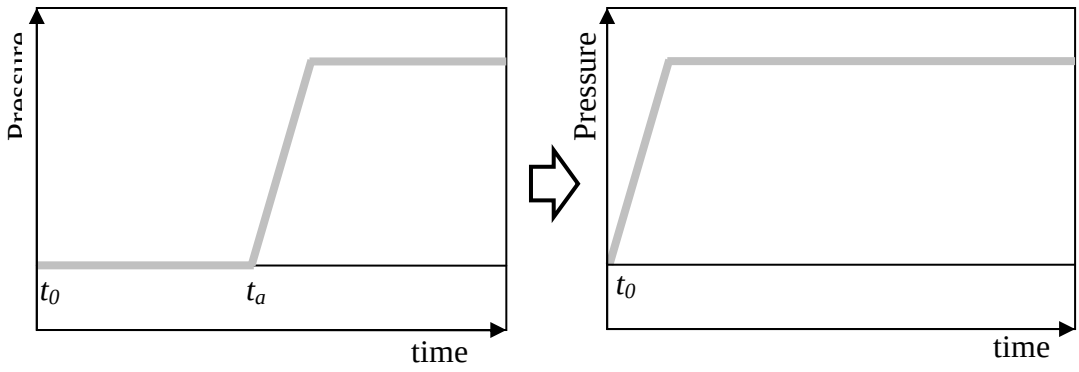

When P_j > atmospheric pressure, set $t_a = t_0$

Figure 4.2 Setting the transient wave arrival time to time zero using a generalised system response as an example

To allow discrimination between natural variations in the measured test system response – due to, for example, measurement errors and system noise – a system threshold level, *h*, is determined which provides the expected signal variation for the defect free system. The threshold level is set as the maximum discrepancy observed between the defect free baseline and each of the *N* defect free system responses used to derive it:

$$h = max\left|P_j^{DF} - P_{j,i}\right|_{i=1}^{i=N} \tag{4.4}$$

All values below *h* are ignored while those that exceed this level are indicative of a variation from the normal defect free baseline. The value of the applied threshold level will undoubtedly influence the sensitivity of the TRACER program. Although low values of *h* will expand the range of detectable traps it will also increase the risk of false alarms. For optimal performance, *h* should be determined specifically for a particular system. As the test for depleted trap seals will normally take place during the night, when the system is quiet, the system noise will be minimal thus improving the performance and accuracy of the technique.

The final set of required information is the pipe period, t_P, of each connected trap seal. This can be obtained from the system geometry by measuring the distance to each trap from the measurement point, or by using the reflected wave technique as a probe to determine the reflection return time for each trap by systematically removing the water seal one at a time.

Figure 4.3 presents a summary of the necessary steps for the collection and assimilation of the required system information.

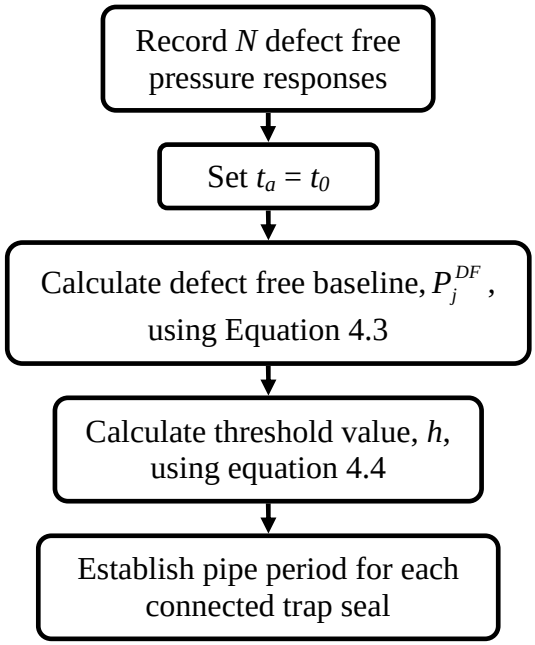

Figure 4.3 System information required by the TRACER program for the automatic detection and location of depleted trap seals

4.5.1.2 Test procedure

Having acquired the necessary system information, the TRACER program is now ready to perform automatic detection and location of depleted trap seals. To determine if a depleted trap induced reflection has occurred, and to estimate its time of arrival, a time series change detection test is carried out by comparing the measured test system response , P_j^M , with the defect free baseline, P_j^{DF} .

Similar to the least squares minimisation test utilised by Stephens *et al.* (2004) and Vitkovsky *et al.* (2007) the absolute difference between P_j^{DF} and P_j^M is used to determine the *goodness-of-fit* between the two system responses.

$$D_t = \left| P_j^{DF} - P_j^M \right| \tag{4.5}$$

If $D_t > h$, then issue alarm and record t_D

where D_t is the absolute difference at a time, t. For every sample of data, the change in system response is then analysed. If D_t exceeds the threshold value, h, then the discrepancy between the two traces is out with the expected variation for a defect free system response, the alarm is issued and time of change t_D is recorded, see **Figure 4.4**.

The time t_D, identified as the reflection return time, is likely to occur after the actual reflection arrive time, t_R, **Figure 4.4(b)**. The discrepancy is due to the dependence on h but in practice the difference is found to be negligible.

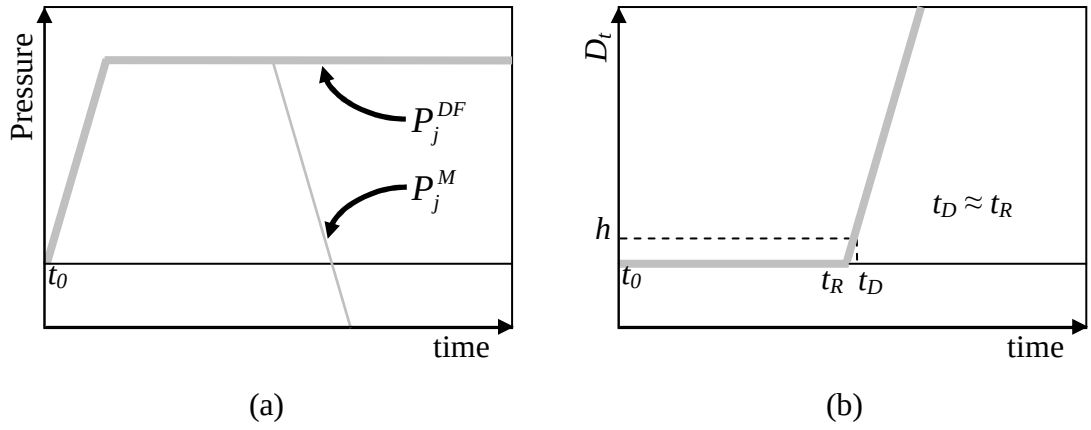

Figure 4.4 The generalised traces of: (a) pressure at measurement point, and (b) absolute difference

Misiunas *et al.* (2005) use a similar time series change detection technique to detect burst-induced transients from the measured system response in water distribution networks, however, they use a modified cumulative sum method which progressively summates any part of the system response which exceeds a drift parameter (expected variation). This technique is more susceptible to the effects of measurement error and signal noise and hence requires additional noise pre-filtering.

4.5.2 Test calibration

Included in the TRACER program is a simple calibration test which is designed to distinguish between a *reliable* system response and an *unreliable* system response. A *reliable* system response is that considered to have been measured under similar system conditions to which the defect free baseline had been measured (i.e. when the system is in a quiescent state) thus allowing direct comparison between the two traces. An *unreliable* system response is that considered to have been measured under different system conditions (i.e. when there is a water flow, or other such influence, which will

alter the pressure regime within the system) thus, in most cases, making direct comparison impossible and generating false alarms. The calibration test is conducted by analysing D_t over the first section (calibration period) of the system response in which no trap-induced reflection can occur as their pipe periods occur after this calibration section, see **Figure 4.5**.

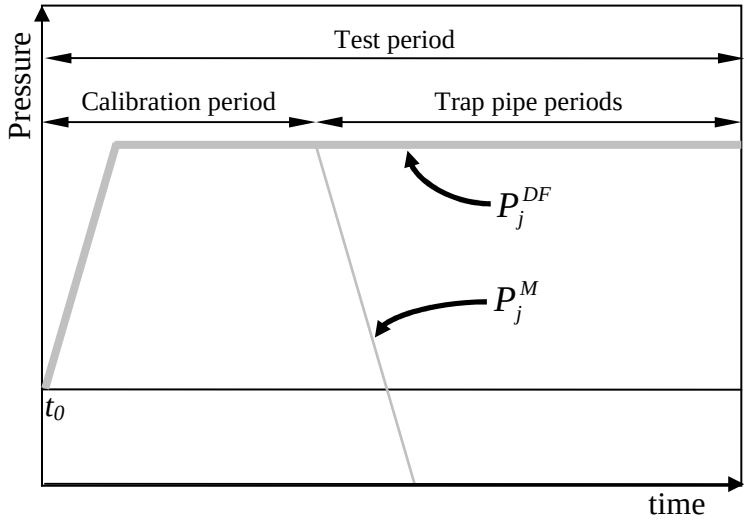

Figure 4.5 Calibration test for the reflected wave technique

If $D_t > h$ during the calibration period then the system response is considered *unreliable* and the system is retested. Otherwise, if $D_t < h$ during the calibration period then the system response is considered to be *reliable* and the data analysis proceeds. Although the proposed test method will take place during the night (i.e. when the system is most likely to be quiescent) this simple calibration test safeguards against false alarms due the unavoidable risk of system usage coinciding with the test. The calibration test will repeat until a reliable system response is obtained.

A schematic view of the complete TRACER program algorithm for the detection and location of depleted trap seals is presented in **Figure 4.6**.

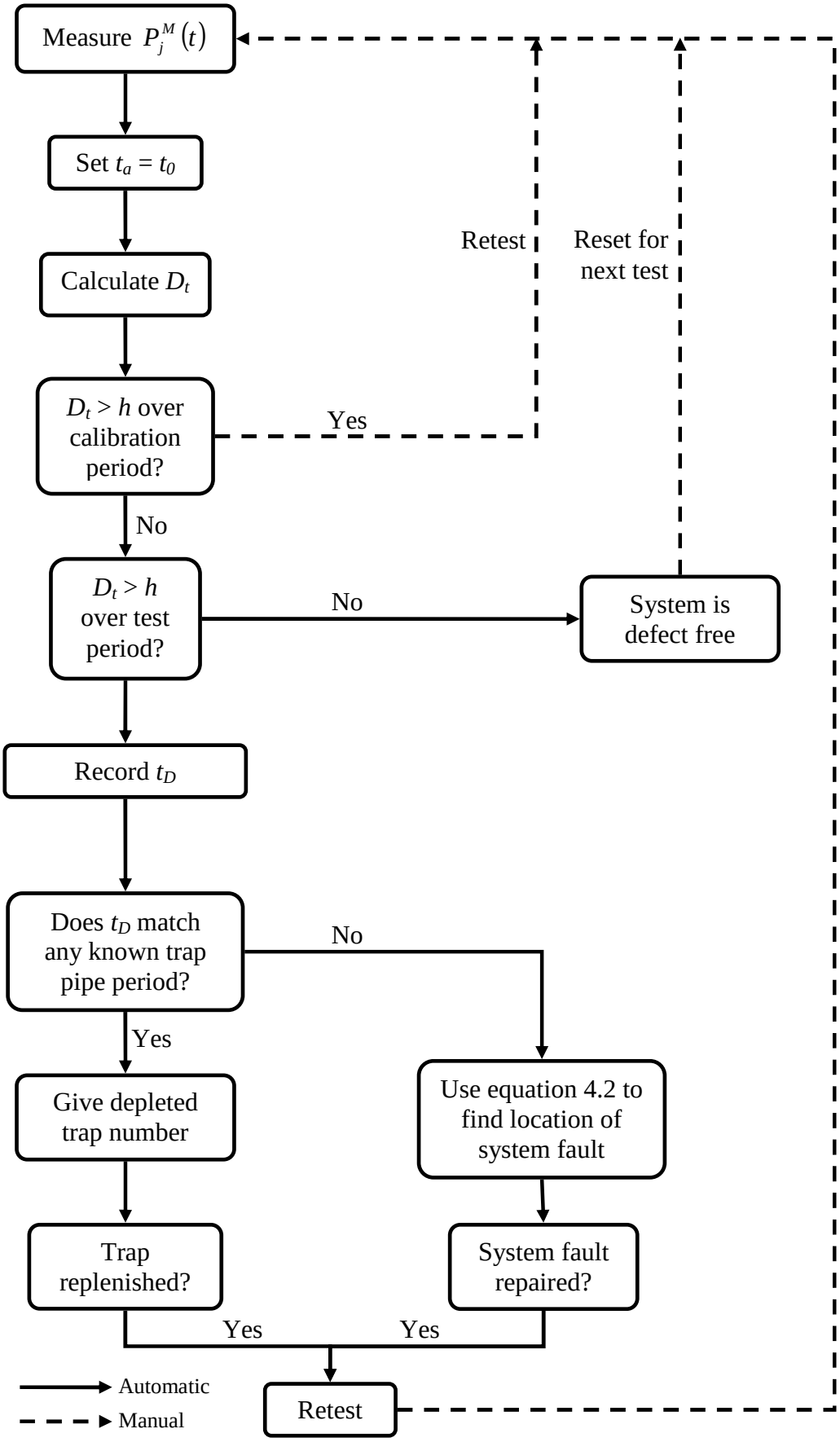

Figure 4.6 Structure diagram of the TRACER program algorithm for the automatic detection and location of depleted trap seals

4.5.3 Dealing with multiple depleted trap seals

Multiple depleted trap seals may also be identified using the TRACER program, however, as the TRACER program determines the presence and location of a depleted trap by performing a change detection test between a test system response and a defect free baseline, to identify more than one depleted trap the number of required baseline traces is increased.

To identify two simultaneously depleted trap seals, baseline traces must be obtained not only for the defect free system, but also for each possible single defect. For three simultaneously depleted trap seals, in addition to the defect free and single defect baselines, those for each combination of two depleted traps must also be obtained, and so no. If the system contains *N* trap seals of which *M* may be depleted simultaneously, then the number of baseline system responses required becomes:

$$\frac{N!}{(M-1)!\,(N-(M-1))!} \tag{4.6}$$

In large building drainage systems, the number of connected trap seals is typically large and so the possible combinations of simultaneously depleted traps make it impractical to have a full baseline database of every permutation. For this reason, the methodology adopted in this study is to use the reflected wave technique to check only for single depleted trap seals during each test. Once the first encountered trap has been detected, located and replenished, the test would then be re-run to determine if the system was now defect free. If a second depleted trap existed in the system then this would be identified in the second test and the process would continue until the system has been confirmed as defect free. This simplifies the test set up and considerably reduces the amounted of information required to carry out the test as only the defect free baseline is required.

In reality, due to the very nature of the building drainage system, the number of trap seals becoming simultaneously depleted is limited. Once a trap seal is lost, it immediately becomes a relief vent to the system, thus, reducing the likelihood of further trap seal loss.

4.6 Numerical study using artificial data

4.6.1 Introduction

Both the reflected wave technique and the TRACER program were tested using artificial transient data simulated using AIRNET. The purpose of this exercise was to verify whether the developed technique and data analysis program were capable of accurately detecting and locating depleted trap seals. A sensitivity analysis to the effects of signal noise was carried out to determine if the accuracy of the proposed method would be compromised when using data obtained from real systems which may be affected by noise.

4.6.2 System configuration

The system used to test and evaluate both the reflected wave technique and the TRACER program is shown in **Figure 4.7**.

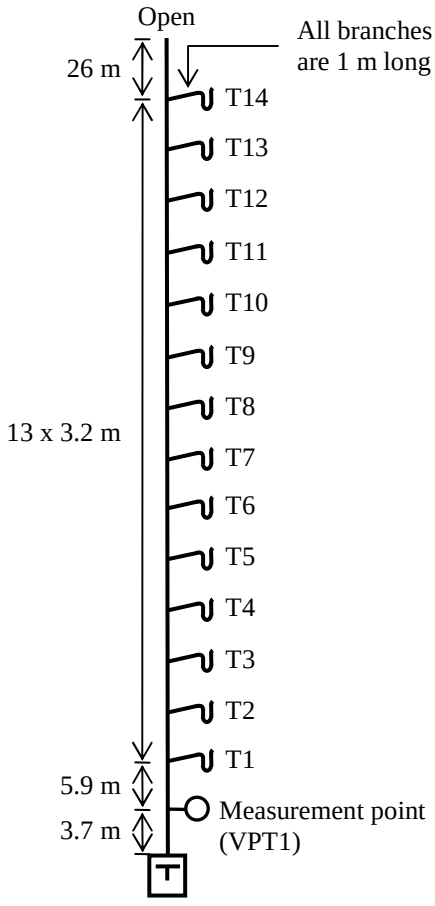

Figure 4.7 System used in numerical study

The stack had a total height L = 77.3 m and an internal diameter D = 100 mm. A single trap seal was connected at each floor level (spaced 3.2 m apart) via a 1 m branch

connection. Both branch and trap have an internal diameter D = 50 mm. The transient generator, from which the controlled test transient was applied to the system, was located at the base of the stack. The boundary condition of the pressure transient generator was based on that used in the real system: a 150 mm diameter piston moving a distance of 200 mm in 0.38 seconds. The top of the stack had an open termination to atmosphere. The measurement point was located at the end of pipe 1 (3.7 m from the stack base). The time step Δt = 0.002 s (equivalent to a 500 Hz sampling rate), the space-step Δx = 0.1 m and the wave propagation speed c = 343m/s.

4.6.3 Analysis using "perfect" numerical data

The test set-up procedure, described in Section 4.5.1.1, was performed to determine the required system data for the TRACER program. The "perfect" numerical data generated by AIRNET provides a special case as it includes no signal noise in the simulated system response. Therefore, only one defect free system response, **Figure 4.8**, is required to form the defect free baseline. **Figure 4.9** shows the defect free baseline once the test set-up procedure has been completed with t_a set to t_0. Only the first 0.6 seconds after the arrival of the incident transient is shown as this covers the pipe period of the whole system. The pipe period of each trap is indicated by the dashed vertical lines. In the absence of any signal noise the threshold value, h = 0.

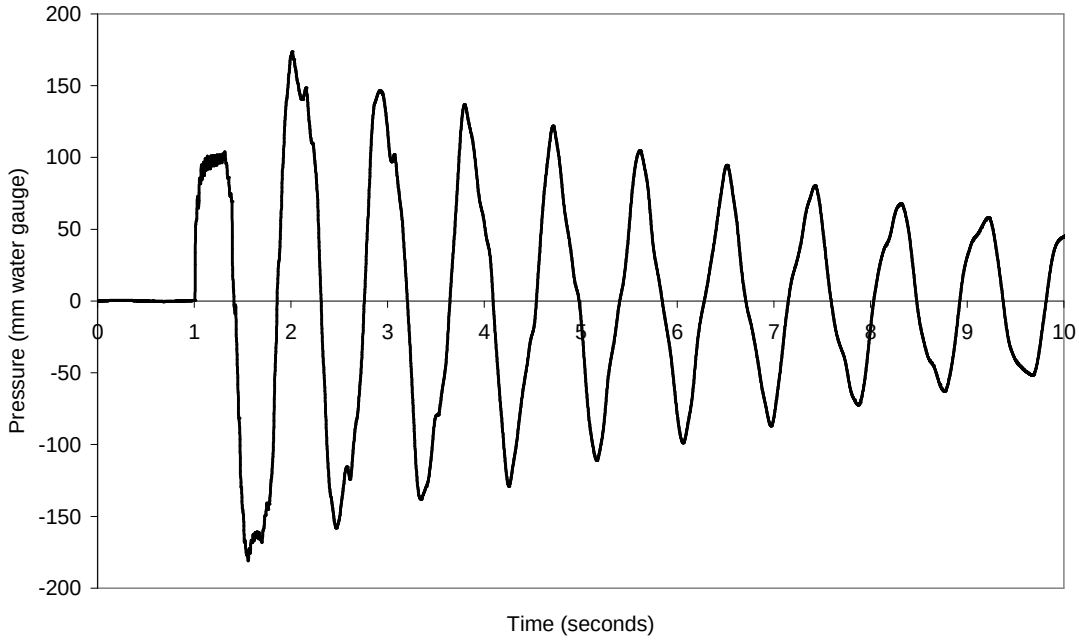

Figure 4.8 Simulated system response using AIRNET for the defect free system recorded at the measurement point (VPT1)

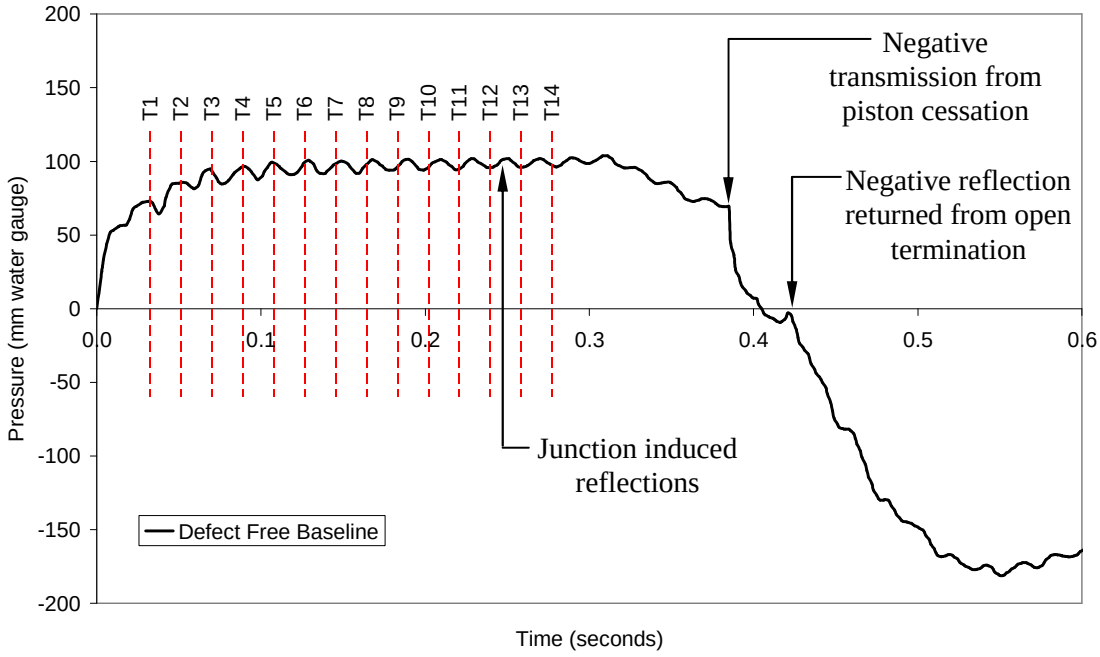

Figure 4.9 Defect free baseline following the test set-up procedure, *h* = 0

Important system information can already be identified from the defect free baseline due to the characteristic reflections imposed by every system boundary: (i) the series of small reflections present within the initial rise of the pressure wave indicates the presence of the junctions at each floor level; (ii) the negative transmission at 0.38 seconds corresponds to the cessation of the piston movement generating an equal and negative transient; and (iii) the negative reflection at 0.43 seconds corresponds with the location of the open stack termination 73.6 m from the measurement point.

System failures were simulated in AIRNET by successively setting each of the connected trap seals to the fully depleted condition. **Figure 4.10** presents the graphical output from the TRACER program for the example of a depleted trap seal at T11. **Figure 4.10(a)** indicates the effect that the depleted trap has on the simulated system response. A negative reflection can be seen to have been returned by the depleted trap which corresponds closely to the pipe period of that trap. By using Equation 4.5 to determine the closeness-of-fit, D_t, between the defect free baseline and the test system response, **Figure 4.10(b),** and determining the time at which $D_t >$ h, **Figure 4.10(c)**, the reflection arrival time, t_D, can be determined. In this example, t_D = 0.232 seconds which, from Equation 4.2, corresponds to an estimated depleted trap distance, $X_D^{estimate}$, of 39.4 m from the measurement point (i.e. [(343x0.232)/2]). The true depleted trap distance, X_D^{true}, was 38.9 m. The discrepancy between $X_D^{estimate}$ and X_D^{true} is 0.5 m, which corresponds to a trap location error of just 0.7% of the total stack height.

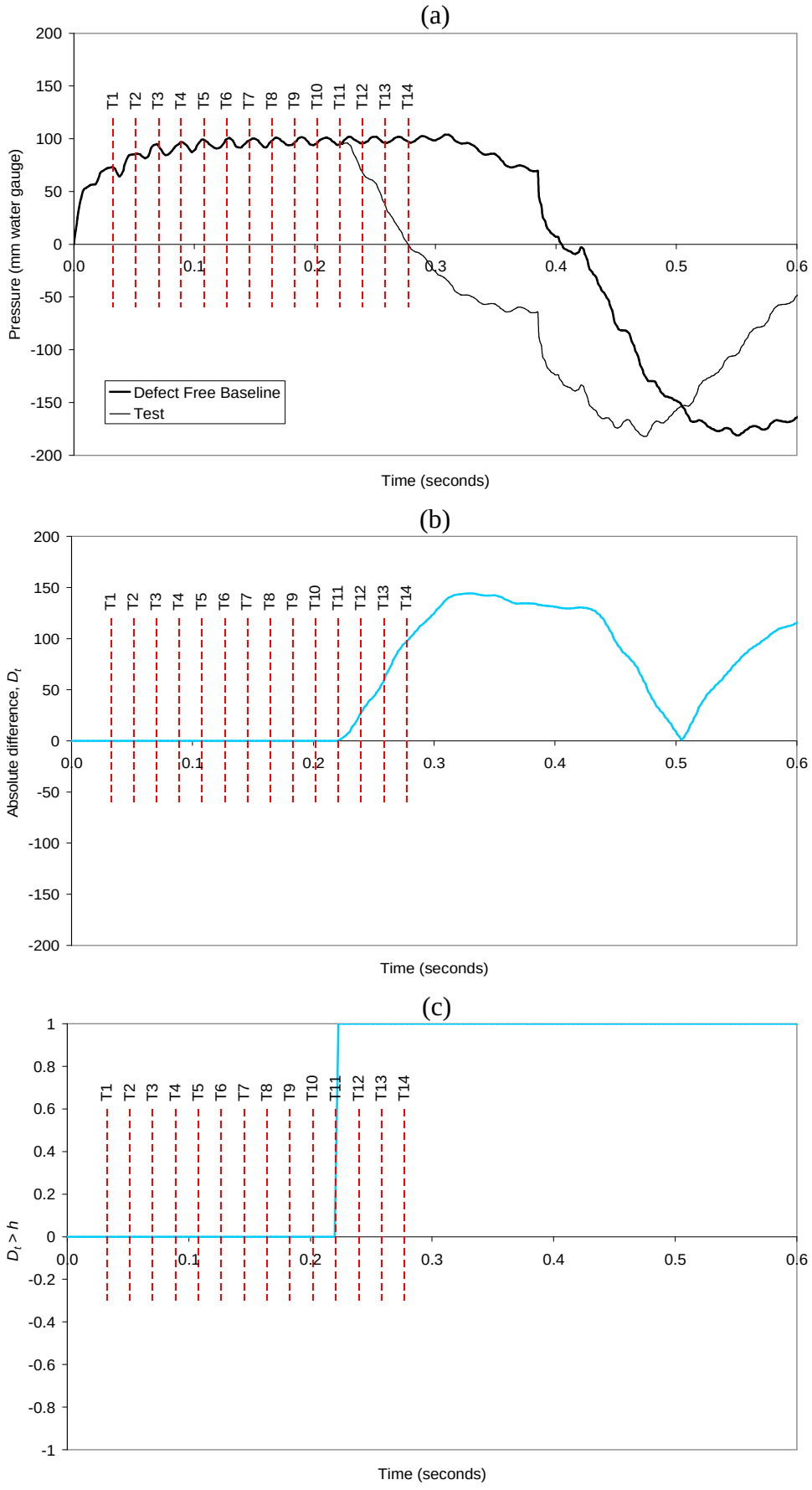

Figure 4.10 Graphical output from TRACER program for a depleted trap at T11, h = 0: (a) comparison of the simulated defect free baseline and test system response; (b) the absolute difference between the simulated defect free baseline and test system response; (c) determination of depleted trap location, $D_t > h$

Depleted trap locations, automatically determined using the TRACER program, are presented in **Table 4.1** (expressed in terms of distance from the measurement point), together with the trap location error, ε. The results show that in each case the depleted trap is detected and the location can be accurately pinpointed by the TRACER program to within 0.5 m of the true trap location (i.e. $\varepsilon < 0.7\%$) when using perfect simulated data. Interestingly, ε appears to increase with trap distance. This phenomenon will be revisited in detail in Chapter 6.

Table 4.1 Estimate of depleted trap location using the TRACER program using perfect data generated by AIRNET

Trap	X_D^{true} (m)	$X_D^{estimate}$ (m)	ε
T1	**7.0**	**7.0**	0.0%
T2	**10.0**	**10.2**	0.2%
T3	**13.3**	**13.6**	0.5%
T4	**16.5**	**16.8**	0.5%
T5	**19.7**	**20.1**	0.5%
T6	**23.0**	**23.3**	0.5%
T7	**26.2**	**26.5**	0.5%
T8	**29.2**	**29.6**	0.5%
T9	**32.5**	**33.0**	0.7%
T10	**35.7**	**36.2**	0.7%
T11	**38.9**	**39.4**	0.7%
T12	**42.2**	**42.7**	0.7%
T13	**45.2**	**45.7**	0.7%
T14	**48.5**	**49.0**	0.7%

A further source of error is attributable to the choice of appropriate time step. If the arrival of the depleted trap induced reflection occurs between two successive time steps then t_D is taken as the greater of the two. In this case, when $\Delta t = 0.002$ seconds (corresponding to a data sampling rate of 500 Hz) the maximum time step error is ≤ 0.686 m, when $c = 343$ m/s. The importance of selecting an appropriate time step, on the accuracy of the test, will be revisited later in Chapter 5.

4.6.4 Analysis using numerical data with added random signal noise

To simulate the effects of measurement interference and system noise, which may be present in real data, and to determine the likely effect these may have on the accuracy of the TRACER program, increasing levels of random signal noise were added to the

"perfect" numerical data, P, generated by the AIRNET model. The signal noise term, S_N, is described by the expression:

$$S_N = sin[\theta\ \psi\ \emptyset_h] \tag{4.7}$$

Where θ is the peak angular deviation in radians, ψ is a random phase with a uniform distribution over the range 0 - 2π, and $\emptyset_h$ is the peak amplitude multiplier corresponding to the desired value of threshold value, h. The final system response, P_o, is given by:

$$P_o = P + S_N \tag{4.8}$$

The noise is randomly distributed and was set to produce maximum threshold values of 5, 10, 15, and 20 mm water gauge when compared to the defect free baseline. In each case, the number of defect free system responses used to determine the defect free baseline and threshold values was N = 20. The graphical outputs are shown for each case in **Figures 4.11** to **4.14** respectively.

Table 4.2 presents the estimated depleted trap locations having been automatically determined using the TRACER program. It can be seen that for all cases the presence of a depleted trap within the system is successfully detected, however, the accuracy of determining the location of the trap decreases with increasing levels of signal noise. While the maximum discrepancy between X_D^{true} and $X_D^{estimate}$ was just 0.5 m (ε = 0.7%) when h = 0, this increased to 1.5 m (ε = 2.0%) for h = 5. The maximum discrepancy then increased further to 2.1 m (ε = 2.9%), 2.4 m (ε = 3.3%) and 2.8 m (ε = 3.8%) when h = 10, h = 15 and h = 20, respectively.

While the relative errors are small, due to the large overall height of the simulated stack, the discrepancy between X_D^{true} and $X_D^{estimate}$ indicate that high levels of signal noise may significantly compromise the sensitivity and effectiveness of the reflected wave technique and the TRACER program, both of which rely on a clear indication of the arrival time of the trap induced reflection.

Signal noise has already been identified as a major concern in the estimation of leakage location and the determination of valve settings in water distribution networks (Beck *et al.* 2002; Stephens *et al.* 2004). However, the methodology discussed here differs from

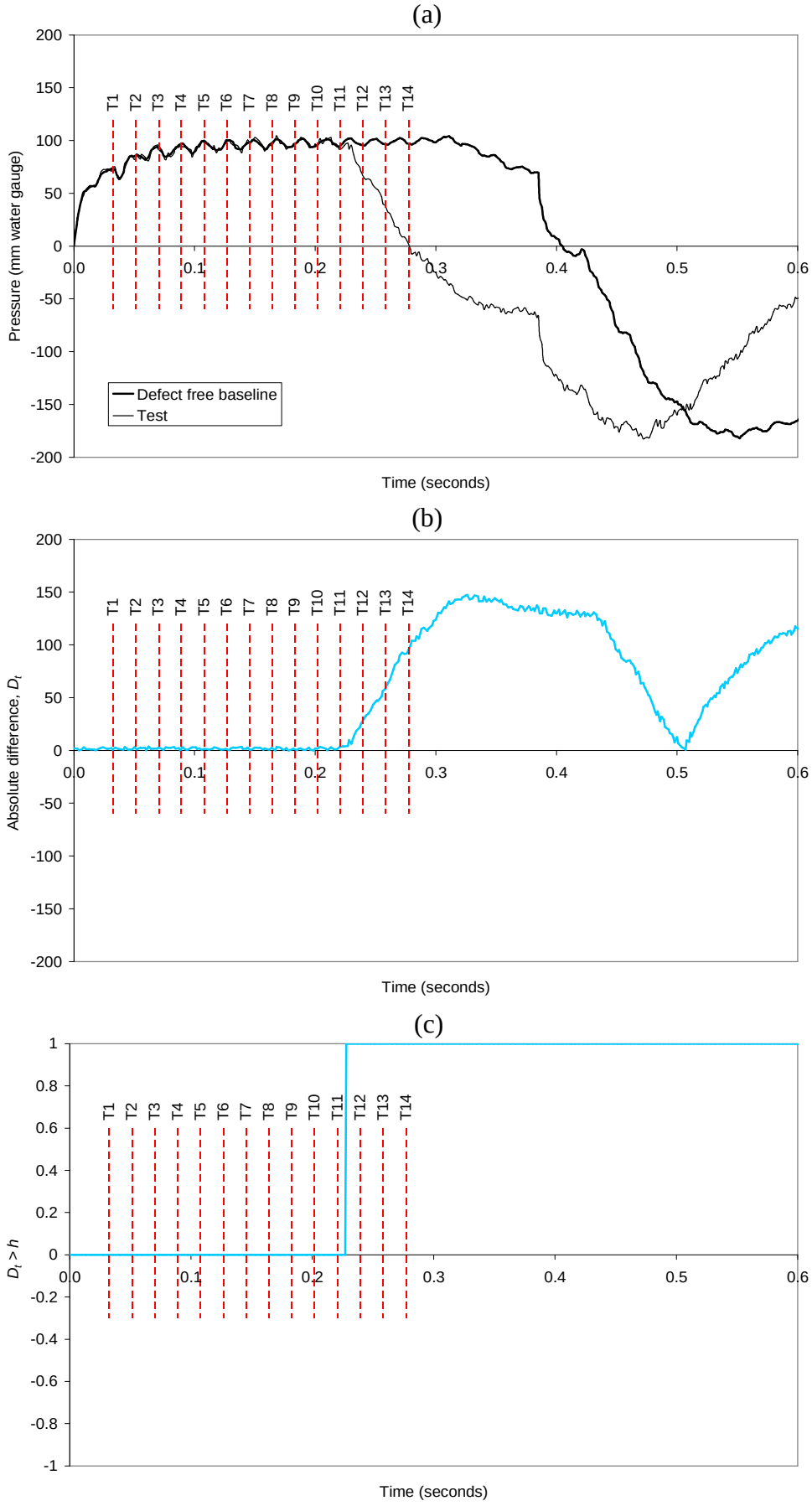

Figure 4.11 Graphical output from TRACER program for a depleted trap at T11, h = 5: (a) comparison of the simulated defect free baseline and test system response; (b) the absolute difference between the simulated defect free baseline and test system response; (c) determination of depleted trap location, $D_t > h$

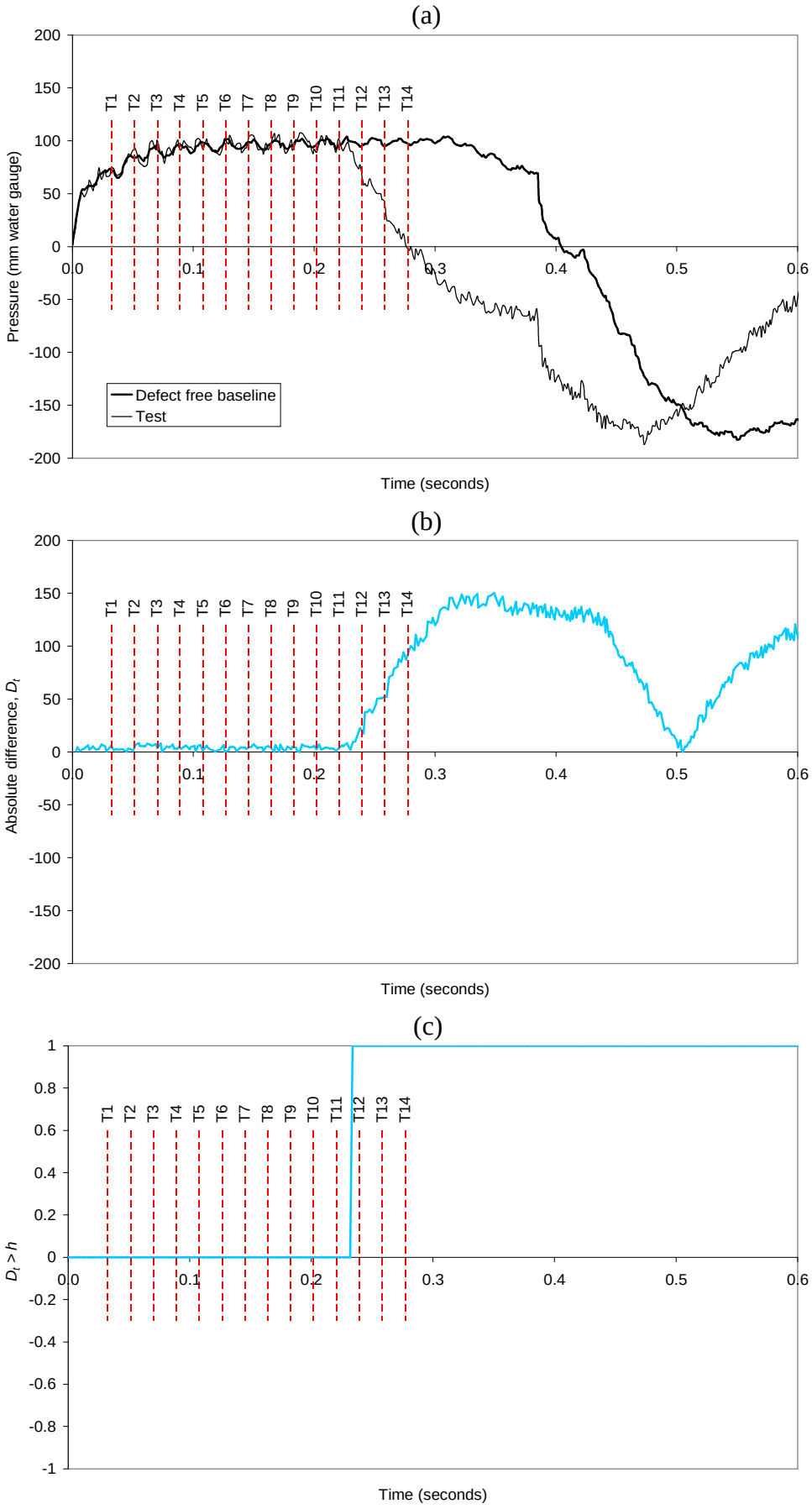

Figure 4.12 Graphical output from TRACER program for a depleted trap at T11, h = 10: (a) comparison of the simulated defect free baseline and test system response; (b) the absolute difference between the simulated defect free baseline and test system response; (c) determination of depleted trap location, $D_t > h$

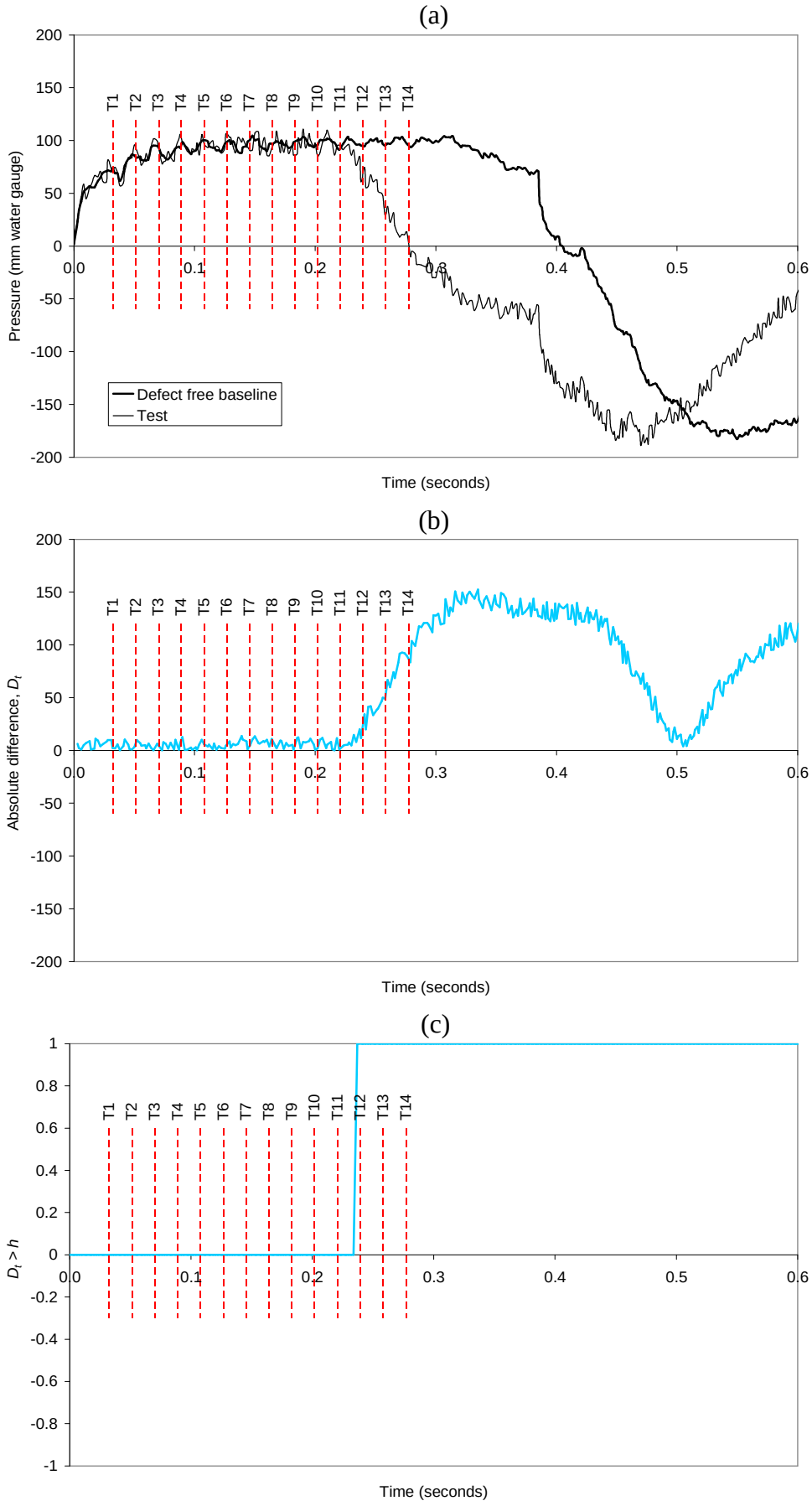

Figure 4.13 Graphical output from TRACER program for a depleted trap at T11, *h* = 15: (a) comparison of the simulated defect free baseline and test system response; (b) the absolute difference between the simulated defect free baseline and test system response; (c) determination of depleted trap location, $D_t > h$

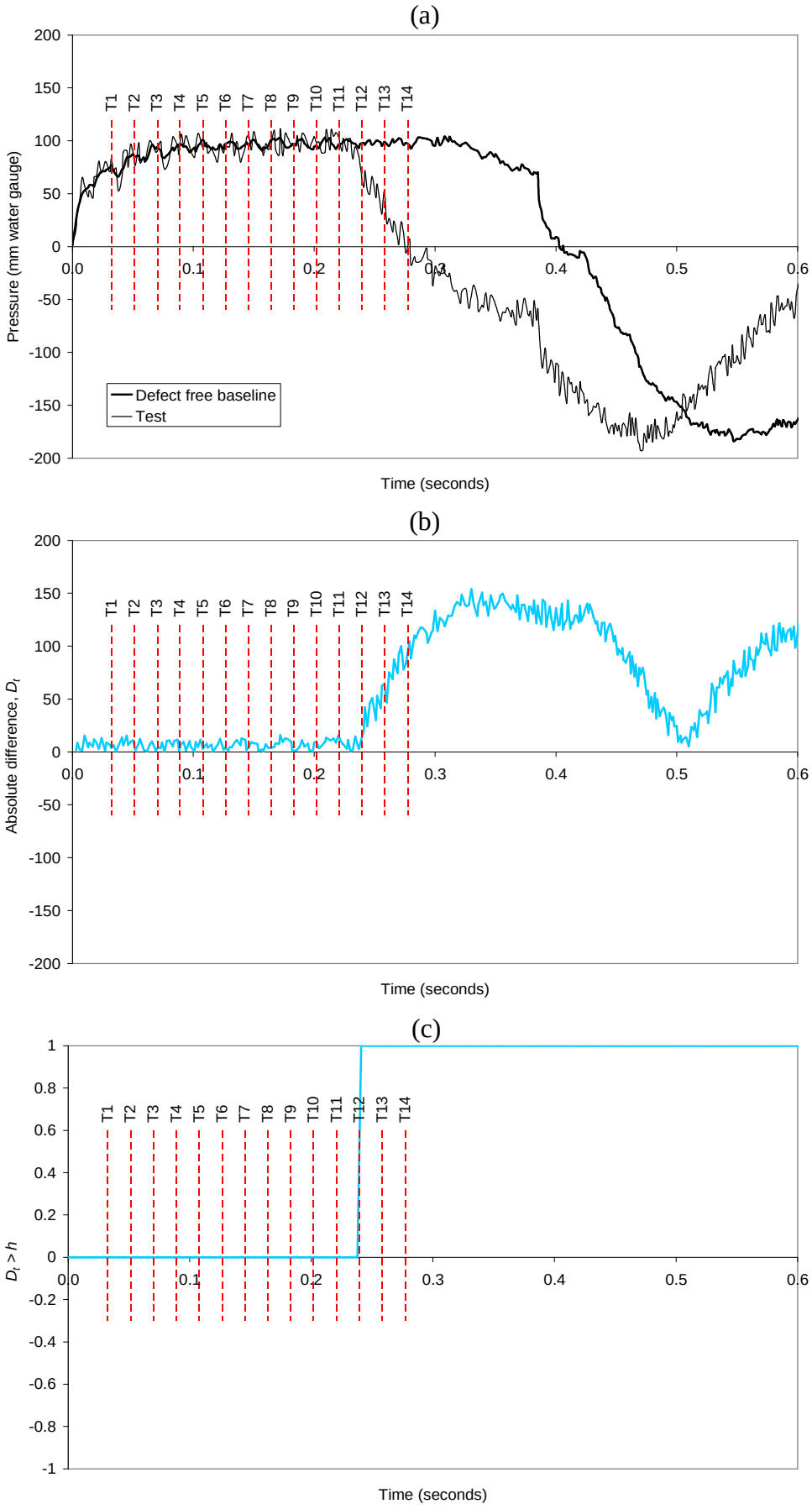

Figure 4.14 Graphical output from TRACER program for a depleted trap at T11, *h* = 20 mm water gauge: (a) comparison of the simulated defect free baseline and test system response; (b) the absolute difference between the simulated defect free baseline and test system response; (c) determination of depleted trap location, $D_t > h$

Table 4.2 Estimate of depleted trap location using the TRACER program for data generated by AIRNET with increasing levels of signal noise

Trap characteristics		***h = 0***		***h = 5***		***h = 10***		***h = 15***		***h = 20***	
Trap No.	X_D^{true} (m)	$X_D^{estimate}$ (m)	ε	$X_D^{estimate}$ (m)	ε	$X_D^{estimate}$ (m)	ε	$X_D^{estimate}$ (m)	ε	$X_D^{estimate}$ (m)	ε
T1	**7.0**	**7.0**	0.0%	**7.8**	1.2%	**7.1**	0.3%	**8.3**	1.9%	**7.1**	0.3%
T2	**10.0**	**10.2**	0.2%	**10.9**	1.1%	**10.9**	1.1%	**11.4**	1.8%	**11.4**	1.8%
T3	**13.3**	**13.6**	0.5%	**14.3**	1.4%	**14.3**	1.4%	**14.6**	1.8%	**15.6**	3.1%
T4	**16.5**	**16.8**	0.5%	**18.0**	2.0%	**18.5**	2.7%	**17.9**	1.9%	**18.7**	3.0%
T5	**19.7**	**20.1**	0.5%	**20.9**	1.6%	**21.1**	1.9%	**22.1**	3.3%	**21.8**	2.9%
T6	**23.0**	**23.3**	0.5%	**23.8**	1.2%	**25.0**	2.9%	**25.0**	2.9%	**25.0**	2.9%
T7	**26.2**	**26.5**	0.5%	**26.9**	1.1%	**28.1**	2.7%	**28.1**	2.7%	**27.5**	1.9%
T8	**29.2**	**29.6**	0.5%	**29.9**	0.8%	**30.4**	1.5%	**31.6**	3.1%	**30.4**	1.5%
T9	**32.5**	**33.0**	0.7%	**33.7**	1.6%	**33.7**	1.6%	**34.7**	3.0%	**34.7**	3.0%
T10	**35.7**	**36.2**	0.7%	**36.9**	1.6%	**37.6**	2.6%	**37.7**	2.7%	**38.1**	3.3%
T11	**38.9**	**39.4**	0.7%	**40.0**	1.5%	**40.8**	2.6%	**40.0**	1.5%	**41.7**	3.8%
T12	**42.2**	**42.7**	0.7%	**42.5**	0.5%	**43.5**	1.9%	**44.2**	2.9%	**43.2**	1.5%
T13	**45.2**	**45.7**	0.7%	**45.9**	0.8%	**47.3**	2.7%	**46.6**	1.8%	**47.9**	3.5%
T14	**48.5**	**49.0**	0.7%	**49.0**	0.7%	**50.0**	2.0%	**50.7**	3.0%	**51.2**	3.7%
		ε_{MAX}	0.7%	ε_{MAX}	2.0%	ε_{MAX}	2.9%	ε_{MAX}	3.3%	ε_{MAX}	3.8%

previous water network applications as the depleted trap detection test will be performed in a quiescent system in which the system noise arising from pre-existing flows will be avoided.

From experience, from both laboratory and field investigations, the actual level of signal noise present in real system data should not normally exceed around 5 mm water gauge which, from this numerical study, can be shown to provide estimated depleted trap locations within satisfactory limits (i.e. within 1.5 m).

The higher levels of signal noise are used in this study for worst case comparative analysis only. It is reassuring that even when subject to unrealistically high levels of signal noise, the reflected wave technique, together with the TRACER program, can estimate the location of a depleted trap to within 3 m and would therefore identify both a floor and bathroom location of the defect if not the exact trap.

4.7 Chapter summary

After reviewing the methods currently available for defect detection in pipe systems, this chapter has introduced the reflected wave technique which has, for the first time, been applied to the detection and location of depleted trap seals within the building drainage system. The presence of a depleted trap seal has been shown to be detectable by virtue of its influence on the overall system response and its location can be determined from the arrival time of the consequent reflection. The condition of the system can be systematically determined by comparing the measured test system response with the defect free baseline.

The TRACER program has been introduced and developed to allow automatic determination of system conditions, removing the requirement for user interrogation. The sensitivity of the TRACER program has been tested using simulated data and has demonstrated an acceptable degree of accuracy even when high levels of signal noise are present in the measured system response data.

Chapter 5
Experimental development of the reflected wave technique for the detection and location of depleted trap seals

5.1 Introduction

5.1.1 General

An extensive series of laboratory and field tests have been undertaken to gather system response data to evaluate the performance and support the development of the reflected wave technique for the detection and location of depleted trap seals. A total of five experimental test programmes were carried out which allowed the technique to be assessed against a number of different building drainage systems of different configurations and sizes. The initial test evaluation used a single positive pressure pulse as the incident transient while subsequent tests used a 10 Hz sinusoidal wave to ensure the technique provides a non-invasive approach to system monitoring. This chapter outlines the development of the technique and describes both the drainage systems used and the test methodologies employed to gather the system response data.

5.1.2 Range of system configurations tested

A number of different drainage stacks were used during these experimental investigations – all of which were of the single stack design (i.e. all appliances drain to one main stack which also provides the system ventilation – a more detailed description of drainage system design can be found in Swaffield and Galowin, 1992). For the preliminary laboratory tests, an existing test-rig was extended to evaluate the test parameters under controlled conditions. A second laboratory test-rig was designed and constructed by this author to allow analysis of the effect of various common system boundaries.

To assess the practical application of the technique, data was collected from three sets of field trials. The first set of field trials were carried out on the drainage system of an unoccupied residential building in Dundee just prior to it being demolished. The second set of field trials were conducted on the drainage system within an academic building at

Heriot-Watt University. The final set of field trials were performed on the drainage system of an office building in Glasgow.

Each of the different drainage stacks will be described in detail, however, **Table 5.1** summarises the most relevant information for each. It can be seen that the stacks selected cover a range of system complexity with the number of connected appliance trap seals ranging from 5 to 112.

5.1.3 Test parameters

As discussed in Chapter 4, to achieve systematic system monitoring, the reflected wave technique is used, in conjunction with the TRACER program, to provide automated test scheduling and data analysis for the automatic detection and location of depleted trap seals. The test procedure involves the estimation of the arrival time of the trap induced reflection using a time series change detection test by comparing the defective system response with a previously determined defect free baseline. The success of the procedure relies on the ability to produce a repeatable test transient and to accurately measure the system response to that transient. Throughout the development of the technique four main factors were identified as being fundamental to its success:

i. to generate and apply a suitable and repeatable test transient to which the system response would be measured and which itself would not pose a threat to the integrity of the system.

ii. to determine the optimum location to introduce the test transient into the system.

iii. to develop a means to accurately measure the system response to the applied test transient.

iv. to develop a knowledge and awareness of the effect of different drainage system components on the measured system response and understand their effect on the accuracy of the reflected wave technique.

These four factors were addressed throughout the experimental test programme and will be discussed in the following sections.

Test set	Stack diameter (mm)	Stack material	Total number of floors	Number of floors with connected appliances	Total number of connected appliances	Incident transient used for testing
HWU 1 *(laboratory)*	75 & 100	uPVC	14	14	14	Single pressure pulse
Dundee *(field)*	150	Cast Iron	17	16	64	Single pressure pulse
HWU 2 *(laboratory)*	100	uPVC	5	5	5	10 Hz sinusoidal wave
HWU Arrol *(field)*	100	uPVC	5	3	21	10 Hz sinusoidal wave
Glasgow WC *(field)*	100	Cast Iron	8	7	28	10 Hz sinusoidal wave
Glasgow WHB *(field)*	100	Cast Iron	8	7	14	10 Hz sinusoidal wave
Glasgow multi-stack *(field)*	100	Cast Iron	8	7	112	10 Hz sinusoidal wave

Table 5.1 Summarised details of the building drainage systems used for testing

5.2 Experimental testing

5.2.1 General

The following section describes the different drainage stacks used and the experimental testing undertaken. The test procedure generally applies to all five test sets, however, where any differences in methodology occur for a particular test set or where the development of the technique has prompted advances to the test method or equipment, details and reasons will be provided.

5.2.2 Preliminary laboratory tests at Heriot-Watt University

5.2.2.1 General

A preliminary evaluation of the reflected wave technique for the detection and location of depleted trap seals was undertaken using an existing experimental test-rig (HWU 1 (*laboratory*) system) constructed at Heriot-Watt University during previous EPSRC funded research.

These initial laboratory-based investigations used a single positive pressure pulse as the incident transient with the purpose of: (i) investigating the effect of a depleted trap on the measured system response; (ii) establishing if a depleted trap can be detected through the analysis of the system response; (iii) determining the level of accuracy in locating a depleted trap; (iv) preparing for future field trial data collection.

5.2.2.2 Experimental test-rig

The test-rig was designed to replicate a 14-storey single stack building drainage system with a single trap connected on each floor, *Configuration I* (**Figure 5.1**). Due to height limitations within the laboratory the test-rig was constructed in a looped configuration using pipes made from unplasticised polyvinyl chloride (uPVC). Looping the system in this way provided the opportunity to simulate a drainage system many times larger than would normally have been possible within the constraints of the laboratory and was made possible by the fact that the proposed monitoring technique is designed to be used during system quiescence when no water flow would be present within the stack thus allowing an air-only test-rig. The effect of the looped bends on the system response was negligible (Wood and Chao, 1971).

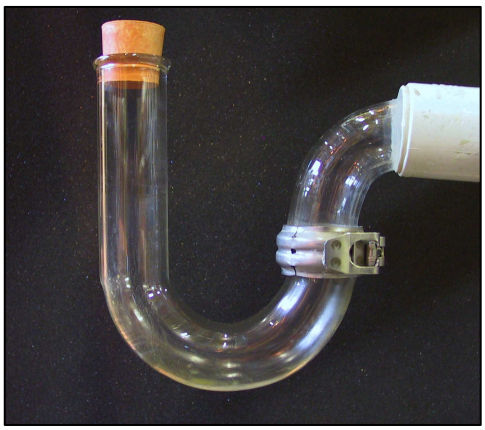

Traps capped using rubber stopper

View of test rig showing the looped pipework

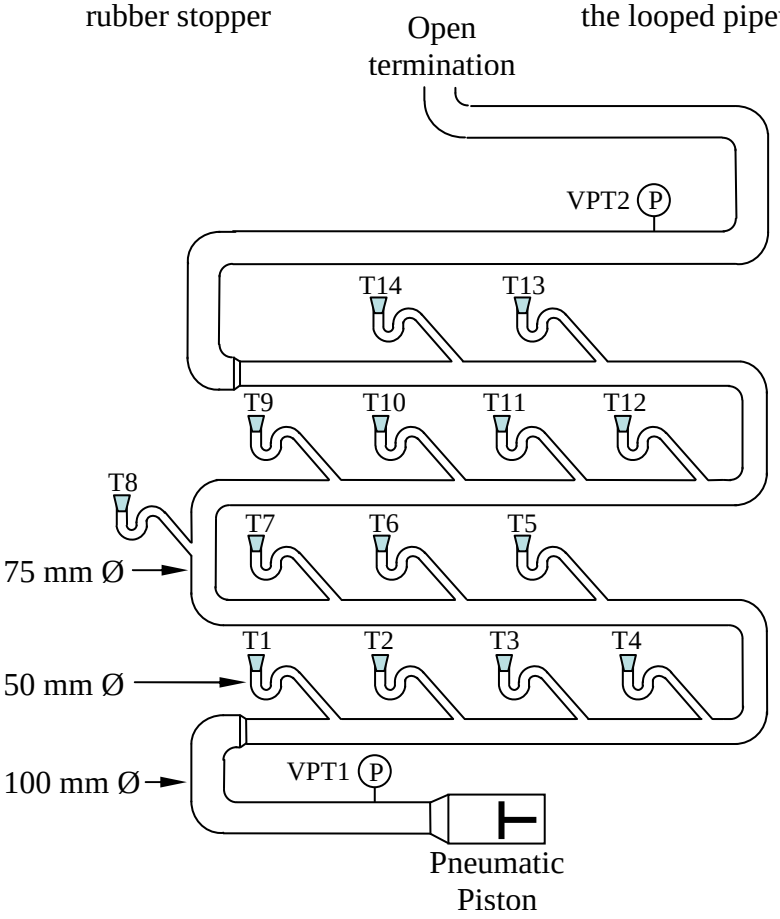

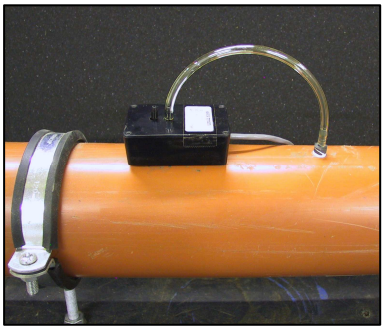

Connection of pressure transducer (VPT1) onto stack

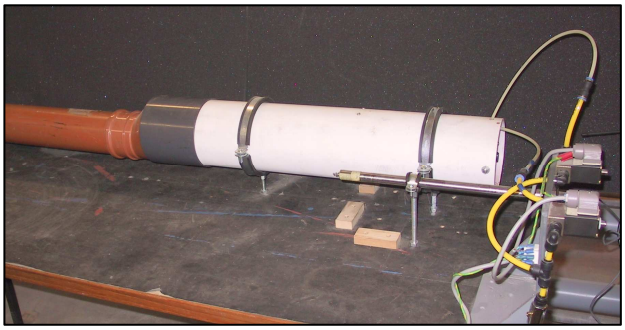

Pneumatic piston installed at base of stack

Figure 5.1 Laboratory test-rig: HWU 1 (laboratory) system, *Configuration I*

Due to limited resources at the time of construction, the test-rig was assembled using both 100 mm and 75 mm diameter uPVC pipes to construct the main stack with 50 mm diameter uPVC traps connected to the stack via 50 mm diameter uPVC branch pipes. The pipework was supported from a scaffold frame using pipe clamps, 2 m spaced, to fix the pipe in place and to restrain it from any movement or vibrations during testing.

5.2.2.3 Generation of the test transient

The single positive pressure pulse, used as the incident transient, was generated by a pneumatic piston connected at the base of the stack. The piston consisted of a 150 mm diameter uPVC cylinder and disc which was driven by a pneumatic ram with a stroke length of 200 mm.

The displacement of the piston was measured using a linear variable differential transformer (LVDT). The LVDT consists of a cylindrical array of three coils (one primary coil and two secondary coils) though which an armature core is passed. The primary coil is excited with an AC current and the movement of the armature core is detected by a differential change in output between the two secondary coils. With the core in the central position, the coupling from the primary to each secondary is equal and opposite and therefore cancel out, thus the resultant output voltage is zero. Movement of the core from this position in either direction causes a proportional change to the voltage output and therefore indicates displacement and direction from the central zero position.

5.2.2.4 LVDT calibration

The LVDT was calibrated before use by measuring the voltage output from a known displacement of the core. The calibration data and derived calibration equation are shown in **Figure 5.2**. The results show a linear relationship for the two variables in the form:

Displacement = m x (voltage) + c

where m is the gradient of the line fit and c is the y-axis intercept.

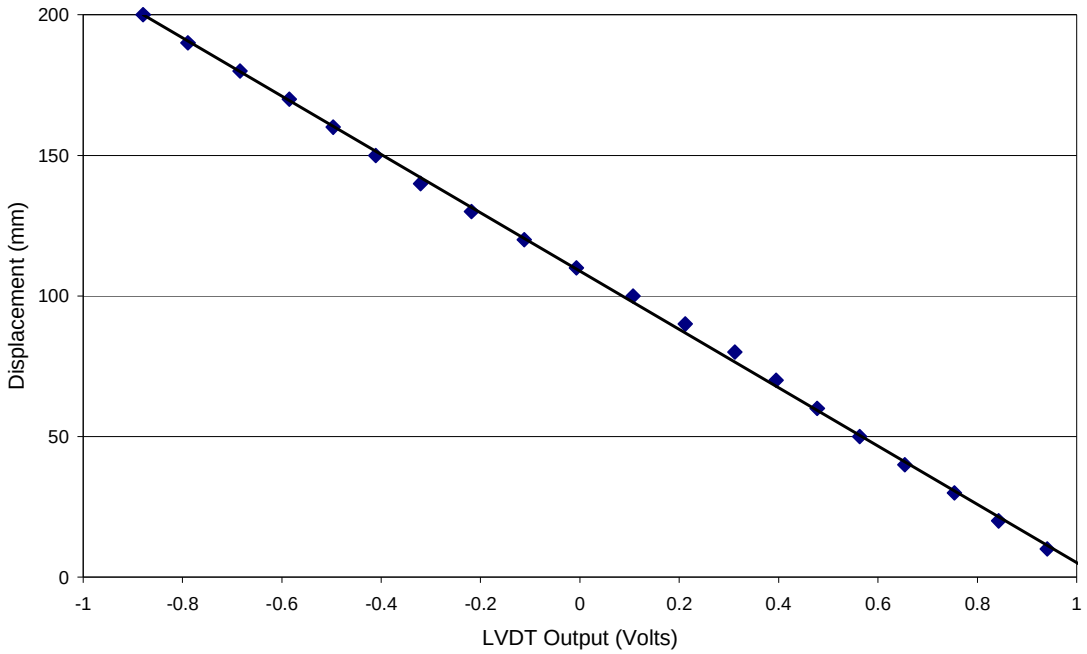

Calibration Equations, LVDT: Displacement = -103.75 x (voltage) + 108.84

(R^2 = 0.9993)

Figure 5.2 LVDT calibration data and calibration equations

5.2.2.5 System response measurement and data acquisition

The system used to measure the pressure response consisted of two pressure transducers, a data acquisition board and a central monitoring computer. Two pressure transducers (VPT1 and VPT2) were located on the main stack at the positions indicated on **Figure 5.1** and were connected into the stack via screwed tappings and small diameter PVC tubing. Measuring the system response at these two locations would allow the wave propagation speed to be later calculated.

The pressure transducers selected were voltage output pressure/vacuum transducers (Sensor Technics, model 113LP25D-PCB) with a voltage output range of 1 to 6 volts and a pressure range of ±250 mm water gauge (approximate non-linearity of ± 0.25%) as these allowed both positive and negative pressures to be monitored and were suitable for the magnitude of pressures that would be experienced during testing. The data acquisition board (Keithley, model KPCI-3116) had 32 analogue input channels and a maximum sampling rate of 250 kHz.

5.2.2.6 Transducer calibration

Each pressure transducer was calibrated before use by measuring the variation in voltage output corresponding to a change of known applied water pressure. The calibration data and derived calibration equations for each transducer are shown in **Figure 5.3**.

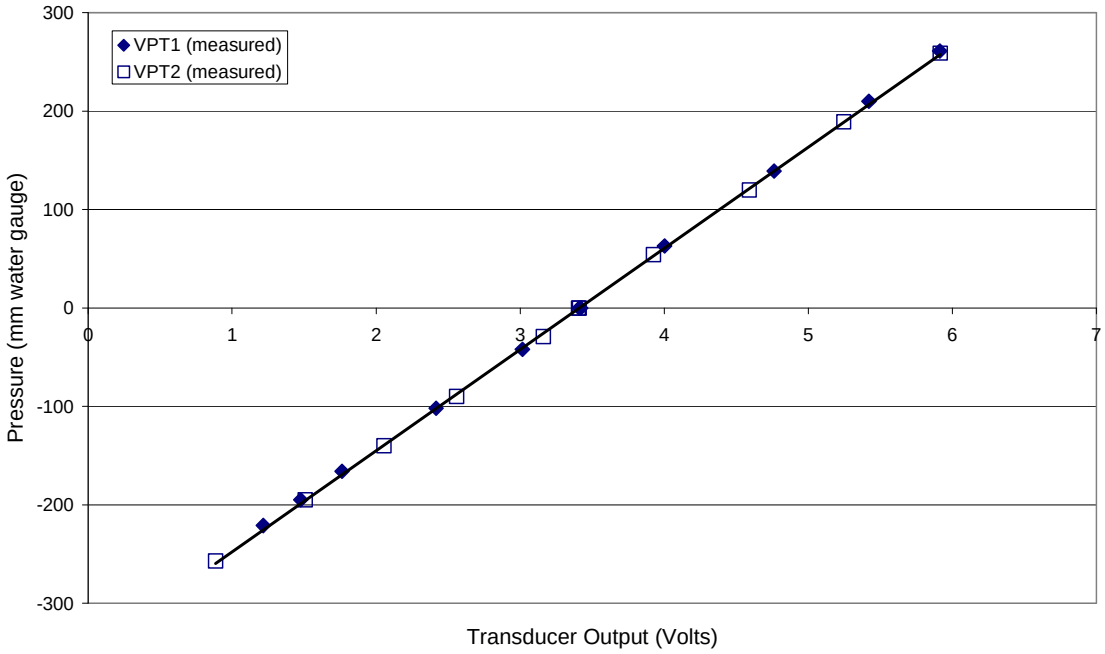

Calibration Equations, VPT1: Pressure = 102.62 x (voltage) + 348.25

(R^2 = 0.9998)

VPT2: Pressure = 102.74 x (voltage) + 350.52

(R^2 = 0.9999)

Figure 5.3 Transducer calibration data and calibration equations

The results gave a linear relationship for the two variables in the form:

Pressure = m x (voltage) + c

where m is the gradient of the line fit and c is the y-axis intercept. To allow for any changes in atmospheric conditions the difference in voltage between that recorded during testing and that recorded during atmospheric conditions just prior to testing was used to calculate pressure, where:

Δ Voltage = Test Voltage – Atmospheric Voltage

Thus ensuring that the calculated pressure values can be attributed only to the imposed transient event. From the voltage difference recorded during testing, it was therefore possible, to calculate the change in pressure using the gradient of the calibration line as the conversion factor, since:

$$\Delta \text{ Pressure} = [\ m \times (\text{voltage}_{test}) + c\ ] - [\ m \times (\text{voltage}_{atmospheric}) + c\ ]$$

which gives:

$$\Delta \text{ Pressure} = m \times (\text{voltage}_{test} - \text{voltage}_{atmospheric})$$

This relationship was then used to convert all subsequent transducer output voltage data into pressure.

5.2.2.7 Simulation of a depleted trap seal

At this initial stage of investigation the traps were not primed with water but instead were capped off using a rubber stopper. The stopper was removed to simulate a defective trap and then replaced to simulate a fully primed trap.

5.2.2.8 Data Collection

The test set-up process, described in Section 4.5.1.1, was used to determine the system information required by the TRACER program. A set of 20 system responses were recorded in order to calculate the defect free baseline. With all traps capped off the system response was measured (using a data sampling rate of 500 Hz) in response to the applied incident transient generated by activation of the piston.

A typical defect free system response is presented in **Figure 5.4** which shows the system response measured at both VPT1 and VPT2. The difference between the transient arrival time measured at VPT1 and VPT2 will be used to estimate the wave propagation speed in Section 6.3 in Chapter 6. It can be seen that the piston travels a forward distance of 200 mm in 0.39 seconds which generates a positive pressure pulse which attains a peak magnitude of 100 mm water gauge (VPT1). The coincidence of the piston stopping (which generates a negative transient equal in magnitude to the incident transient) and the arrival and re-reflection with a +1 reflection coefficient at the stationary piston of the negative reflection induced by the open termination (which is

also equal in magnitude to the incident transient) have the combined effect of reducing the pressure by 300 mm to around -200 mm water gauge. It is these transients which are then propagated back and forth within the system until they eventually attenuate due to pipe frictional effects.

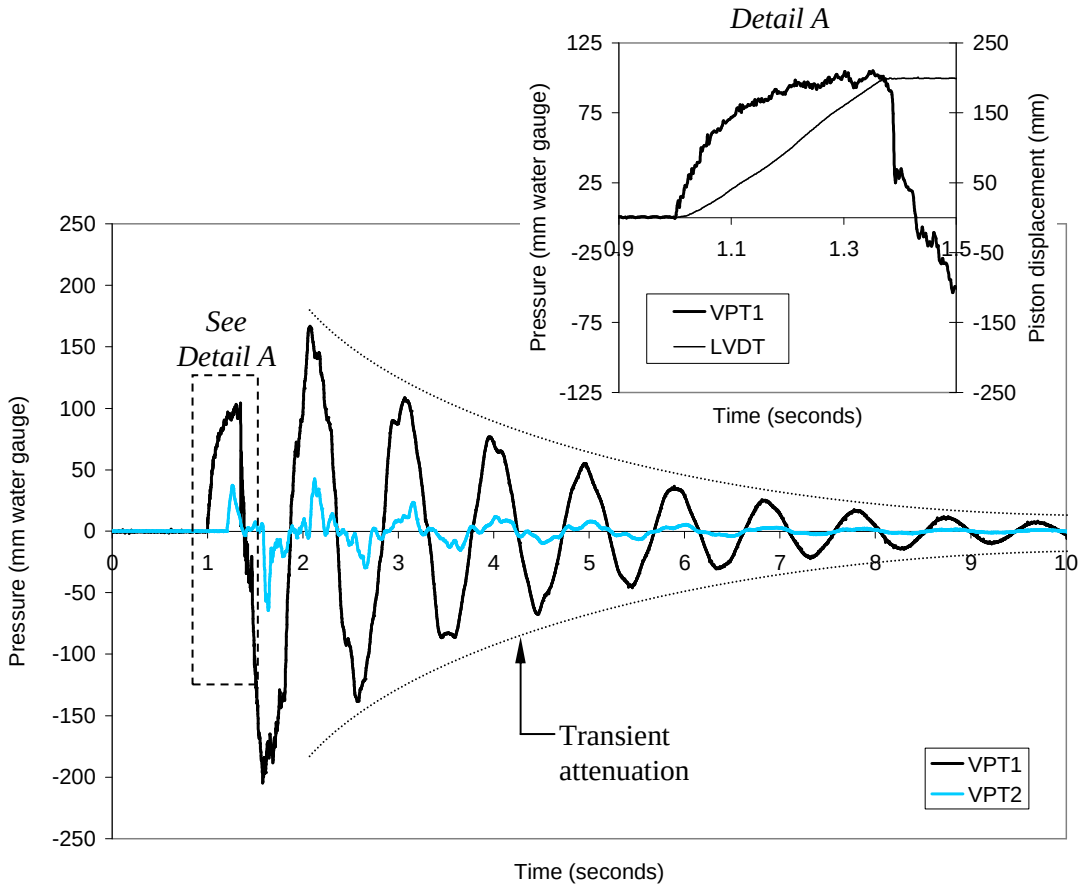

Figure 5.4 Typical defect free system response measured at VPT1 and VPT2 in response to a single positive pressure pulse for *Configuration I*. Detail A shows the system response between 0.9 and 1.5 seconds and includes the piston displacement as measured by the LVDT

Once all 20 traces were collected, and the transient arrive time, t_a, set to time zero, t_0, the defect free baseline, P_j^{DF}, and the threshold value, h, were calculated using Equations (4.3) and (4.4), respectively, **Figure 5.5**. In this case, h = 6 mm water gauge, thus providing the expected signal variation for the defect free system.

Once all of the required system information had been acquired, the system response was measured for each failure condition by opening each trap in turn.

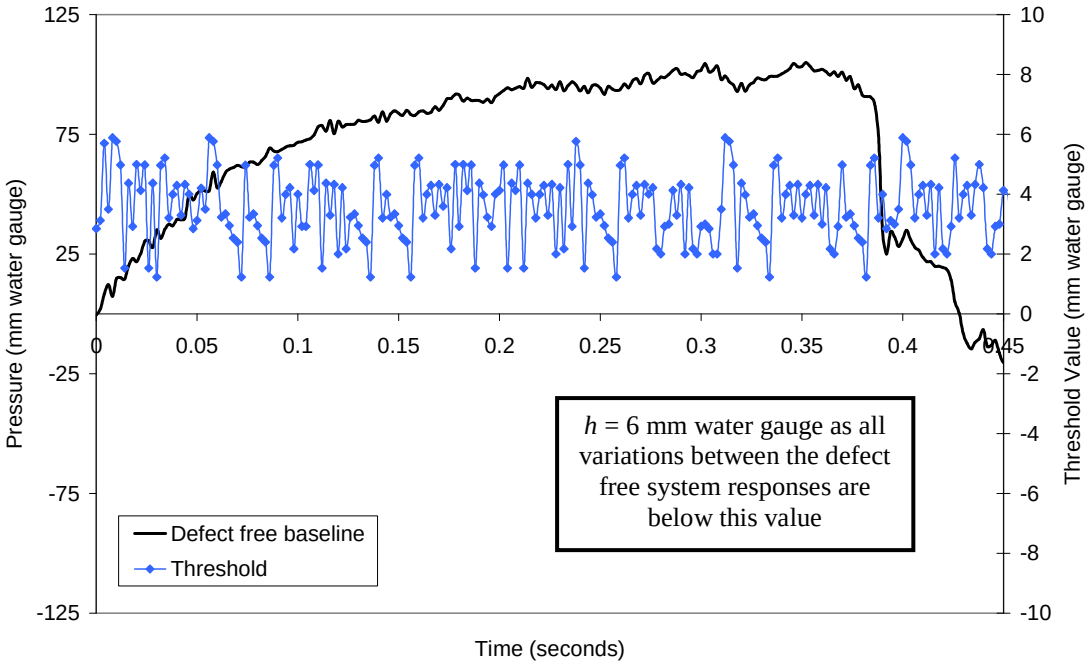

Figure 5.5 Calculated defect free baseline, P_j^{DF}, and threshold value, *h*, for *Configuration I*, *h* = 6 mm water gauge

5.2.3 Experimental field trials in a residential building in Dundee

5.2.3.1 General

Access to test the drainage system of an unoccupied 17-storey residential building in Dundee was granted by the Sanctuary Scotland Housing Association and allowed the practical assessment of the reflected wave technique using the single positive pressure pulse as the incident transient. Constructed around 1965 the building was awaiting demolition as part of the City of Dundee's regeneration project, thus allowing full and unrestricted access for testing. The building was divided into three blocks each containing six flats per floor. The ground floor housed a double height internal clothes drying area and so the flats were located on Floors 2 to 17 only.

5.2.3.2 System description

The building drainage system consisted of multiple single stacks, each collecting the waste from a single flat on each floor, and each terminating through the roof with an open end penetration. Just below this termination there was a branch connection into the stack from the roof rainwater collection drain.

For the purposes of this investigation one stack was selected for testing and this was chosen by its ease of access. Prior to testing, a full and exhaustive survey of the stack

was carried out to determine the system configuration and dimensions. **Figure 5.6** provides a summary of the results together with a schematic of the system showing the branch connection arrangement at each floor. It will be seen that the stack has a diameter of 150mm and collects the waste from the wc, wash-hand-basin, sink and bath from each flat.

5.2.3.3 Generation of the test transient

The pneumatic piston was used to generate a single positive pressure pulse. To minimise disruption to the system and to facilitate easy installation of the test equipment, the piston was connected onto the stack via an existing 75 mm diameter access panel. A connector was manufactured to allow the piston branch to be bolted into place using the original access panel screw holes, thus facilitating a secure and airtight connection to the stack, see **Figure 5.7**.

5.2.3.4 System response measurement and data acquisition

The data acquisition system was the same as that used for the HWU 1 (*laboratory*) system tests, consisting of a pressure/vacuum transducer (Sensor Technics, model 113LP25D-PCB, with a pressure range of ±250 mm water gauge and non-linearity of ± 0.25%), a data acquisition board (Keithley, model KPCI-3116, with 32 analogue input channels and a maximum sampling rate of 250 kHz) and a central monitoring computer. The pressure transducer, VPT1, was located on the transient inlet branch.

5.2.3.5 Standardisation of the stack

Although the layout of each flat was the same there had been some minor alterations made to the drainage system in a number of the flats. These alterations mainly consisted of additional connections for washing machine drains or a second connection for a double basin kitchen sink. All of these miscellaneous connections were removed and capped.

The original stack termination on the roof was fitted with a cone-shaped cover to prevent debris from entering the drainage system. However, a fully open termination was preferred as to act as a clear indicator of the top of the stack and so this cover was removed. As the tests were being conducted during the summer months and as conditions were regularly monitored during testing, the risk of debris entering the system during testing was considered to be small. To prevent confusion between the true stack termination and the rainwater collection drain, the rainwater collection drain was sealed using a foam plug and sealing compound during testing.

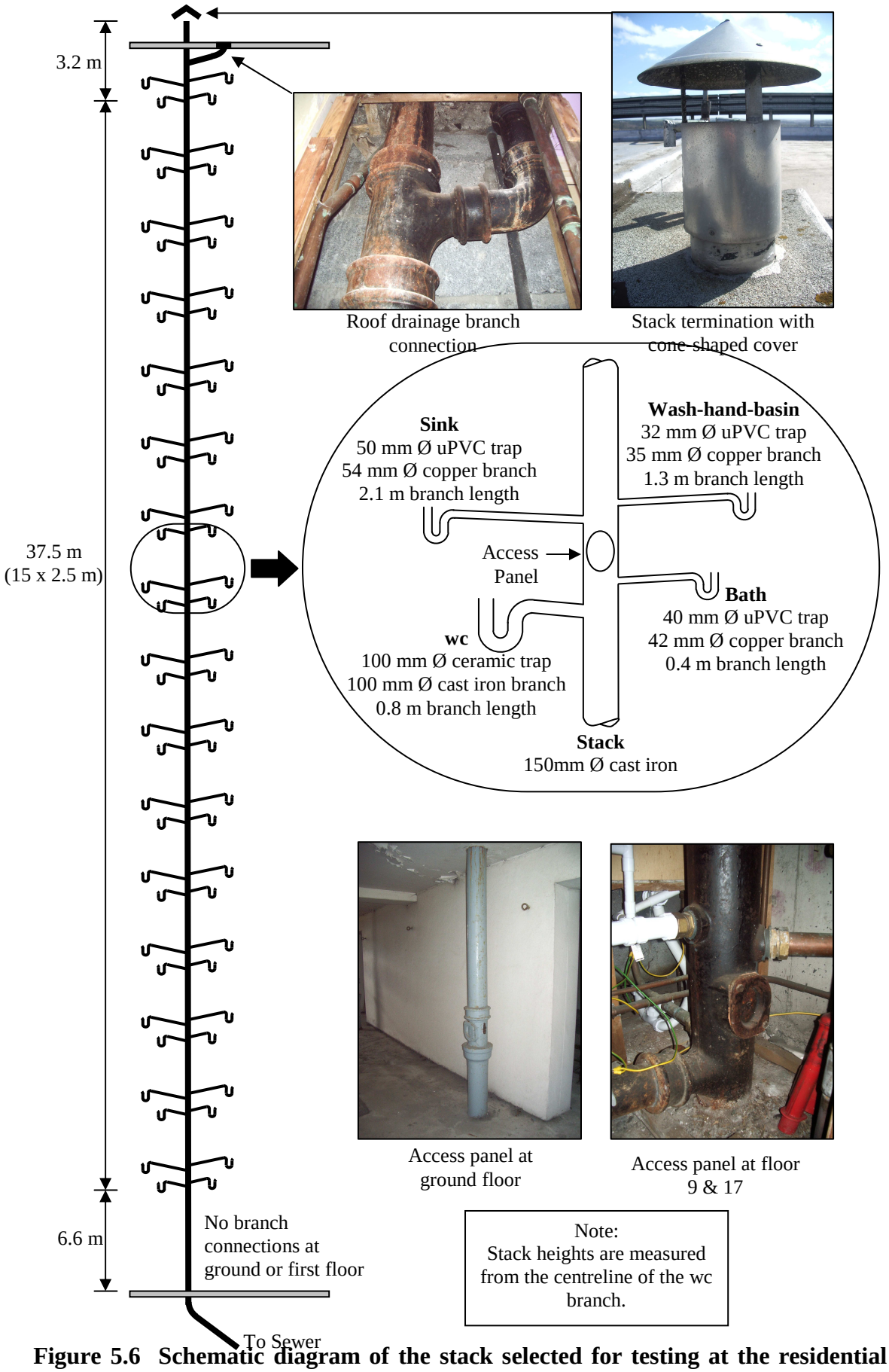

Figure 5.6 Schematic diagram of the stack selected for testing at the residential building in Dundee: Dundee (*Field*) system

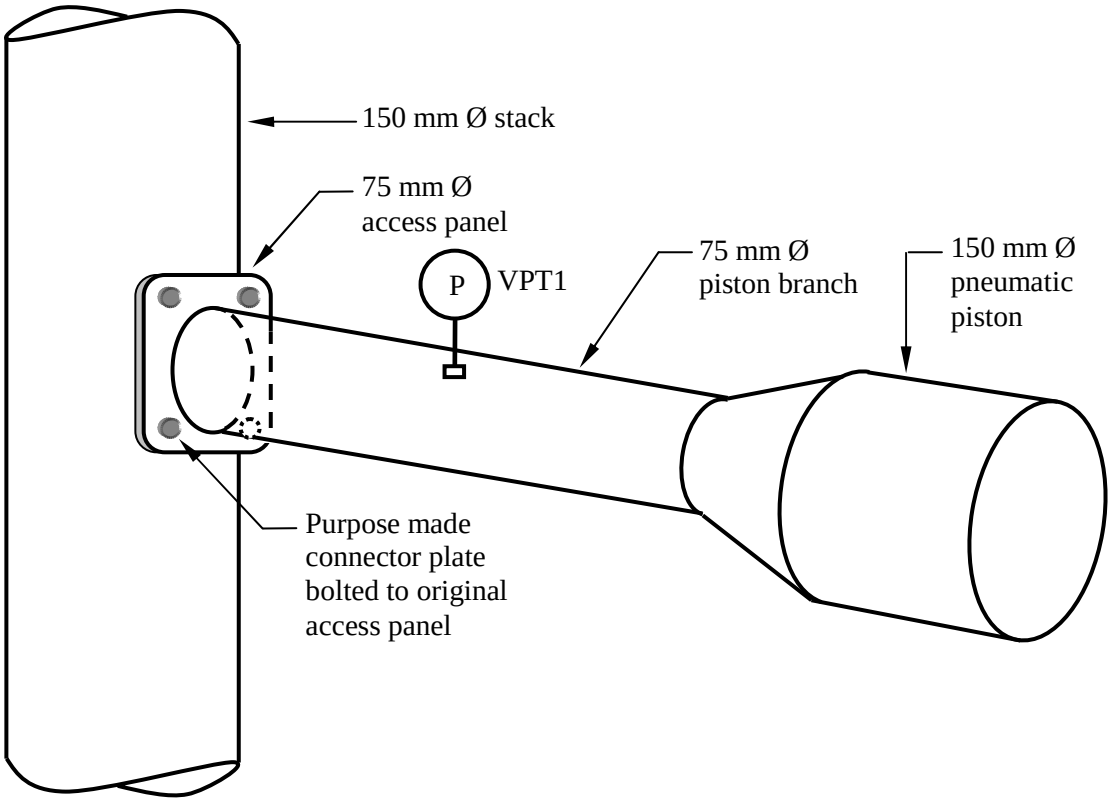

Figure 5.7 Method used to connect the pneumatic piston to the drainage stack via an existing access panel

5.2.3.6 Simulation of a depleted trap seal

The wc traps were selected to simulate the depleted traps as these were the easiest to access. As many of the flats had been empty for some time it was likely that the water would have evaporated from the traps and so each was checked and replenished prior to testing. A depleted trap was created by removing the water seal from one wc trap per test using a hand suction pump. All other traps were regularly monitored and kept fully primed throughout testing.

5.2.3.7 Transient entry point

Assessment of the optimum transient entry point was investigated by introducing the incident transient at three different stack locations: Floor 9 (*Configuration II*), Ground Floor (*Configuration III*), and Floor 17 (*Configuration IV*) were all selected to investigate introducing the transient to the middle, bottom and top of the stack, respectively, see **Figure 5.8**.

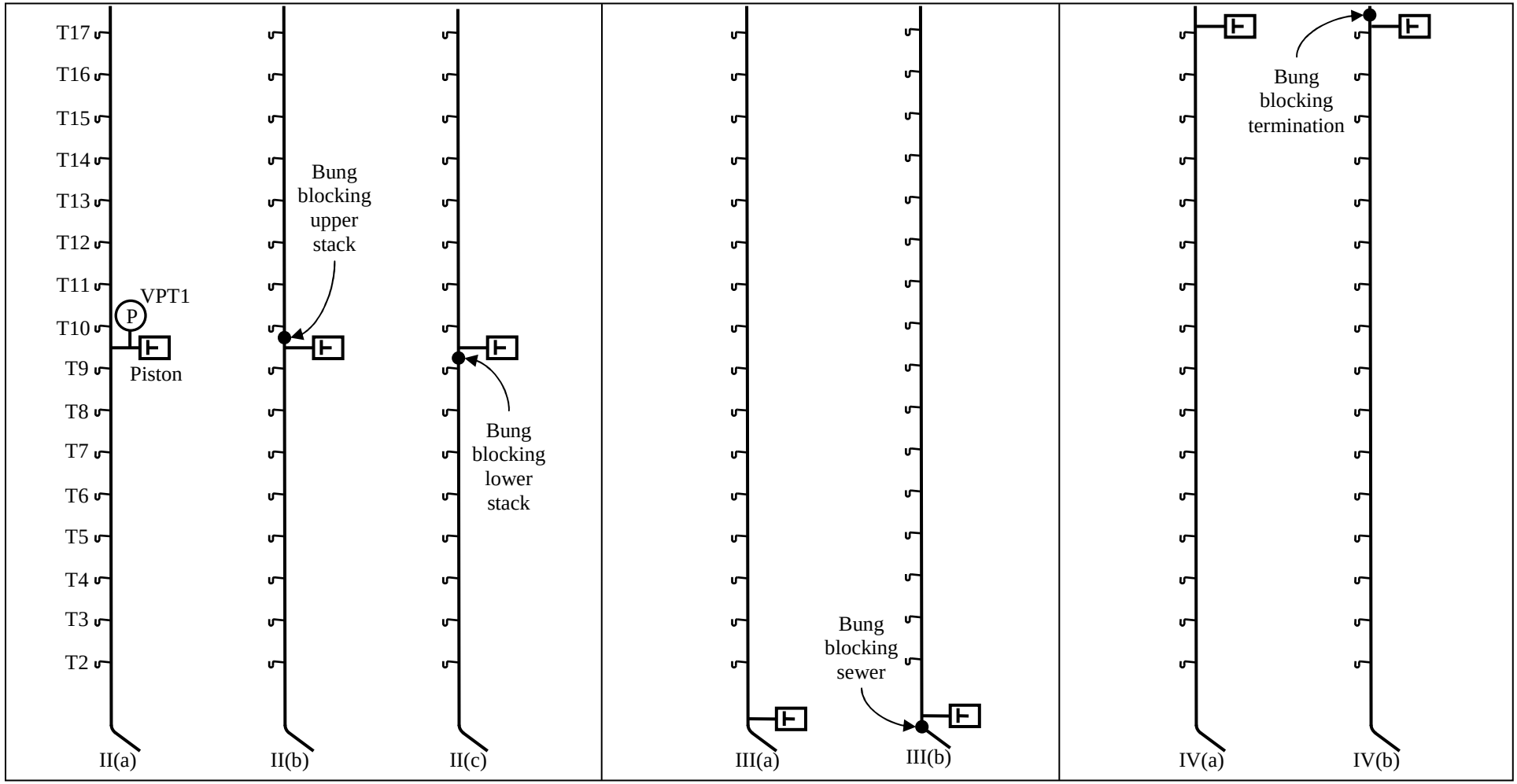

Figure 5.8 System configurations used during the Dundee (*field*) system tests. *Configuration II* (transient applied to Floor 9), *Configuration III* (transient applied to Ground Floor), *Configuration IV* (transient applied to Floor 17). For simplicity only the wc branches are shown here.

5.2.3.8 Data Collection

Floor 9 was selected to house the central data logging system as this provided the logistical benefit of being mid-way up the building (and, therefore, provided best access to all other floors during testing) as well as the economic benefit of reducing the cable length required to connect to the pressure transducer located at the piston.

With the central data logging system at Floor 9, it was convenient to begin testing at this floor also and so the piston was connected onto the stack via the access panel connection piece at this floor.

The test procedure was the same as that outlined in Section 5.2.2.7 where the test set-up process was used to determine the system information required by the TRACER program. System responses of the defect free system were measured (using a data sampling rate of 500 Hz) in order that the defect free baseline, P_j^{DF}, and threshold value, *h*, could be determined.

On checking the defect free system response an unexpected and sudden pressure drop was observed which occurred almost immediately after the arrival of the incident transient at the measurement point, **Figure 5.9(a)**.

To find the cause of the pressure drop, attention focused on the geometry and configuration of the transient entry pipework as this is the only parameter that had changed from the laboratory tests.

The transient entry pipework, shown previously in **Figure 5.7**, consisted of a 150 mm diameter piston which reduced to a 75 mm diameter inlet branch to facilitate the connection to the 75 mm diameter access panel on the stack, which itself was 150 mm diameter. From the transient theory presented in Chapter 2 it is known that discontinuities such as changes in pipe diameter and pipe junctions will induce a reflection and transmission process which can alter the system response. **Figure 5.9(b)** provides a simplified examination of the discontinuities present within the transient entry pipework and, using Equations (2.12) and (2.13), identifies the resultant reflection and transmission coefficients. It can be seen that the change in pipe diameter from 150 mm to 75 mm generates a reflection coefficient of +0.6 and transmission coefficient of +1.6. The three pipe junction created by the 75 mm diameter inlet branch and the 150 mm diameter stack generates a further reflection coefficient of -0.78 and a transmission

coefficient of +0.22. Therefore, to remove the pressure drop from the system response these discontinuities would need to be removed.

First, the discontinuity created by the pipe diameter change was removed by increasing the inlet branch diameter to 150 mm to match that of the piston. **Figure 5.10(a)** shows that although the system response is improved a pressure drop can still be observed which is attributed to the entry to the three pipe junction created between the inlet branch and the stack which generates a reflection coefficient of -0.33 and a transmission coefficient of +0.66, **Figure 5.10(b)**. Note that although the transient must still pass the orifice created by the 75 mm access panel, its influence is considered to be negligible.

To remove the discontinuity created by the three pipe junction the lower section of the stack was closed off using an inflatable balloon bung which effectively created a two pipe junction of equal diameter. **Figure 5.11(a)** shows that the pressure drop has now been removed as the reflection coefficient tends to zero and the transmission coefficient tends to +1, thus permitting total through flow, **Figure 5.11(b)**.

Now that the pressure response had been improved and now resembled a full pressure pulse it was possible to proceed with testing. Therefore, during these tests at Floor 9, and the subsequent tests at Ground Floor and Floor 17 a 150 mm diameter inlet branch was used in conjunction with closing off a section of the stack (either above or below the inlet branch, depending on which section was to be tested). As a result, all subsequent analysis will focus on the tests carried out using *Configurations II(b), II(c), III(b) and IV(b)*.

Figures 5.12 to **5.15** show the calculated defect free baseline, P_j^{DF}, and threshold value, *h*, for each configuration respectively.

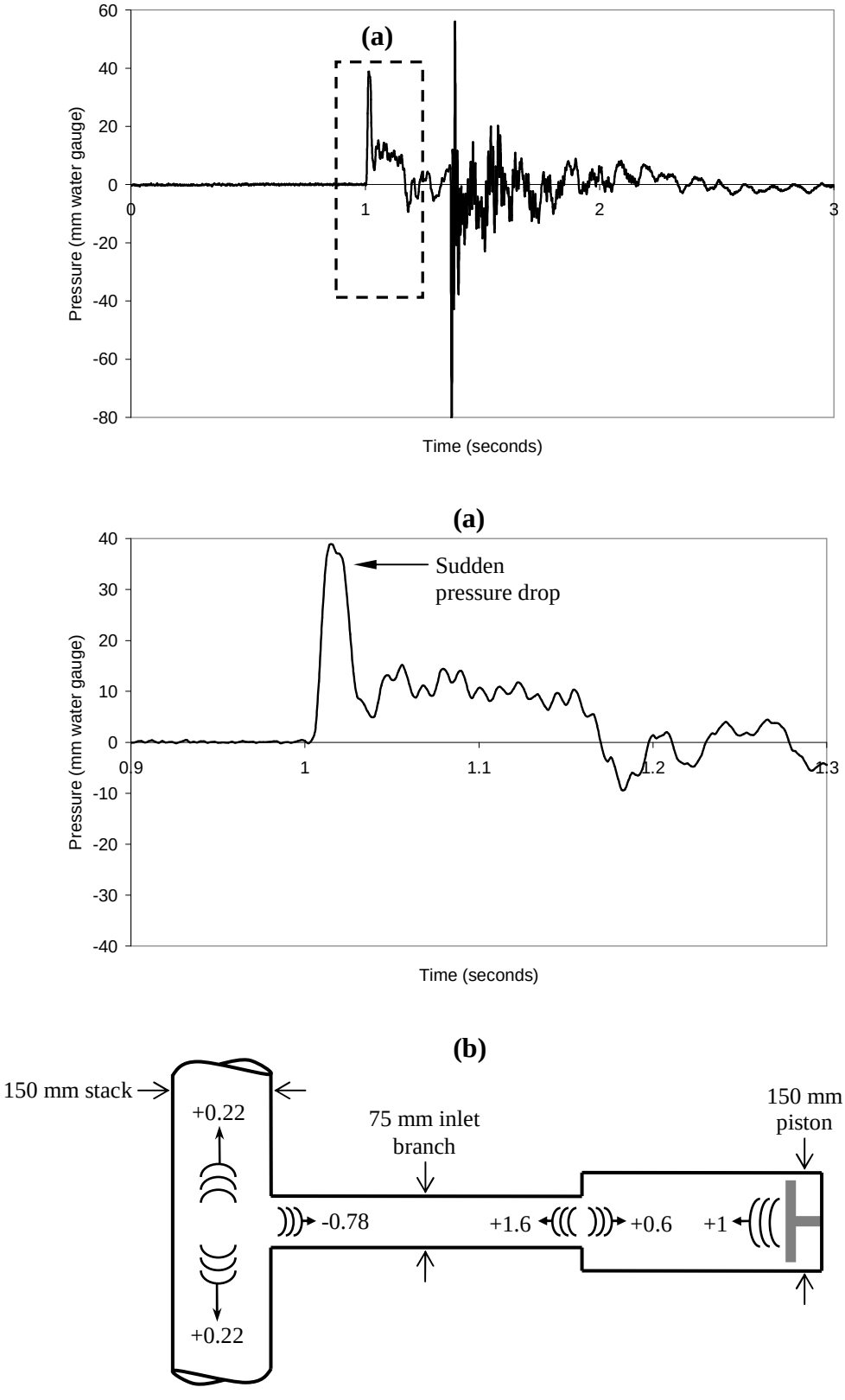

Figure 5.9 System response measured at VPT1 on *Configuration II(a)* in response to a single positive pressure pulse; (a) shows the arrival of the incident transient followed by a sudden pressure drop; (b) provides a simplified examination of the reflection and transmission coefficients at each discontinuity at the transient entry pipework – namely a pipe diameter change and three pipe junction

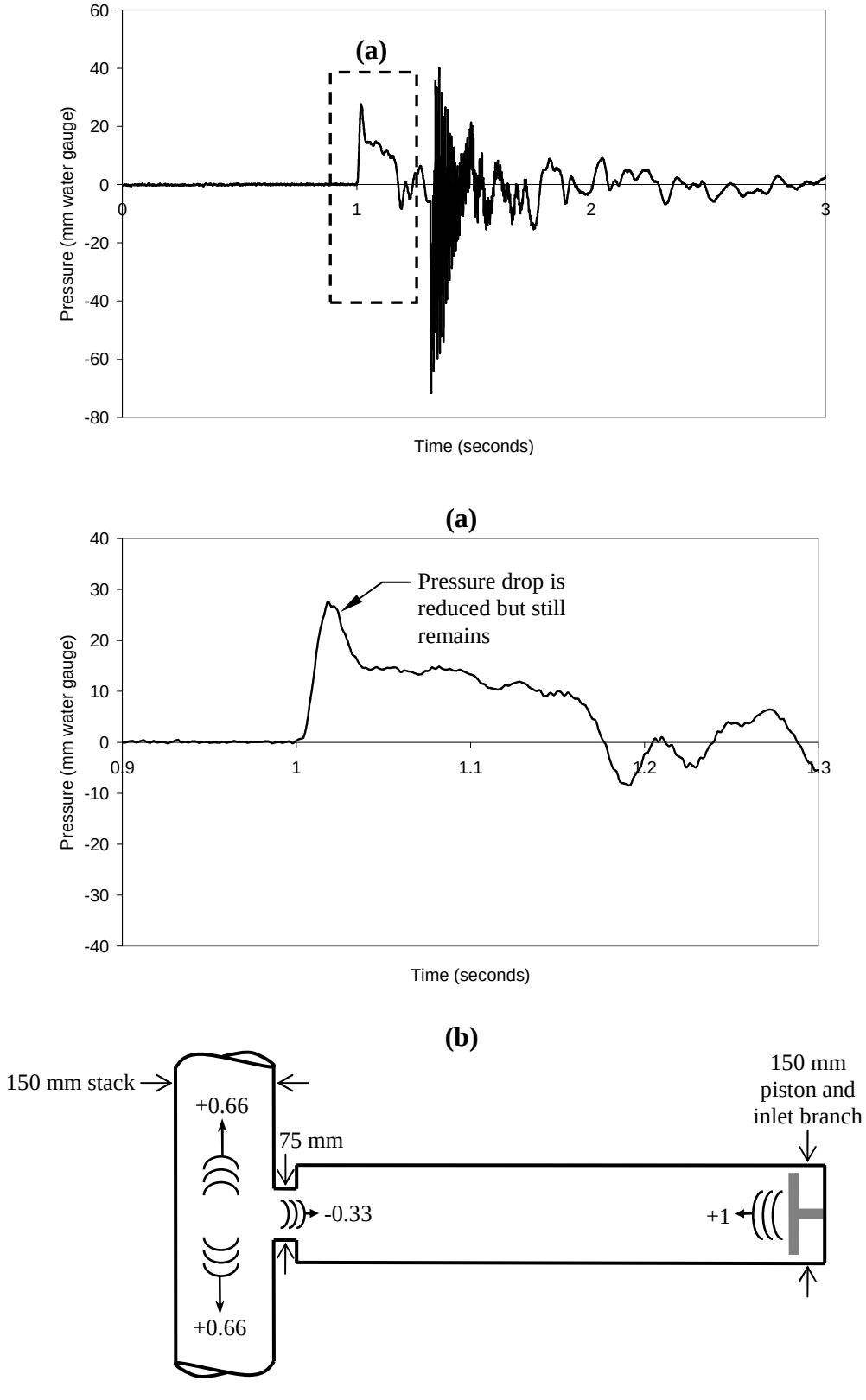

Figure 5.10 System response measured at VPT1 on *Configuration II(a)* in response to a single positive pressure pulse; (a) shows the arrival of the incident transient followed by a sudden pressure drop; (b) provides a simplified examination of the reflection and transmission coefficients at each discontinuity at the transient entry pipework – namely a three pipe junction

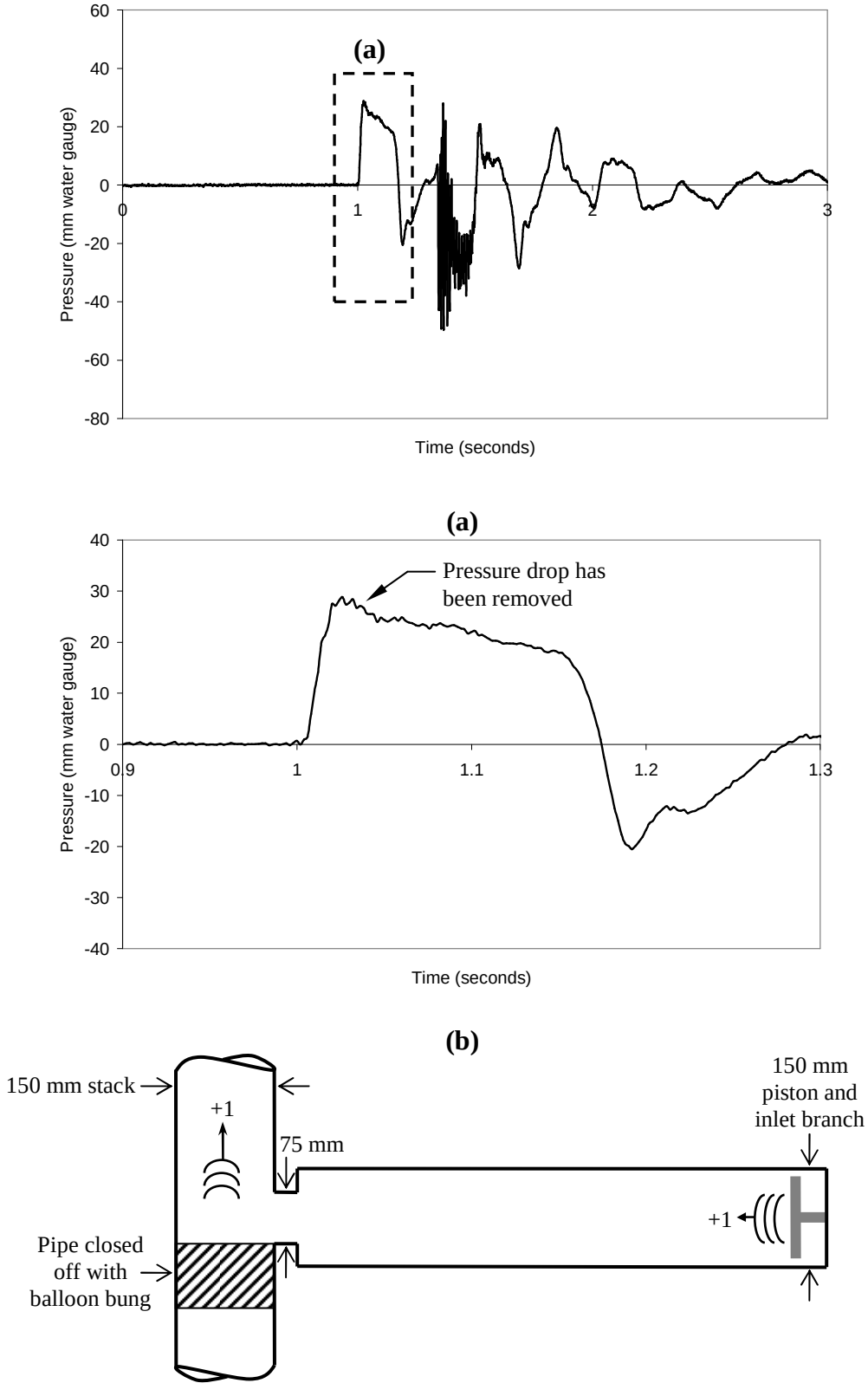

Figure 5.11 System response measured at VPT1 on *Configuration II(c)* in response to a single positive pressure pulse; (a) shows the arrival of the incident transient now with no sudden pressure drop; (b) provides a simplified examination of the reflection and transmission coefficients at each discontinuity at the transient entry pipework – both the diameter change and the 3-pipe junction have been removed

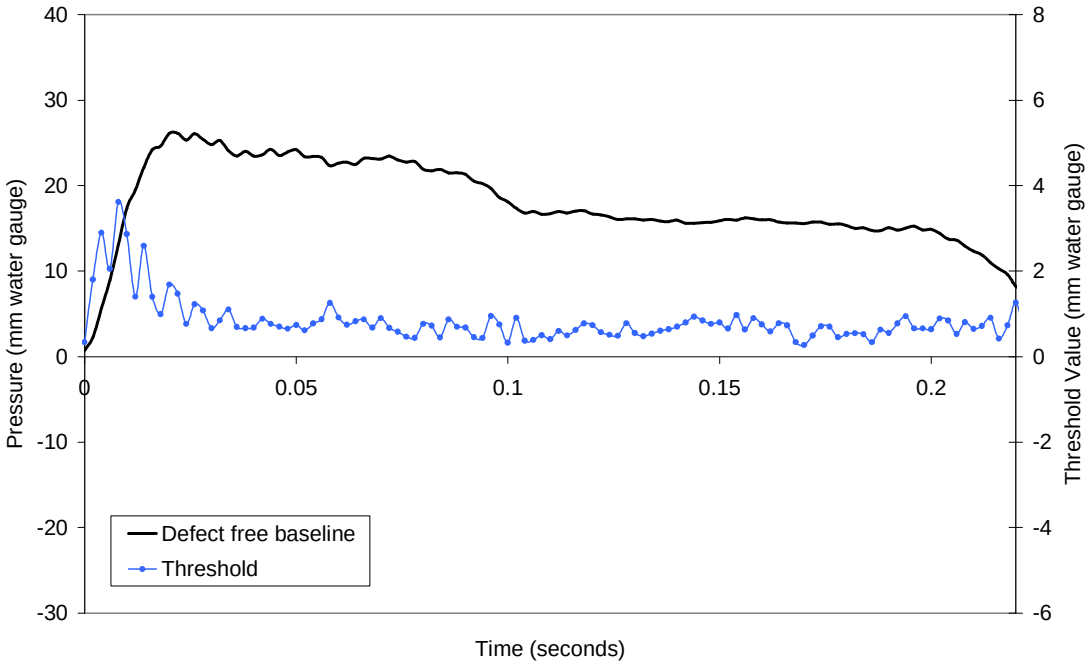

Figure 5.12 Calculated defect free baseline, P_j^{DF}, and threshold value, *h*, for *Configuration II(b)*, *h* = 5 mm water gauge

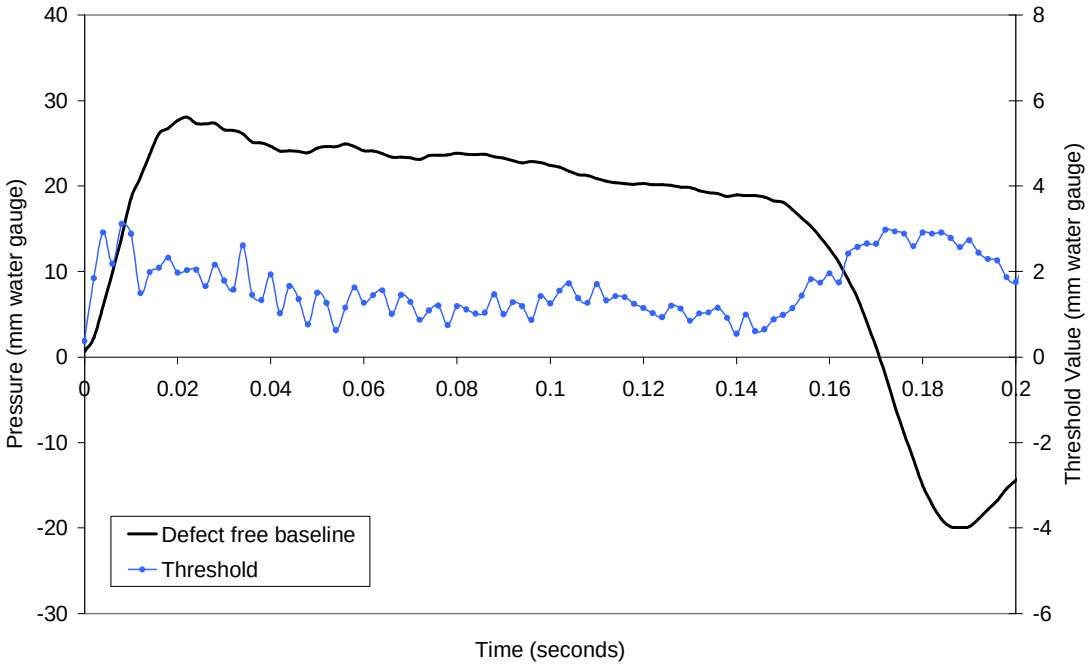

Figure 5.13 Calculated defect free baseline, P_j^{DF}, and threshold value, *h*, for *Configuration II(c)*, *h* = 4 mm water gauge

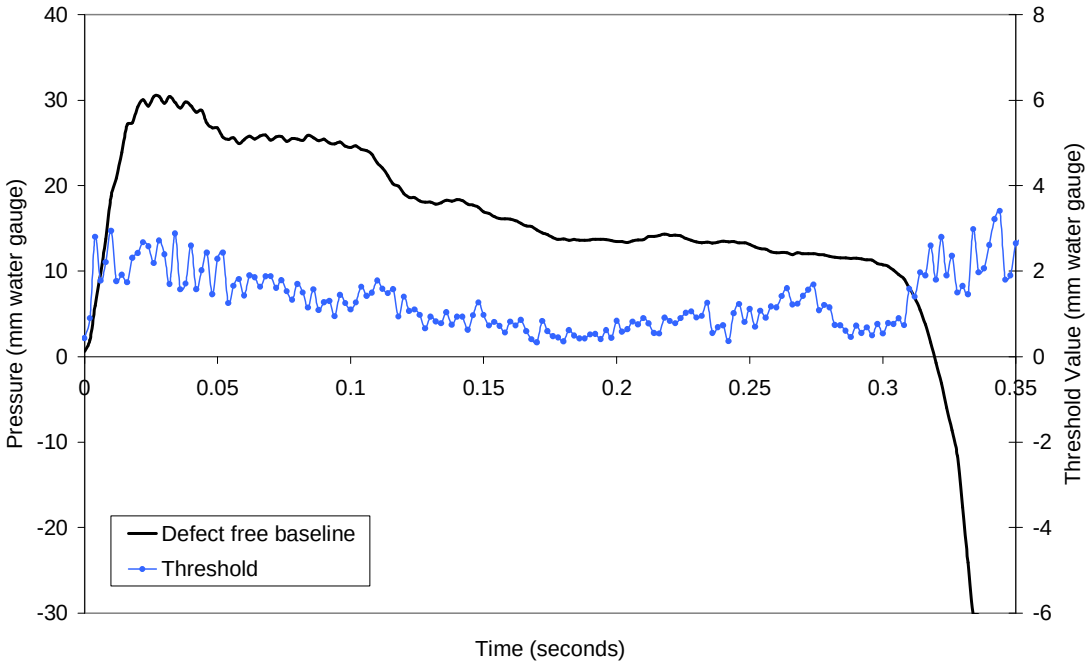

Figure 5.14 Calculated defect free baseline, P_j^{DF}, and threshold value, *h*, for *Configuration III(b)*, *h* = 4 mm water gauge

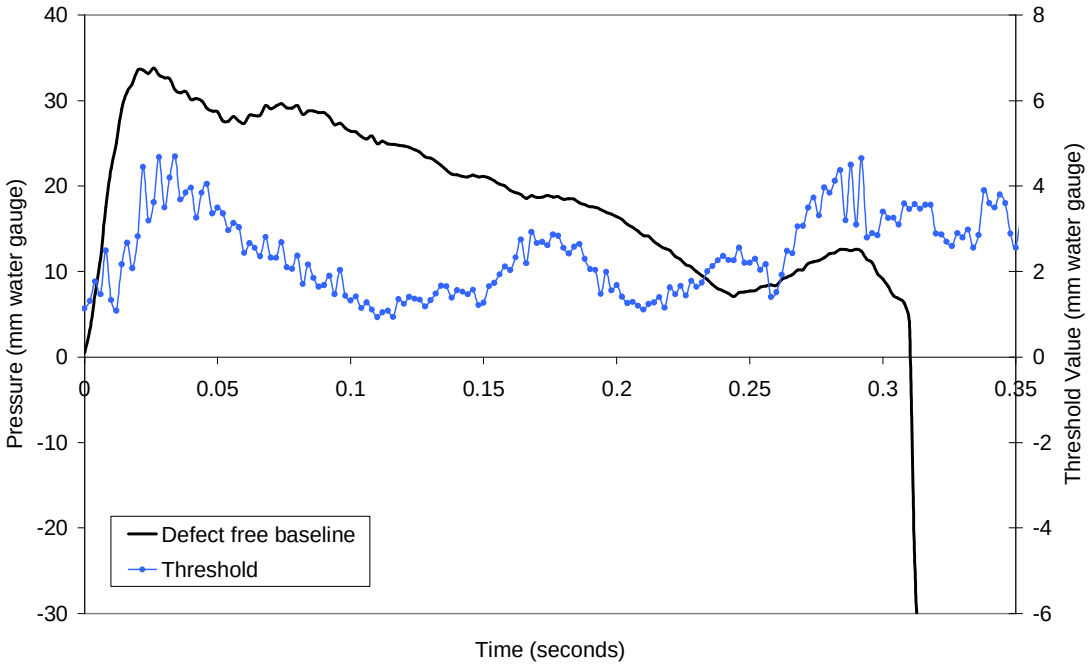

Figure 5.15 Calculated defect free baseline, P_j^{DF}, and threshold value, *h*, for *Configuration IV(b)*, *h* = 5 mm water gauge

5.2.3.9 Test Observations

These initial field trials provided valuable insight into the practical implications of performing the reflected wave technique in a real building drainage system. Three main observations were made which were used later to develop the test methodology:

i. As discussed in the previous section, any extraneous reflections which may adversely affect the system response should be removed from the transient entry pipework. In particular, the entry of the transient into the stack must be controlled on order to avoid reflections from the three pipe junction created with the inlet branch and stack;

ii. While no trap was ever depleted as a result of introducing the single positive pressure pulse into the system, oscillations in the surface of the water seal were observed on a number of occasions which raised concerns regarding the potentially destructive consequence of applying the pressure pulse into the system;

iii. Performing the tests at the three transient entry points (i.e. at the top, middle and bottom of the stack) it became apparent that introducing the transient into the top of the stack (i.e. within the dry stack section) would be the most practical option for the following two reasons: (a) the internal pipe surface of the dry stack would be cleaner, as it is above any waste discharge, and therefore more hygienic; (b) if the system were to be used during testing then any waste discharge would enter the system below the transient entry point and so would not interfere with the test equipment.

These observations prompted the development of a new transient entry device which would provide a combined solution to each of the concerns raised during these field trials. The development of this device will be discussed in the following section.

5.2.4 Development of the transient entry device

Developed to address each of the three concerns raised in the previous section, the transient entry device, shown in **Figure 5.16**, consists of a sinusoidal piston exciter, an automated 3-port valve with integrated pressure transducer, and an inlet branch. Each component will be discussed in turn:

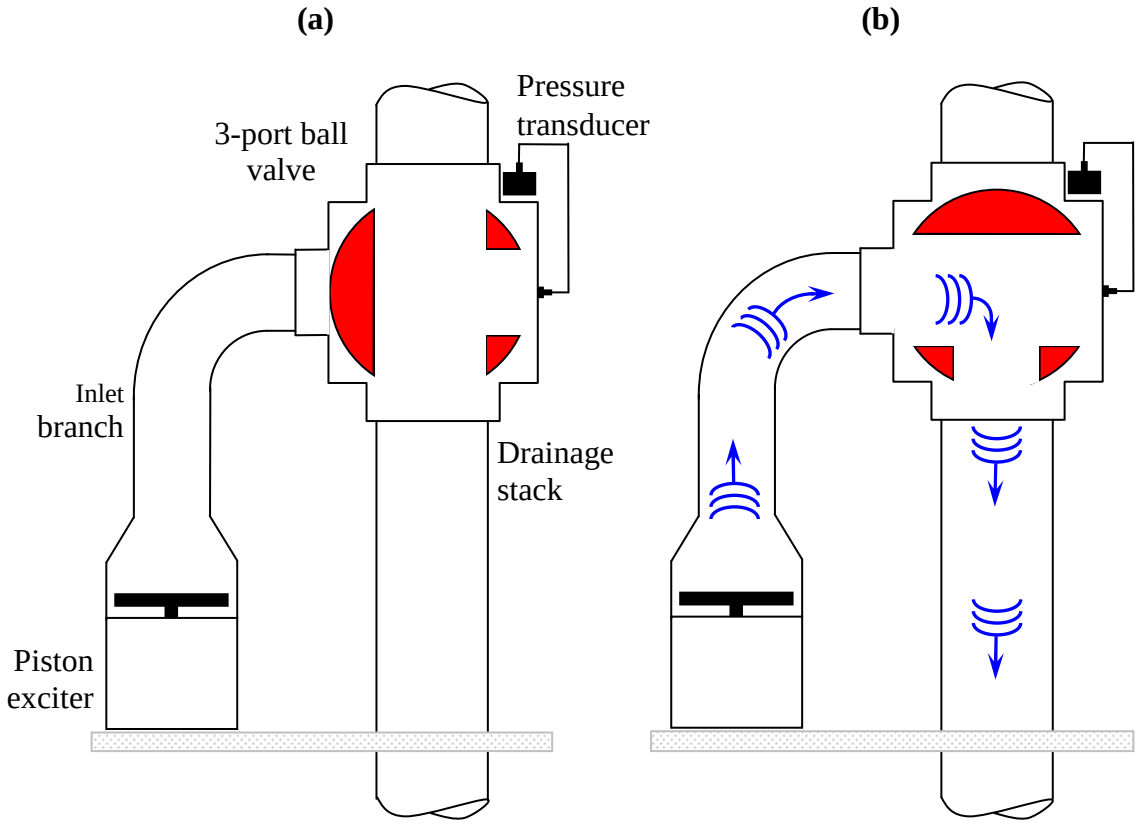

Figure 5.16 The new transient entry device showing the system under (a) normal mode "stack open" and (b) test mode "stack closed"

Sinusoidal piston exciter. As discussed in Section 3.6.6.4, initial investigations by Kelly (2007) provided evidence that the application of a 10 Hz sinusoidal transient offered a non-destructive alternative to the single positive pressure pulse by protecting the integrity of the trap seal by limiting the impact of the transient on the water surface. This was later confirmed by experimental investigation by Beattie (2007) while Swaffield (2007) confirmed that AIRNET was capable of simulating these effects.

The pneumatic piston was replaced with a frequency adjustable piston exciter connected to a frequency generator and amplifier. The piston exciter (LDS Shaker, model V406/8) consisted of a permanent magnet which houses and supports the drive coil which itself is formed from copper wire. Movement of the piston exciter is generated once a current is passed through the copper drive coil. The frequency of the movement is the same as the frequency of the applied current which is determined by the frequency generator via the amplifier (LDS amplifier, model PA 100E). The excitation frequency was generated using a widely available audio media software programme called *Audacity* which was installed onto the central computer. The frequency was set to 10 Hz.

Automated 3-port valve and integrated pressure transducer. The automated 3-port ball valve provides directional control over the propagation of the test transient as it enters the stack. Designed to be installed within the upper dry stack (i.e. above all discharging appliances), the 3-port valve would remain in the "stack open" position during normal conditions and would be switched to the "stack closed" position during test conditions which closes off the top section of the stack, effectively removing the three pipe junction, and directs the test transient down the stack in the direction of all the connected appliances. The valve is controlled by a relay controlled actuator which has a failsafe reset function which returns the valve to the "stack open" position in the event of a power failure. During these investigations the actuator was switched manually between the "stack open" and "stack closed" position, however, this can be timer controlled as part of a scheduled system test. The operational control method is shown in **Figure 5.17**. The test duration is relatively short, with a full test cycle lasting less than 30 seconds.

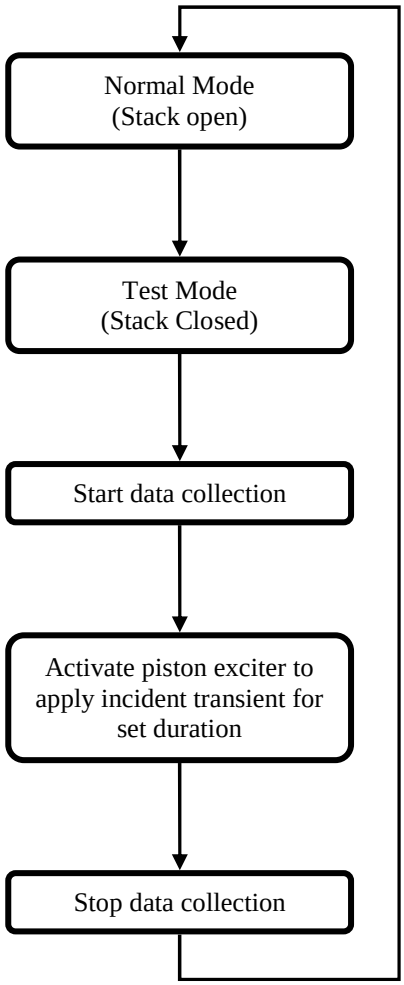

Figure 5.17 Operational control method for the transient entry device

A number of different transducer locations were investigated during the equipment development. These included the inlet branch, the stack, and the 3-port valve. No one location provided any significant improvements to the measured system response and so, in order to consolidate the test equipment and simplify its installation, it was decided to locate the transducer on the 3-port valve.

Transient inlet branch. The inlet branch diameter, together with that of the piston, was designed to achieve the optimum system response. AIRNET offered the easiest and quickest method of investigating different diameter combinations without the need for extensive laboratory experiments. A simple system was designed and simulated consisting only of the piston, inlet branch and stack, as shown in **Figure 5.18**.

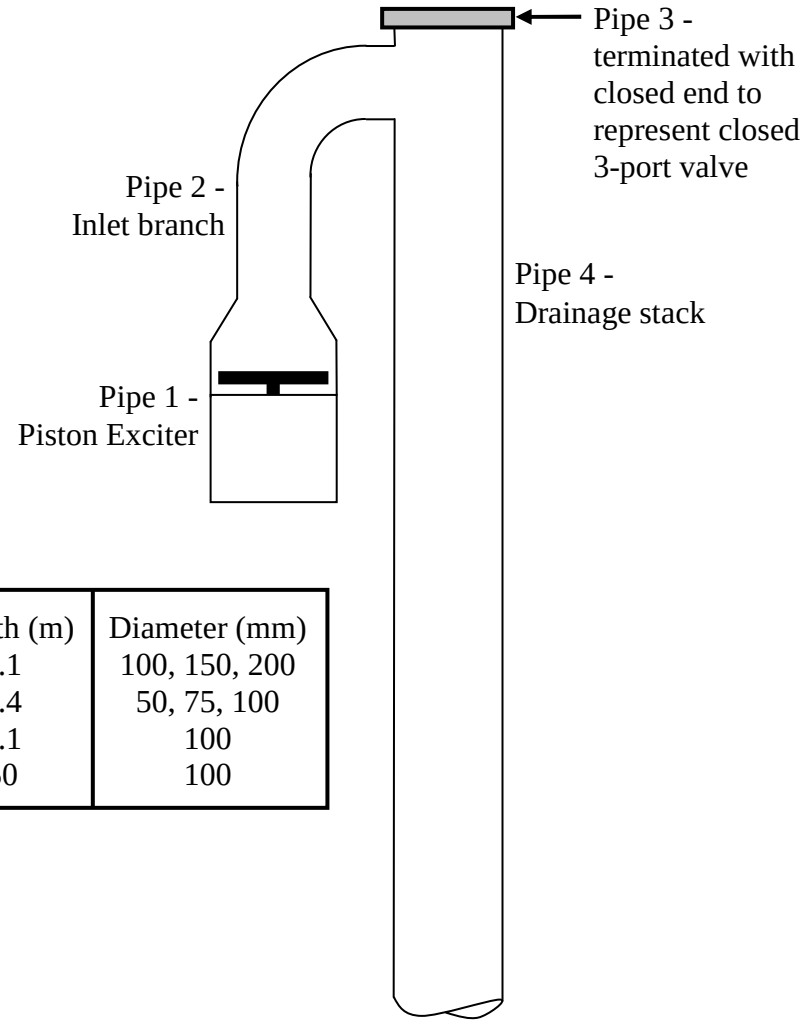

Pipe	Length (m)	Diameter (mm)
1	0.1	100, 150, 200
2	0.4	50, 75, 100
3	0.1	100
4	50	100

Figure 5.18 System simulated by AIRNET to assess the effect of piston, inlet branch and stack diameter combination on the measured system response

First, the influence of the piston diameter was investigated. Piston diameters of 100 mm, 150 mm and 200 mm were simulated while the inlet branch was set at 75 mm. **Figure 5.19** shows the simulated system response to the applied 10 Hz sinusoidal wave for each piston diameter. While the peak pressure produced by the 100 mm diameter piston was 14.9 mm water gauge, this increased to 33.6 mm water gauge for the 150 mm diameter piston. Increasing the piston diameter again to 200 mm water gauge produced a peak pressure of 59.8 mm water gauge. There is a clear increase in peak pressure and this is directly related to the increase in surface area of the piston plate as a result of the diameter increase. As the largest peak pressure would be least affected by system noise by helping to reduce the signal/noise ratio the 200 mm diameter piston was selected. However, preliminary laboratory tests showed that it was difficult to obtain a repeatable system response due to vibrations generated by the piston. Reducing to a 150 mm diameter piston, however, generated no noticeable vibration and, thus, provided an improved system response. It was, therefore, decided to proceed with a 150 mm diameter piston.

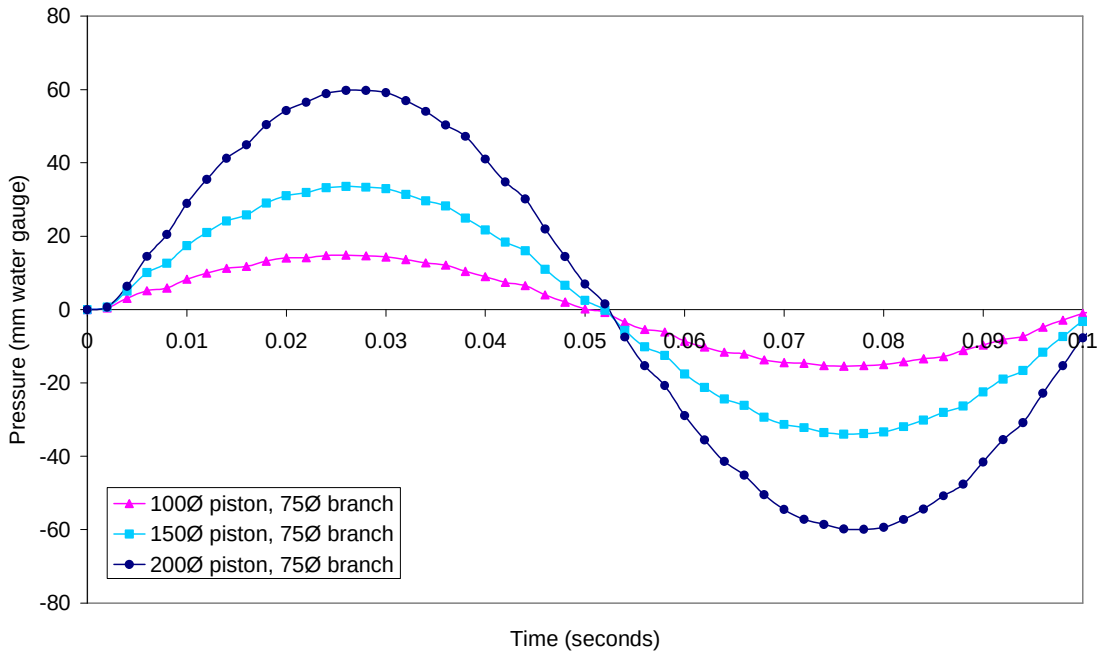

Figure 5.19 Results from an AIRNET simulation showing effect of piston diameter on the system response to an applied 10 Hz sinusoidal excitation

The effect of different inlet branch diameters was then investigated and the results are shown in **Figure 5.20**. The peak pressure is found to increase from 33.49 mm water gauge to 33.58 mm water gauge and then to 33.99 mm water gauge for inlet diameter branches of 100 mm, 75 mm and 50 mm respectively. Although the peak pressure is increased by reducing the diameter of the inlet branch due the to the amplification effects that a diameter reduction imposes, the increase is very small and provides no great benefit. Therefore, as the spigot connection on the valve is already 75 mm, it was decided to proceed with a 75 mm diameter inlet branch.

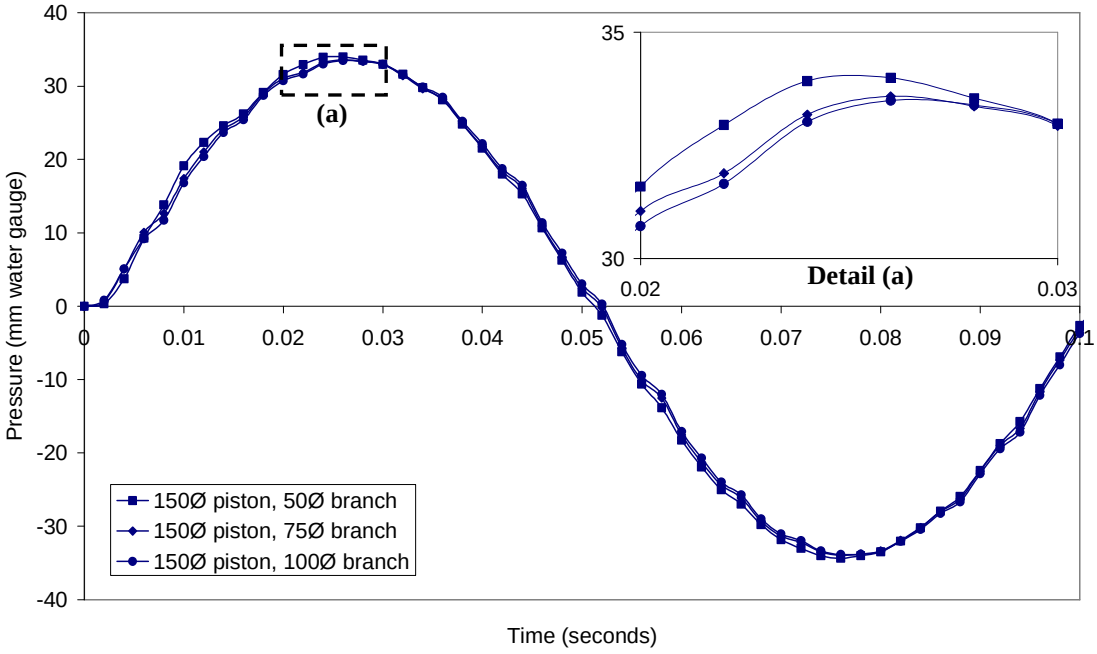

Figure 5.20 Results from AIRNET simulation showing effect of inlet branch diameter on the system response to an applied 10 Hz sinusoidal excitation

Installation of the transient entry device is facilitated by the use of standard pipe sizes which allow it to be slotted into any new or existing stack. As the transient entry device is intended to be installed within the dry stack, reducing the stack diameter locally to accept a 100 mm diameter 3-port valve would not be a problem in normal stack operation if the stack was a greater diameter. Alternatively, the 3-port valve could be made available in a range of sizes compatible with all common stack diameters.

5.2.5 Experimental field trials at Heriot-Watt University

5.2.5.1 General

An appraisal of the new transient entry device was carried out during field trials on the drainage system within the Arrol Building at Heriot-Watt University (HWU Arrol (*field*) system). These tests aimed to: (i) evaluate the use of a sinusoidal wave as the incident transient for the reflected wave technique; and (ii) optimise the reliability, repeatability and accuracy of the test method in order to provide confidence in the technique as a long term option for building drainage maintenance.

5.2.5.2 System description

A schematic of the HWU Arrol (*field*) system, *Configuration V*, is shown in **Figure 5.21**. The stack was 100 mm in diameter and spanned 5 storeys before terminating through the roof with an open end penetration. Appliances were located only on the top 3 floors, with a number of wcs, urinals, wash-hand-basins and showers connected at Floor 3 and 4, and only a floor gully connected at Floor 5.

The transient entry device was installed into the dry section at the top of the stack. The stack was exposed within the boiler room at the top of the building thus providing ease of access and facilitating installation. The central monitoring computer and data acquisition system were located directly beneath the boiler room in a storage cupboard on Floor 4 and the power and data cables were run through an existing services hole between the two floors.

In addition to the pressure transducer located on the transient entry device (i.e. VPT1), additional transducers were located at the horizontal branch on both Floor 3 and Floor 4 (i.e. VPTL3 and VPTL4, respectively). These two distributed pressure transducers were required to distinguish between equidistant traps occurring on Floor 3 and Floor 4 and also to improve the clarity of the reflection return time from a depleted trap located near the end of each branch. These issues will be discussed in more detail in Chapter 6.

5.2.5.3 Simulation of a depleted trap seal

When required, a depleted trap was created by removing the water seal from the trap using a hand suction pump. All other traps were monitored regularly during testing to ensure they remained fully primed. The trap serving the urinals and showers were not used to create depleted traps as they were generally found to be inaccessible. They were, however, kept fully primed throughout testing.

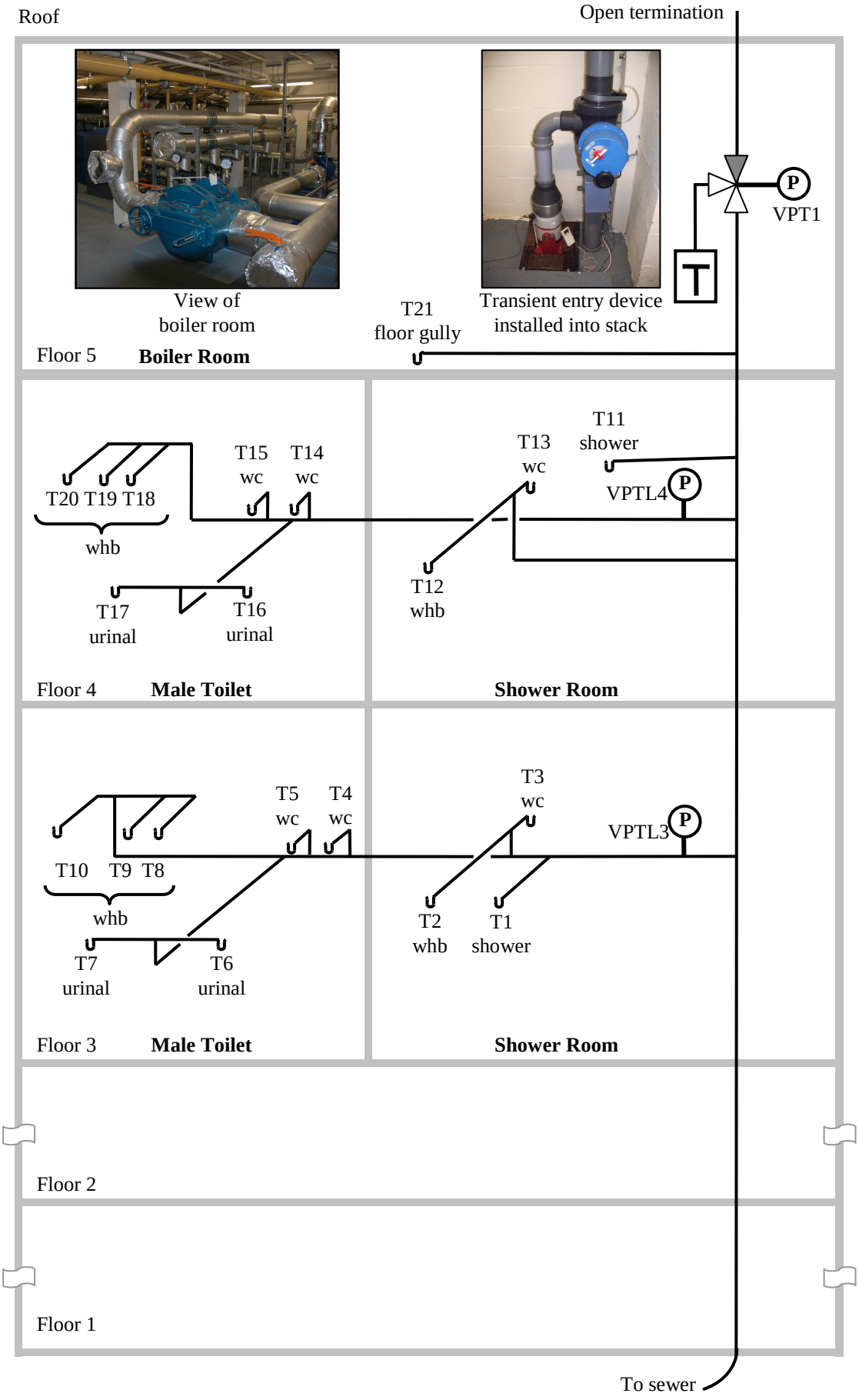

Figure 5.21 Schematic of the HWA Arrol (field) system, *Configuration V*

5.2.5.4 Data collection

The test set-up process, described in Section 4.5.1.1, was used in conjunction with the operational control method shown in **Figure 5.17** to determine the system information required by the TRACER program. First, the system was set to *test mode* by switching the 3-port valve to the *stack closed* position. The data collection system was then started and the sinusoidal exciter activated to introduce the incident transient into the system. After 5 seconds the exciter was halted and the data collection system stopped before switching the 3-port valve to the *stack open* position, thus reverting the system to *normal mode*. The test procedure lasted around 20 seconds per test when taking account of the valve motion and data collection period which is a practical time frame when testing in real building situations. A set of 20 system responses were recorded in order to calculate the defect free baseline, P_j^{DF}, and threshold value, *h*. A typical defect free system response measured at VPT1 is presented in **Figure 5.22**.

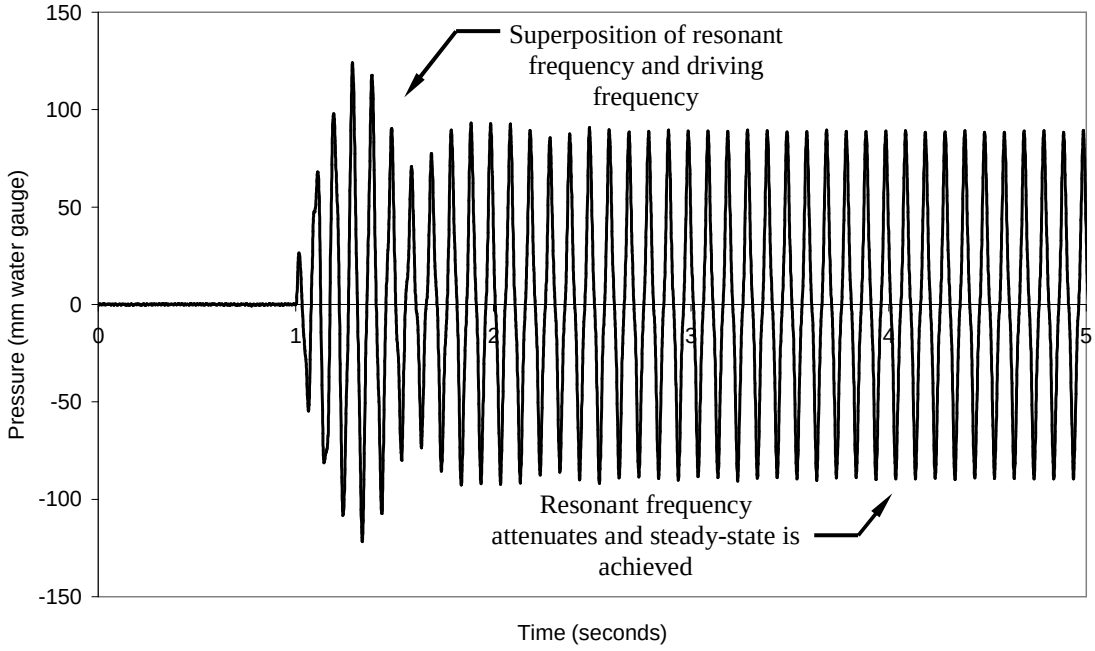

Figure 5.22 Typical defect free system response measured at VPT1 during the HWU Arrol (*field*) system tests, *Configuration V*

The application of the 10 Hz sinusoidal wave provides a very different system response to those observed earlier in response to the single positive pressure pulse. The resultant system response is the product of two main harmonic elements: (i) the natural resonance of the system; and (ii) the 10 Hz sinusoidal driving frequency. The sudden start of the piston excites the natural resonance of the system which is dependant upon the physical geometry of the system. The 10 Hz sinusoidal driving frequency combines with the

natural resonance frequency and the resultant system response is a superposition of these two frequencies. The natural frequency eventually attenuates and the pressure response settles to steady-state.

It is worth mentioning that although resonance frequencies have been used in various pipeline leak and blockage detection methods, as discussed in Chapter 4 (Covas *et al.*, 2005; Lee *et al.*, 2005; Sattar and Chaudhry, 2008; Antonopoulous-Domis, 1980; Qunli and Fricke, 1989, 1991; De Salis and Oldham, 1999, 2001), these have had limited success in this application for monitoring depleted trap seals within the building drainage system (Kelly *et al.*, 2008).

Figure 5.23, **5.24** and **5.25** show the defect free baseline, P_j^{DF}, and threshold value, *h*, measured at VPT1, VPTL3 and VPTL4, respectively, and show only the first 0.12 seconds, 0.08 seconds and 0.05 seconds, respectively, following the arrival of the transient at the measurement point. Before this information could be successfully obtained, it was necessary to make a number of adjustments and improvements to the test method in order to give confidence in the reliability, repeatability and accuracy of the technique for successful application within the field. The steps taken to achieve these improvements will be discussed in the following section.

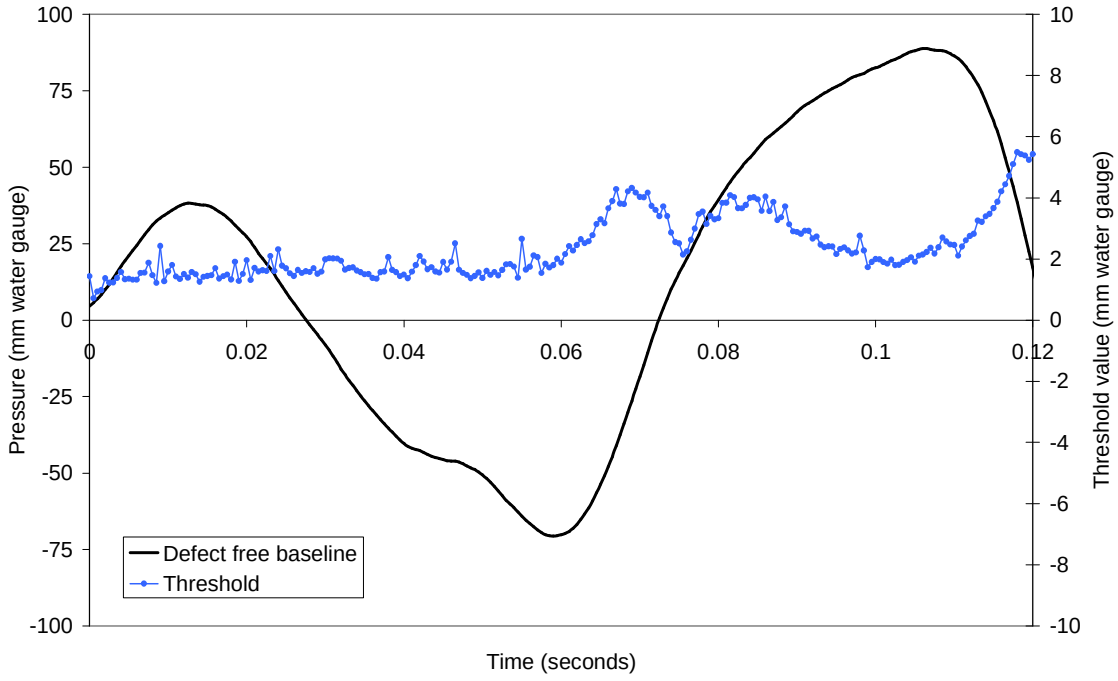

Figure 5.23 Calculated defect free baseline, P_j^{DF}, and threshold value, *h*, for *Configuration V* measured at VPT1, *h* = 6 mm water gauge

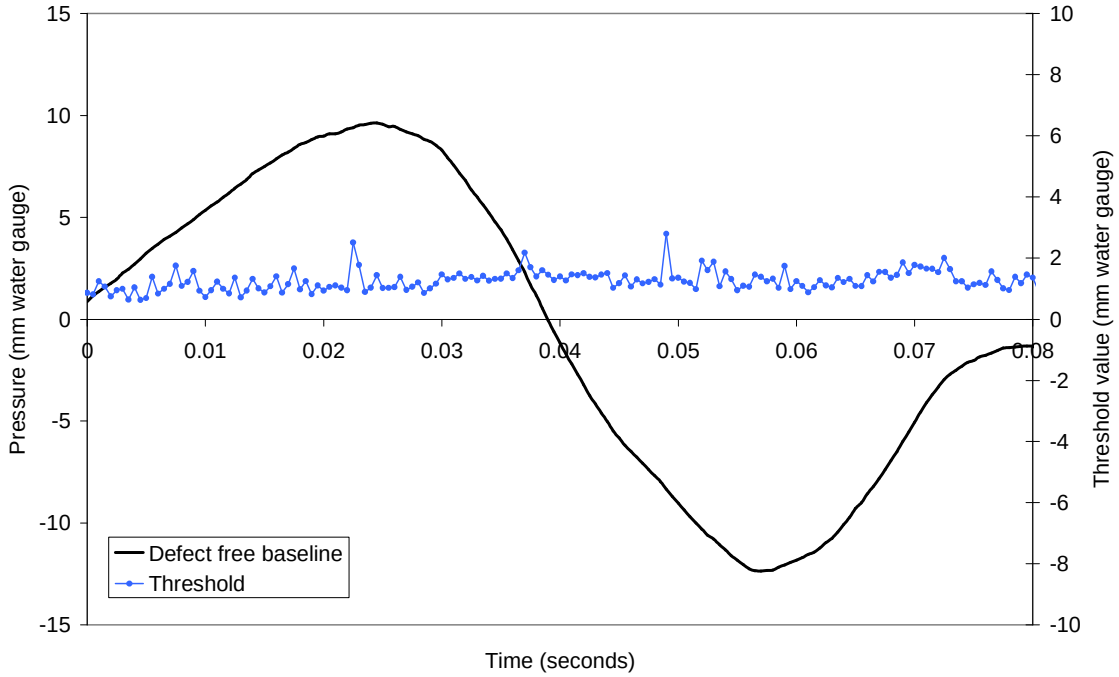

Figure 5.24 Calculated defect free baseline, P_j^{DF}, and threshold value, *h*, for *Configuration V* measured at VPTL3, *h* = 3 mm water gauge

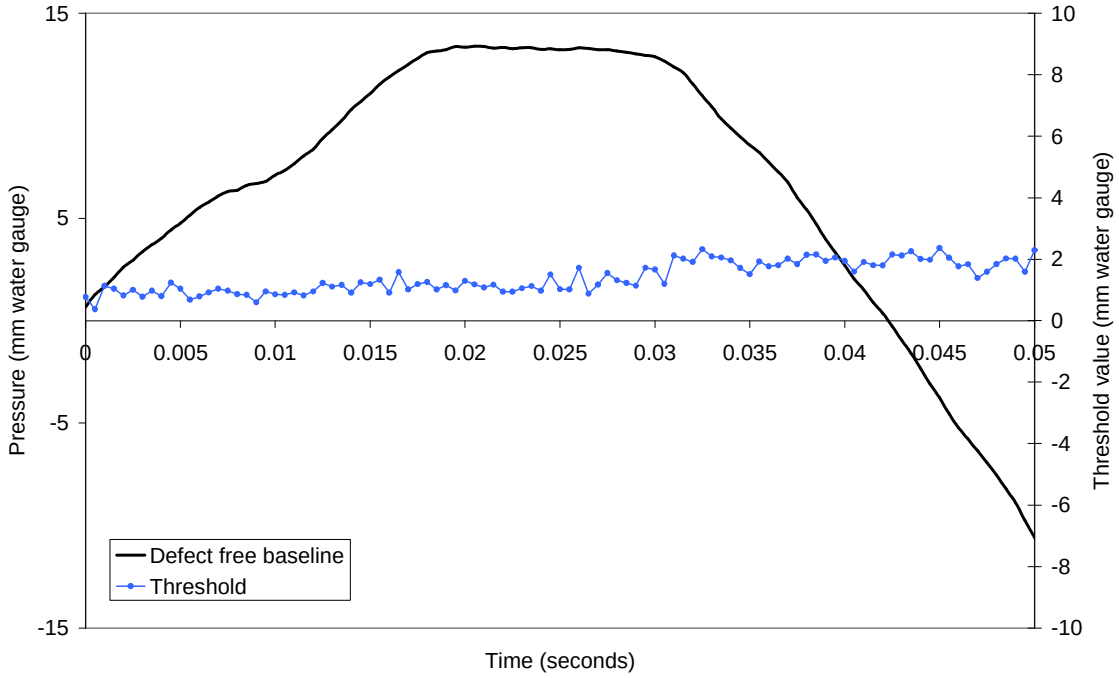

Figure 5.25 Calculated defect free baseline, P_j^{DF}, and threshold value, *h*, for *Configuration V* measured at VPTL4, *h* = 3 mm water gauge

5.2.5.5 Problems encountered during data collection

5.2.5.5.1 Data sampling rate

As detailed in Chapter 4, the TRACER program automatically detects and locates depleted trap seals by comparing the test system response with the defect free baseline. If the absolute difference between the two traces is within the threshold value (i.e. $D_t < h$) then the system is deemed defect free, but if the absolute difference exceeds the threshold value (i.e. $D_t > h$) then this indicates the presence of a depleted trap and the time at which the exceedance occurs, t_D, is recorded and used to locate the defect using Equation (4.2).

The reliability of the technique is dependant upon the successful alignment of the two traces. The TRACER program automatically aligns the traces by setting the transient wave arrival time, t_a, to time zero, t_0, (i.e. $t_0 = t_a = P_j >$ atmospheric pressure). If t_a occurs between data points then t_0 is set to the succeeding data point in the time series. Using a data scan rate of 500 Hz the time step between each data point is only 0.002 seconds, however, this has been found on occasion to allow a misalignment between the two traces, **Figure 5.26**.

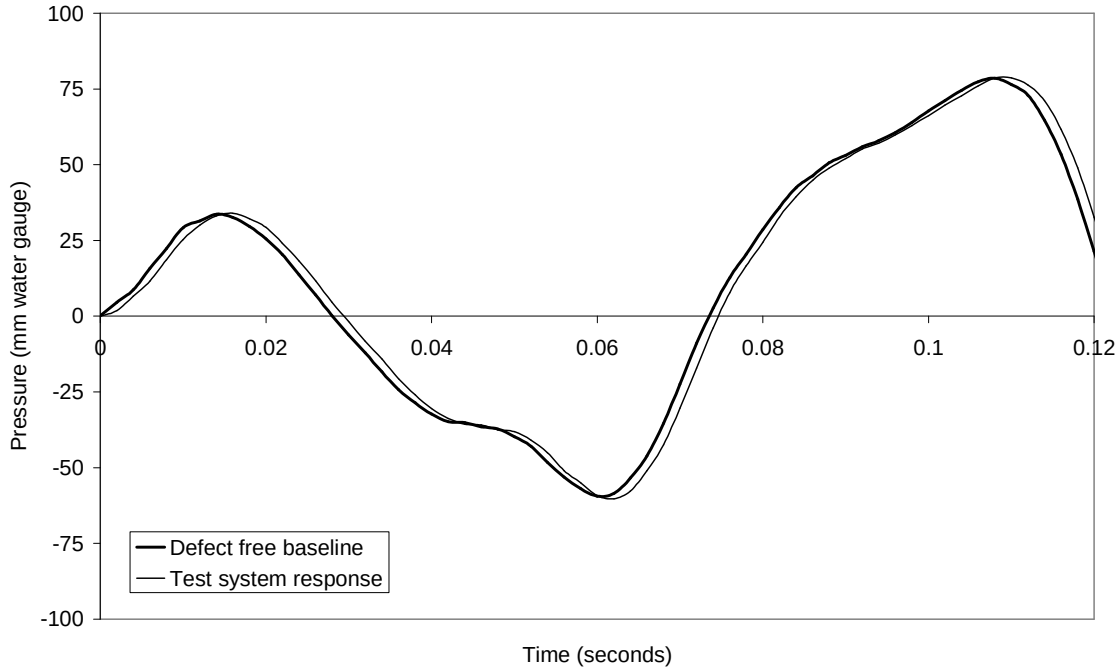

Figure 5.26 Example showing the misalignment of the test system response with the defect free baseline using a data sampling rate of 500 Hz

If misalignment were to occur during calculation of the defect free baseline then this would increase the threshold value and thus reduce the sensitivity of the technique. On the other hand, if misalignment were to occur during testing then this would potentially

generate a false alarm, indicating the presence of a depleted trap when, in fact, the system was defect free.

To improve the test reliability a series of tests were conducted using higher data scan rates (i.e. 1,000 Hz, 2,000 Hz, 3,000 Hz, 4,000 Hz and 5,000 Hz) with the expectation that with more data points being recorded per second the potential or extent of the misalignment would be reduced. A total of 70 defect free system responses were recorded at each scan rate and the defect free baseline and threshold values were calculated using Equations (4.3) and (4.4), respectively. **Figure 5.27** shows that as the scan rate increases the threshold value decreases, thus indicating an improvement to the successful alignment of the pressure responses. For example, at 500 Hz, h = 11.65 mm water gauge, while for 5,000 Hz, h = 4.22 mm water gauge, constituting a 64% reduction. It shows that the higher the data sampling rate, the better the alignment and, therefore, the more reliable the test will be. The consequences of using a high data scan rate, however, are larger file sizes and increased computer processing times. A balance must be made between the accuracy of the technique and the practicality of performing the test. Therefore, a compromise has been made by using a scan rate of 2,000 Hz. This provides a 51% reduction in threshold value while still producing manageable file sizes and tolerable processing times.

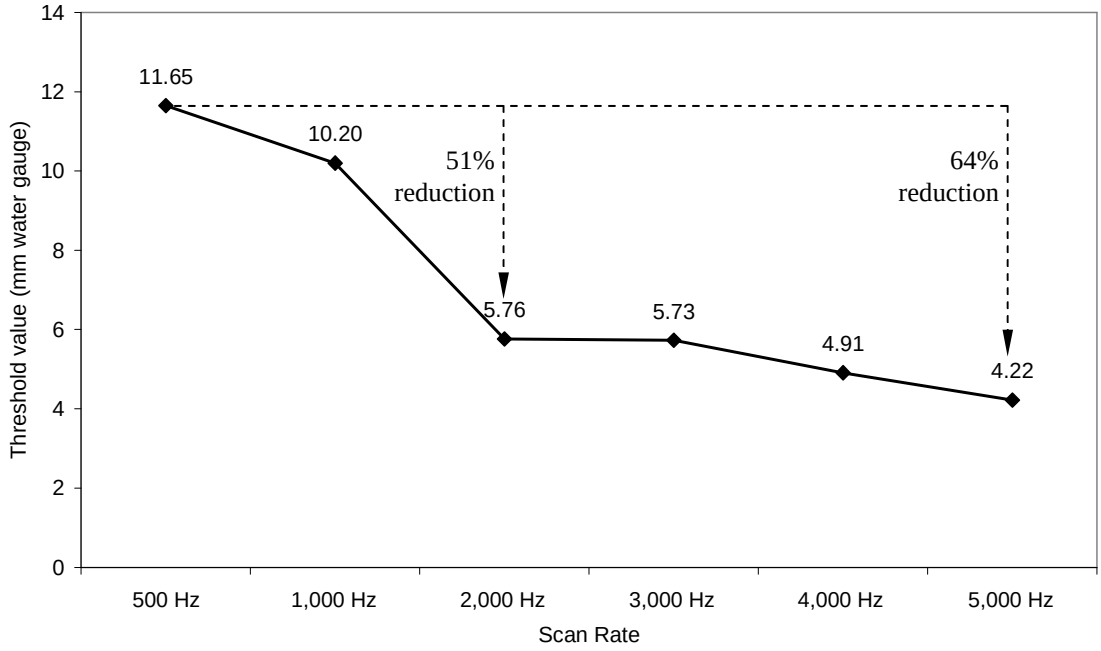

Figure 5.27 Threshold values calculated for different data scan rates

5.2.5.5.2 Signal repeatability

It is essential to the success of the technique that the incident transient, to which every system response is measured, is repeatable. This is especially important for the automatic detection and location of a depleted trap using the TRACER program as this uses a time series change detection test to estimate the arrival time of a depleted trap induced reflection by comparing the measured test system response with the defect free baseline. Any variation to the incident transient will alter the system response, thus making a direct comparison impossible and would potentially cause false alarms or incorrect system diagnosis.

This requirement was highlighted during these investigations as the test system response was sometimes found to have varied from the defect free baseline despite the conditions within the system remaining unchanged. Take the example shown in **Figure 5.28**. The test system response appears to match with the defect free baseline until around 0.01 seconds when it can be seen to deviate from the baseline. This deviation could be mistaken as the influence of a reflection returned from a depleted trap at a distance of 1.72 m (i.e. (0.01 x 343)/2). However, with the closest appliance located 5.4 m away this was clearly not possible.

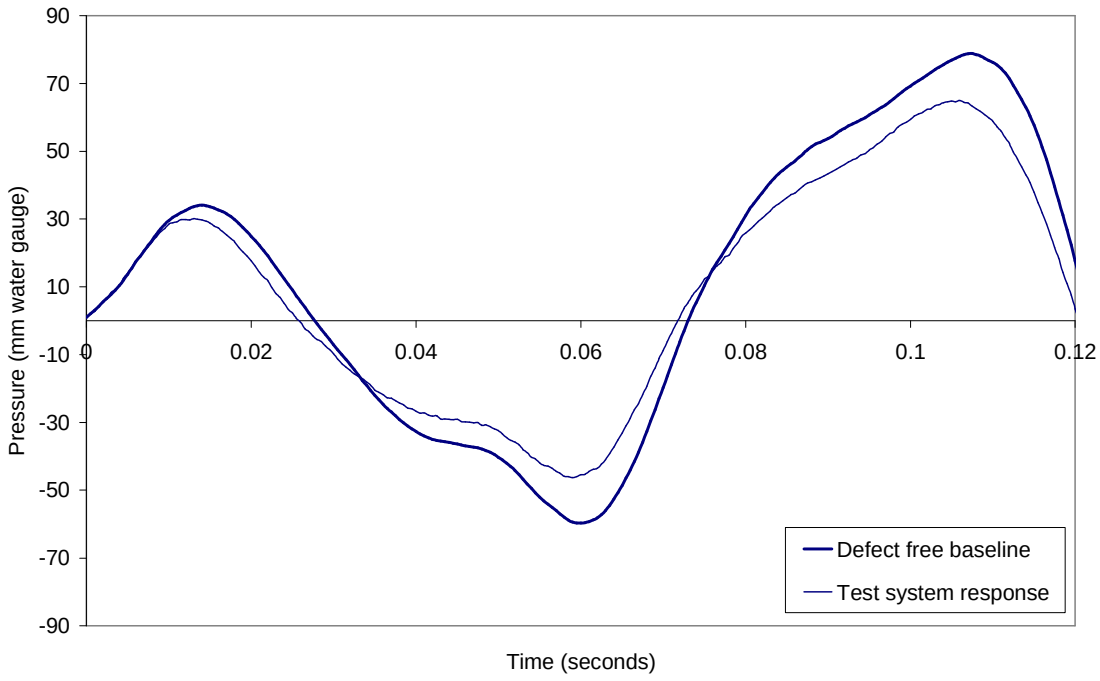

Figure 5.28 Comparison of a test system response, recorded while the system was defect free, with the defect free baseline. The two traces are unmatched as the test system response is seen to be of a lower magnitude thus causing an incorrect system diagnosis

A series of tests were conducted to determine the cause of the variation. It was discovered that the output from the piston exciter was susceptible to external temperature changes and, therefore, the applied incident transient was not consistent throughout the tests. **Figure 5.29(a)** clearly illustrates the effect of changing the external temperature by comparing the threshold value (or maximum deviation) calculated between the test system response and the defect free baseline with the external temperature recorded at the time of testing over a 16 day period. The threshold value can be seen to fluctuate in direct response to the natural variation of daily external temperature. On the days when the external temperature was low, the threshold value was high, thus confirming a variation in the test system response (i.e. on 24-Oct, the external temperature was 2.4 ^{o}C and the threshold value was 23.8 mm water gauge, see **Figure 5.29(b)**). Conversely, on days when the external temperate was high, the threshold value was low, thus confirming a close match between the defect free baseline and the test system response (i.e. on 02-Nov, the external temperature was 14.5 ^{o}C and the threshold value was only 4.8 mm water gauge, see **Figure 5.29(c)**).

It should be noted that the relationship between external temperature and the resultant threshold value is dependant upon the conditions at the time the defect free baseline was measured. Had it been measured on a day when the external temperature was low then the effect on the threshold value would be reversed.

To evaluate the influence that changing temperature had on the output from the piston exciter and to determine its effect on the resultant incident transient and measured system response, a series of temperature-controlled laboratory tests were conducted. The transient entry device and data acquisition system were placed within an environmental chamber and a simple 5-storey single-stack test-rig was extended to connect to the 3-port valve on the transient entry device, **Figure 5.30**. The temperature within the environmental chamber was varied between 5 ^{o}C and 35 ^{o}C in increments of 5 ^{o}C. The system response was measured at each increment once the temperature at the piston exciter had stabilised. The temperature at the piston exciter was measured using a simple thermocouple (Temperature Control Ltd., Type K) with a temperature range of -40 ^{o}C to 375 ^{o}C, a resolution of 0.1 ^{o}C, and a tolerance of ±1.5 ^{o}C.

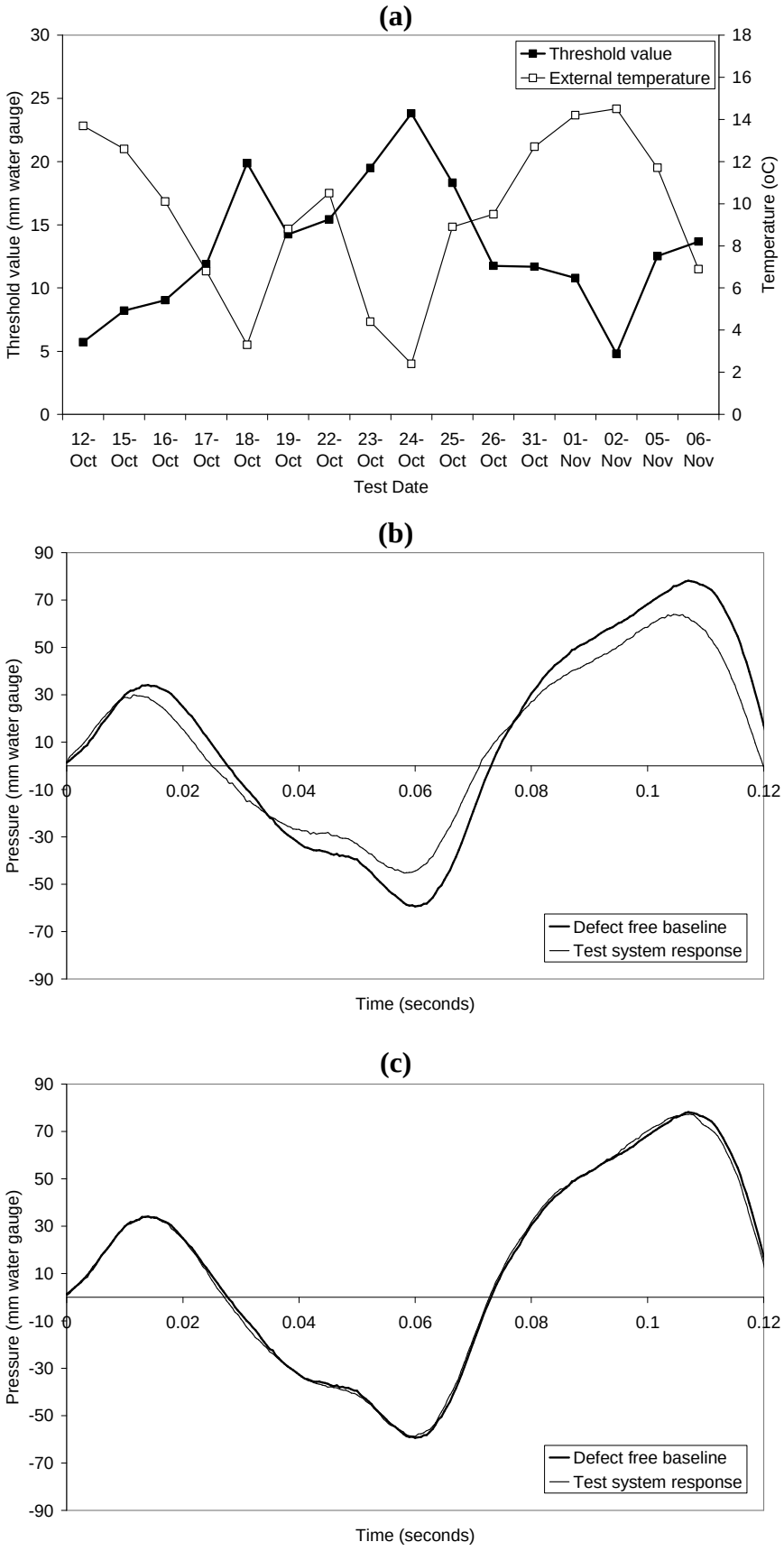

Figure 5.29 Effect of fluctuations in external temperature on the repeatability of the test: (a) comparison of the threshold value and external temperature; (b) the test system response measured on 24-Oct; (c) the test system response measured on 02-Nov

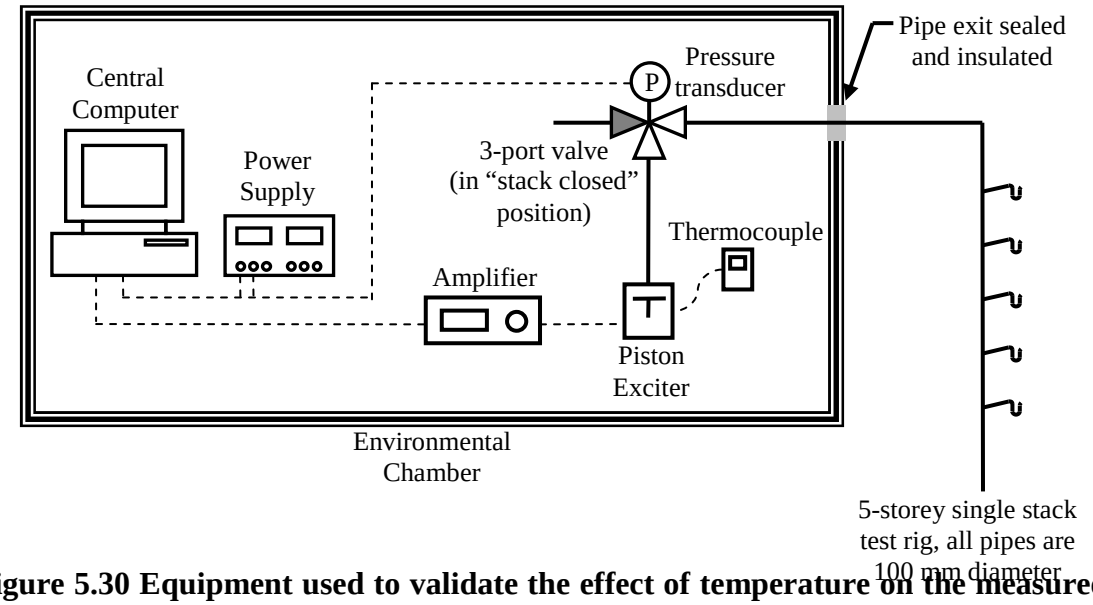

Figure 5.30 Equipment used to validate the effect of temperature on the measured system response

Figure 5.31 compares the system response measured at each temperature. Note that the response measured at 20 ^{o}C (representing nominal ambient conditions) has been set as the defect free baseline to provide a benchmark for comparison. The magnitude of the measured system response clearly varies with temperature. The magnitude increases with increasing temperature.

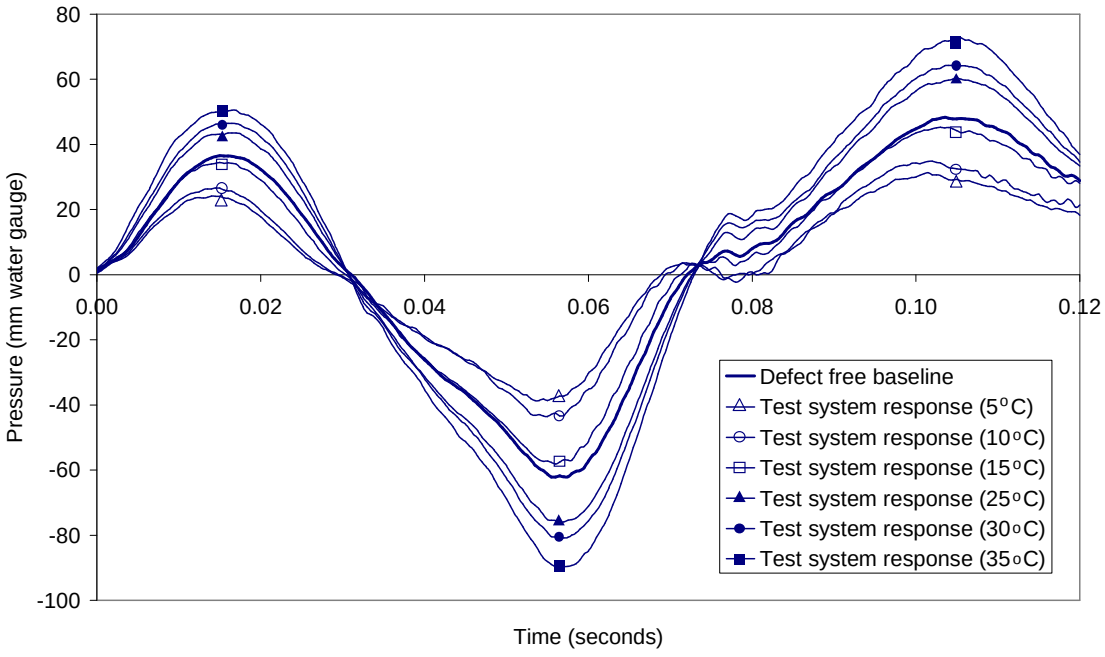

Figure 5.31 Variation in the recorded test system response to different environmental temperatures

The threshold value calculated for each temperature is plotted in **Figure 5.32**. Note that those calculated from the system responses measured below 20 ^{o}C have been plotted as negative values to indicate the direction of variance from the defect free baseline.

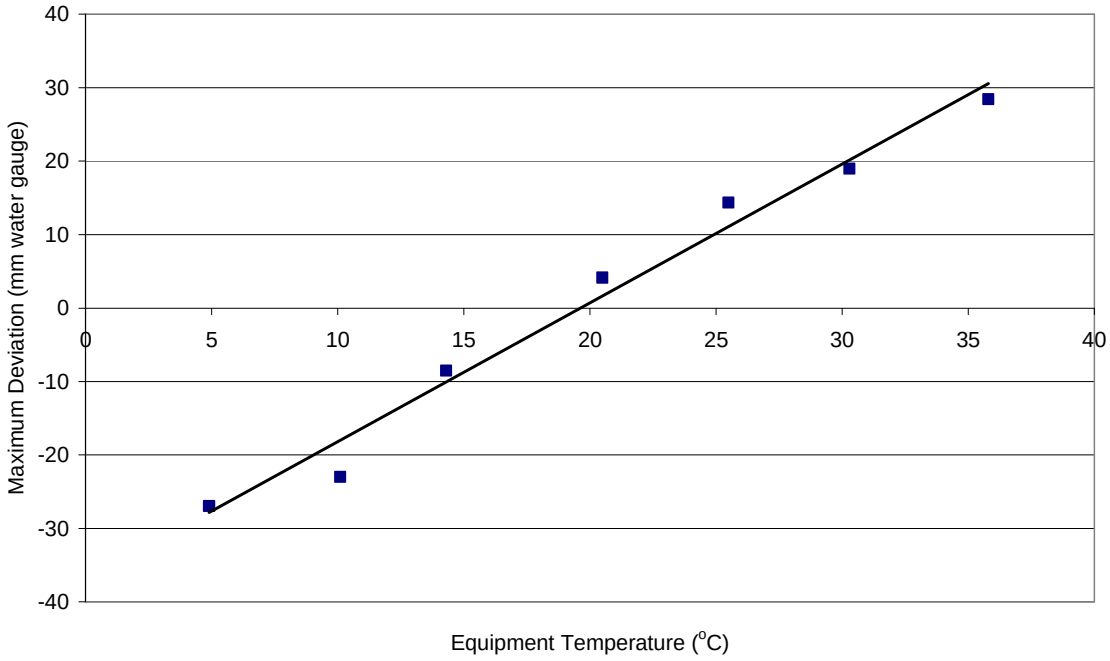

Figure 5.32 Maximum Deviation of the initial test system responses against temperature

The relationship between threshold value and temperature is clearly linear. It is assumed from these results that the likely cause of this linear variation is due to the changing resistance of the copper drive coil used to control the movement of the piston exciter. It is known that the resistance of copper is a linear function of temperature. As temperature increases, the resistance of the copper coil will also increase resulting in a larger power output. This coincides with the results from both **Figure 5.31** and **5.32** which show the magnitude of the incident transient and the threshold values increasing with rising temperature.

Therefore, to improve test repeatability it was necessary to ensure that the piston exciter was maintained at a stable temperature. This was achieved by using a 3.0 kW electric warm air heater to control the local ambient temperature at the exciter.

It must be emphasised that the effect of external temperature fluctuations was worsened in this case by the close proximity of the piston exciter to an external air louvre within the boiler room. The susceptibility of the piston exciter to changes in external

temperature and the effect that this had on the applied incident transient is a function of the exciter used in these investigations and not a fundamental problem with the technique. Subsequent tests on the Glasgow (*field*) system, Section 5.2.6, did not require additional temperature control as the piston was located in an internal plantroom where the temperature was stable.

5.2.5.6 General observations

During the initial system survey the boiler room floor gully was found to be completely dry and filled with debris, **Figure 5.33**. The gully trap was cleaned, the debris removed, and the trap was primed with water in preparation for testing.

Figure 5.33 The boiler room floor gully was found to be completely dry and was filled with debris

The purpose of the floor gulley was to collect condensate from the six boilers, however, due to insufficient volumes of condensate generated by the boilers and the high temperatures within the boiler room, the water seal was found to evaporate on a daily basis. Recurring problems such as this would be easily identified by the maintenance technique proposed in this thesis, allowing necessary system alterations to be made. In this case, the existing water sealing floor gully could be replaced with a waterless trap which would not be affected by the high temperatures within the boiler room.

5.2.6 Experimental field trials in a 7-storey insurance building in Glasgow

5.2.6.1 General

The final set of field trials combines the knowledge and practical experience gained from the previous investigations to apply the reflected wave technique for the identification of depleted trap seals in the multi-stack drainage system of a fully operational commercial building which was not under the direct control of the investigators.

Permission to test the drainage system of the Direct Line Insurance building at Atlantic Quay in Glasgow was granted by the Royal Bank of Scotland. This 7-storey building was constructed in 2001 and is currently used by the bank as a call centre.

To avoid disruption to the business, the tests were conducted out of hours (i.e. between 10pm and 5am).

5.2.6.2 System description

Before testing commenced, a full survey was carried out to determine the configuration and geometry of the building drainage system. The Glasgow (*field*) system consisted of multiple single-stacks which collected the waste from the staff toilets on Floor 1 to Floor 7, **Figure 5.34**. There were six 100 mm diameter stacks in total, two collecting the waste from wcs only and four collecting waste from wash-hand-basins only. Each stack connected to a horizontal drain pipe located at high level in the basement before exiting the building to connect to the main sewer. Each stack was terminated with an AAV within the plantroom on Floor 8. The majority of the system was constructed in cast iron, only changing to uPVC at each of the branch connections on each floor.

Three sets of tests were conducted. The first tested only one wc stack (Stack 2), *Configuration VI* in **Figure 5.35**; the second tested only one wash-hand-basin stack (Stack 3), *Configuration VII* in **Figure 5.35**; and the third tested all six stacks, *Configuration VIII* in **Figure 5.36**.

For the tests conducted on only the single stacks (*Configuration VI* and *VII*) the transient entry device was installed at the top of each stack in turn. Installation was straightforward as the device slotted easily onto the existing stack using standard connections. The AAV was re-connected to the stack termination to ensure usual operation during *normal mode*.

For the multi-stack tests (*Configuration VIII*) the transient entry device was located on Stack 3 and distributed pressure transducers were located on each of the remaining stacks at Floor 3. The decision to install distributed pressure transducers was taken following the experience at the HWU Arrol (*field*) system tests where it was found that when relying solely on one measurement point at the transient entry device, the arrival time of reflections returned from distant traps were sometimes difficult to measure accurately due to dissipation of the returning reflection caused by the effects of the system junctions.

The optimum location for the distributed measurement points was would have been the base of each stack. However, due to problems of accessibility the distributed measurement points had to be installed at Floor 3 instead, thus allowing only those traps on Floors 4 to 7 to be monitored.

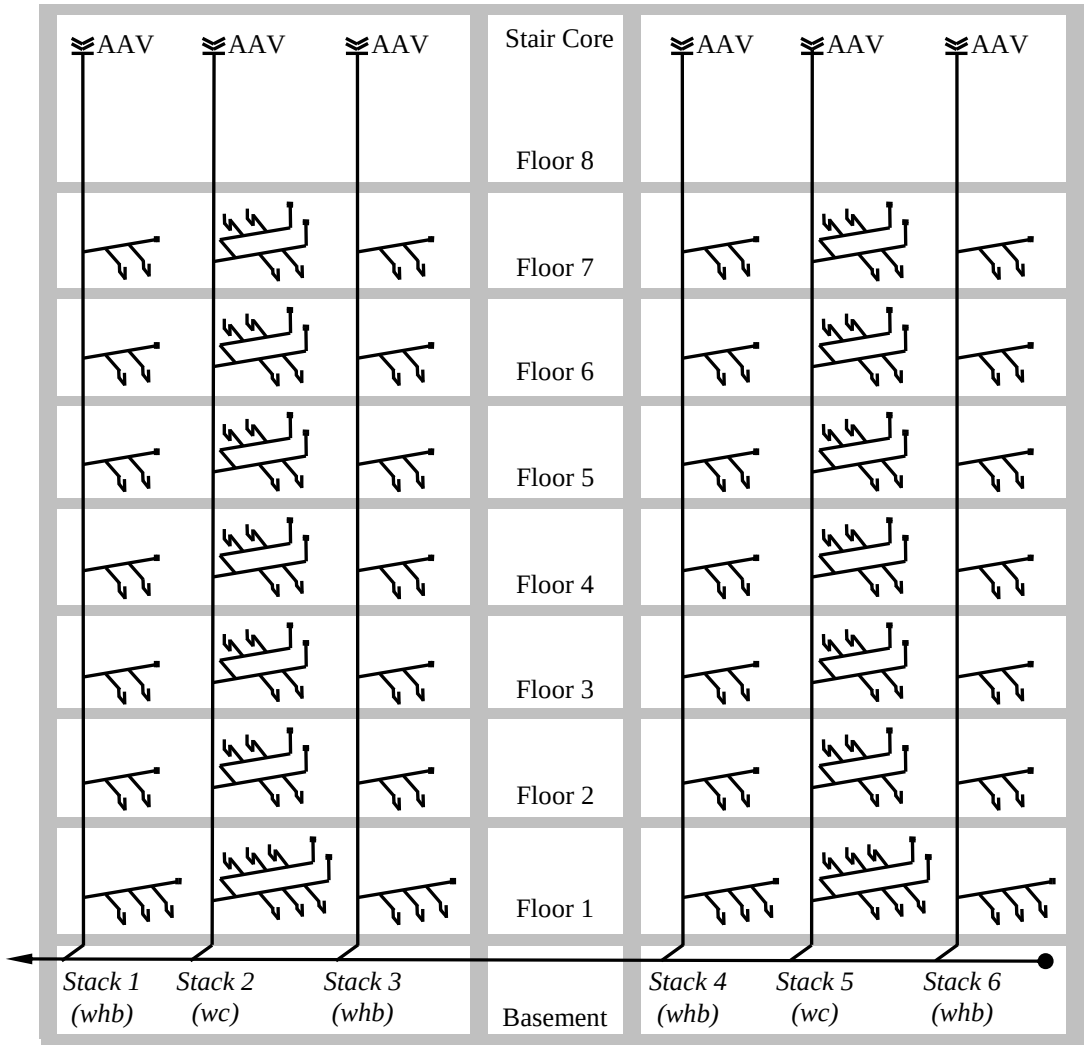

Figure 5.34 Schematic of the Glasgow (*field*) system

Transient entry device
installed on Stack 2

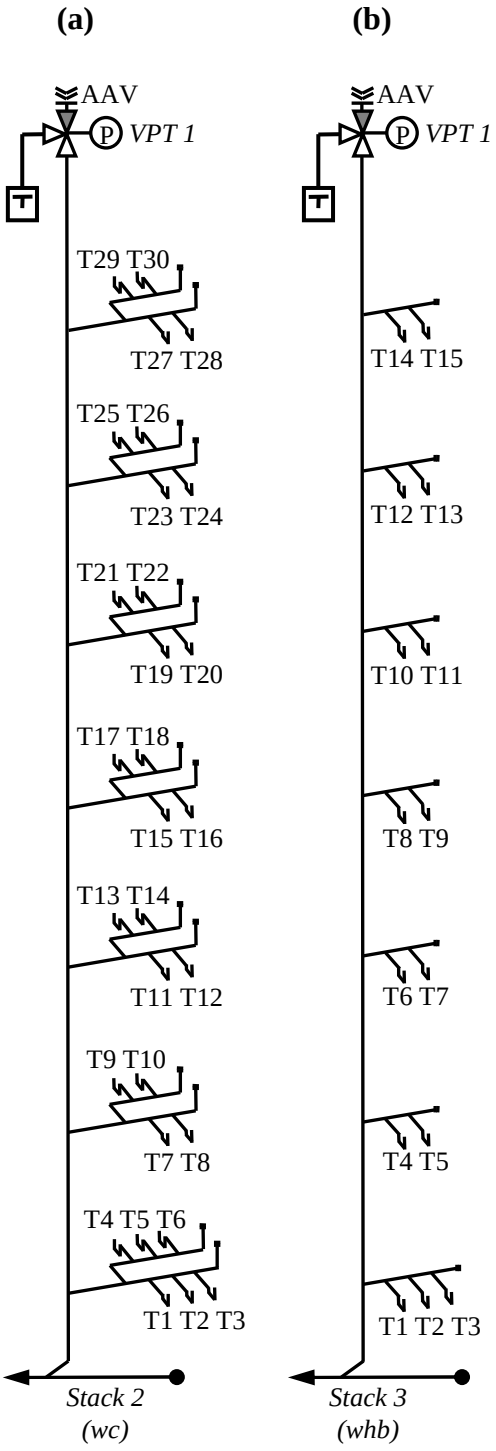

Transient entry device
installed on Stack 3

wc branch connection
into stack

whb branch
connection into stack

Drainage exit point
from building

Notes:
All stack diameters are 100 mm.
wc branch diameters are 100 mm.
wc trap diameters are 100 mm.
whb branch diameters are 50 mm.
whb trap diameters are 40 mm.

Stack connection to
drain pipe at high level
in basement

Figure 5.35 Schematics of (a) *Configuration VI*; and (b) *Configuration VII*

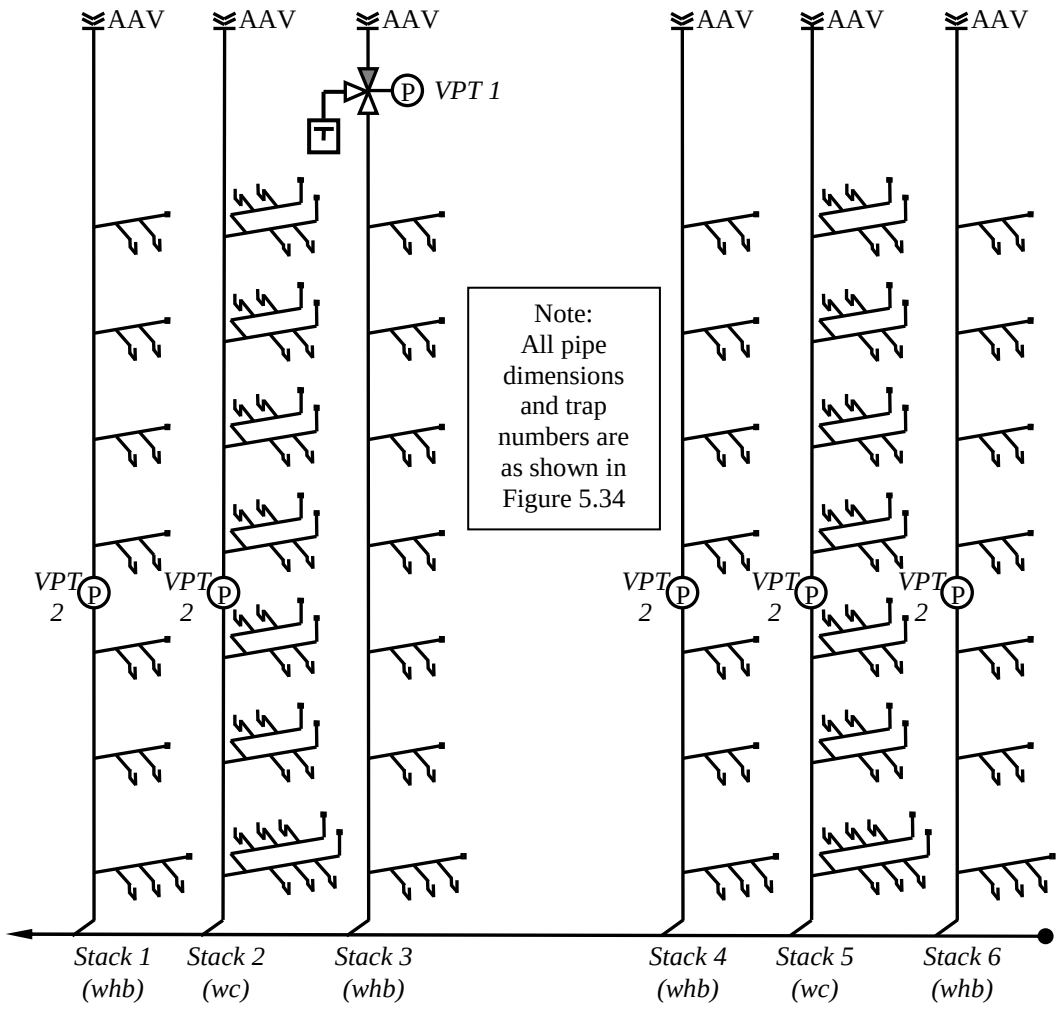

Figure 5.36 Schematic of *Configuration VIII*

5.2.6.3 Simulation of a depleted trap seal

Depleted traps were created by removing the water seal from each trap in turn using a hand suction pump. All other traps were monitored regularly during testing to ensure they remained fully primed.

5.2.6.4 Data Collection

The test set-up procedure outlined in Section 5.2.2.7, in conjunction with the operational control method shown in **Figure 5.17**, was used to determine the relevant system information required by the TRACER program. Each set of tests began by switching the transient entry device to *test mode* before the transient was introduced and the resultant system response was measured. **Figure 5.37**, **5.38** and **5.39** show the defect free baseline and threshold value measured for *Configuration VI*, *VII* and *VIII*, respectively.

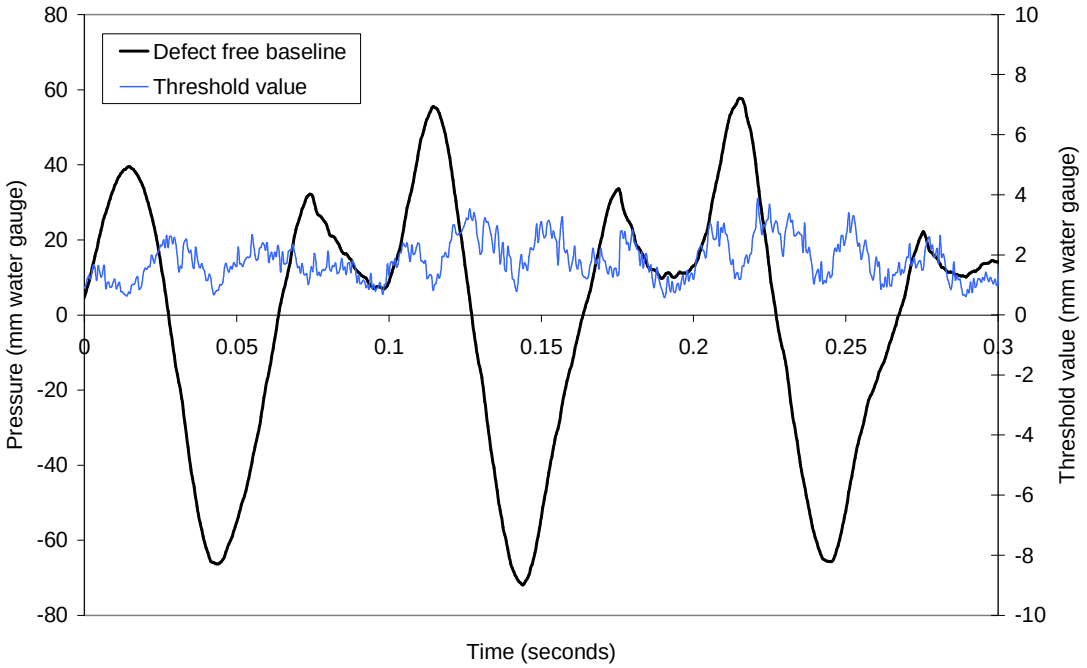

Figure 5.37 Calculated defect free baseline, P_j^{DF}, and threshold value, *h*, for *Configuration VI* measured at VPT1, *h* = 4 mm water gauge

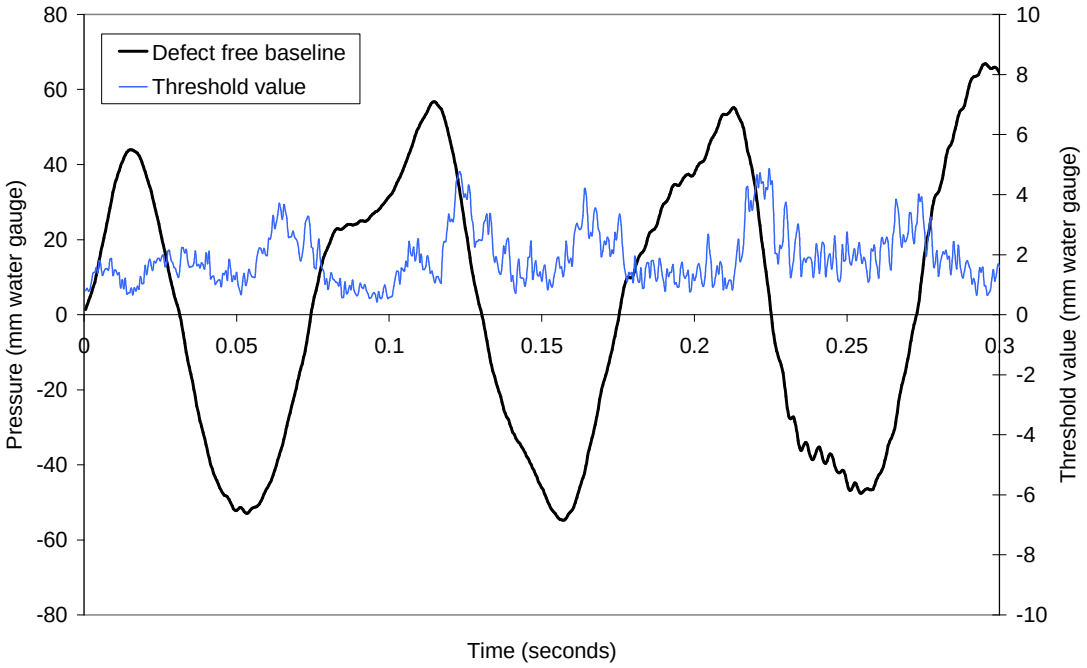

Figure 5.38 Calculated defect free baseline, P_j^{DF}, and threshold value, *h*, for *Configuration VII* measured at VPT1, *h* = 5 mm water gauge

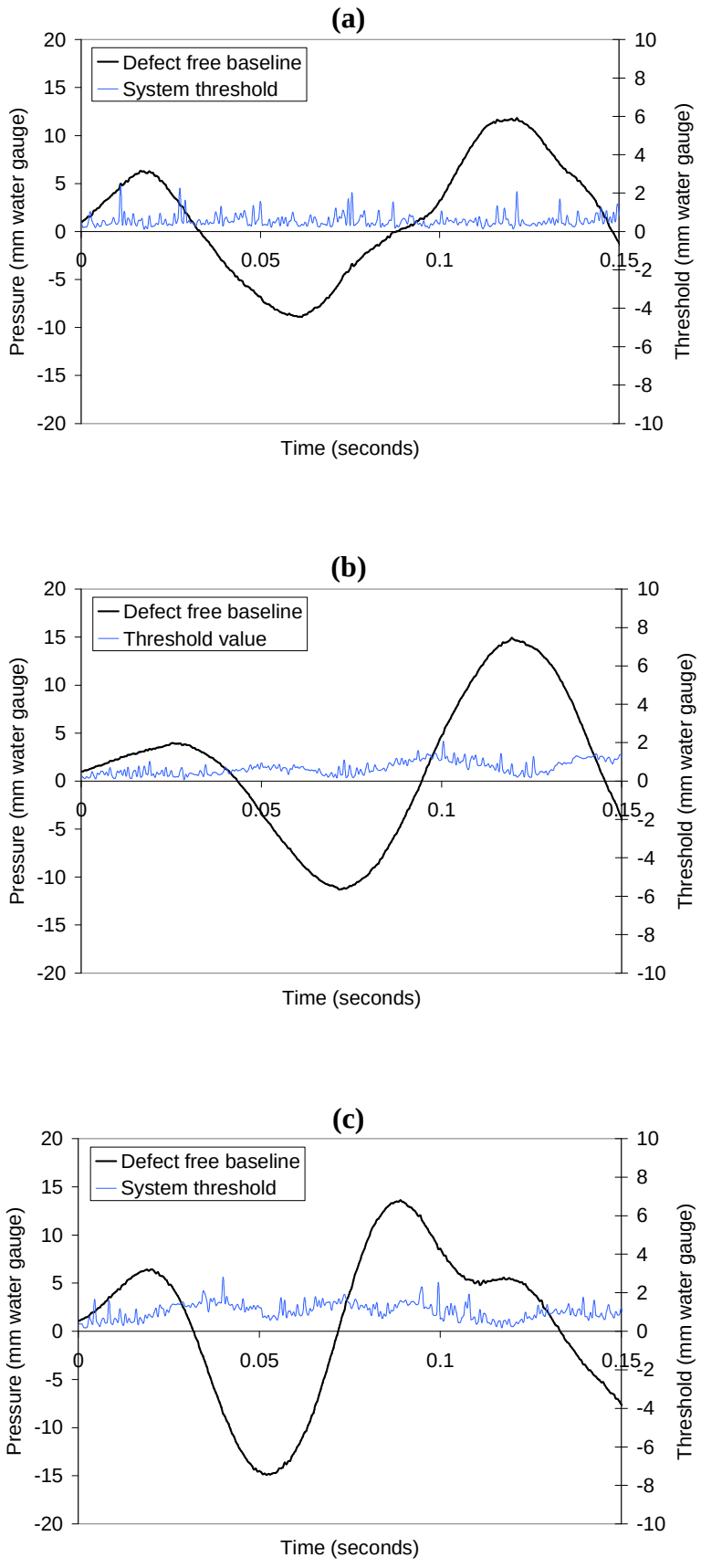

Figure 5.39 Calculated defect free baseline, P_j^{DF}, and threshold value, *h*, for *Configuration VIII* measured at VPT2: (a) stack 1, *h* = 2 mm water gauge; (b) stack 2, *h* = 2 mm water gauge; (c) stack 4, *h* = 2 mm water gauge

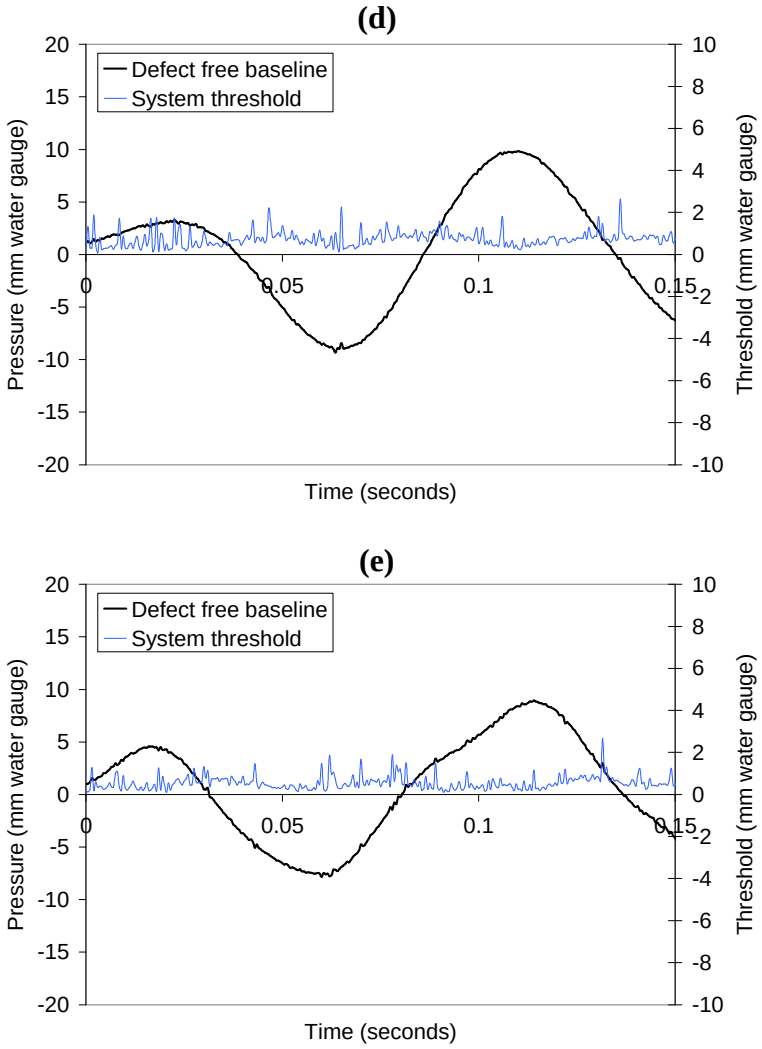

Figure 5.39 cont. Calculated defect free baseline, P_j^{DF}, and threshold value, *h*, for *Configuration VIII* measured at VPT2: (d) stack 5, *h* = 3 mm water gauge; (e) stack 6, *h* = 3 mm water gauge

5.3 Laboratory tests at Heriot-Watt University to investigate the influence of different system boundaries

As detailed in Chapter 4 every boundary that a transient encounters will induce a characteristic reflection while the remainder of the wave is transmitted forwards. This reflection and transmission process modifies the shape of the propagating transient and ultimately alters the resultant system response. As this boundary mechanism underpins the basis of the reflected wave technique it is essential that the influence of each boundary is understood. This not only enables a more accurate interpretation of the information contained within the system response but also determines how the presence

of a specific boundary condition within the system may influence the success of the technique to accurately identify depleted trap seals.

The effect of three system boundaries will be examined through a series of laboratory investigations. The boundaries include: branch/trap diameter, an AAV and a PAPA.

5.3.1 Experimental test-rig

For these investigations a second experimental test-rig was designed and constructed at Heriot-Watt University by this author: the HWU 2 (*laboratory*) system. Simulating a 5-storey single stack system, the test-rig was constructed using uPVC pipes and was designed to be easily adjustable allowing different diameter branches and AAVs and PAPAs to be added and removed when required. Three-pipe spigots were connected at each floor level (Spaced at 3.2 m intervals) which allowed a single branch of either 32 mm, 40 mm, 50 mm, 75 mm or 100 mm diameter to be installed onto the 100 mm diameter stack. Each branch was 1.2 m long. The pipes were secured to a scaffolding rig using pipe clamps, spaced at 2 m intervals, to restrain the pipe from movement or vibration. The transient entry device was connected to the top of the stack (i.e. the section representing the dry stack).

5.3.2 Data collection

To determine the effect of each boundary condition the system response was measured for the system both with and without the test boundary installed, thus allowing the effect of each boundary to be easily identified by direct comparison of the two traces.

To allow the effect of each boundary to be checked against the accuracy of the reflected wave technique the relevant system information required by the TRACER program was collected by following the test set-up process described in Section 4.5.1.1 in conjunction with the operational control method shown in **Figure 5.17**. The system without the boundary installed was used as the defect free baseline.

The effect of branch/trap diameter was investigated using *Configuration IX(a-f)*, **Figure 5.40**. First, the defect free baseline was determined using *Configuration IX(a)* – the single stack with no branches connected. The system response was then measured for each branch location and for each branch diameter using *Configuration IX(b-f)*. The system response was first measured while the trap was fully primed so that only the effect of the new junction could be analysed. Next, the system response was measured while the trap was depleted so that the effect of branch/trap diameter could be analysed.

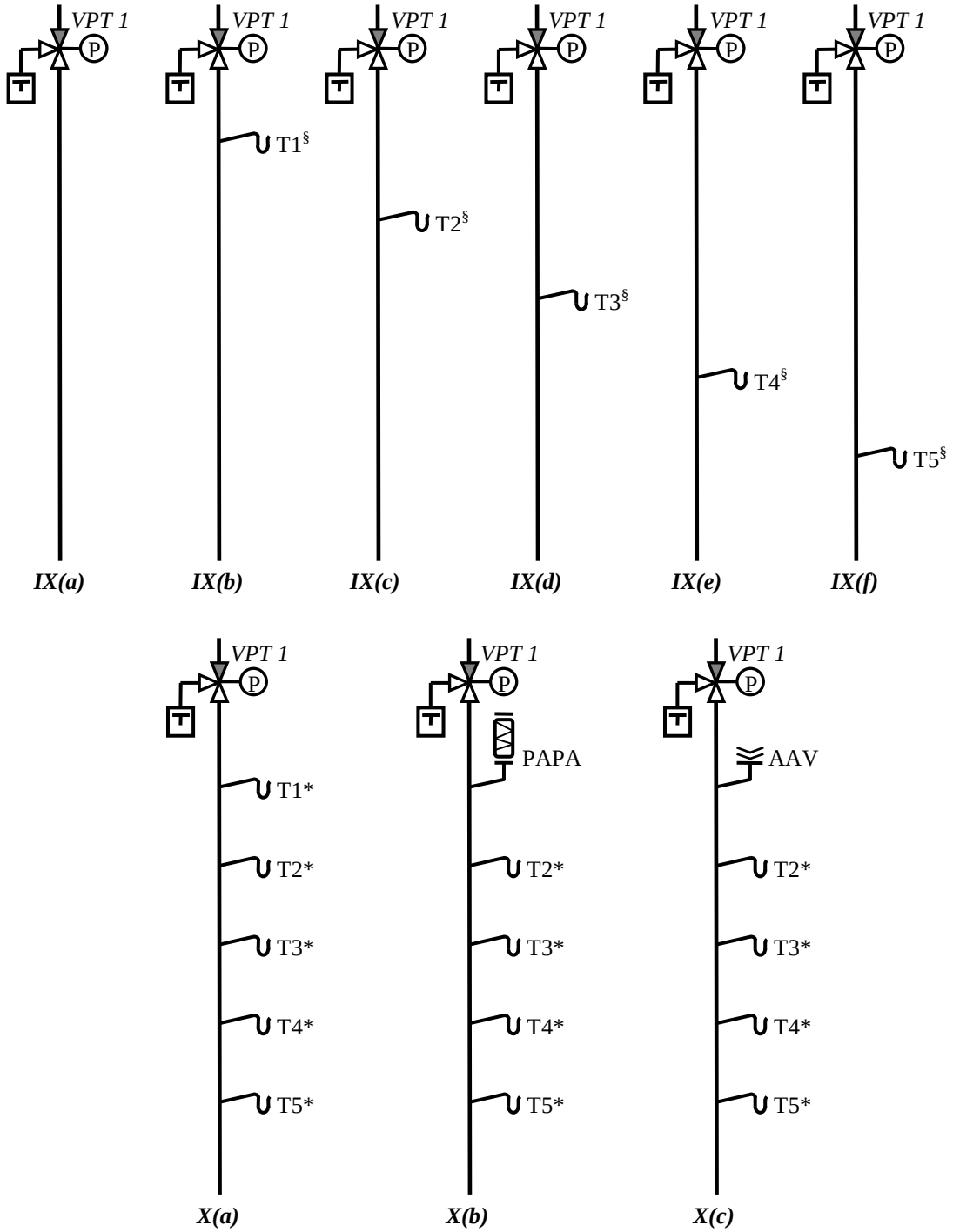

Notes
1. All pipes are uPVC.
2. The stacks are 100 mm diameter.
3. All branches are 1.2 m long and are spaced at 3.2 m centers
4. § branch/trap diameters of 32 mm, 40 mm, 50 mm, 75 mm and 100 mm investigated at each location.
5. * branch/trap diameter of 100 mm.

Figure 5.40 The HWU 2 (*laboratory*) system showing each configuration tested

Configuration X(a-c), **Figure 5.40**, was used to determine the influence of both the PAPA and AAV. First, the defect free baseline was measured using *Configuration X(a)* without either the PAPA or AAV installed. The system response for each depleted trap was then measured in order to provide a benchmark to which the effect of installing the PAPA or AAV on the accuracy of the reflected wave technique could be compared. Next the system response was measured for *Configuration X(b)* and then *Configuration X(c)* to determine the effect of the PAPA and AAV, respectively. With each new boundary installed the system response for each depleted trap was measured.

Figures 5.41 presents the defect free baseline and threshold value for both *Configuration IX(a)* and *X(a)*.

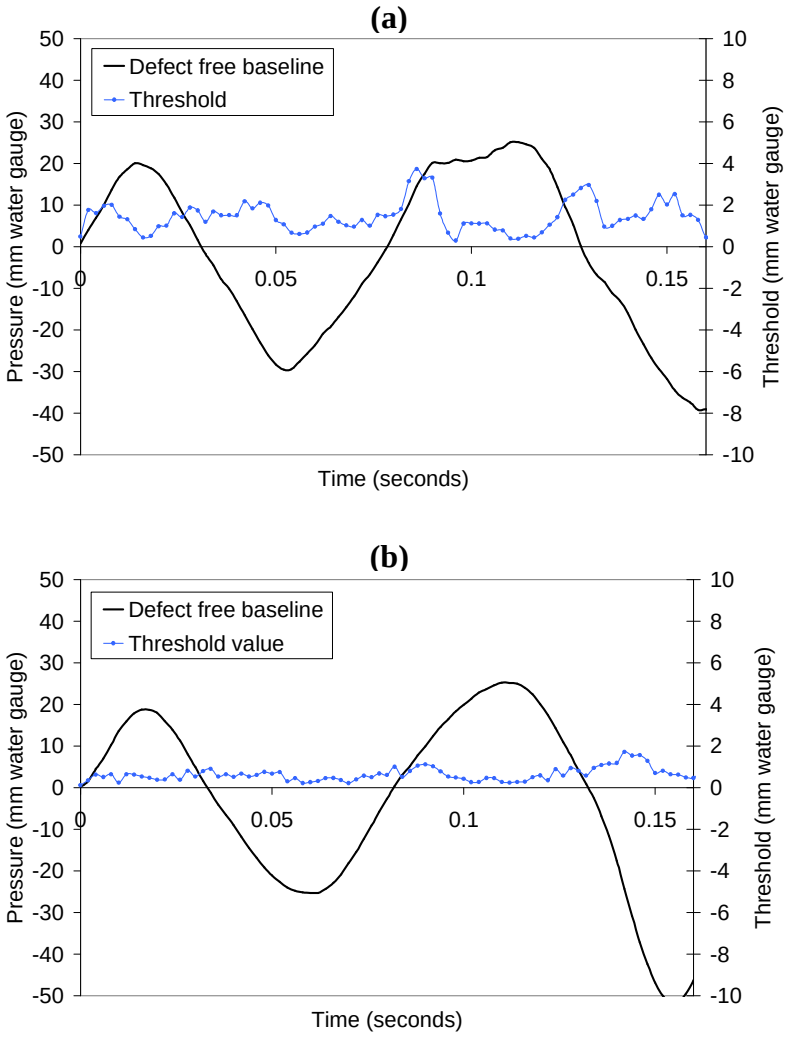

Figure 5.41 Calculated defect free baseline, P_j^{DF}, and threshold value, *h*, for (a) *Configuration IX(a)*, *h* = 4 mm water gauge; (b) *Configuration X(a)*, *h* = 2 mm water gauge

5.4 Errors and accuracy

The accuracy of the reflected wave technique relies heavily on the equipment used to gather all of the required data. The successful application of the technique for the detection and location of depleted trap seals requires the accurate measurement of the system response together with a detailed knowledge of the pipe lengths and distances to each trap which are all subject to experimental uncertainties, or errors, due to instrumental, physical and human limitations.

The experimental uncertainties associated with the transient data collected during these investigations have been quantified and summarised in **Table 5.2** below.

Parameter	Logger	Uncertainty (%)	Uncertainty (SI units)
Pressure	Pressure Transducer	± 0.25% of full range (± 250 mm water gauge)	± 1.25 mm water gauge
Piston stroke	LVDT	± 0.5% of full range (± 300 mm)	± 3 mm
Pipe diameter	Measured	Not perfectly circular	± 1.5 mm
Pipe length	Measured	Human error	± 2.0 mm
	Acquisition board (sampling rate)	250 kHz and c~343 m/s	0.00137 m ($\Delta x = c/f$)
	Acquisition board (scan rate)	500 Hz and c~343 m/s	0.69 m ($\Delta x = c/f$)
	Acquisition board (scan rate)	2,000 Hz and c~343 m/s	0.17 m ($\Delta x = c/f$)

Table 5.2 Summary of data errors

As the reflected wave technique is used ultimately to determine the distance to the depleted trap seal, the errors affecting pipe length measurement are of most interest here. The maximum error can be estimated by summing the likely uncertainty associated with each source of error. For a scan rate of 2,000 Hz, the maximum error will be 0.17337 m (0.002 m + 0.00137 m + 0.17 m). The significance of this error on the accuracy of the reflected wave technique can be estimated by determining its effect on both the largest system (i.e. *Configuration I*, 77 m high) and the smallest system (i.e. *Configuration V*, 15 m high) tested during these investigations. The maximum relative error, while using a scan rate of 2,000 Hz, associated with experimental uncertainty is, therefore, 0.2% for *Configuration I* and 1.2% for *Configuration V*.

The associated experimental uncertainties can, therefore, be assumed to have a negligible influence over the accuracy of the technique.

5.5 Summary and Conclusions

Extensive experimental investigations were conducted under both controlled laboratory conditions and field conditions. Many transient tests were carried out by measuring the system response to an applied incident transient with and without simulated depleted trap seals.

Several problems were encountered during the data collection phase, requiring various changes and developments to be made to the test technique, including: design of a controllable transient entry device; application of a non-destructive incident transient; ensuring accurate alignment of the test system response with the defect free baseline; improving test repeatability and reliability. Modifications were made during the development of the technique to either resolve or mitigate these problems.

Despite the difficulties faced, much reliable data was collected and used to validate the reflected wave technique as a potential method for monitoring the building drainage system against the threat of cross-contamination from depleted trap seals. The ability of the TRACER program to effectively detect and locate a depleted trap within the system by automatically analysing the test system response and its potential as a systematic maintenance tool will be reviewed.

Finally, the accuracy of the equipment used to collect data and the methods used to determine system dimensions were quantified and summarised. These experimental uncertainties were found to have a negligible influence over the accuracy of the technique.

Chapter 6
Test results and analysis

6.1 Introduction

This chapter presents the results of the investigations outlined in Chapter 5. Using physical data collected during both controlled laboratory conditions (HWU 1 and HWU 2) and field conditions (Dundee, HWU Arrol and Glasgow), the analysis aims to both evaluate the reflected wave technique as a means of detecting and locating depleted trap seals within the building drainage system, and analyse the effect that some system components can have on the accuracy of the technique. This chapter is organised into the following parts:

i. the trap location error, used as a performance indicator for the proposed technique, is derived,

ii. the reflected wave technique is applied and sensitively analysis is carried out to assess the effectiveness of the proposed technique in detecting depleted traps,

iii. the influence of some common system components will be analysed to determine their effect on the accuracy of the technique,

6.2 Depleted trap location performance indicator

To evaluate the effectiveness of the proposed technique in estimating the location of depleted trap seals, and to enable comparisons between the different data sets acquired during these investigations, a performance indicator is required. This is defined by the *relative error* between the true trap location and the predicted trap location as follows:

$$\varepsilon = \frac{\left| X_D^{true} - X_D^{predicted} \right|}{L} \tag{6.1}$$

in which ε is the trap location error, X_D^{true} and $X_D^{predicted}$ are the true trap location and the predicated trap location, respectively, and L is the total stack height (from the measurement point to the stack termination). This is a similar performance indicator as that used by Covas (2003) and Han *et al.* (2004) to evaluate, respectively, the performance of pipe leak and cable fault detection techniques.

Brunone and Ferrante (2001) use a modified version of this equation to evaluate the performance of a leak detection technique by defining the leak location error with respect to the distance from the leak to the measurement section (i.e. $\varepsilon = \left| X_D^{true} - X_D^{predicted} \right| / X_D^{true}$). Although mathematically correct, this definition depends on the location of the defect from the measurement point so, for the same $\left| X_D^{true} - X_D^{estimate} \right|$, ε can be significantly large or relatively small, depending on whether the defect is very close or far from the measurement point. This definition cannot, therefore, be used as a consistent performance indicator to evaluate the reflected wave technique. The trap location error (or performance indicator) defined above in Equation (6.1) represents the efficiency of the technique in terms of the total stack height and allows assessment of the technique in application to any building drainage system.

6.3 Initial evaluation of the reflected wave technique

The results of the preliminary laboratory investigation are analysed in this section. The AIRNET model is then used to simulate the system in order to evaluate the correlation between the measured and simulated data.

6.3.1 Preliminary laboratory investigation

Data collected using the HWU 1 (*laboratory*) system, *Configuration I* (**Figure 6.1**), using the single positive pressure pulse as the incident transient, were first used to evaluate the reflected wave technique as a potential method for the identification of depleted trap seals within the building drainage system.

Four trap locations (T1, T3, T4 and T12) were selected for comparison and **Figure 6.2** shows the effect of the depleted trap location on the measured system response.

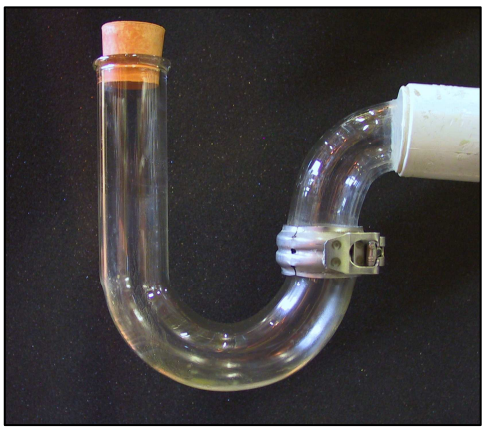

Traps capped using rubber stopper

View of test rig showing the looped pipework

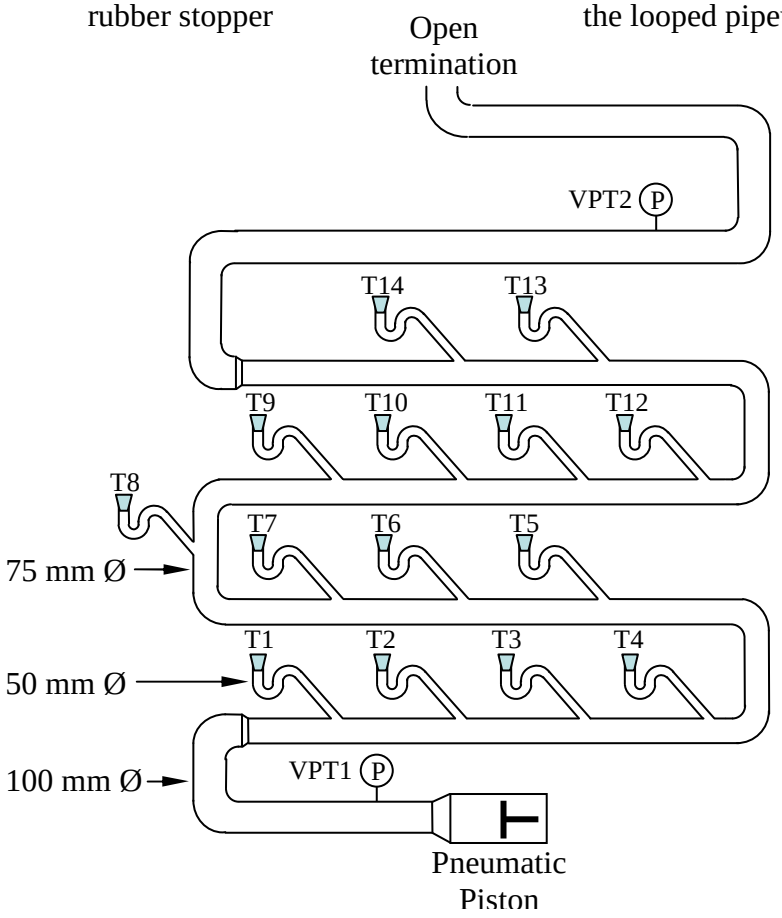

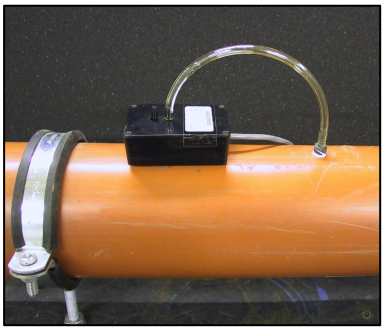

Connection of pressure transducer (VPT1) onto stack

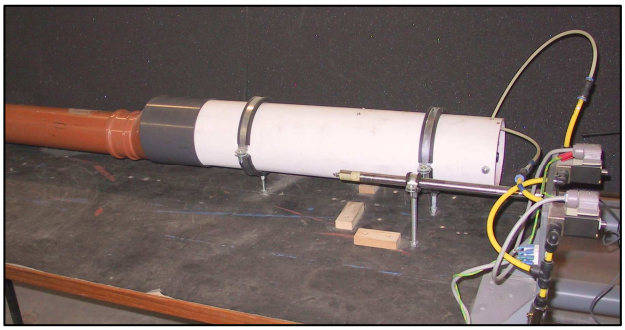

Pneumatic piston installed at base of stack

Figure 6.1 Laboratory test-rig: HWU 1 (laboratory) system, *Configuration I*. Shown previously in Figure 5.1 but repeated here for convenience

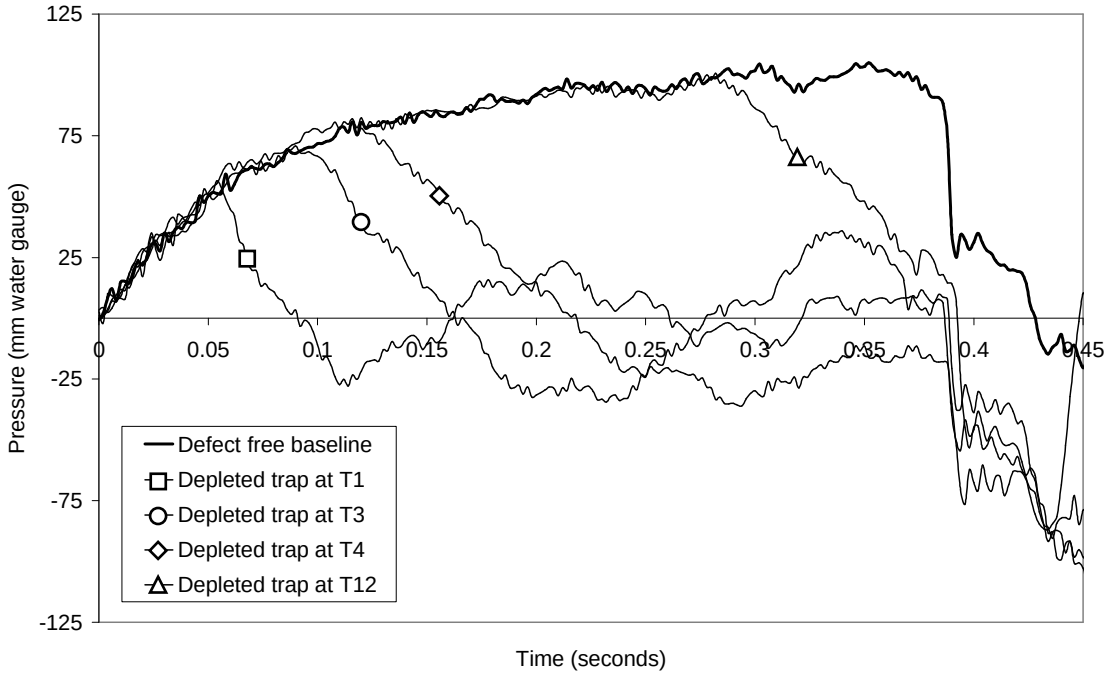

Figure 6.2 Measured pressure response at transducer VPT1 for a selection of depleted trap seals using the HWU 1 (*laboratory*) system, *Configuration I*

It can be seen that each depleted trap induces a negative reflection in response to the applied single positive pressure pulse which alters the measured system response at a time specific to that trap (i.e. the trap pipe period). The success of the reflected wave technique relies on the accurate detection of the arrival time of this negative reflection. However, before the location of the depleted trap can be assessed, the wave propagation speed c must first be determined. An accurate estimate of the wave propagation speed will allow the depleted trap location to be predicted more precisely. Three different methods were used to estimate the wave propagation speed for the system, the results of which are presented in **Table 6.1**.

- ***Method I*** is the theoretical wave speed formula (i.e. Equation 2.2). c was calculated considering air at 20 ^{o}C (p = 1.10913x10^{5} Pa, γ= 1.4 and ρ = 1.32 kg m^{-3}).

- ***Method II*** is based on the travelling times between transducers positioned at different locations on the stack (i.e. $c = L/(t_{VPT2} - t_{VPT1})$ where t_{VPT1} and t_{VPT2} are the arrival times of the transient pressure wave at *pressure transducer 1* and *pressure transducer 2*, respectively).

- ***Method III*** is based on frequency analysis of the transient pressure response using Fast Fourier Transform (FFT) (i.e. $c = 4Lf$, where L = total stack height and f = dominant frequency of the transient pressure response obtained by FFT analysis).

Table 6.1 Estimation of wave propagation speed in the building drainage system

Theoretical formula	**Measurement between transducers**	**Frequency analysis**	
Method I	***Method II***	***Method III***	
c (m/s)	***c*** (m/s)	***f*** (Hz)	***c*** (m/s)
343	333	1.163	327

The wave propagation speed calculated using *Method I* (i.e. 343 m/s) is 3% and 5% higher than those calculated by *Method II* (i.e. 333 m/s) and *Method III* (i.e. 327 m/s) respectively. The arrival time of the negative reflection is determined by the TRACER program using the time series change detection test discussed in Section 4.5.1 where the measured reflection return time $t_D^{measured}$ is taken as the time when the absolute difference between the *defect free baseline* P_j^{DF} and the *measured system response* P_j^M exceeds the threshold value *h* (i.e when $D_t > h$), **Figure 6.3**. The measured depleted trap locations $X_D^{measured}$ determined using Equation (4.2) for each of the three methods is presented in **Table 6.2** together with the trap location errors ε.

Table 6.2 Assessment of the depleted trap location by the reflected wave technique

Trap characteristics		**Measured system response**	**Theoretical formula**		**Measurement between transducers**		**Frequency analysis**	
			Method I **(*c* = 343 m/s)**		***Method II*** **(*c* = 333 m/s)**		***Method III*** **(*c* = 327 m/s)**	
Trap	X_D^{true} (m)	$t_D^{measured}$ (s)	$X_{D(I)}^{measured}$ (m)	$\varepsilon_{(I)}$	$X_{D(II)}^{measured}$ (m)	$\varepsilon_{(II)}$	$X_{D(III)}^{measured}$ (m)	$\varepsilon_{(III)}$
T1	**9.1**	0.056	**9.6**	0.6%	**9.3**	0.3%	**9.2**	0.1%
T3	**15.3**	0.096	**16.5**	1.6%	**16.0**	0.9%	**15.7**	0.5%
T4	**19.6**	0.124	**21.3**	2.2%	**20.6**	1.3%	**20.3**	0.9%
T12	**46.6**	0.290	**49.7**	4.0%	**48.3**	2.2%	**47.4**	1.0%

$$\varepsilon_{(II)} = \frac{\left| X_{D(I)}^{measured} - X_D^{true} \right|}{L} \qquad \varepsilon_{(II)} = \frac{\left| X_{D(II)}^{measured} - X_D^{true} \right|}{L} \qquad \varepsilon_{(II)} = \frac{\left| X_{D(III)}^{measured} - X_D^{true} \right|}{L}$$

When L = 77.0 m (the total stack height)

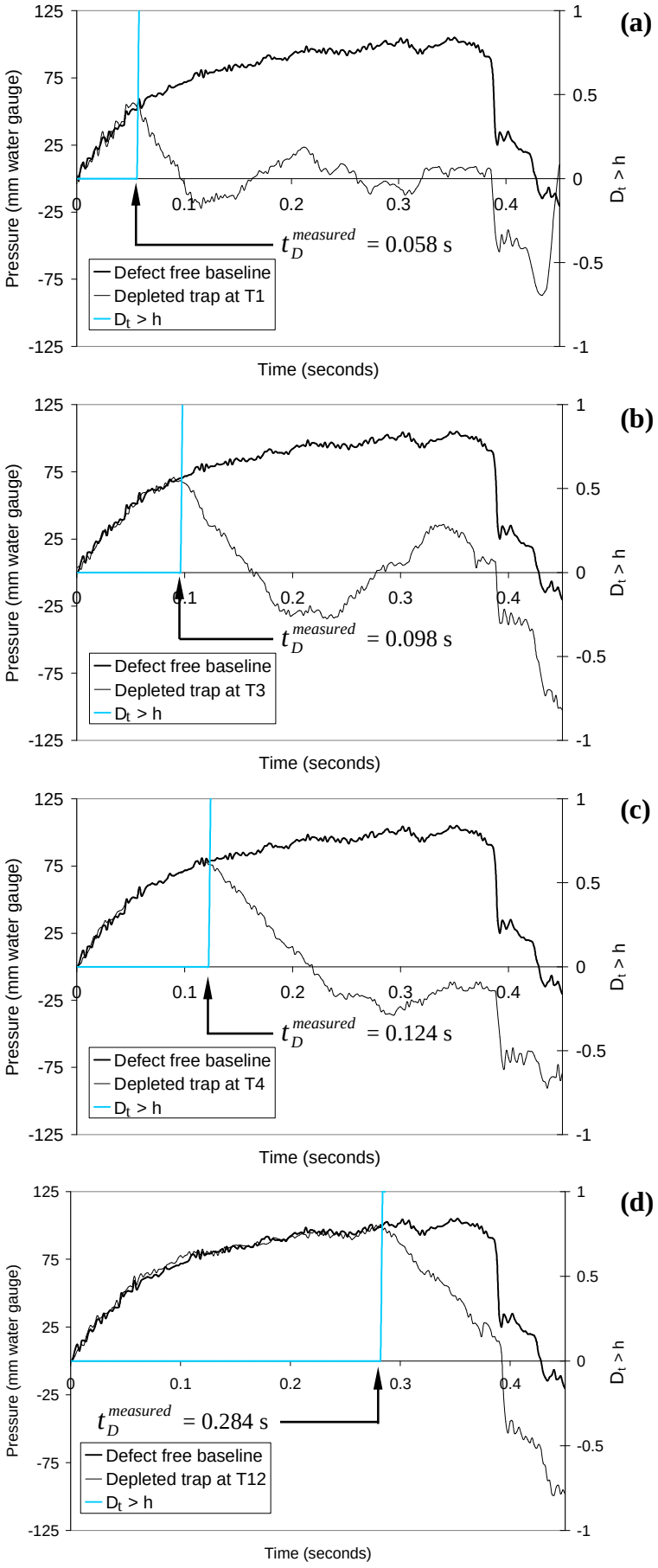

Figure 6.3 Using the TRACER program to identify $t_D^{measured}$ for a depleted trap at (a) trap T1; (b) trap T3; (c) trap T4; and (d) trap T12

The following conclusions can be made:

i. It can be seen from **Figure 6.3** that the TRACER program is capable of automatically identifying the measured reflection return time $t_D^{measured}$ with good accuracy. $t_D^{measured}$ corresponds well with the point of divergence between the defect free baseline and measured system response.

ii. Trap location error ε decreases with the decrease of wave propagation speed, **Table 6.2**. For the highest value of wave propagation speed (i.e. *Method I* = 343 m/s) the location error ε varies between 0.6% and 4.0%, whereas for the lowest value of wave propagation speed (i.e. *Method III* = 327 m/s), ε varies between 0.1% and 1.0%.

iii. Trap location error ε increases with the increase of trap distance (i.e. with an increasing value of X_D^{true}), **Table 6.2**. Whilst ε varies across each of the three methods between 0.1% and 0.6% for trap T1 (i.e. X_D^{true} = 9.1 m), it increases to between 1.0% and 4.0% for trap T12 (i.e. X_D^{true} = 46.6 m).

The wave propagation speed estimated by *Method III* is the most accurate in determining the measured depleted trap locations. However, as will be discussed in Section 6.4 both *Method II* and *Method III* are affected by the *junction effect* which wrongly suggests a lower wave propagation speed than is actually present.

Therefore, the theoretical wave propagation speed estimated using *Method I*, which is unaffected by the *junction effect*, will instead be used throughout the following data analysis. It has already been shown in Chapter 3 and Appendix A that any variation in wave propagation speed, due to its dependency on air pressure, is insignificant within the limits of the pressure excursions experienced within the building drainage system. Wave propagation speed will, therefore, be assumed to be sensibly constant within the context of these test parameters.

6.3.2 Preliminary AIRNET investigations

The HWU 1 (*laboratory*) system, *Configuration I* (**Figure 6.1**), was modelled using AIRNET. The time step used was Δt = 0.002 seconds (equivalent to the 500 Hz data scan rate used during the preliminary laboratory investigations) and the space step was Δx = 0.1 m. The piston displacement data measured in the laboratory by the LVDT (**Figure 5.4**) was used to characterise the piston boundary condition in the form of time-distance pairs. **Figure 6.4** compares the simulated defect free baseline with that determined from the real data measured in the laboratory. It can be seen that the simulated data correlates extremely well with the real system data.

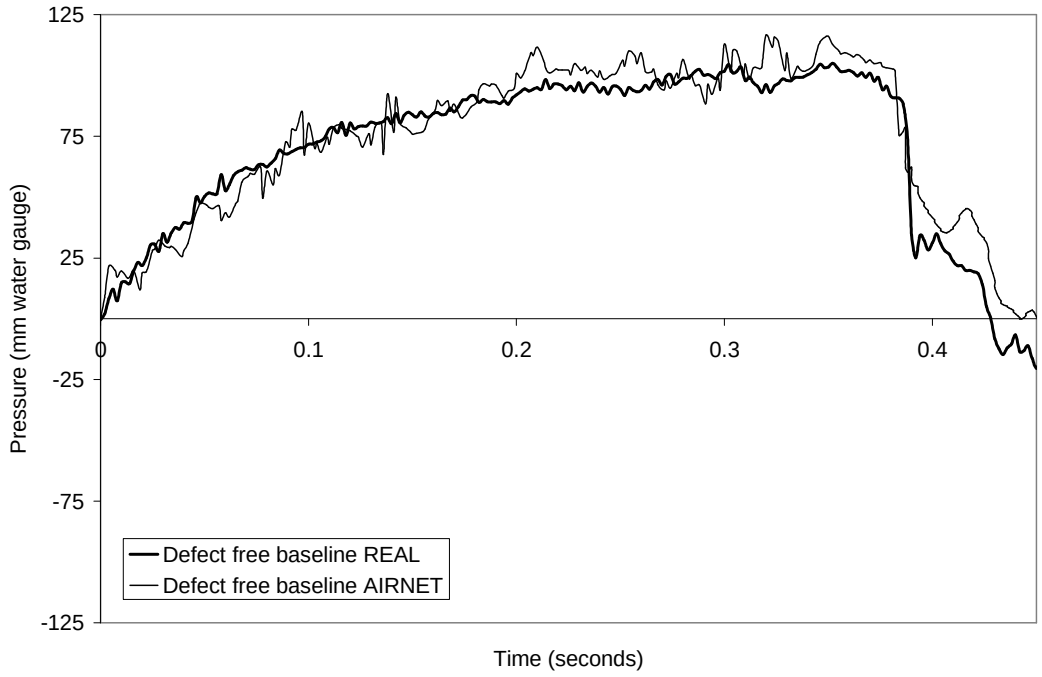

Figure 6.4 Comparison of the measured and AIRNET simulated system response applied as the defect free baseline

The same four depleted trap locations as those used in the laboratory experiments (i.e. T1, T3, T4 and T12) were then simulated for comparison, **Figure 6.5**. Each depleted trap is shown to return a negative reflection in response to the imposed single positive pressure pulse, matching that of the real system data. The TRACER program was used to identify the reflection return times from the simulated data. Note that the threshold value *h* determined from the laboratory data (i.e. *h* = 6 mm water gauge, **Figure 5.5**) was used in the TRACER program to determine the reflection return time from the simulated data.

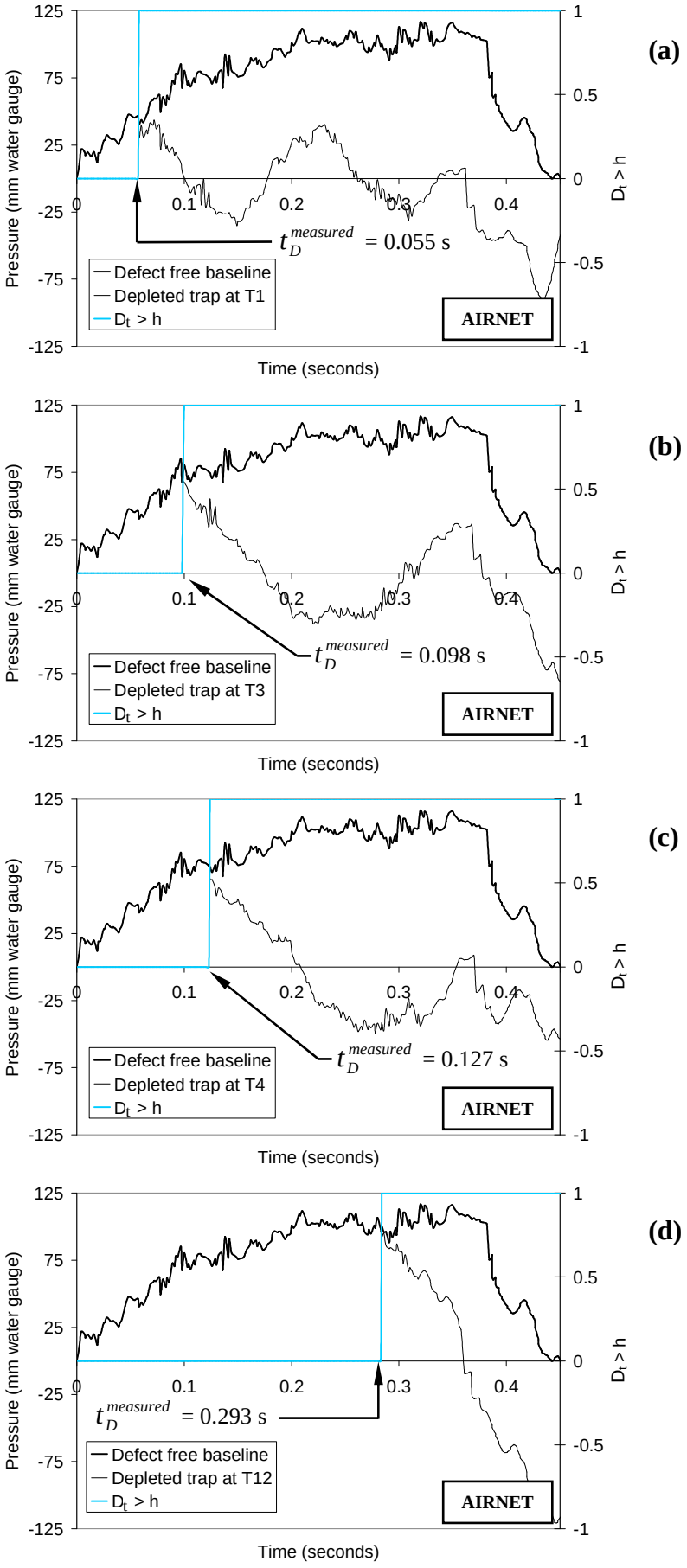

Figure 6.5 Using the TRACER program to identify $t_D^{measured}$ for a depleted trap at (a) trap T1; (b) trap T3; (c) trap T4; (d) trap T12 using AIRNET simulated data

While the analysis of the real system data required the wave propagation speed to be determined, this is not necessary for the AIRNET simulation as the base value of the wave propagation speed, $c_{base,}$ is user defined (i.e. c_{base} = 343 m/s which is based on theoretical formula of *Method I*). Measured depleted trap locations $X_D^{measured}$ calculated by Equation (4.2) by using the measured reflection return time $t_D^{measured}$ (determined by the TRACER program from the AIRNET predictions, **Figure 6.3**) and the wave propagation speed c = 343 m/s are presented in **Table 6.3** together with the trap location errors ε.

Table 6.3 Assessment of the depleted trap location using the reflected wave technique to analyse AIRNET simulated data

Trap characteristics		**AIRNET system response**	**Theoretical formula**	
			Equation (4.2)	
Trap	X_D^{true} (m)	$t_D^{measured}$ (s)	$X_D^{measured}$ (m)	ε*
T1	**9.1**	0.055	**9.4**	0.4%
T3	**15.3**	0.095	**16.3**	1.3%
T4	**19.6**	0.127	**21.8**	2.8%
T12	**46.6**	0.289	**49.6**	3.8%

$$*\varepsilon = \frac{\left| X_D^{measured} - X_D^{true} \right|}{L}$$

When L = 77.0 m (the total stack height)

Comparing **Table 6.2** and **Table 6.3** it can be seen that the measured trap location $X_D^{measured}$ derived from the real system data matches well with that derived from the AIRNET simulation. For example, the measured trap location for T12 derived from the real system data is 49.7 m, while that derived from the simulated data is 49.6 m. The simulated data shows a similar increase in the trap location error ε with the increase of trap distance (i.e. with an increasing value of X_D^{true}). For trap T1 (i.e. X_D^{true} = 9.1 m), ε is 0.4% which corresponds to a trap location estimation error of 0.3 m, however, for trap T12 (i.e. X_D^{true} = 46.6 m), ε is 3.8% giving a trap location estimation error of 3.0 m. In each case, the measured trap location, $X_D^{measured}$, is overestimated when compared with the true trap location, X_D^{true}. This implies that AIRNET is accurately modelling whatever is causing the laboratory data overestimate of trap location.

6.4 Identifying the cause of overestimating the depleted trap location

The results from the preliminary laboratory investigations and AIRNET simulation, Section 6.3.1 and 6.3.2, respectively, have shown an increase in the trap location error with trap distance (i.e. as X_D^{true} increases) which corresponds to an increasing *overestimation* of the measured trap location $X_D^{measured}$. At the time of testing, no cause of this discrepancy was apparent so to allow further investigation the AIRNET model, which has been shown in Section 6.3 to be capable of accurately simulating the system response to an applied pressure transient, was used to simulate a simple drainage system to allow a more thorough consideration of potential causes.

The physical characteristics of the simple system, **Figure 6.6(a)**, remained similar to *Configuration I*. However, the system was simplified by setting all the pipes and branches, including the piston, to a single internal diameter D = 100 mm to avoid any influence from changes in pipe diameter. In addition, the distance between floor levels was increased to 4 m and the branch lengths increased to 3 m in the attempt to allow the pressure response to be more easily analysed without superposition of information caused by the reflection and transmission of the pressure wave at system boundaries.

Further simplification was introduced by using an instantaneous positive pressure pulse as the incident transient, generated by simulating a rapid piston movement of 1 m/s for 0.2 seconds, thus providing a simple square wave transient. A dry stack height of 20 m was used to ensure that the reflection generated by the open termination to atmosphere could not interfere with that from any of the traps, and so could be discounted from the analysis. The time step was again Δt = 0.002 s (equivalent to a 500 Hz sampling rate) and the space-step was Δx = 0.5 m. Once these simulations were complete, they were repeated after changing the branch diameter to D = 32 mm, while the stack remained at D = 100 mm.

Measured depleted trap locations, $X_D^{measured}$, calculated by Equation (4.2) using the defined wave propagation speed c = 343 m/s and a measured reflection return time, $t_D^{measured}$, determined by the TRACER program are presented in **Table 6.4** together with the trap location errors ε.

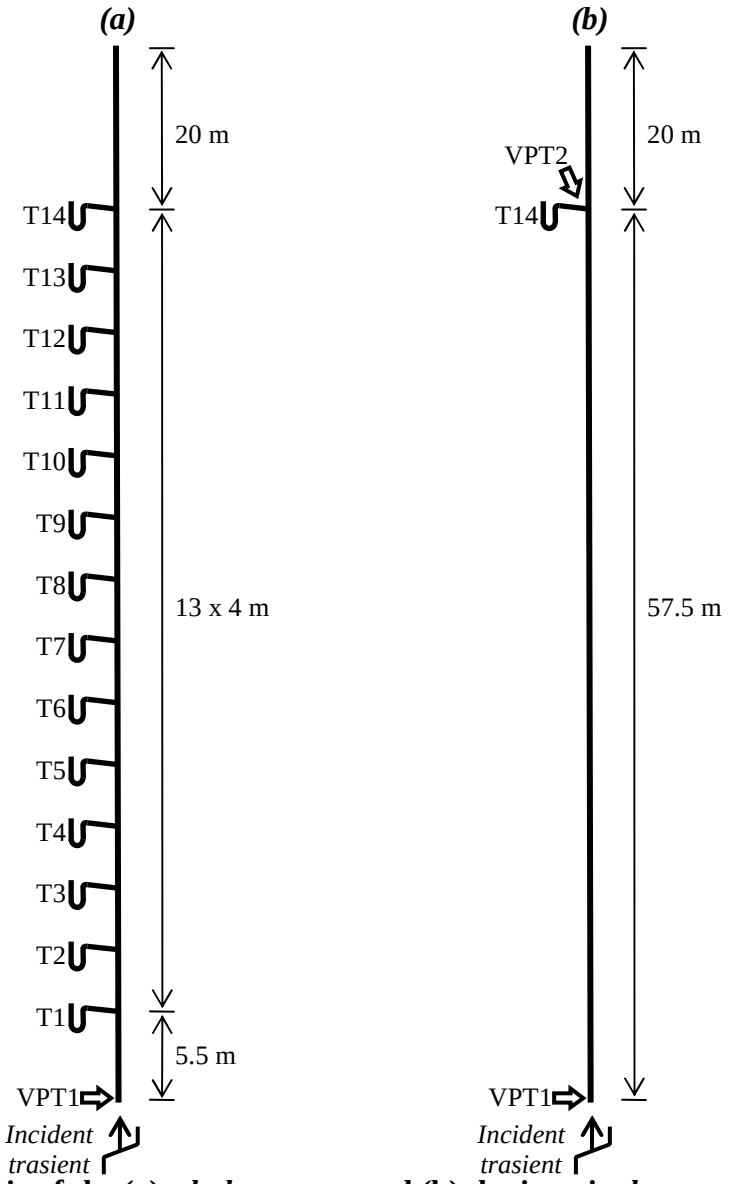

Figure 6.6 Schematic of the (a) *whole system*; and (b) the *junctionless system* used in the AIRNET investigation into the effect of system junctions

In both cases, the results show a similar increase in the trap location error ε with an increase of trap distance X_D^{true} as observed in the results of both the preliminary laboratory investigations and AIRNET simulation reported earlier in **Table 6.2** and **Table 6.3**, respectively, which corresponds to an overestimation of $X_D^{measured}$. It can be seen, however, that ε becomes progressively greater for the 100 mm branch/100 mm stack configuration as X_D^{true} increases than for the 32 mm branch/100 mm stack configuration. For example, for T14, $\varepsilon_{(100)}$ = 18.2% while $\varepsilon_{(32)}$ = 3.2%.

Table 6.4 Assessment of the depleted trap location using the reflected wave technique to analyse data simulated by AIRNET for the *whole system* shown in Figure 6.6 having both 100 mm and 32 mm diameter branches

Trap characteristics		100 mm branch/100 mm stack			32 mm branch/100 mm stack		
		AIRNET system response	Theoretical formula *Equation (4.2)*		AIRNET system response	Theoretical formula *Equation (4.2)*	
Trap	X_D^{true} (m)	$t_{D(100)}^{measured}$ (s)	$X_{D(100)}^{measured}$ (m)	$\varepsilon_{(100)}^{*}$	$t_{D(32)}^{measured}$ (s)	$X_{D(32)}^{measured}$ (m)	$\varepsilon_{(32)}^{*}$
T1	**8.5**	0.050	**8.5**	0.0%	0.050	**8.5**	0.0%
T2	**12.5**	0.073	**12.6**	0.1%	0.075	**12.7**	0.2%
T3	**16.5**	0.098	**16.8**	0.3%	0.099	**16.7**	0.3%
T4	**20.5**	0.123	**21.1**	0.7%	0.123	**20.9**	0.5%
T5	**24.5**	0.163	**27.9**	4.1%	0.148	**25.2**	0.9%
T6	**28.5**	0.188	**32.3**	4.9%	0.172	**29.2**	1.0%
T7	**32.5**	0.214	**36.7**	5.4%	0.197	**33.4**	1.2%
T8	**36.5**	0.253	**43.4**	9.0%	0.222	**37.7**	1.5%
T9	**40.5**	0.279	**47.9**	9.5%	0.246	**41.7**	1.6%
T10	**44.5**	0.307	**52.7**	10.6%	0.271	**46.0**	1.9%
T11	**48.5**	0.344	**59.0**	13.5%	0.295	**50.2**	2.1%
T12	**52.5**	0.371	**63.6**	14.3%	0.320	**54.4**	2.5%
T13	**56.5**	0.395	**67.8**	16.8%	0.345	**58.6**	2.7%
T14	**60.5**	0.435	**74.6**	18.2%	0.371	**63.0**	3.2%

$$*\varepsilon = \frac{\left| X_D^{measured} - X_D^{true} \right|}{L}$$

When L = 77.5 m (the total stack height)

Inspection of the results found that $t_D^{measured}$ was being affected by the reflection and transmission process occurring at each of the system junctions, such that the *perceived* arrival time of the trap induced reflection was dependant upon both the *number* and *geometry* (i.e. the branch to stack area ratio) of each of the junctions traversed by the propagating wave.

The most straight forward method of demonstrating the influence of the system junctions on $t_D^{measured}$ is to compare the pressure response of the system *with* junctions (i.e. the *whole system* **Figure 6.6(a)**) with that of a system *without* junctions (i.e. the *junctionless system* **Figure 6.6(b)**). To allow comparison of the two systems, a single junction - that serving trap T14 - was retained on the *junctionless system*. The AIRNET simulation permitted this comparison relatively easily and quickly, without having to rely on costly and time consuming laboratory investigations.

Figure 6.7(a) compares the simulated pressure response at VPT1 of the *junctionless system* (see **Figure 6.6(b)**) with a depleted trap at T14 with that of the defect free baseline. The simulated reflection return time can be seen to correspond well with the predicted reflection return time (the trap pipe period, calculated using Equation (4.2)) indicated by the dashed vertical line. **Figure 6.7(b)** shows the same information but for the *whole system* (see **Figure 6.6(a)**). There is a clearly visible delay in the simulated reflection return time which occurs some time after the predicted reflection return time. A reasonable explanation can be found by considering the reflection and transmission process which takes place at each junction and acknowledging the effect that each junction has on the propagating transient.

As the transient wave propagates throughout the system, each junction will cause part of the wave to be reflected back along the index pipe while the remainder will be transmitted forwards equally into the receiving pipes. Equations (2.12) and (2.13) respectively determine what proportion of an incoming transient is reflected and transmitted based on the area ratios of the connecting pipes. This reflection and transmission process takes place at every junction, with the result that the original incident pressure transient is effectively divided into many smaller reflected and transmitted parts as it moves through the system.

The magnitude of the transient's leading edge, Δp_l, is thus proportional to the number of junctions traversed, n, and the junction transmission coefficient, $C_T^{junction}$, which itself is dependant upon the branch to stack area ratio:

$$\Delta p_l = \Delta p_I \times \left(C_{T_1}^{junction} \times C_{T_2}^{junction} \times ... \times C_{T_n}^{junction} \right) \quad (6.2)$$

where Δp_I is the initial incident pressure transient. For identical junctions, with identical transmission coefficients, this becomes:

$$\Delta p_l = \Delta p_I \times \left(C_T^{junction} \right)^n \quad (6.3)$$

The identical three pipe junctions (consisting of 100 mm diameter pipes) used in the AIRNET simulation each have a reflection coefficient of $C_R^{junction}$ = -0.33 and a transmission coefficient of $C_T^{junction}$ = +0.67 of the incident transient, Equations (2.12) and (2.13) respectively. Therefore, from Equation (6.3), having encountered a total of

14 junctions along the way, the magnitude of the transient leading edge arriving at trap T14 is only 0.4% of the incident transient, having been progressively "eroded" by each junction encountered.

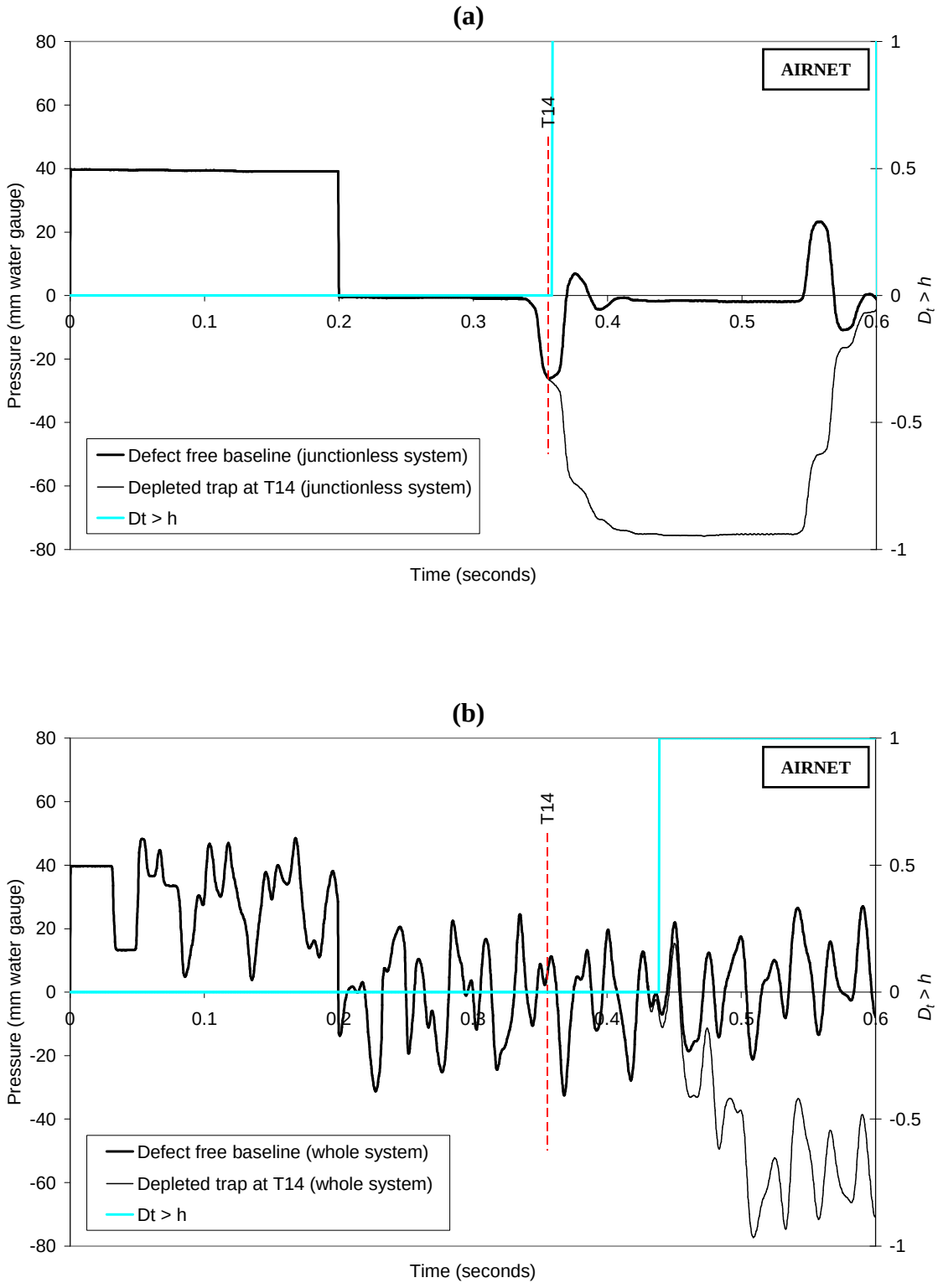

Figure 6.7 Comparison of the AIRNET simulated defect free baseline and the test system response measured for a depleted trap at T14 for (a) the *junctionless system*; and (b) the *whole system*

This is clearly illustrated in **Figure 6.8** which compares the pressure response predicted at VPT2 (at the start of the branch connected to T14) for both the *whole system* and the *junctionless system*. For the *junctionless system*, the transient arrives sharply at 0.157 seconds (i.e. $T = L/c$) and almost immediately attains peak pressure. Note that the transient is no longer a perfect square wave as it now shows the reflection from the junction as it passes into the branch towards trap T14. For the *whole system*, by the time the transient arrives at VPT2 the magnitude of the leading edge has been dampened by the junctions and is now so small (i.e. 0.4% of the incident transient) that it makes no impact on the system response. It is some time later, at 0.179 seconds, that it first registers on the pressure response. It continues to build gradually until, it too attains peak pressure at 0.258 seconds, some 0.079 seconds later.

This demonstrates that although the magnitude of the transient leading edge arriving at trap T14 is only 0.4% of the incident transient, the remaining 99.6% is not lost. Although divided and dispersed into smaller and smaller reflected and transmitted parts by each junction, these continue to be re-reflected and re-transmitted such that eventually they too arrive at trap T14 and the wave is effectively *reconstructed*. In practice, if the junction is not restrained from motion it is possible that small movements of the pipework may exacerbate this effect by attenuating the incident transient (Wood and Chao, 1971).

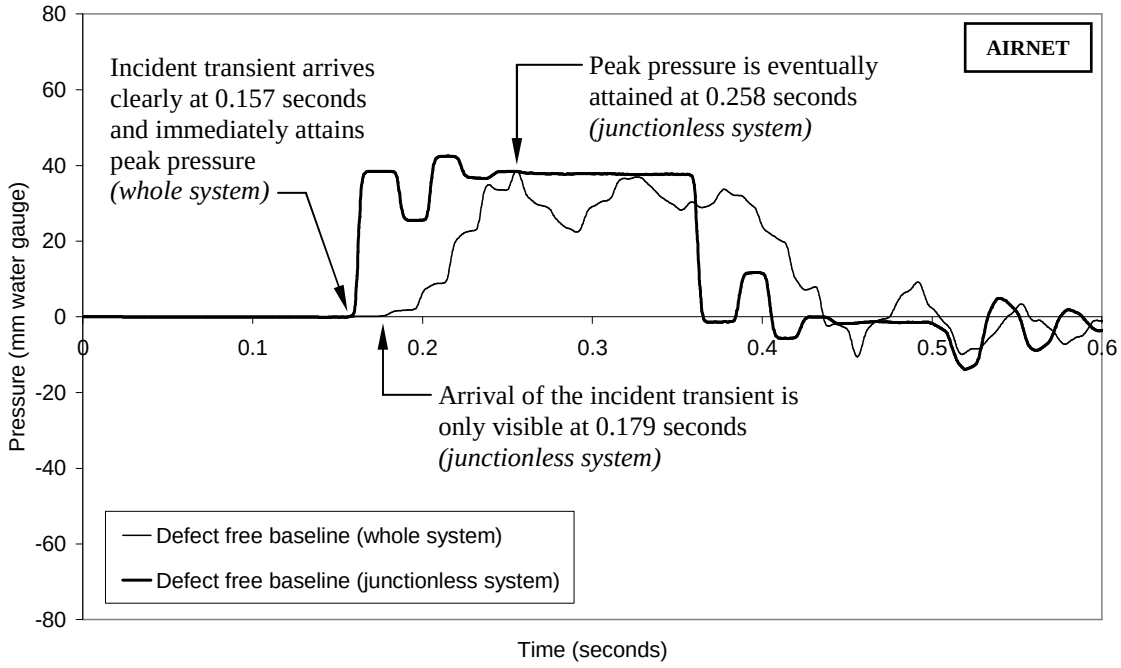

Figure 6.8 Comparison of the defect free baseline measured at VPT2 for both the *whole system* and *junctionless system*

6.5 Overcoming the junction effect

It has been demonstrated experimentally and theoretically that the *junction effect* induces a delay in the perceived arrival time of the trap induced reflection, $t_D^{measured}$. This results in an overestimation of the measured trap location, $X_D^{measured}$, and an underestimation of the wave propagation speed, *c*, as observed earlier in Section 6.3.1. Equation (4.2), which allows the true trap pipe period, t_D^{true}, to be calculated for a known trap location X_D^{true} and wave propagation speed, *c*, takes no account of this *junction effect*. Accurately predicting the location of a depleted trap is, therefore, not possible by relying solely on Equation (4.2). Consequently, three methods for predicting the actual trap pipe period will be compared:

- ***Method A*** uses Equation (4.2) to calculate the theoretical trap pipe period t_D^{true} from the true trap location, X_D^{true}, (measured from the physical system), and the wave propagation speed calculated from *Method I* (i.e. c = 343 m/s).
- ***Method B*** uses AIRNET to predict the simulated trap pipe period t_D^{AIRNET} from the system response of the simulated system. The simulated trap distance, X_D^{AIRNET}, and the base value of the wave propagation speed, c_{base}, are known as they are both user defined (i.e. c_{base} = 343 m/s).
- ***Method C*** uses the reflected wave technique as a probe to determine the perceived trap pipe period t_D^{probe}. The method requires all depleted trap seal cases to be sequentially simulated experimentally. Neither X_D^{probe} or *c* need to be known prior to using this method as t_D^{probe} is measured directly from the physical system.

These three methods will be used in the following sections to evaluate the reflected wave technique through the analysis of the data collected during the experimental investigations discussed in Chapter 5. Particular attention will be paid to determine if the *junction effect* is evident in the experimental data and which of the three methods (i.e. Method A, B and C) provides the greatest accuracy.

Note: to aid cross-reference between different system tests, the following data analysis is presented in a repetitive format covering all tests in the following order: Dundee (*field*) system *Configuration II(b), II(c), III(b)* and *IV(b)*; HWU Arrol (*field*) system *Configuration V*; Glasgow (*field*) system *Configuration VI*, *VII*, and *VIII*.

6.6 Application to the Dundee (*field*) system

Data collected from the Dundee (*field*) system allowed the reflected wave technique to be validated for the first time under field conditions. This section presents the results from the four test sets *Configuration II(b), II(c), III(b)* and *IV(b),* see **Figure 6.9**.

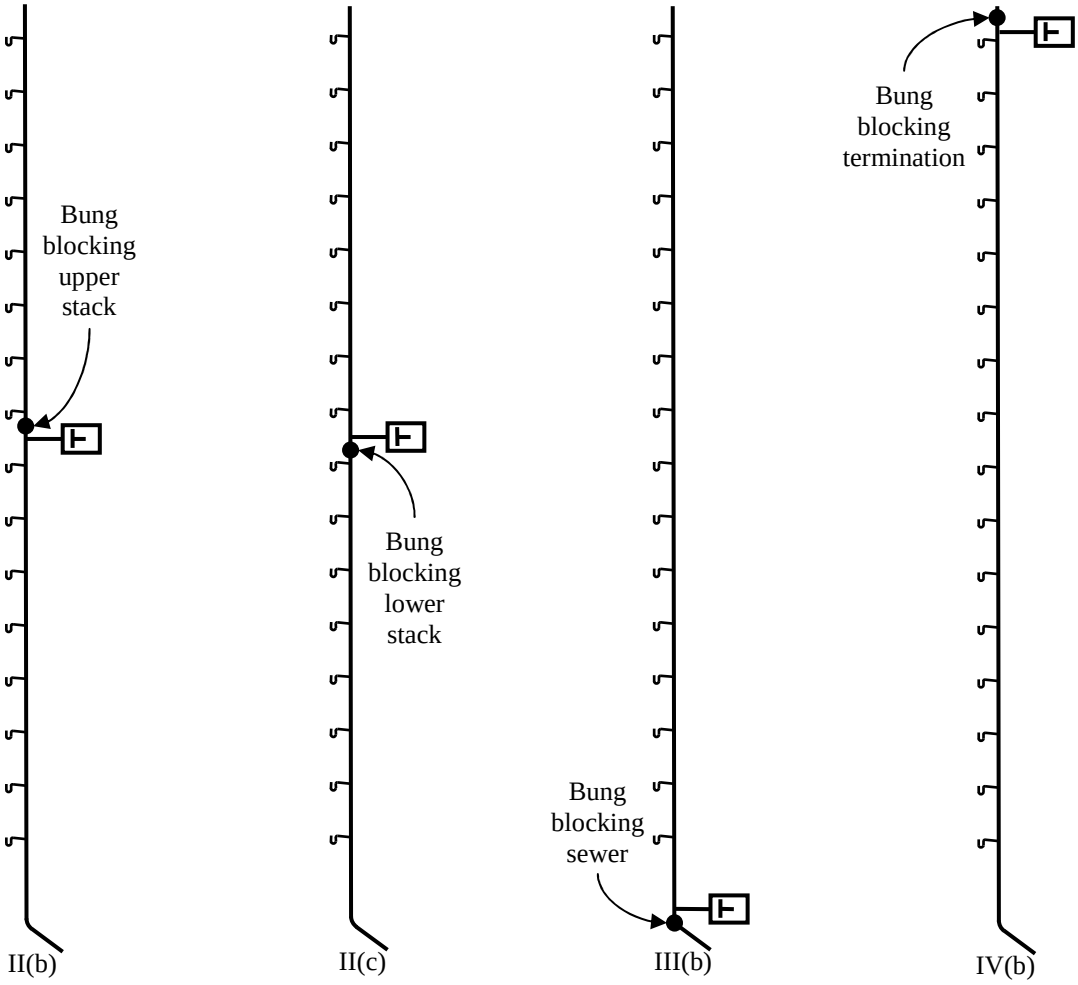

Figure 6.9 System configurations used in the Dundee (*field*) system tests shown previously in Figure 5.8 but repeated here for convenience. *Configuration II* (transient applied to Floor 9), *Configuration III* (transient applied to Ground Floor), *Configuration IV* (transient applied to Floor 17). For simplicity only the wc branches are shown here.

6.6.1 Dundee (field) system Configuration II(b)

Figure 6.10 shows the measured system response for the set of depleted trap seals (i.e. T2 to T9) for *Configuration II(b)*, **Figure 6.9**. The negative reflection, induced by each depleted trap in response to the applied single positive pressure pulse can be seen to alter the measured system response by generating a corresponding pressure drop at a time specific to the location of that trap.

Predicted depleted trap locations, estimated by the three methods (i.e. *Method A, B* and *C*) are presented in **Table 6.5** together with the trap location errors ε. **Figure 6.11** compares the measured depleted trap location with that predicted by each method. The following conclusions can be made:

i. Trap location error ε, for *Method A,* increases with the increase of trap distance (i.e. as X_D^{true} increases). For trap T9 (i.e. X_D^{true} = 3.5 m) ε is only 0.2% which corresponds to a trap location estimation error of only 0.1 m.

   However, the trap location error ε increases until, for trap T2 (i.e. X_D^{true} = 21.0 m), ε is 4.1% giving a trap location estimation error of 2.0 m.

ii. In comparison, the trap location error, for *Methods B* and *C*, each demonstrate considerably better accuracy (i.e. ε = 0.2% to 0.8% and ε = 0.6% to 0.8%, respectively) as both of these methods take account of the *junction effect*.

   Figure 6.11 shows the excellent correlation of X_D^{AIRNET} and X_D^{probe} with $X_D^{measured}$. The maximum trap location estimation error for *Method B* and *C* is 0.4 m.

iii. The trap location error for *Method C* is a function of the low data scan rate (i.e. 500 Hz) used during these tests which gives a time step between data points of 0.002 seconds and provides the maximum difference between $t_D^{measured}$ and t_D^{probe}.

The depleted trap location can be accurately estimated by both *Methods B* and *C* (ε < 1%). *Method A* is shown to be influenced by the *junction effect* which causes ε to increase with increasing trap distance.

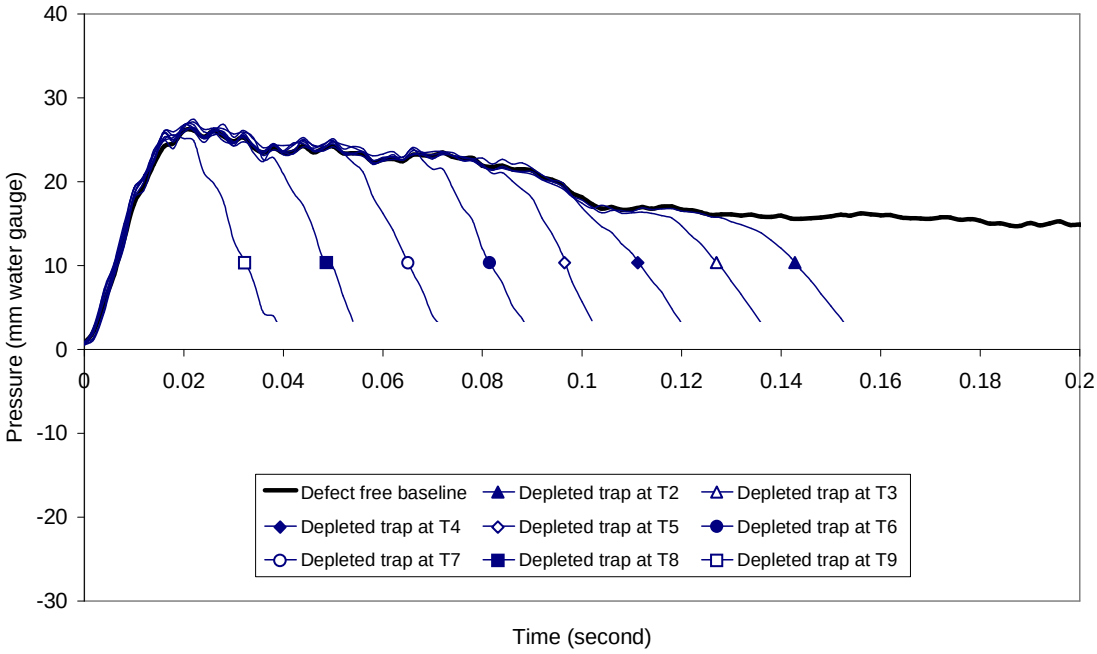

Figure 6.10 Measured system response at VPT1 showing the effect of depleted trap distance for *Configuration II(b)*. Note: for clarity each pressure trace has been discontinued shortly after its deviation from the defect free baseline.

Table 6.5 Assessment of the depleted trap location by the reflected wave technique for *Configuration II(b)*

Measured trap characteristics from system response			**True trap location and pipe period**			**AIRNET simulated trap location and pipe period**			**Probed trap location and pipe period**		
			Method A			***Method B***			***Method C***		
No	$t_D^{measured}$ (s)	$X_D^{measured}$ (m)	t_D^{true} (s)	X_D^{true} (m)	ε_A	t_D^{AIRNET} (s)	X_D^{AIRNET} (m)	ε_B	t_D^{probe} (s)	X_D^{probe} (m)	ε_C
T2	0.134	**23.0**	0.122	**21.0**	4.1%	0.134	**22.9**	0.2%	0.132	**22.6**	0.8%
T3	0.118	**20.2**	0.108	**18.5**	3.5%	0.120	**20.5**	0.6%	0.120	**20.6**	0.8%
T4	0.100	**17.2**	0.093	**16.0**	2.4%	0.101	**17.3**	0.2%	0.102	**17.5**	0.6%
T5	0.084	**14.4**	0.079	**13.5**	1.8%	0.086	**14.7**	0.6%	0.086	**14.7**	0.6%
T6	0.070	**12.0**	0.064	**11.0**	2.0%	0.071	**12.2**	0.4%	0.072	**12.3**	0.6%
T7	0.052	**8.9**	0.050	**8.5**	0.8%	0.054	**9.3**	0.8%	0.054	**9.3**	0.8%
T8	0.036	**6.2**	0.035	**6.0**	0.4%	0.037	**6.4**	0.4%	0.038	**6.5**	0.6%
T9	0.020	**3.4**	0.020	**3.5**	0.2%	0.020	**3.5**	0.2%	0.022	**3.8**	0.8%

$$\varepsilon_A = \frac{\left| X_D^{measured} - X_D^{true} \right|}{L} \qquad \varepsilon_B = \frac{\left| X_D^{measured} - X_D^{AIRNET} \right|}{L} \qquad \varepsilon_C = \frac{\left| X_D^{measured} - X_D^{probe} \right|}{L}$$

When L = 49.0 m (the total stack height)

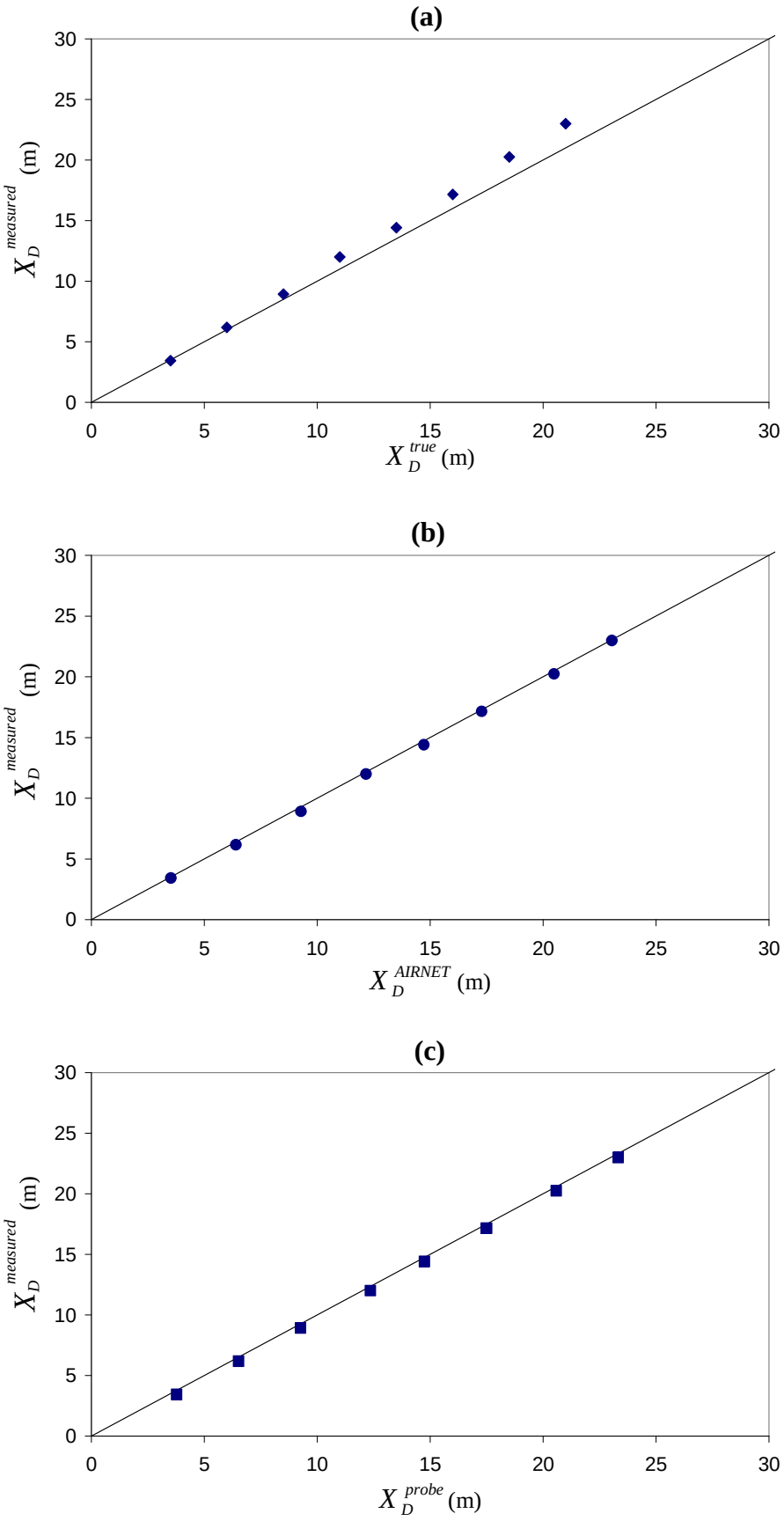

Figure 6.11 Comparison of the measured and predicted depleted trap locations for *Configuration II(c)* for (a) *Method A*; (b) *Method B* and (c) *Method C*

6.6.2 Dundee (field) system Configuration II(c)

Figure 6.12 shows the measured system response for the set of depleted trap seals (i.e. T10 to T17) for *Configuration II(c)*, **Figure 6.9**. The effect of each depleted trap is clear by the induced negative reflection (pressure drop) generated in response to the applied single positive pressure pulse which corresponds to the location of that trap.

Predicted depleted trap locations, estimated by the three methods (i.e. *Method A, B* and *C*) are presented in **Table 6.6** together with the trap location errors ε. **Figure 6.13** compares the predicted depleted trap locations for each method with the measured depleted trap location. The following conclusions can be made:

i. For *Method A* the trap location error ε, increases with the increase of trap distance. For trap T10 (i.e. X_D^{true} = 5.1 m) ε is only 0.8% which corresponds to a trap location estimation error of only 0.4 m. However, the trap location error ε increases until, for trap T17 (i.e. X_D^{true} = 22.6 m), ε is 5.7% giving a trap location estimation error of 2.8 m.

ii. In comparison, the trap location error ε, for *Methods B* and *C*, each show a considerably higher level of accuracy (i.e. ε = 0.0% to 0.8% and ε = 0.6% to 0.8%, respectively) as both of these methods take account of the *junction effect*. The maximum trap location estimation error for both *Method B* and *C* is 0.4 m.

iii. The trap location error ε for *Method C* is a function of the low data scan rate (i.e. 500 Hz) used during these tests which provides a time step between data points of 0.002 seconds and which provides the maximum difference between $t_D^{measured}$ and t_D^{probe}.

The location of the depleted trap can be accurately estimated by both *Methods B* and *C* (ε < 1%). *Method A* is shown to be influenced by the *junction effect* which causes ε to increase with increasing trap distance.

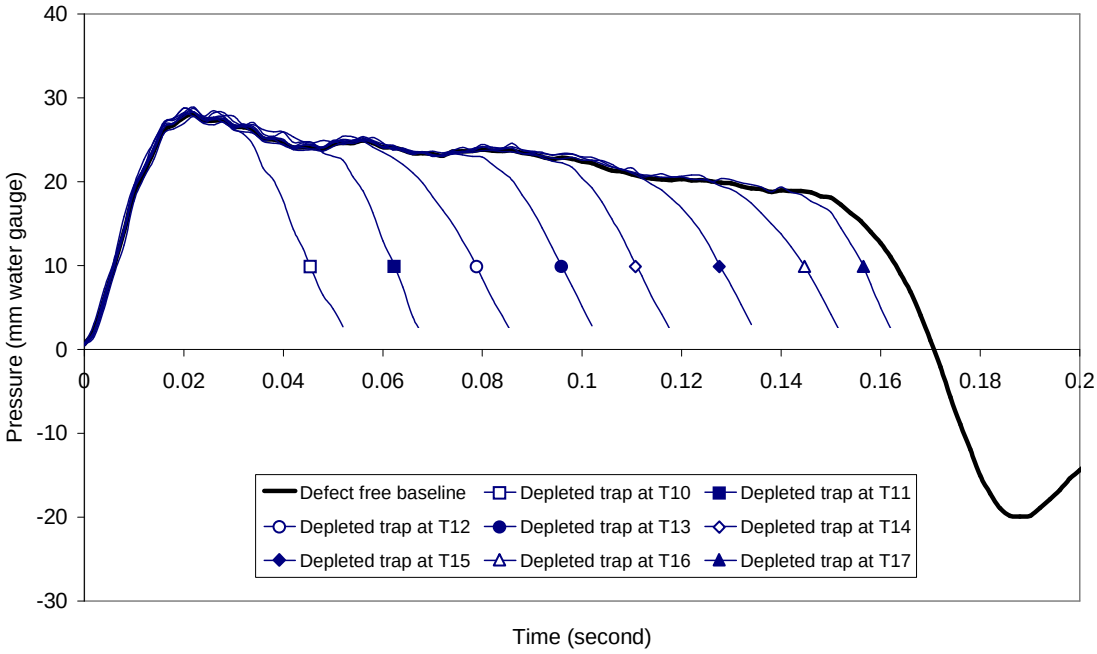

Figure 6.12 Measured system response at VPT1 showing the effect of depleted trap distance for *Configuration II(c)*. Note: for clarity each pressure trace has been discontinued shortly after its deviation from the defect free baseline.

Table 6.6 Assessment of the depleted trap location by the reflected wave technique for *Configuration II(c)*

Measured trap characteristics from system response			**True trap location and pipe period**			**AIRNET simulated trap location and pipe period**			**Probed trap location and pipe period**		
			Method A			***Method B***			***Method C***		
No	$t_D^{measured}$ (s)	$X_D^{measured}$ (m)	t_D^{true} (s)	X_D^{true} (m)	ε_A	t_D^{AIRNET} (s)	X_D^{AIRNET} (m)	ε_B	t_D^{probe} (s)	X_D^{probe} (m)	ε_C
T10	0.032	**5.5**	0.030	**5.1**	0.8%	0.031	**5.3**	0.4%	0.034	**5.8**	0.6%
T11	0.048	**8.2**	0.044	**7.6**	1.2%	0.048	**8.3**	0.2%	0.050	**8.6**	0.8%
T12	0.062	**10.6**	0.059	**10.1**	1.0%	0.064	**11.0**	0.8%	0.064	**11.0**	0.8%
T13	0.080	**13.7**	0.073	**12.6**	2.2%	0.080	**13.8**	0.2%	0.082	**14.1**	0.8%
T14	0.098	**16.8**	0.088	**15.1**	3.5%	0.098	**16.8**	0.0%	0.100	**17.2**	0.8%
T15	0.114	**19.6**	0.103	**17.6**	4.1%	0.114	**19.5**	0.2%	0.116	**19.9**	0.6%
T16	0.132	**22.6**	0.117	**20.1**	5.1%	0.132	**22.6**	0.0%	0.134	**23.0**	0.8%
T17	0.148	**25.4**	0.132	**22.6**	5.7%	0.150	**25.7**	0.6%	0.150	**25.7**	0.6%

$$\varepsilon_A = \frac{\left| X_D^{measured} - X_D^{true} \right|}{L} \qquad \varepsilon_B = \frac{\left| X_D^{measured} - X_D^{AIRNET} \right|}{L} \qquad \varepsilon_C = \frac{\left| X_D^{measured} - X_D^{probe} \right|}{L}$$

When L = 49.0 m (the total stack height)

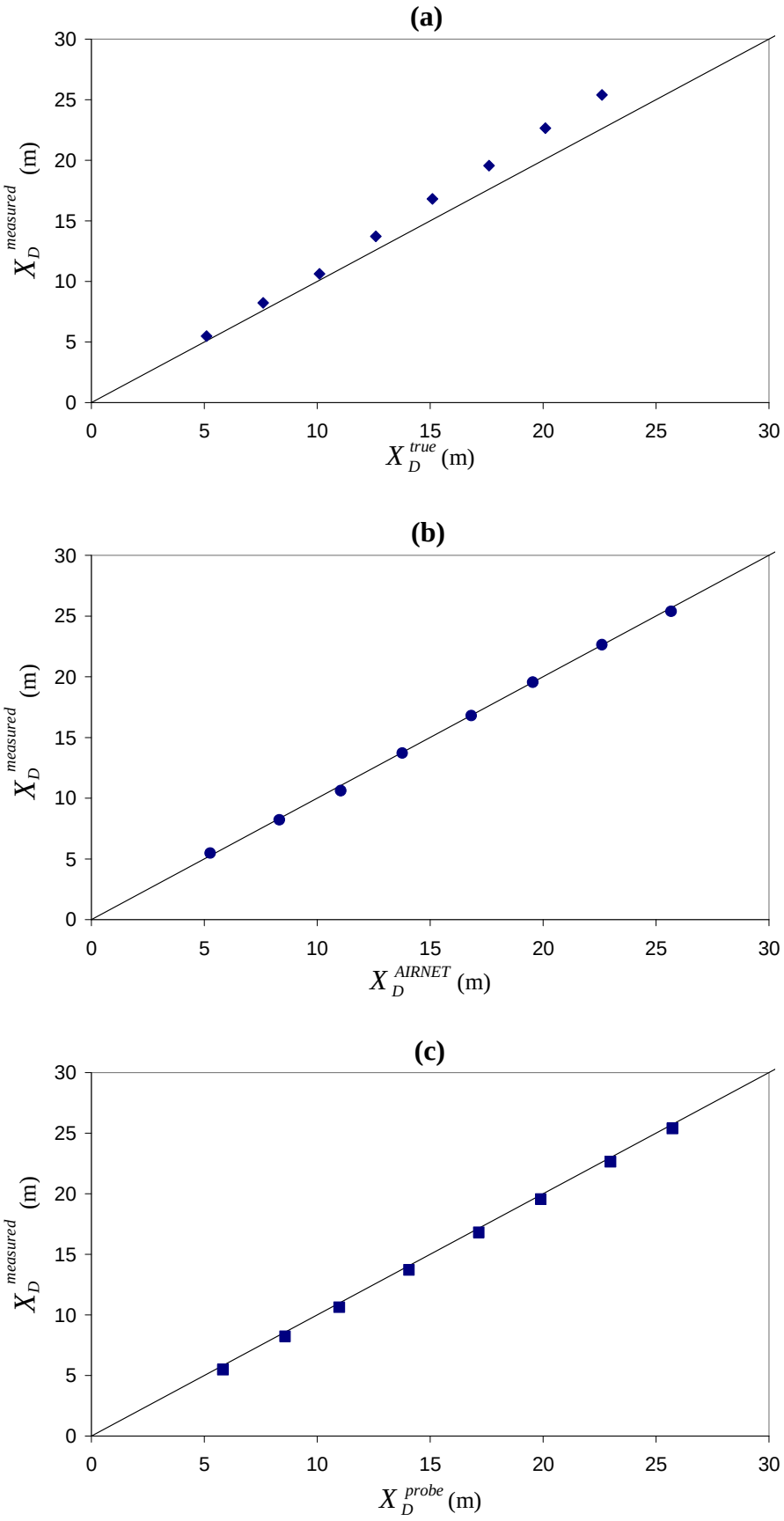

Figure 6.13 Comparison of the measured and predicted depleted trap locations for *Configuration II(c)* for (a) *Method A*; (b) *Method B* and (c) *Method C*

6.6.3 Dundee (field) system Configuration III(b)

Figure 6.14 shows the measured system response for the set of depleted trap seals (i.e. T2 to T17) for *Configuration III(b)*, **Figure 6.9**. The effect of each depleted trap is clear by the induced negative reflection (pressure drop) generated in response to the applied single positive pressure pulse which corresponds to the location of that trap.

Predicted depleted trap locations, estimated by the three methods (i.e. *Method A, B* and *C*) are presented in **Table 6.7** together with the trap location errors ε. **Figure 6.15** compares the predicted depleted trap locations for each method with the measured depleted trap location. The following conclusions can be made:

i. Trap location error ε, for *Method A,* increases with the increase of trap distance (i.e. as X_D^{true} increases). For trap T2 (i.e. X_D^{true} = 8.0 m) ε is only 0.4% which corresponds to a trap location estimation error of only 0.2 m. However, the trap location error ε increases until, for trap T17 (i.e. X_D^{true} = 45.5 m), ε is 11.4% giving a trap location estimation error of 5.6 m.

ii. In comparison, the trap location error ε, for *Methods B* and *C*, each show a considerably higher level of accuracy (i.e. ε = 0.2% to 1.6% and ε = 0.6% to 0.8%, respectively) due to these methods both taking account of the *junction effect*. The maximum trap location estimation error for *Method B* and *C* is 0.8 m and 0.4 m, respectively.

iii. The trap location error ε for *Method C* is a function of the low data scan rate (i.e. 500 Hz) used during these tests which provides a time step between data points of 0.002 seconds and which provides the maximum difference between $t_D^{measured}$ and t_D^{probe}.

The location of the depleted trap can be accurately estimated by both *Methods B* and *C* (ε < 2.0%). *Method A* is shown to be influenced by the *junction effect* which causes ε to increase with increasing trap distance.

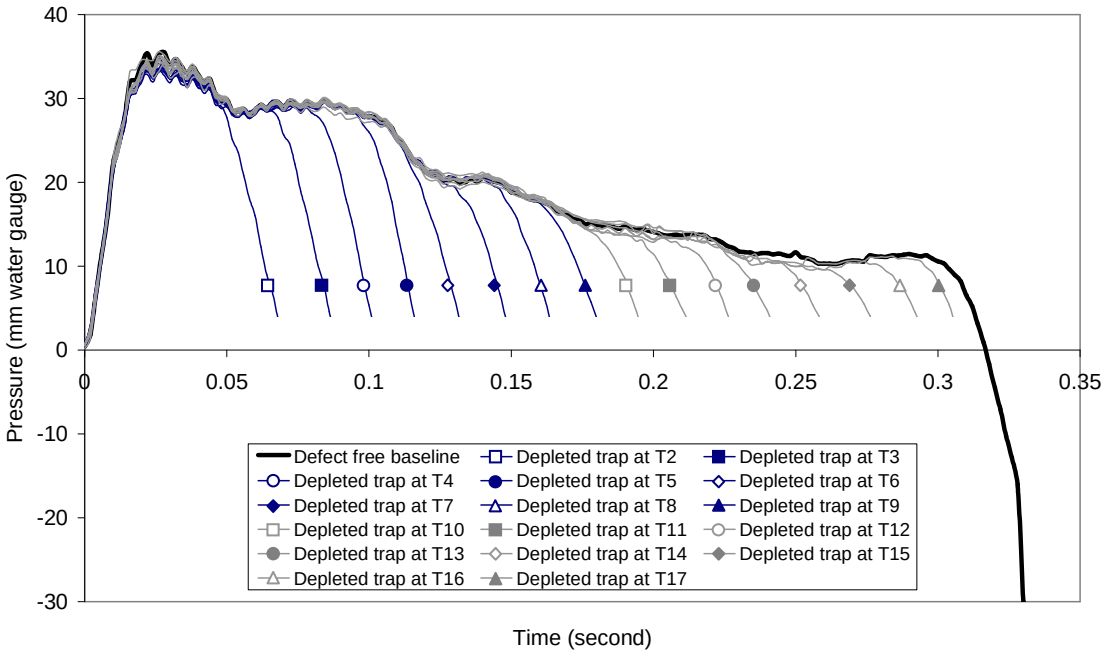

Figure 6.14 Measured system response at VPT1 showing effect of depleted trap distance for *Configuration III(b)*. Note: for clarity each pressure trace has been discontinued shortly after its deviation from the defect free baseline.

Table 6.7 Assessment of the depleted trap location by the reflected wave technique for *Configuration III(b)*

Measured trap characteristics from system response			True trap location and pipe period *Method A*			AIRNET simulated trap location and pipe period *Method B*			Probed trap location and pipe period *Method C*		
No	$t_D^{measured}$ (s)	$X_D^{measured}$ (m)	t_D^{true} (s)	X_D^{true} (m)	ε_A	t_D^{AIRNET} (s)	X_D^{AIRNET} (m)	ε_B	t_D^{probe} (s)	X_D^{probe} (m)	ε_C
T2	0.048	**8.2**	0.047	**8.0**	0.4%	0.044	**7.5**	1.4%	0.050	**8.6**	0.8%
T3	0.066	**11.3**	0.061	**10.5**	1.6%	0.061	**10.5**	1.6%	0.068	**11.7**	0.8%
T4	0.082	**14.1**	0.076	**13.0**	2.2%	0.079	**13.6**	1.0%	0.084	**14.4**	0.6%
T5	0.098	**16.8**	0.090	**15.5**	2.7%	0.095	**16.3**	1.0%	0.100	**17.2**	0.8%
T6	0.116	**19.9**	0.105	**18.0**	3.9%	0.113	**19.4**	1.0%	0.118	**20.2**	0.6%
T7	0.132	**22.6**	0.120	**20.5**	4.3%	0.129	**22.1**	1.0%	0.134	**23.0**	0.8%
T8	0.148	**25.4**	0.134	**23.0**	4.9%	0.147	**25.2**	0.4%	0.150	**25.7**	0.6%
T9	0.166	**28.5**	0.149	**25.5**	6.1%	0.164	**28.2**	0.6%	0.168	**28.8**	0.6%
T10	0.182	**31.2**	0.163	**28.0**	6.5%	0.183	**31.3**	0.2%	0.184	**31.6**	0.8%
T11	0.198	**34.0**	0.178	**30.5**	7.1%	0.200	**34.3**	0.6%	0.200	**34.3**	0.6%
T12	0.214	**36.7**	0.192	**33.0**	7.6%	0.216	**37.1**	0.8%	0.216	**37.0**	0.6%
T13	0.230	**39.4**	0.207	**35.5**	8.0%	0.232	**39.8**	0.8%	0.232	**39.8**	0.8%
T14	0.248	**42.5**	0.222	**38.0**	9.2%	0.252	**43.2**	1.4%	0.250	**42.9**	0.8%
T15	0.266	**45.6**	0.236	**40.5**	10.4%	0.268	**45.9**	0.6%	0.268	**46.0**	0.8%
T16	0.282	**48.4**	0.251	**43.0**	11.0%	0.286	**49.0**	1.2%	0.284	**48.7**	0.6%
T17	0.298	**51.1**	0.265	**45.5**	11.4%	0.303	**51.9**	1.6%	0.300	**51.5**	0.8%

$$\varepsilon_A = \frac{\left| X_D^{measured} - X_D^{true} \right|}{L} \qquad \varepsilon_B = \frac{\left| X_D^{measured} - X_D^{AIRNET} \right|}{L} \qquad \varepsilon_C = \frac{\left| X_D^{measured} - X_D^{probe} \right|}{L}$$

When L = 49.0 m (the total stack height)

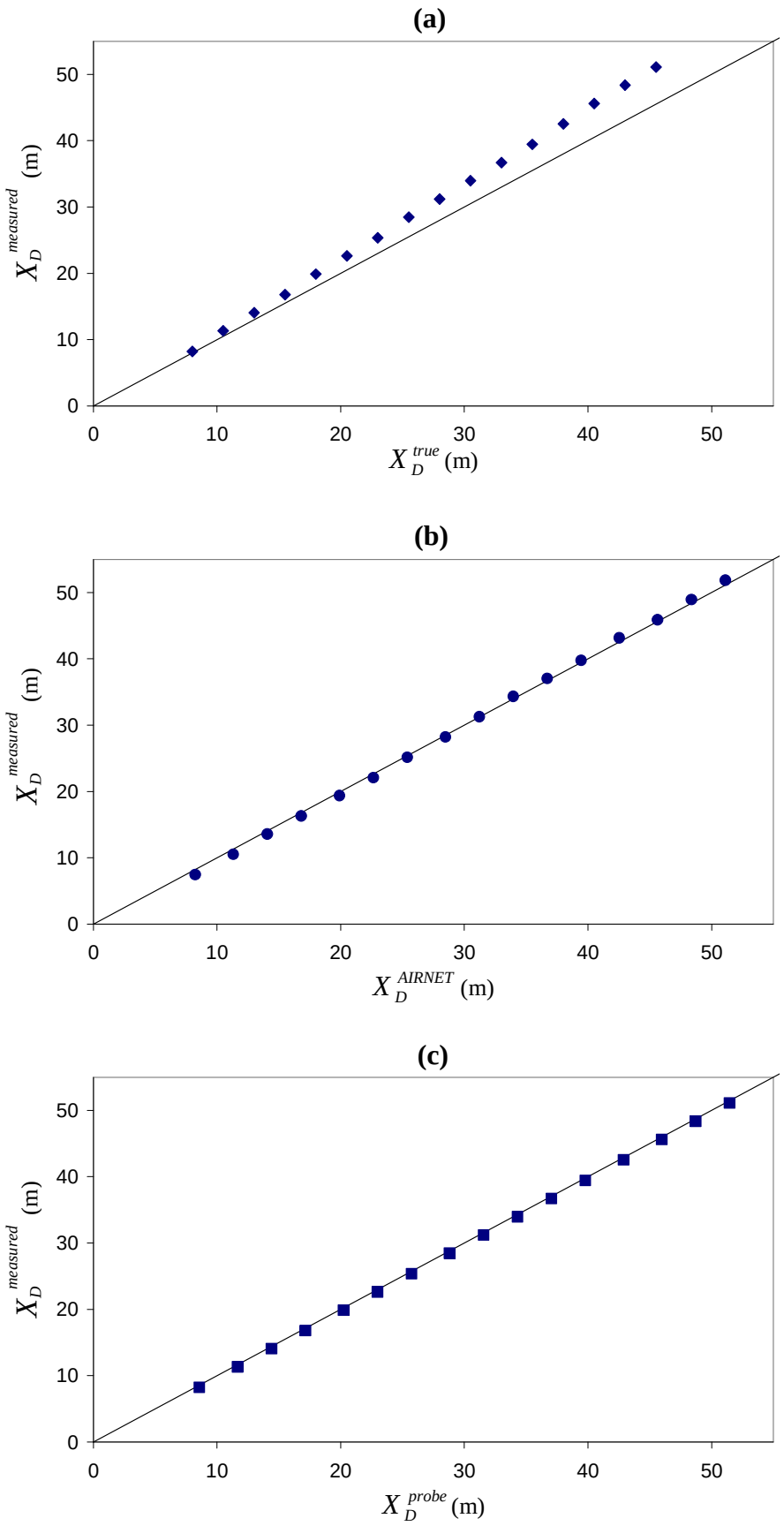

Figure 6.15 Comparison of the measured and predicted depleted trap locations for *Configuration III(b)* for (a) *Method A*; (b) *Method B* and (c) *Method C*

6.6.4 Dundee (field) system Configuration IV(b)

Figure 6.16 shows the measured system response for the set of depleted trap seals (i.e. T2 to T17) for *Configuration IV(b)*, **Figure 6.9**. The effect of each depleted trap is clear by the induced negative reflection (pressure drop) generated in response to the applied single positive pressure pulse which corresponds to the location of that trap.

Predicted depleted trap locations, estimated by the three methods (i.e. *Method A, B* and *C*) are presented in **Table 6.8** together with the trap location errors ε (L = 49.0 m, the total stack height). **Figure 6.17** compares the predicted depleted trap locations for each method with the measured depleted trap location. The following conclusions can be made:

i. Trap location error ε, for *Method A*, increases with the increase of trap distance (i.e. as X_D^{true} increases). For trap T17 (i.e. X_D^{true} = 3.5 m) ε is only 0.6% which corresponds to a trap location estimation error of only 0.3 m. However, the trap location error ε increases until, for trap T2 (i.e. X_D^{true} = 41.0 m), ε is 10.2% giving a trap location estimation error of 5.0 m.

ii. In comparison, the trap location error ε, for *Methods B* and *C*, each show a considerably higher level of accuracy (i.e. ε = 0.0% to 1.4% and ε = 0.6% to 0.8%, respectively) due to these methods both taking account of the *junction effect*. The maximum trap location estimation error for *Method B* and *C* is 0.7 m and 0.4 m, respectively.

iii. The trap location error ε for *Method C* is a function of the low data scan rate (i.e. 500 Hz) used during these tests which provides a time step between data points of 0.002 seconds and which provides the maximum difference between $t_D^{measured}$ and t_D^{probe}.

The location of the depleted trap can be accurately estimated by both *Methods B* and *C* (ε < 1.5%). *Method A* is shown to be influenced by the *junction effect* which causes ε to increase with increasing trap distance.

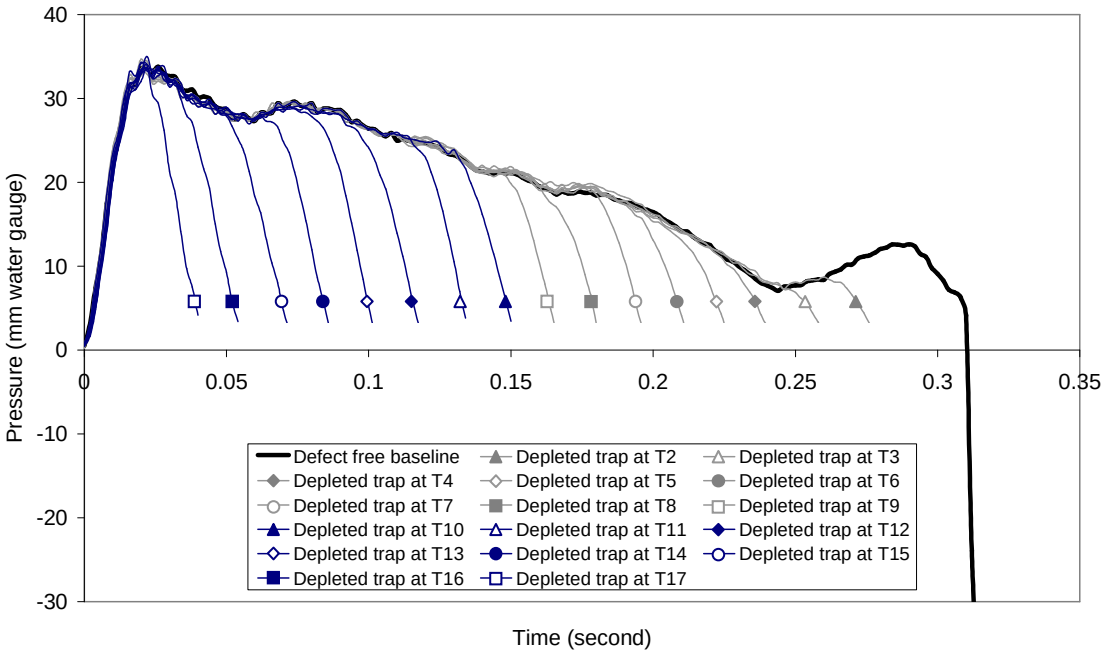

Figure 6.16 Measured system response at VPT1 showing effect of depleted trap distance for *Configuration IV(b)*. Note: for clarity each pressure trace has been discontinued shortly after its deviation from the defect free baseline.

Table 6.8 Assessment of the depleted trap location by the reflected wave technique for *Configuration IV(b)*

Measured trap characteristics from system response			**True trap location and pipe period**			**AIRNET simulated trap location and pipe period**			**Probed trap location and pipe period**		
			Method A			***Method B***			***Method C***		
No	$t_D^{measured}$ (s)	$X_D^{measured}$ (m)	t_D^{true} (s)	X_D^{true} (m)	ε_A	t_D^{AIRNET} (s)	X_D^{AIRNET} (m)	ε_B	t_D^{probe} (s)	X_D^{probe} (m)	ε_C
T2	0.268	**46.0**	0.239	**41.0**	10.2%	0.267	**45.8**	0.4%	0.270	**46.3**	0.6%
T3	0.254	**43.6**	0.224	**38.5**	10.4%	0.250	**42.9**	1.4%	0.256	**43.9**	0.6%
T4	0.236	**40.5**	0.210	**36.0**	9.2%	0.233	**40.0**	1.0%	0.238	**40.8**	0.6%
T5	0.216	**37.0**	0.195	**33.5**	7.1%	0.218	**37.4**	0.8%	0.218	**37.4**	0.8%
T6	0.198	**34.0**	0.181	**31.0**	6.1%	0.199	**34.2**	0.4%	0.200	**34.3**	0.6%
T7	0.184	**31.6**	0.166	**28.5**	6.3%	0.185	**31.7**	0.2%	0.186	**31.9**	0.6%
T8	0.168	**28.8**	0.152	**26.0**	5.7%	0.168	**28.8**	0.0%	0.170	**29.2**	0.8%
T9	0.152	**26.1**	0.137	**23.5**	5.3%	0.153	**26.2**	0.2%	0.154	**26.4**	0.6%
T10	0.136	**23.3**	0.122	**21.0**	4.7%	0.136	**23.4**	0.2%	0.138	**23.7**	0.8%
T11	0.120	**20.6**	0.108	**18.5**	4.3%	0.120	**20.5**	0.2%	0.122	**20.9**	0.6%
T12	0.100	**17.2**	0.093	**16.0**	2.4%	0.104	**17.9**	1.4%	0.102	**17.5**	0.6%
T13	0.084	**14.4**	0.079	**13.5**	1.8%	0.087	**15.0**	1.2%	0.086	**14.7**	0.6%
T14	0.070	**12.0**	0.064	**11.0**	2.0%	0.071	**12.2**	0.4%	0.072	**12.3**	0.6%
T15	0.054	**9.3**	0.050	**8.5**	1.6%	0.054	**9.3**	0.0%	0.056	**9.6**	0.6%
T16	0.036	**6.2**	0.035	**6.0**	0.4%	0.039	**6.7**	1.0%	0.038	**6.5**	0.6%
T17	0.022	**3.8**	0.020	**3.5**	0.6%	0.022	**3.8**	0.0%	0.024	**4.1**	0.6%

$$\varepsilon_A = \frac{\left| X_D^{measured} - X_D^{true} \right|}{L} \qquad \varepsilon_B = \frac{\left| X_D^{measured} - X_D^{AIRNET} \right|}{L} \qquad \varepsilon_C = \frac{\left| X_D^{measured} - X_D^{probe} \right|}{L}$$

When L = 49.0 m (the total stack height)

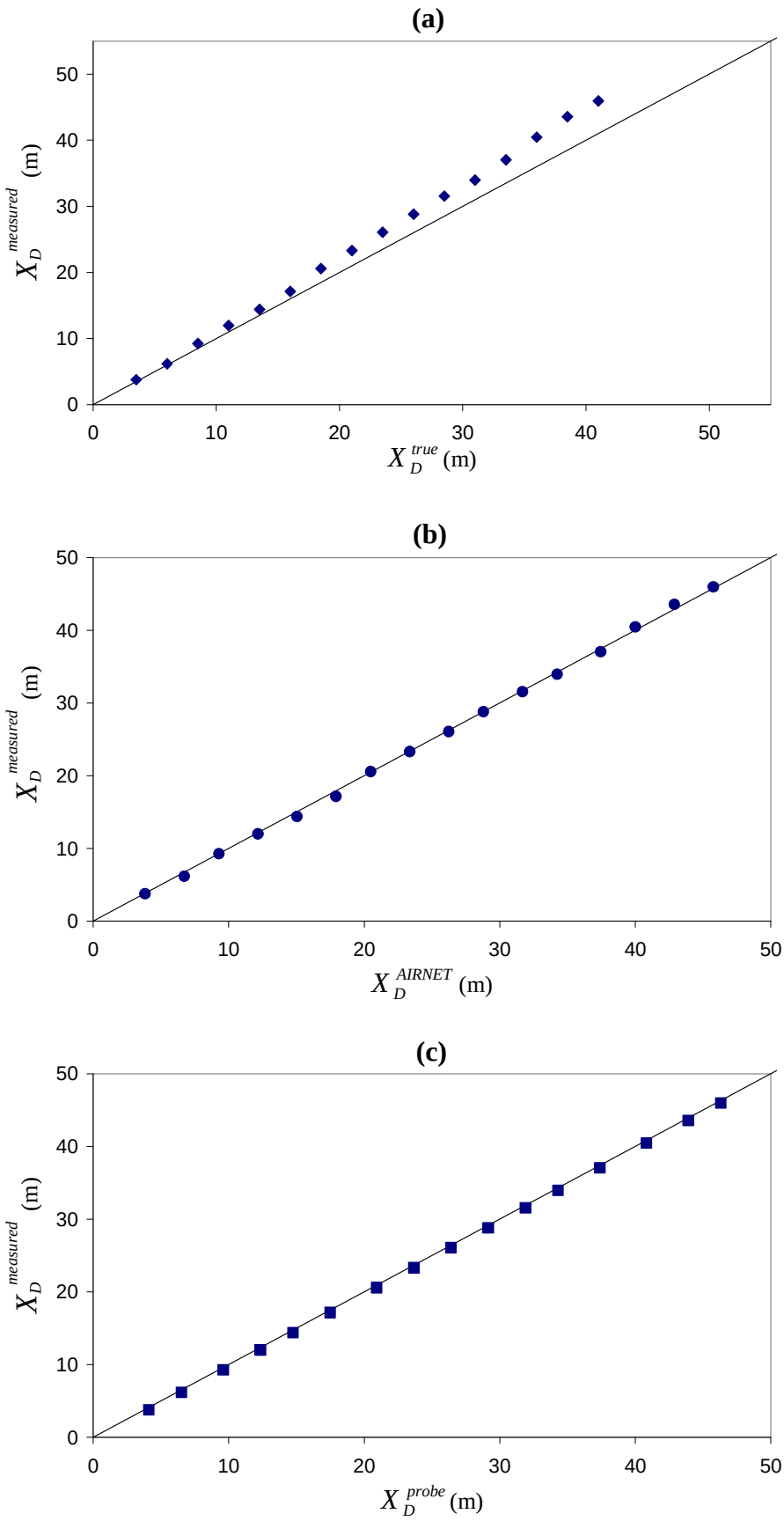

Figure 6.17 Comparison of the measured and predicted depleted trap locations for *Configuration IV (b)* for (a) *Method A*; (b) *Method B* and (c) *Method C*

6.6.5 Summary

The results of these initial field trials show that relying on the theoretical determination of the expected reflection return time (*Method A*) results in a trap location error that increases as the distance to that trap increases. To be more precise, as the number of junctions traversed by the incident transient increases, before it reaches the depleted trap, the higher the trap location error. From the results of *Configuration III(b)* and *IV(b)* the maximum trap location error, having traversed 16 junctions, was between 10% to 12%. When the number of junctions traversed was halved, *Configurations II(b)* and *II(c)*, the maximum trap location error was also halved to between 5% to 6% showing a clear relationship between the number of junctions traversed and trap location error.

Determining the expected reflection return times using the AIRNET simulation and the reflected wave technique itself (*Methods B* and *C*, respectively) showed a marked improvement in accuracy, with a maximum trap location error < 2% across all tests and all system configurations.

6.7 Application to the HWU Arrol (*field*) system

The tests undertaken at the HWU Arrol (*field*) system (*Configuration V* in **Figure 6.18**) provided the first opportunity of incorporating the new combined test equipment configuration (including the sinusoidal exciter and 3-port directional control valve) in the application of the reflected wave technique under field conditions. These tests were also the first field trials of the reflected wave technique using the 10 Hz sinusoidal wave as the incident transient.

The HWU Arrol (*field*) system differed from all the systems tested previously as instead of being connected directly to the stack, the majority of the appliances were connected to a long horizontal branch on either Level 3 or Level 4. This was found to introduce two challenges for the reflected wave method: (i) the large number of junctions encountered by the transient as it propagated the horizontal branch had the effect of reducing the magnitude of the returned refection; (ii) a number of traps were found to be spaced equidistant from the measurement point, despite being on separate floors, such that they displayed similar reflection return times. However, it will be shown that by providing distributed measurement points within the system, these issues were overcome.

6.7.1 HWU Arrol (field) system Configuration V

Figures 6.19 and **6.20** show the measured system response, recoded at VPT1, for the set of depleted water traps on Level 3 (i.e. traps T2 to T10) and Level 4 and 5 (i.e. traps T12 to T20 and T21) respectively. It can be seen that, apart from traps T13 and T21 which are connected directly to the stack, the reflections returned by the depleted traps connected too the horizontal branches are, in some instances, so small that they have little effect on the system response. This is attributed to the *junction effect* which divides and disperses both the incident transient and the returning reflection as they propagate along the horizontal branches. Those traps connected at Level 3 (**Figure 6.19**) are worse affected as these are located further from the measurement point and therefore traverse a greater number of junctions.

Despite being less visible on the measured system response, the TRACER program successfully identified the measured reflection return time for each trap. Predicted depleted trap locations, estimated by the three methods (i.e. *Methods A*, *B* and *C*) are compared with the measured pressure response in **Figure 6.21** and **Table 6.9** presents a summary of these results together with the trap location errors ε.

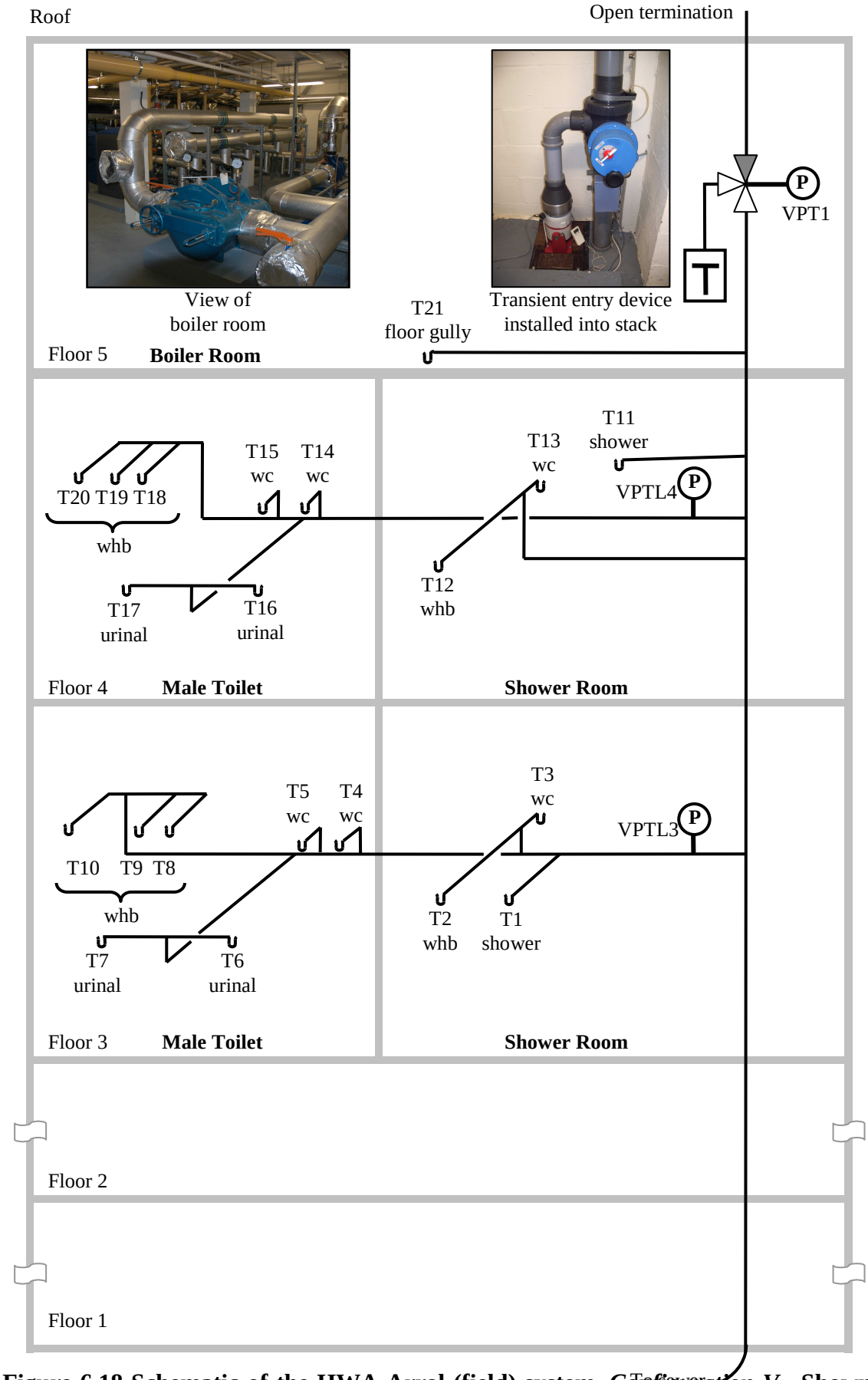

Figure 6.18 Schematic of the HWA Arrol (field) system, *Configuration V*. Shown previously in Figure 5.21 but repeated here for convenience

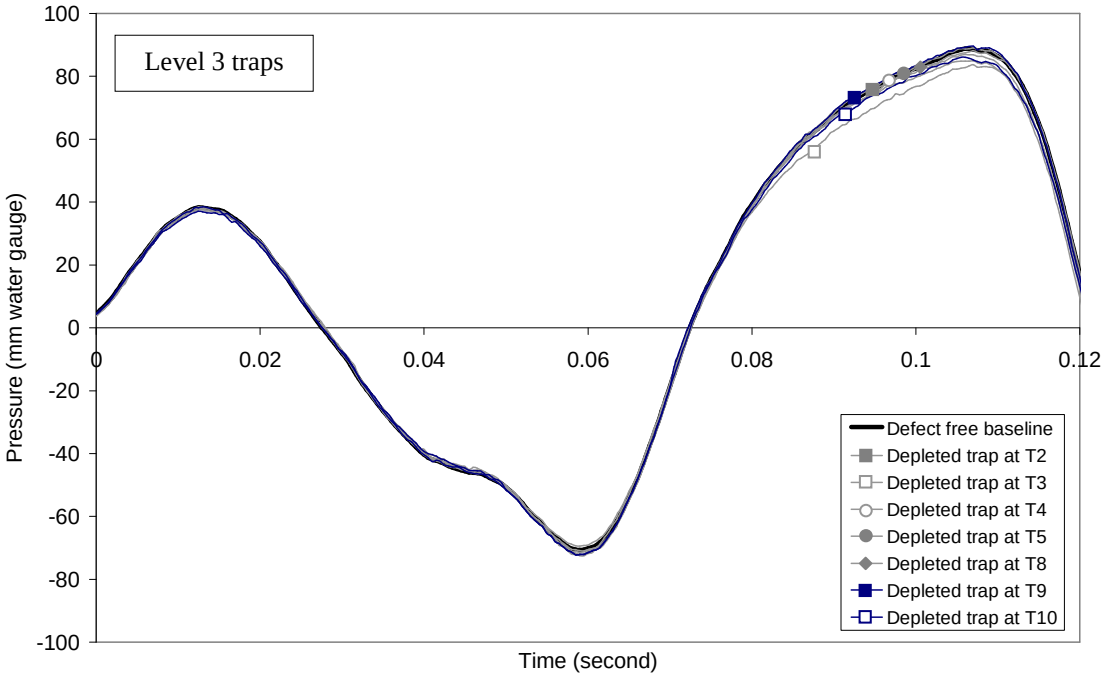

Figure 6.19 Measured system response at VPT1 showing effect of depleted trap distance for *Configuration V* (Level 3 traps only)

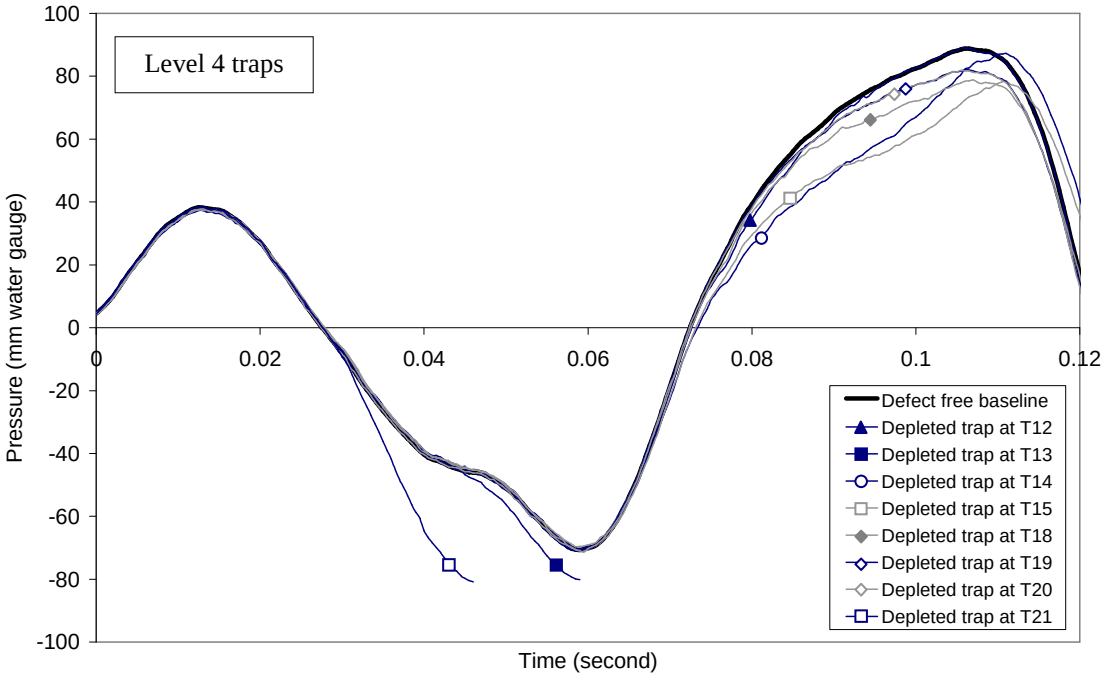

Figure 6.20 Measured system response at VPT1 showing effect of depleted trap distance for *Configuration V* (Level 4 traps only). Note: for clarity each pressure trace has been discontinued shortly after its deviation from the defect free baseline.

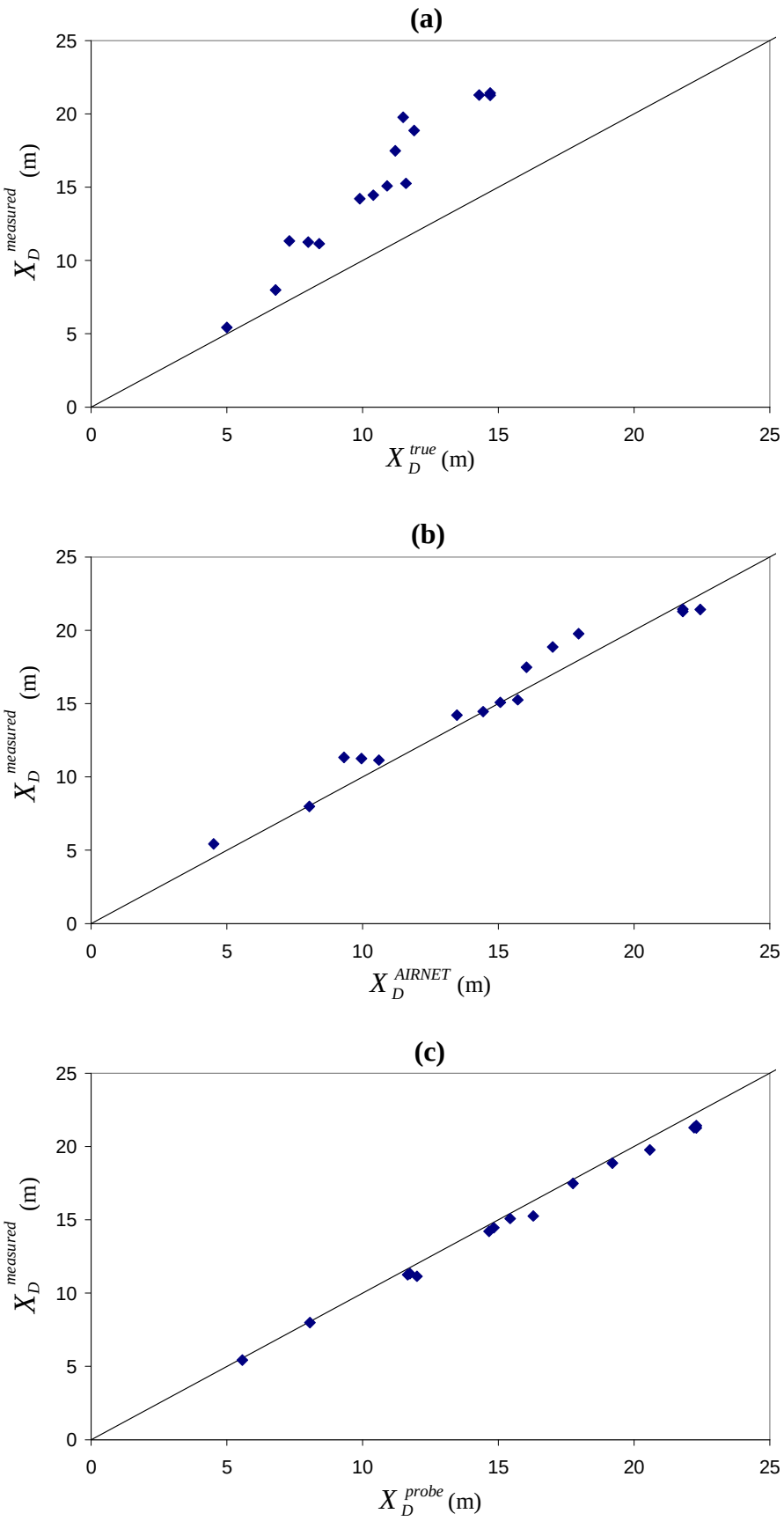

Figure 6.21 Comparison of the measured and predicted depleted trap locations for *Configuration V* using data measured at VPT1 for (a) *Method A*; (b) *Method B* and (c) *Method C*

Table 6.9 Assessment of the depleted trap location by the reflected wave technique for *Configuration V* using data measured at VPT1

Measured trap characteristics from system response			True trap location and pipe period			AIRNET simulated trap location and pipe period			Probed trap location and pipe period		
			Method A			***Method B***			***Method C***		
No	$t_D^{measured}$ (s)	$X_D^{measured}$ (m)	t_D^{true} (s)	X_D^{true} (m)	ε_A	t_D^{AIRNET} (s)	X_D^{AIRNET} (m)	ε_B	t_D^{probe} (s)	X_D^{probe} (m)	ε_C
T2	0.1155	**19.8**	0.0671	**11.5**	55.3%	0.1050	**18.0**	12.0%	0.1201	**20.6**	5.3%
T3	0.0828	**14.2**	0.0577	**9.9**	28.7%	0.0787	**13.5**	4.7%	0.0857	**14.7**	3.3%
T4	0.1020	**17.5**	0.0653	**11.2**	42.0%	0.0933	**16.0**	10.0%	0.1038	**17.8**	2.0%
T5	0.1102	**18.9**	0.0694	**11.9**	46.7%	0.0991	**17.0**	12.7%	0.1120	**19.2**	2.0%
T8	0.1248	**21.4**	0.0857	**14.7**	44.7%	0.1306	**22.4**	6.7%	0.1300	**22.3**	6.0%
T9	0.1242	**21.3**	0.0834	**14.3**	46.7%	0.1271	**21.8**	3.3%	0.1294	**22.2**	6.0%
T10	0.1242	**21.3**	0.0857	**14.7**	44.0%	0.1271	**21.8**	3.3%	0.1300	**22.3**	6.7%
T12	0.0647	**11.1**	0.0490	**8.4**	18.0%	0.0618	**10.6**	3.3%	0.0700	**12.0**	6.0%
T13	0.0466	**8.0**	0.0397	**6.8**	8.0%	0.0466	**8.0**	0.0%	0.0472	**8.1**	0.7%
T14	0.0659	**11.3**	0.0426	**7.3**	26.7%	0.0542	**9.3**	13.3%	0.0682	**11.7**	2.7%
T15	0.0659	**11.3**	0.0466	**8.0**	22.0%	0.0583	**10.0**	8.7%	0.0682	**11.7**	2.7%
T18	0.0845	**14.5**	0.0606	**10.4**	27.3%	0.0822	**14.1**	2.7%	0.0886	**15.2**	4.6%
T19	0.0880	**15.1**	0.0636	**10.9**	28.0%	0.0886	**15.2**	0.7%	0.0915	**15.7**	4.0%
T20	0.0892	**15.3**	0.0676	**11.6**	24.7%	0.0927	**15.9**	4.0%	0.0950	**16.3**	6.7%
T21	0.0315	**5.4**	0.0292	**5.0**	2.7%	0.0262	**4.5**	6.0%	0.0327	**5.6**	1.3%

$$\varepsilon_A = \frac{\left| X_D^{measured} - X_D^{true} \right|}{L} \qquad \varepsilon_B = \frac{\left| X_D^{measured} - X_D^{AIRNET} \right|}{L} \qquad \varepsilon_C = \frac{\left| X_D^{measured} - X_D^{probe} \right|}{L}$$

When L = 15.0 m (the total stack height)

The following conclusions can be made:

i. For *Method A*, the trap location error ε is considerably lower for the traps connected directly to the stack. Traps T21, T13 and T12 each have a trap location error of 2.7%, 8.0% and 18.0%, respectively, (which, incidentally increase with trap distance). However, those traps connected at Level 4 have a trap location error of between 22.0% and 28.0%, and even worse, those connected at Level 3 have a trap location error of between 28.7% and 55.3%.

ii. *Method B* shows an improvement to the trap location error ε for both Level 4 (i.e. ε = 0.7% to 13.3%) and Level 3 (ε = 3.3% to 12.7%).

iii. While *Method C* shows a further improvement: Level 4 (i.e. ε = 2.0% to 6.7%) and Level 3 (ε = 2.0% to 6.7%).

While the location of the depleted trap can be determined with good accuracy using *Method C* (i.e. $\varepsilon < 7\%$) it was found that some traps were located at similar distances from the measurement point and, therefore, had similar reflection return times making it difficult to determine which was the correct location of the depleted trap.

Figure 6.22 shows an example of the measured system response of both trap T3 and T18 which, despite being located on different floors, were positioned equidistantly from the measurement point such that the reflection return times identified by the TRACER program were almost matched (T3, t_D^{probe} = 0.086 seconds; T18, t_D^{probe} = 0.087 seconds) making it impossible to distinguish which was the correct depleted trap location.

AIRNET was used to determine if a more optimal measurement point could be identified which would improve the clarity of the returned reflection and also allow defects on different floors to be distinguished. Two additional measurement points were identified which, in conjunction with VPT1, could be used to optimise the test procedure. Pressure transducers were connected directly onto the Level 3 branch (VPTL3) and the Level 4 branch (VPTL4). The following sections analyse the system response measured at these two locations.

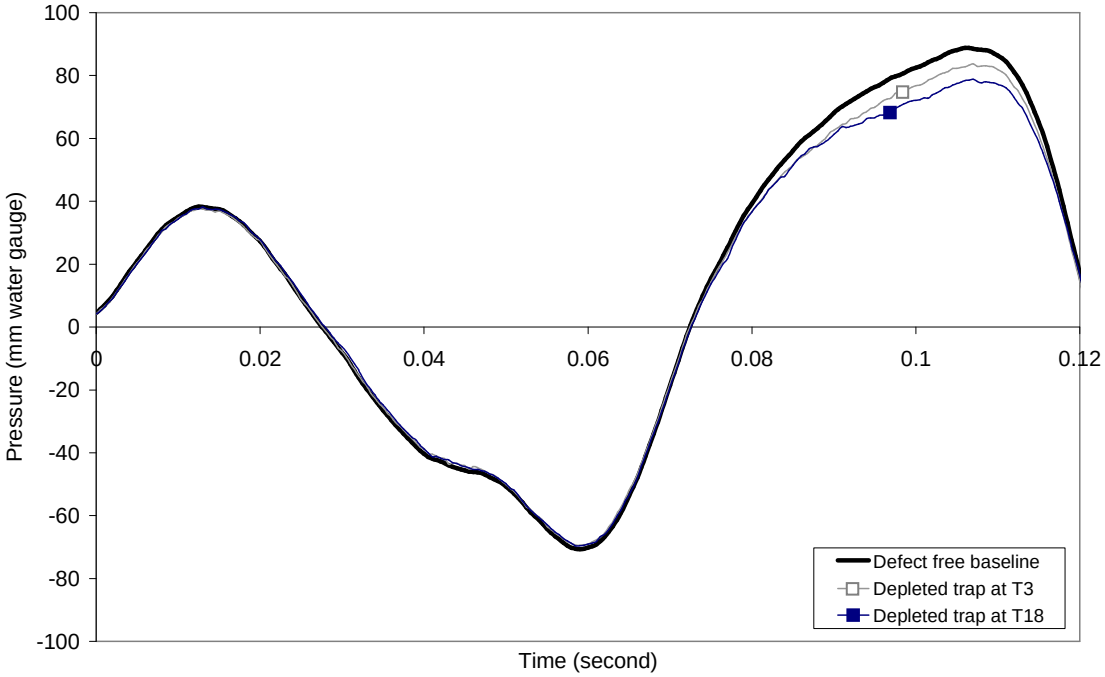

Figure 6.22 Measured system response at VPT1 showing effect of depleted trap distance for *Configuration V*

6.7.1.1 Pressure response measured at VPTL3 (Level 3)

Figure 6.23 shows the measured system response at VPTL3 (*Configuration V* in **Figure 6.18**) for the set of depleted water traps on Level 3 (i.e. traps T2 to T10). All depleted traps are shown to alter the measured system response by inducing a reflection, in response to the applied pressure transient. **Table 6.10** presents the predicted depleted trap locations and the corresponding trap location errors as estimated by each of the three methods (i.e. *Method A*, *B* and *C*). **Figure 6.24** compares the predicted depleted trap locations with the measured depleted trap locations for each method.

The following conclusions can be made:

i. By analysing the system response measured at VPTL3, it can be seen that the trap location error ε is reduced considerably for every trap and for every method. The only exceptions are T9 in *Method B* and T5 in *Method C* which both remained unchanged at 3.3% and 2.0%, respectively.

ii. With *Method A*, the trap location error ε for T8, T9 and T10 (i.e. ε = 16.7%, 13.3% and 28.7%, respectively) are much higher than those observed for the other traps (i.e. all have $\varepsilon < 5\%$). There are two reasons for this. Firstly, as traps T8, T9 and T10 are located at the end of the horizontal branch, the incident transient and returning reflection must pass a greater number of junctions before arriving back at the measurement point. So, due to the *junction effect*, which divides and disperses the waves, the leading edge magnitude of the returning reflection is smaller. Secondly, these traps have a diameter of just 32 mm and so, as will be discussed in more detail in Section 6.9.1 when considering the effect of a single junction, the smaller the branch to stack area ratio, the smaller the returned trap induced reflection will be. Methods *B* and *C*, which take account of the *junction effect*, show a considerable improvement with all traps having a trap location error of $\varepsilon \leq 4\%$ and $\varepsilon < 5.0\%$ respectively.

The distributed measurement point at VPTL3 provides a greater accuracy in detecting and locating the depleted trap seals located on the horizontal branch at Level 3. *Methods B* and *C* are capable of determining the depleted trap location with good accuracy ($\varepsilon < 5.0\%$). However, by not taking account the *junction effects*, Method A introduces greater uncertainties ($\varepsilon < 30\%$).

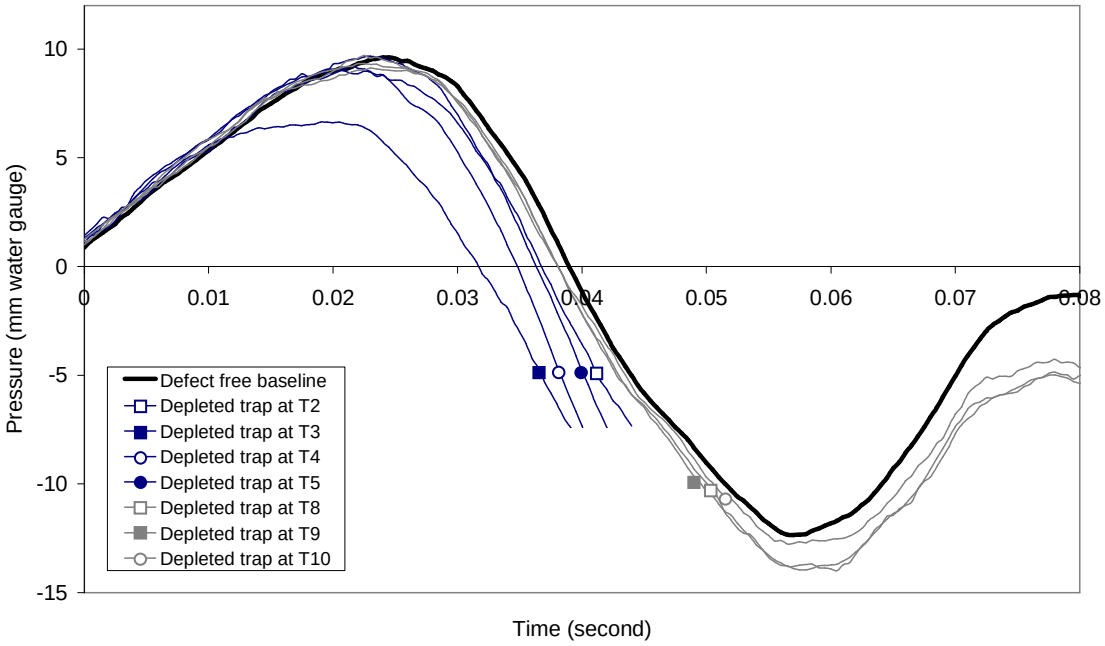

Figure 6.23 Measured system response at VPTL3 showing effect of depleted trap distance for *Configuration V*. Note: for clarity each pressure trace has been discontinued shortly after its deviation from the defect free baseline.

Table 6.10 Assessment of the depleted trap location by the reflected wave technique for *Configuration V* using data measured at VPTL3

Measured trap characteristics from system response			**True trap location and pipe period**			**AIRNET simulated trap location and pipe period**			**Probed trap location and pipe period**		
			Method A			***Method B***			***Method C***		
No	$t_D^{measured}$ (s)	$X_D^{measured}$ (m)	t_D^{true} (s)	X_D^{true} (m)	ε_A	t_D^{AIRNET} (s)	X_D^{AIRNET} (m)	ε_B	t_D^{probe} (s)	X_D^{probe} (m)	ε_C
T2	0.0262	**4.5**	0.0222	**3.8**	4.7%	0.0280	**4.8**	2.0%	0.0286	**4.9**	2.7%
T3	0.0134	**2.3**	0.0128	**2.2**	0.7%	0.0111	**1.9**	2.7%	0.0134	**2.3**	0.0%
T4	0.0251	**4.3**	0.0239	**4.1**	1.3%	0.0222	**3.8**	3.3%	0.0262	**4.5**	1.3%
T5	0.0309	**5.3**	0.0297	**5.1**	1.3%	0.0280	**4.8**	3.3%	0.0327	**5.6**	2.0%
T8	0.0525	**9.0**	0.0379	**6.5**	16.7%	0.0560	**9.6**	4.0%	0.0542	**9.3**	2.0%
T9	0.0472	**8.1**	0.0356	**6.1**	13.3%	0.0501	**8.6**	3.3%	0.0507	**8.7**	4.0%
T10	0.0671	**11.5**	0.0420	**7.2**	28.7%	0.0647	**11.1**	2.7%	0.0630	**10.8**	4.7%

$$\varepsilon_A = \frac{\left| X_D^{measured} - X_D^{true} \right|}{L} \qquad \varepsilon_B = \frac{\left| X_D^{measured} - X_D^{AIRNET} \right|}{L} \qquad \varepsilon_C = \frac{\left| X_D^{measured} - X_D^{probe} \right|}{L}$$

When L = 15.0 m (the total stack height)

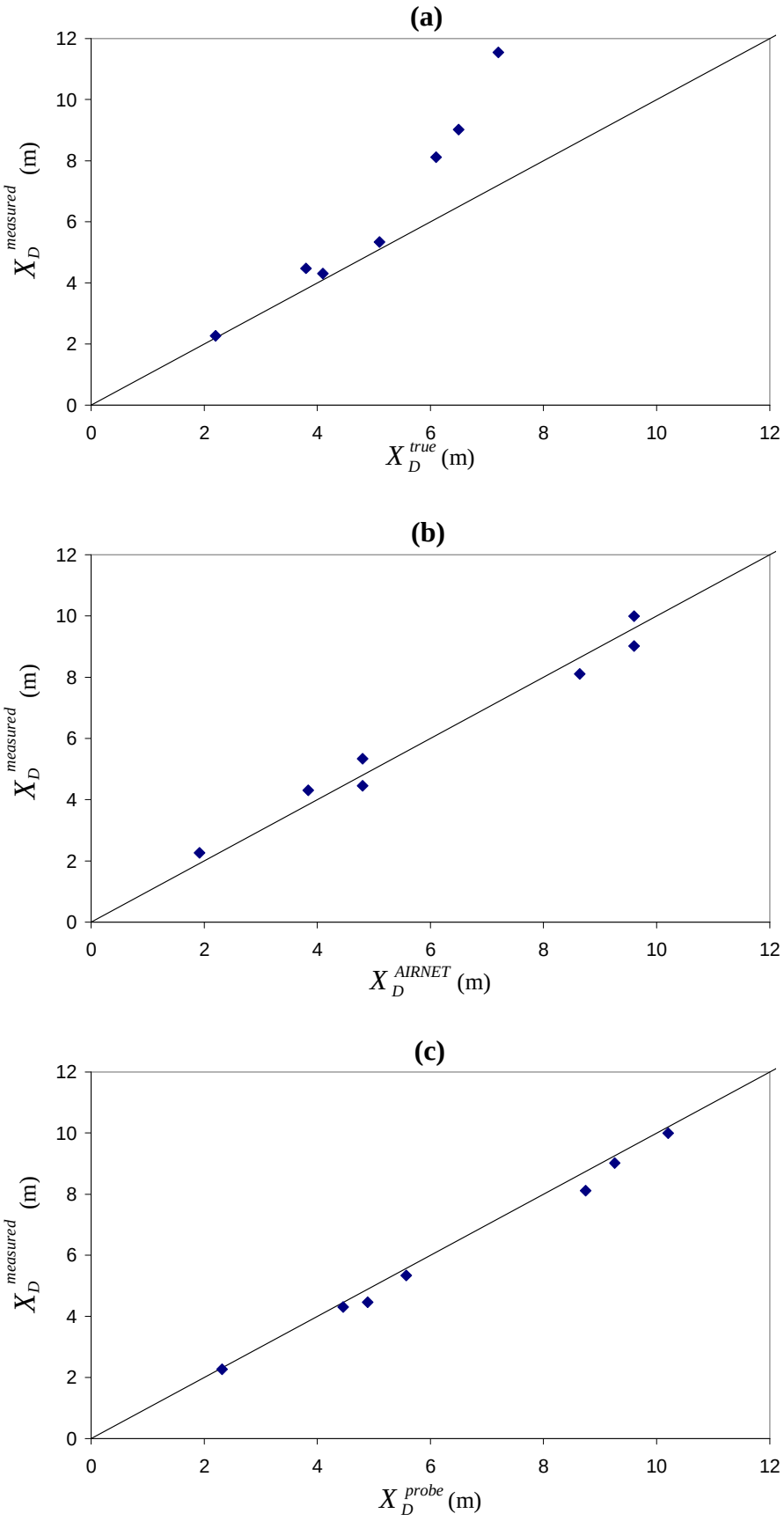

Figure 6.24 Comparison of the measured and predicted depleted trap locations for *Configuration V* using data measured at VPTL3 for (a) *Method A*; (b) *Method B* and (c) *Method C*

6.7.1.2 Pressure response measured at VPTL4 (Level 4)

Figure 6.25 shows the measured system response at VPTL4 (*Configuration V* in **Figure 6.18**) for the set of depleted traps on Level 4 (i.e. traps T14 to T20). All depleted traps are shown to alter the measured system response by inducing a reflection, in response to the applied pressure transient.

Table 6.11 presents the predicted depleted trap locations and the corresponding trap location errors as estimated by each of the three methods (i.e. *Method A*, *B* and *C*). **Figure 6.26** compares the predicted depleted trap locations with the measured depleted trap locations for each method.

The following conclusions can be made:

i. By analysing the system response measured at VPTL4, the trap location error ε is considerably reduced for every trap and for every method, **Table 6.11**.

ii. For Method A, all depleted trap locations can be identified to within 1.3 m (i.e. $\varepsilon \leq 8.7\%$), while for Method B, this improves to 1.0 m (i.e. $\varepsilon \leq 6.7\%$) and for Method C this improves again to 0.6 m (i.e. $\varepsilon \leq 4.0\%$).

The distributed measurement point at VPTL4 provides a greater accuracy in detecting and locating the depleted trap seals located on the horizontal branch at Level 4. *Methods B* and *C* are capable of determining the depleted trap location with good accuracy (i.e. $\varepsilon \leq 6.7\%$). However, by not taking account the *junction effect*s, *Method A* introduces greater uncertainties (i.e. $\varepsilon \leq 8.7\%$)

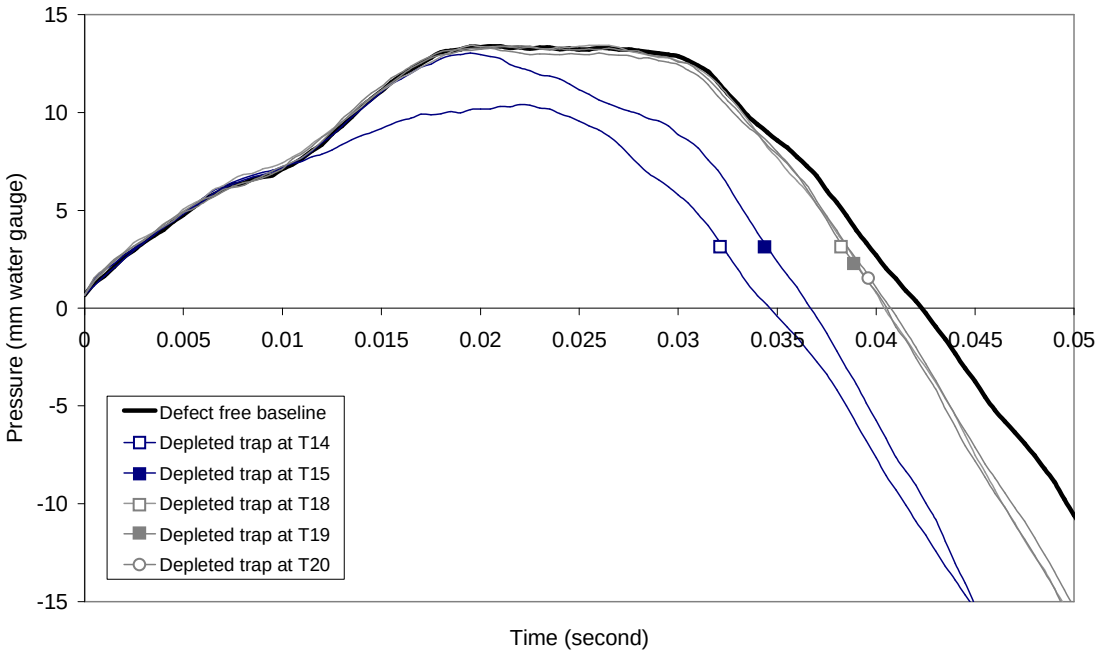

Figure 6.25 Measured system response at VPTL4 showing effect of depleted trap distance for *Configuration V*

Table 6.11 Assessment of the depleted trap location by the reflected wave technique for *Configuration V* using data measured at VPTL4

Measured trap characteristics from system response			True trap location and pipe period			AIRNET simulated trap location and pipe period			Probed trap location and pipe period		
			Method A			*Method B*			*Method C*		
No	$t_D^{measured}$ (s)	$X_D^{measured}$ (m)	t_D^{true} (s)	X_D^{true} (m)	ε_A	t_D^{AIRNET} (s)	X_D^{AIRNET} (m)	ε_B	t_D^{probe} (s)	X_D^{probe} (m)	ε_C
T14	0.0122	**2.1**	0.0105	**1.8**	2.0%	0.0093	**1.6**	3.3%	0.0122	**2.1**	0.0%
T15	0.0210	**3.6**	0.0187	**3.2**	2.7%	0.0152	**2.6**	6.7%	0.0222	**3.8**	1.3%
T18	0.0350	**6.0**	0.0274	**4.7**	8.7%	0.0338	**5.8**	1.3%	0.0385	**6.6**	4.0%
T19	0.0373	**6.4**	0.0303	**5.2**	8.0%	0.0373	**6.4**	0.0%	0.0402	**6.9**	3.3%
T20	0.0362	**6.2**	0.0344	**5.9**	2.0%	0.0391	**6.7**	3.3%	0.0367	**6.3**	0.7%

$$\varepsilon_A = \frac{\left| X_D^{measured} - X_D^{true} \right|}{L} \qquad \varepsilon_B = \frac{\left| X_D^{measured} - X_D^{AIRNET} \right|}{L} \qquad \varepsilon_C = \frac{\left| X_D^{measured} - X_D^{probe} \right|}{L}$$

When L = 15.0 m (the total stack height)

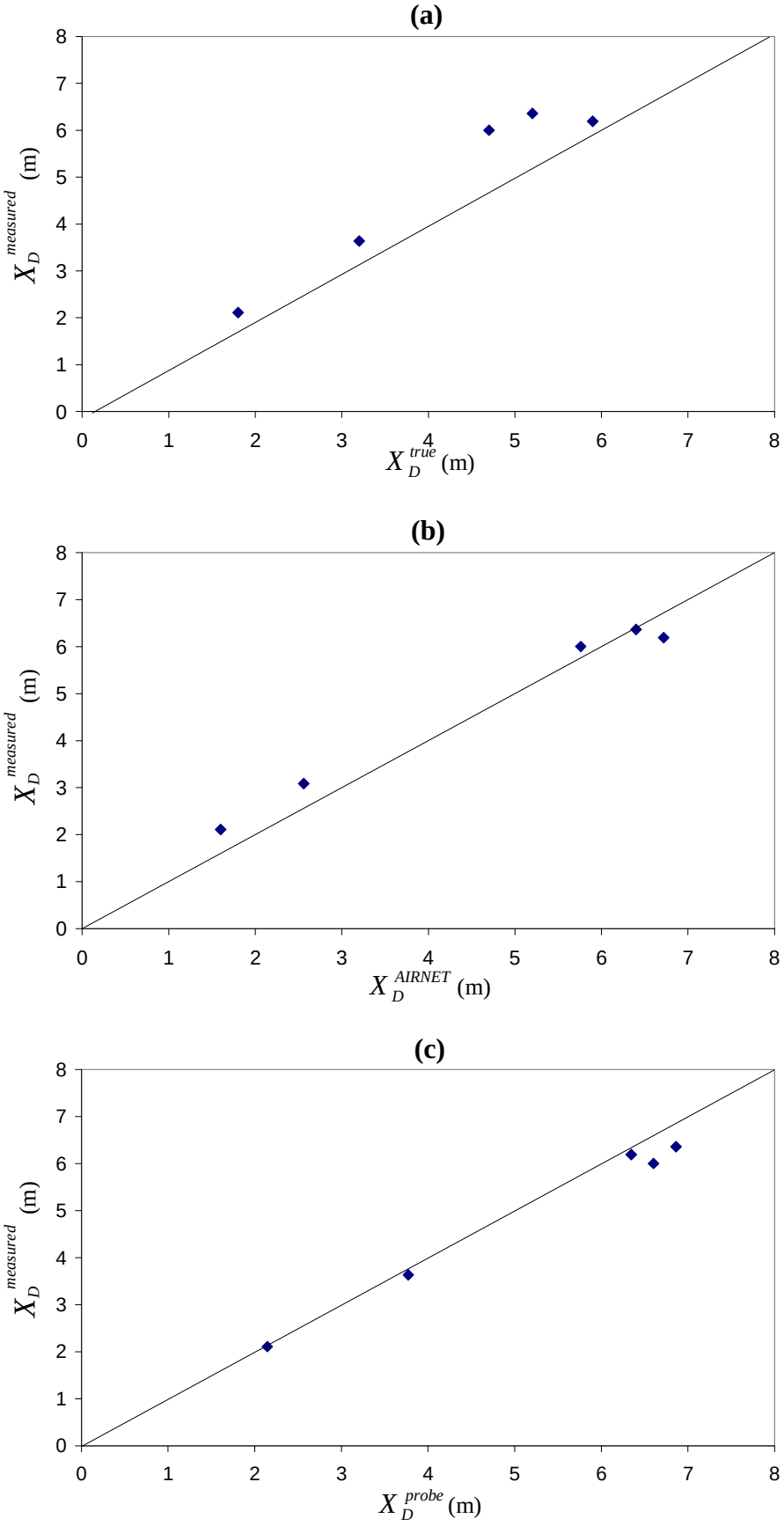

Figure 6.26 Comparison of the measured and predicted depleted trap locations for *Configuration V* using data measured at VPTL4 for (a) *Method A*; (b) *Method B* and (c) *Method C*

6.7.2 Summary

The tests undertaken on the HWU Arrol (*field*) system provided new challenges for the successful application of the reflected wave technique. Collecting the majority of the appliances into a horizontal branch on either Level 3 or Level 4 the magnitude, and therefore the clarity, of the returned reflection from a depleted trap was reduced due to the *junction effect*. Furthermore, the traps located at similar distance from the measurement point were difficult to distinguish so the correct location of the depleted trap was sometimes difficult to identify.

Distributed measurement points have been shown to overcome these problems. By installing a pressure transducer on each of the horizontal branches, the *junction effect* was minimised as the number of junctions that the returning reflection must traverse before arriving at the measurement point is reduced. The problem of equidistant traps is also overcome as the system response from the distributed measurement point can be used in conjunction with VPT1 to triangulate the true location of the depleted trap.

6.8 Application to the Glasgow (*field*) system

The tests undertaken at the Glasgow (*field*) system provided the first opportunity to test the reflected wave technique in a fully operational commercial building not under the control of the investigators. The data from three system tests - (i) *Configuration VI*, (ii) *Configuration VII* (both shown in **Figure 6.27**), and (iii) *Configuration VIII* (shown in **Figure 6.28**) - were analysed to investigate the effect of depleted trap distance X_D^{true} on the accuracy of the technique.

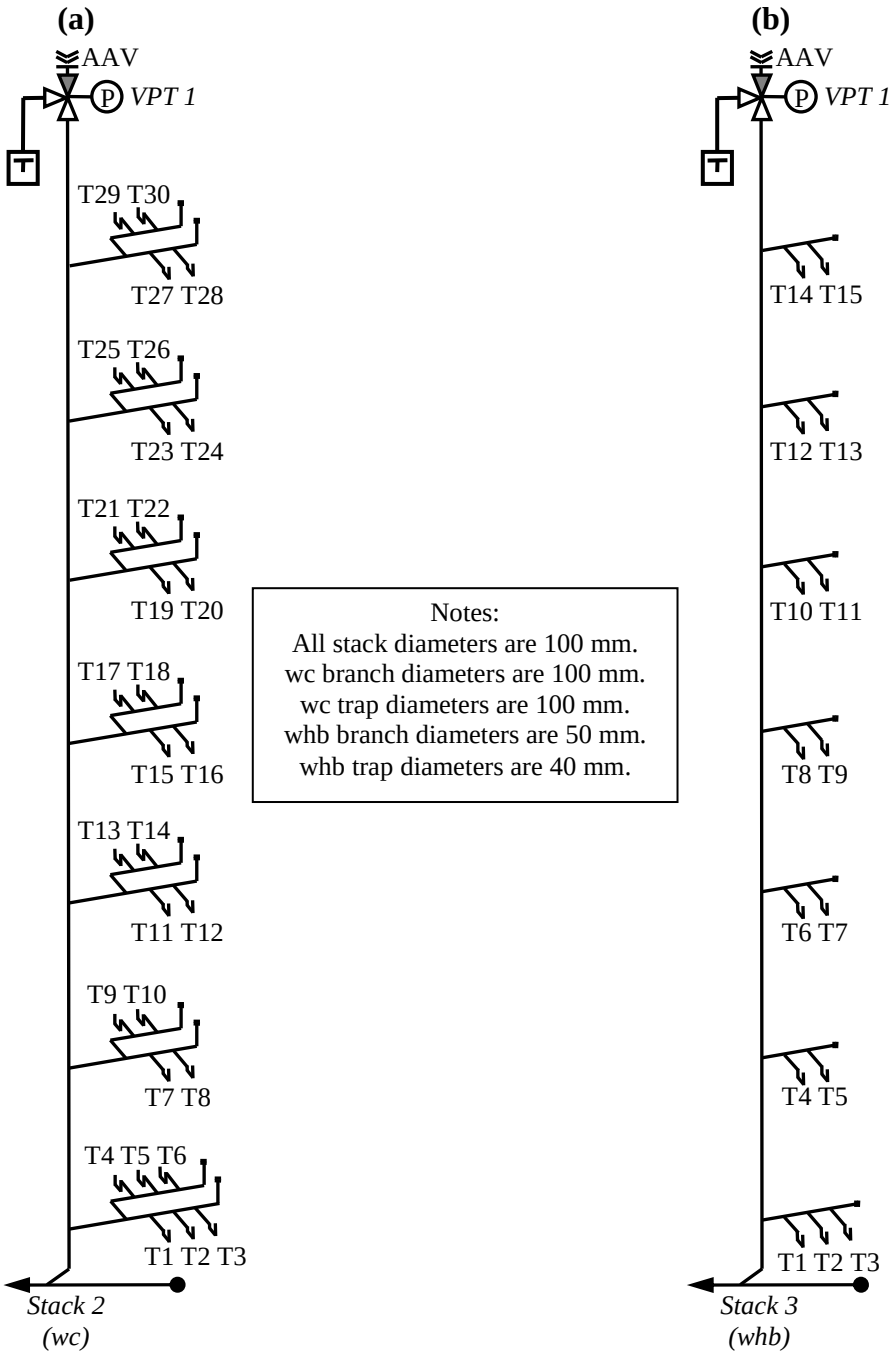

Figure 6.27 Schematics of (a) *Configuration VI*; and (b) *Configuration VII*. Shown previously in Figure 5.35 but repeated here for convenience.

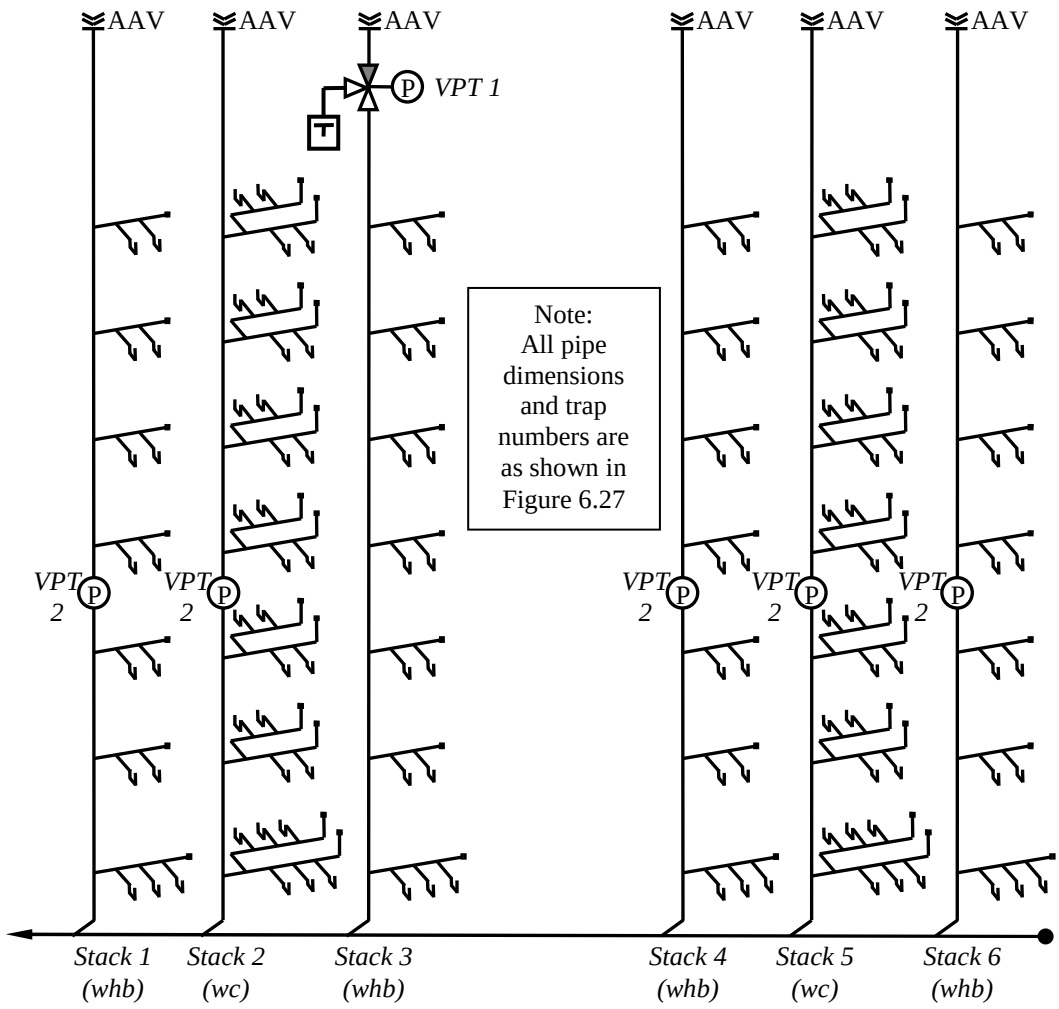

Figure 6.28 Schematic of *Configuration VIII*. Shown previously in Figure 5.36 but repeated here for convenience.

6.8.1 Glasgow WC (field) system

Figure 6.29 presents the measured pressure response at VPT1 for the selected set of depleted traps (i.e. T6, T10, T14, T18, T22, T26 and T30) for *Configuration VI*, **Figure 6.27**.

It can be seen that the reflection induced by each depleted trap in response to the applied pressure transient becomes visibly smaller in magnitude as the distance to the depleted trap increases. This is attributed to the *junction effect* which, as demonstrated in Section 6.4, has been shown to alter the waveform of the transient leading edge due to the reflection and transmission process which takes place at each junction.

Each time the incident transient encounters a junction it is reduced by the proportion of the transient which is reflected backwards. Therefore, not only does the leading edge magnitude of the incident transient arriving at the depleted trap become smaller and smaller in relation to the number of junctions encountered on the way, the returning reflection, which is also subject to the same effect, becomes smaller and smaller as it returns along the system.

The result is that traps located further from the measurement point and which are therefore preceded by a larger number of junctions are identified with a smaller diameter reflection.

As the junctions within the system consist of three identical pipes then, from Equations (2.12) and (2.13), the reflection coefficient $C_R^{junction}$ = -0.33 and the transmission coefficient $C_T^{junction}$ = +0.67. It can be seen from Equation 6.3 that the leading edge magnitude of the returning reflection from, for example trap T6, having traversed a total of 16 junctions during both the outward and returning propagation is only 0.2% of the incident transient. Whereas, for trap T30, having traversed only 8 junctions the leading edge magnitude of the returning reflection is 4% of the incident transient, some twenty times greater than that for T6.

It should be noted that the reflection magnitudes quoted here refer only to the *initial* leading edge of the returning reflection. The measured system response show reflections which eventually attain a much larger magnitude as these include the re-reflected and re-transmitted parts of the wave which eventually arrive at the measurement point to *reconstruct* the pressure wave.

Despite the reducing influence of the *junction effect* on the leading edge magnitude of the trap induced reflection the TRACER program is able to determine the reflection return times from the measured pressure response. Predicted depleted trap locations, estimated by the three methods (i.e. *Methods A*, *B* and *C*) are presented in **Table 6.12** together with the trap location errors ε.

Figure 6.30 compares the measured and predicted depleted trap locations for each method. The following can be concluded:

i. Trap location error for *Method A* increases with trap distance (i.e. as X_D^{true} increases). For trap T30 (i.e. X_D^{true} = 6.5 m) ε is 1.7% which corresponds to a trap location estimation error of 0.6 m. The trap location error continues to increase until, for trap T6 (i.e. X_D^{true} = 33.6 m), ε is 41.1% giving a trap location estimation error of 14.4 m.

   This level of error is unacceptable and confirms the need for alternative methods of predicting trap location.

ii. *Methods B* and *C* each demonstrate considerably better accuracy (i.e. ε = 1.4% to 3.1% and ε = 0.6% to 2.6%, respectively). **Figure 6.30** demonstrates the excellent correlation that both X_D^{AIRNET} and X_D^{probe} have with $X_D^{measured}$.

   The maximum trap location estimation error for *Methods B* and *C* are 1.1 m and 0.9 m, respectively which is greatly more acceptable than that for *Method A.*

The location of the depleted trap can be accurately estimated by both *Methods B* and *C* ($\varepsilon \leq$ 3.1%). *Method A* is shown to be influenced by the *junction effect* which causes ε to increase with increasing trap distance.

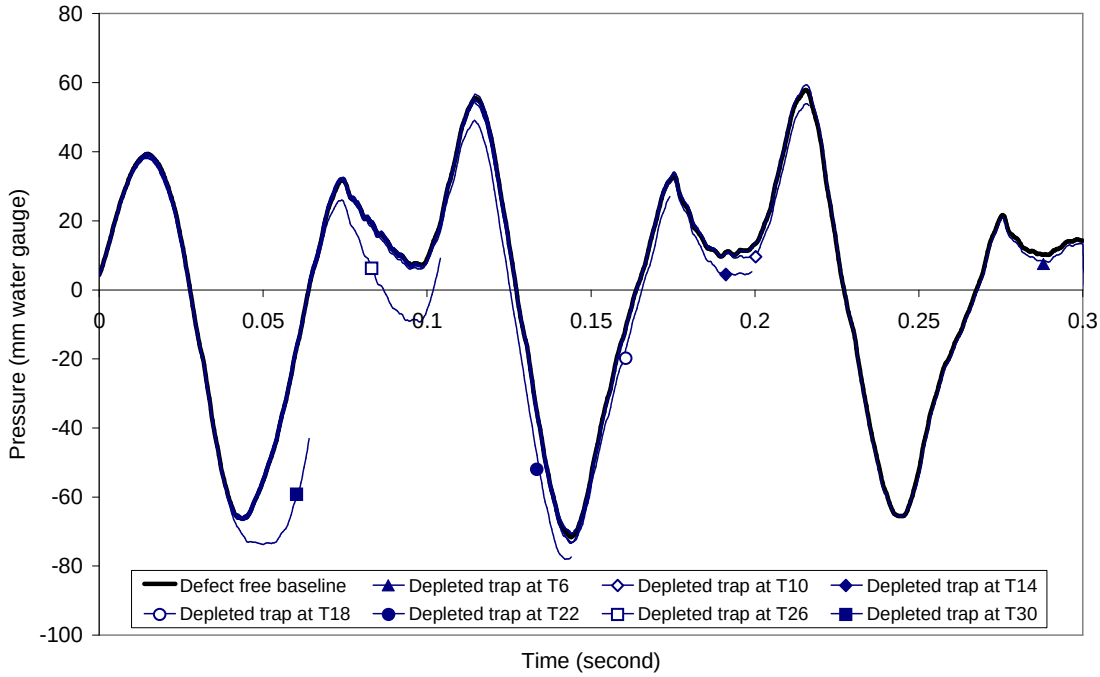

Figure 6.29 Measured system response at VPT1 showing effect of depleted trap distance for *Configuration VI*. Note: for clarity each pressure trace has been discontinued shortly after its deviation from the defect free baseline.

Table 6.12 Assessment of the depleted trap location by the reflected wave technique for *Configuration VI* using data measured at VPT1

Measured trap characteristics from system response			**True trap location and pipe period**			**AIRNET simulated trap location and pipe period**			**Probed trap location and pipe period**		
			Method A			***Method B***			***Method C***		
No	$t_D^{measured}$ (s)	$X_D^{measured}$ (m)	t_D^{true} (s)	X_D^{true} (m)	ε_A	t_D^{AIRNET} (s)	X_D^{AIRNET} (m)	ε_B	t_D^{probe} (s)	X_D^{probe} (m)	ε_C
T6	0.2799	**48.0**	0.1959	**33.6**	41.1%	0.2752	**47.2**	2.3%	0.2851	**48.9**	2.6%
T10	0.2099	**36.0**	0.1545	**26.5**	27.1%	0.2146	**36.8**	2.3%	0.2052	**35.2**	2.3%
T14	0.1819	**31.2**	0.1312	**22.5**	24.9%	0.1790	**30.7**	1.4%	0.1802	**30.9**	0.9%
T18	0.1487	**25.5**	0.1079	**18.5**	20.0%	0.1440	**24.7**	2.3%	0.1464	**25.1**	1.1%
T22	0.1050	**18.0**	0.0845	**14.5**	10.0%	0.1096	**18.8**	2.3%	0.1061	**18.2**	0.6%
T26	0.0682	**11.7**	0.0612	**10.5**	3.4%	0.0746	**12.8**	3.1%	0.0694	**11.9**	0.6%
T30	0.0414	**7.1**	0.0379	**6.5**	1.7%	0.0472	**8.1**	2.9%	0.0402	**6.9**	0.6%

$$\varepsilon_A = \frac{\left| X_D^{measured} - X_D^{true} \right|}{L} \qquad \varepsilon_B = \frac{\left| X_D^{measured} - X_D^{AIRNET} \right|}{L} \qquad \varepsilon_C = \frac{\left| X_D^{measured} - X_D^{probe} \right|}{L}$$

When L = 35.0 m (the total stack height)

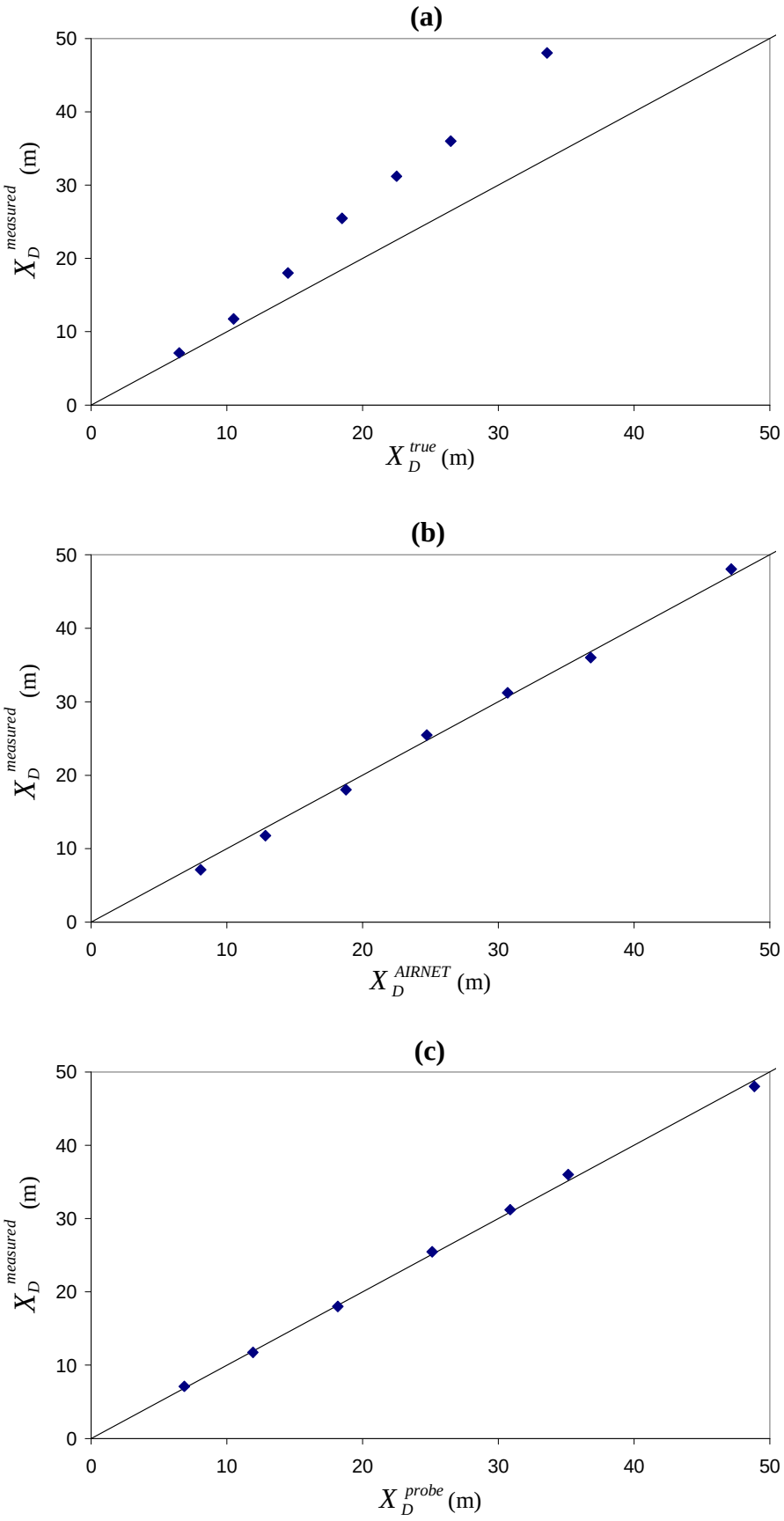

Figure 6.30 Comparison of the measured and predicted depleted trap locations for *Configuration VI* using data measured at VPT1 for (a) *Method A*; (b) *Method B* and (c) *Method C*

6.8.2 Glasgow WHB (field) system

Figure 6.31 presents the measured pressure response at VPT1 for the selected set of depleted traps (i.e. T1 to T15) for *Configuration VII*, **Figure 6.27**. Each trap can be seen to induce a clear reflection, in response to the applied pressure transient. The influence of the *junction effect* is less obvious than that observed from *Configuration VI*. This is due to the difference of the branch to stack area ratios of the two systems. The side branches on the *Configuration VII* system have a diameter of 50 mm and so, with a 100 mm diameter stack, the reflection coefficient is $C_R^{junction}$ = -0.11 and the transmission coefficient is $C_T^{junction}$ = +0.89; while for *Configuration VI* the junction reflection and transmission coefficients are $C_R^{junction}$ = -0.33 and $C_T^{junction}$ = +0.66, respectively. Although when considering the effect of a single junction, as will be discussed in Section 6.9.1, the greater the branch to stack area ratio is, the larger the magnitude of the trap induced reflection, it is the process that occurs at each preceding junction that determines the leading edge magnitude of both the transient arriving at the depleted trap and the subsequent reflection which arrives at the measurement point. Therefore, when the branch to stack area ratio is small, the overall significance of the *junction effect* is reduced and the returned trap induced reflection will be larger.

Using the TRACER program to determine the reflection return times, the predicted depleted trap locations, estimated by the three methods (i.e. *Method A*, *B* and *C*) are presented in **Table 6.13** together with the trap location errors ε. **Figure 6.32** compares the measured depleted trap location with that predicted by each method. The following conclusions can be made:

i. Trap location error ε, for *Method A*, increases with trap distance. For trap T14 (i.e. X_D^{true} = 6.9 m) ε is 3.1% which corresponds to a trap location estimation error of 1.1 m. The trap location error continues to increase until, for trap T3 (i.e. X_D^{true} = 34.3 m), ε is 7.4% giving a trap location estimation error of 2.6 m.

ii. *Methods B* and *C* both give considerably better accuracy (i.e. ε = 0.0% to 3.1% and ε = 0.0% to 2.0%, respectively). **Figure 6.32** demonstrates the excellent correlation of both X_D^{AIRNET} and X_D^{probe} with $X_D^{measured}$. The maximum trap location estimation error for *Methods B* and *C* are 1.1 m and 0.7 m, respectively. The location of the depleted trap can be accurately estimated by both *Methods B* and *C* ($\varepsilon \leq$ 3.1% and $\varepsilon <$ 2.0%, respectively).

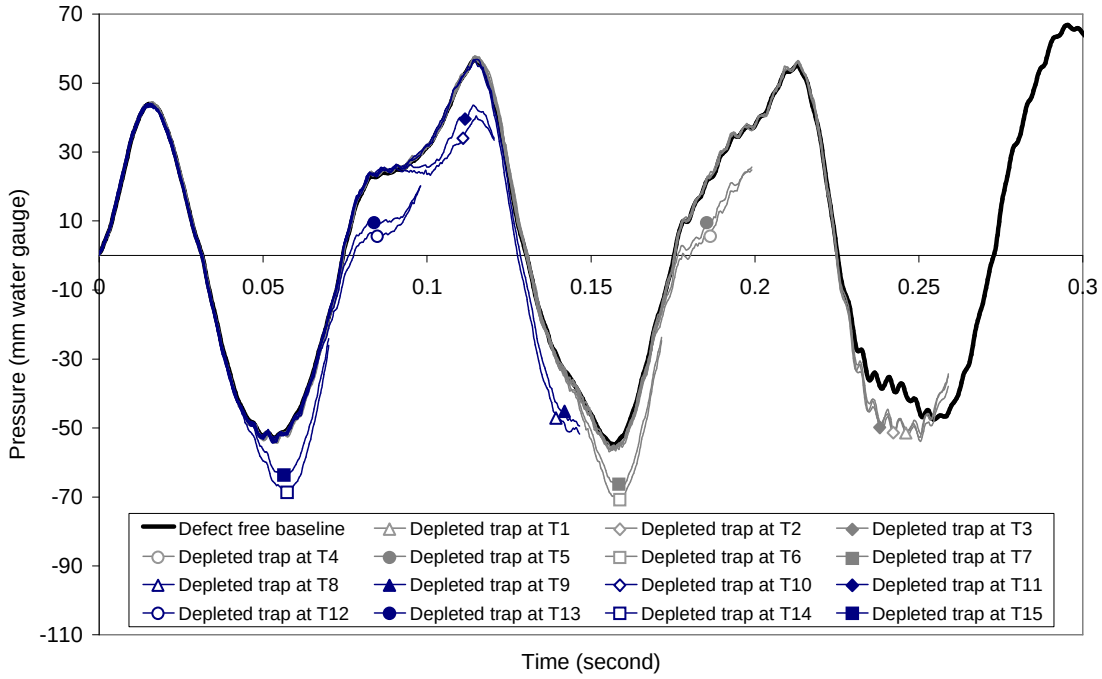

Figure 6.31 Measured system response at VPT1 showing effect of depleted trap distance for *Configuration VII*. Note: for clarity each pressure trace has been discontinued shortly after its deviation from the defect free baseline.

Table 6.13 Assessment of the depleted trap location by the reflected wave technique for *Configuration VII* using data measured at VPT1

Measured trap characteristics from system response			**True trap location and pipe period**			**AIRNET simulated trap location and pipe period**			**Probed trap location and pipe period**		
			Method A			***Method B***			***Method C***		
No	$t_D^{measured}$ (s)	$X_D^{measured}$ (m)	t_D^{true} (s)	X_D^{true} (m)	ε_A	t_D^{AIRNET} (s)	X_D^{AIRNET} (m)	ε_B	t_D^{probe} (s)	X_D^{probe} (m)	ε_C
T1	0.2099	**36.0**	0.1953	**33.5**	7.1%	0.2058	**35.3**	2.0%	0.2122	**36.4**	1.1%
T2	0.2122	**36.4**	0.1977	**33.9**	7.1%	0.2076	**35.6**	2.3%	0.2128	**36.5**	0.3%
T3	0.2152	**36.9**	0.2000	**34.3**	7.4%	0.2087	**35.8**	3.1%	0.2140	**36.7**	0.6%
T4	0.1697	**29.1**	0.1569	**26.9**	6.3%	0.1638	**28.1**	2.9%	0.1679	**28.8**	0.9%
T5	0.1732	**29.7**	0.1592	**27.3**	6.9%	0.1685	**28.9**	2.3%	0.1738	**29.8**	0.3%
T6	0.1452	**24.9**	0.1335	**22.9**	5.7%	0.1399	**24.0**	2.6%	0.1411	**24.2**	2.0%
T7	0.1475	**25.3**	0.1359	**23.3**	5.7%	0.1434	**24.6**	2.0%	0.1452	**24.9**	1.1%
T8	0.1207	**20.7**	0.1102	**18.9**	5.1%	0.1155	**19.8**	2.6%	0.1178	**20.2**	1.4%
T9	0.1242	**21.3**	0.1125	**19.3**	5.7%	0.1184	**20.3**	2.9%	0.1230	**21.1**	0.6%
T10	0.0956	**16.4**	0.0869	**14.9**	4.3%	0.0956	**16.4**	0.0%	0.0962	**16.5**	0.3%
T11	0.0980	**16.8**	0.0892	**15.3**	4.3%	0.0968	**16.6**	0.6%	0.0991	**17.0**	0.6%
T12	0.0711	**12.2**	0.0636	**10.9**	3.7%	0.0706	**12.1**	0.3%	0.0688	**11.8**	1.1%
T13	0.0735	**12.6**	0.0659	**11.3**	3.7%	0.0729	**12.5**	0.3%	0.0711	**12.2**	1.1%
T14	0.0466	**8.0**	0.0402	**6.9**	3.1%	0.0472	**8.1**	0.3%	0.0466	**8.0**	0.0%
T15	0.0490	**8.4**	0.0426	**7.3**	3.1%	0.0496	**8.5**	0.3%	0.0490	**8.4**	0.0%

$$\varepsilon_A = \frac{\left| X_D^{measured} - X_D^{true} \right|}{L} \qquad \varepsilon_B = \frac{\left| X_D^{measured} - X_D^{AIRNET} \right|}{L} \qquad \varepsilon_C = \frac{\left| X_D^{measured} - X_D^{probe} \right|}{L}$$

When L = 35.0 m (the total stack height)

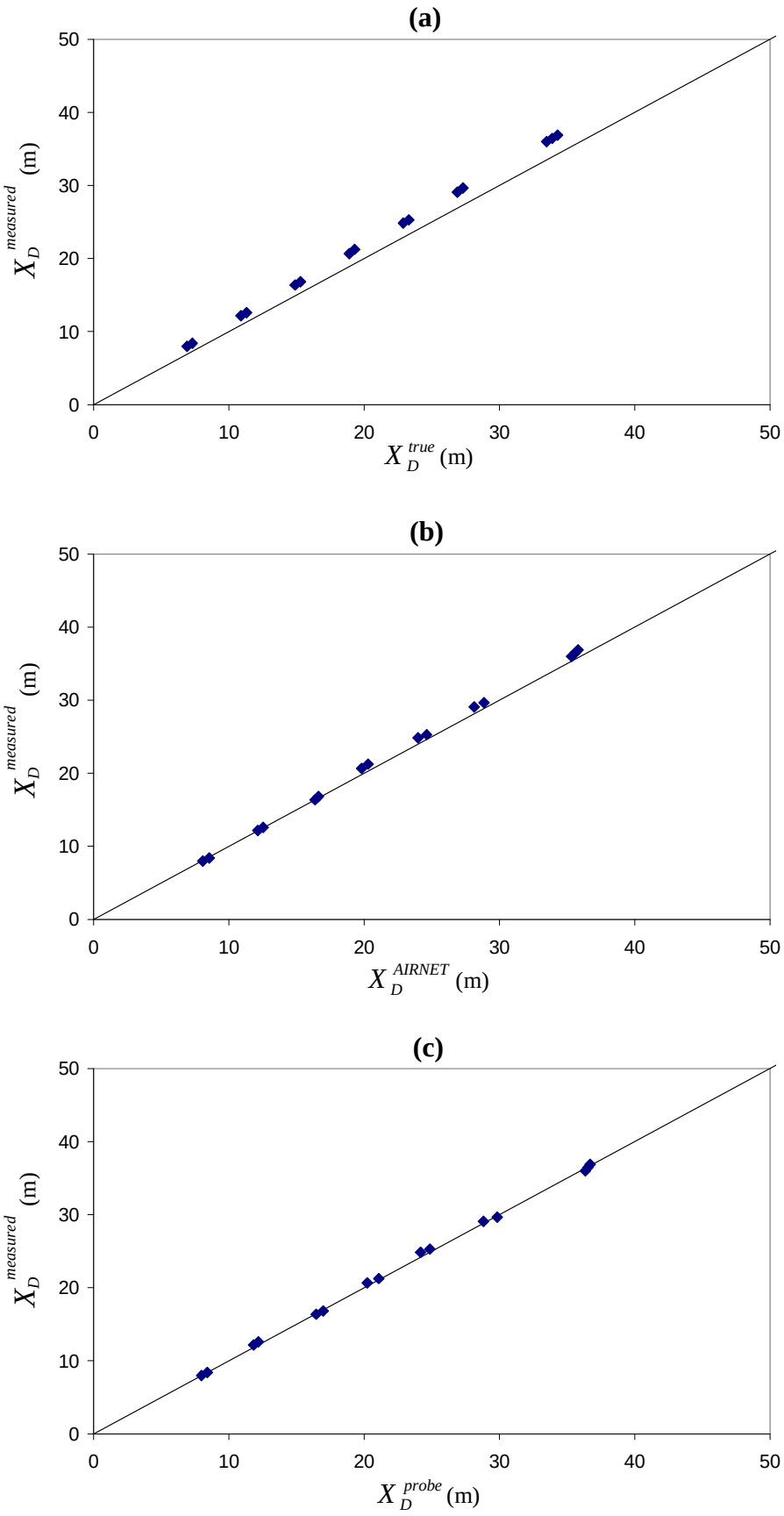

Figure 6.32 Comparison of the measured and predicted depleted trap locations for *Configuration VII* using data measured at VPT1 for (a) *Method A*; (b) *Method B* and (c) *Method C*

6.8.3 Glasgow multi-stack (field) system

Until now the reflected wave technique has been applied to determine the system status of only one single stack drainage system at a time. This section analyses the results of the tests carried out at the Glasgow multi-stack (*field*) system, *Configuration VIII* **Figure 6.28**, where the technique was applied to a multi-single-stack system (i.e. consisting of six single stacks connected at a common horizontal drain pipe). The combined test equipment was installed at Stack 3 and distributed measurement points were located at Floor 2 on each of the remaining stacks.

Figures 6.33 to **6.37** show the system response measured at VPT2 for Stack 1, Stack 2, Stack 4, Stack 5 and Stack 6, respectively, for the selected set of depleted traps (i.e. T8, T10, T12 and T14 on Stack 1, Stack 4 and Stack 6; and T15, T19, T23 and T27 on Stack 2 and Stack 5). The system response obtained from these downstream measurement points can be seen to have a considerably lower amplitude than the input transient wave, **Figure 6.31**, which can be mainly attributed to the reflection and transmission effects of the numerous junctions traversed before arriving at the VPT2, each of which attenuate the wave by an amount determined by the junction geometry, Equations (2.12) and (2.13), respectively. Nevertheless, the depleted trap seals can be seen to generate a negative reflection in response to the applied positive pressure transient that alters the system response at a time specific to that trap. Although the induced pressure drop is, in most cases, quite subtle, the TRACER program was capable of identifying the reflection return times, $t_D^{measured}$, from the measured system response. In some instances, however, to obtain an accurate value for $t_D^{measured}$ the threshold level, *h*, had to be reduced from 4 mm water gauge to only 1 mm water gauge; potentially increasing the likelihood of false alarms.

The predicted depleted trap locations, estimated by the three methods (i.e. *Method A*, *B* and *C*) for every stack are presented in **Table 6.14** together with the trap location errors ε. **Figure 6.38** compares the measured depleted trap location, again for every stack, with that predicted by each method. The following conclusions can be made:

i. In general, the trap location error ε, for *Method A*, increases with increasing trap distance. Taking Stack 2 for example, the trap location error ε for trap T15 (i.e. X_D^{true} = 3.9 m) is 6.0% which corresponds to a trap location estimation error

of 2.1 m. ε continues to increase until for trap T27 (i.e. X_D^{true} = 15.9 m), ε is 32.9% giving a trap location estimation error of 11.5 m.

ii. For *Method A*, the trap location error for Stack 2 and 5 (i.e. ε < 33%) is considerably greater than that for Stack 1, 4 and 6 (i.e. ε < 10.0%). This difference is a function of the *junction effect*, and in particular, of the branch to stack area ratio of each junction present within each stack. The junctions in Stack 2 and 5 consist of three identical pipes (i.e. A_{branch}/A_{stack} = 1.0) and so from Equations (2.12) and (2.13) the reflection coefficient is $C_R^{junction}$ = -0.33 and the transmission coefficient is $C_T^{junction}$ = +0.67. However, for Stacks 1, 4 and 6, where the junctions consist of a 50 mm diameter branch and a 100 mm diameter stack (i.e. A_{branch}/A_{stack} = 0.3), $C_R^{junction}$ = -0.11 and $C_T^{junction}$ = +0.89. Therefore, in Stacks 1, 4 and 6, as more of the incident transient is transmitted forwards at each junction, and less is reflected backwards, the magnitude of the transient arriving at the depleted trap is larger which, in turn, generates a larger returning reflection which allows its arrival time to be more clearly determined. The effect of the different branch to stack area ratios is clearly demonstrated in **Figure 6.38(a)**. Section 6.10 considers this point in more detail by quantifying the influence on the trap location error of both the branch to stack area ratio and the number of junctions traversed.

iii. *Method B* improves the accuracy of the technique. While the traps located on Stack 2 and 5 continue to have the highest trap location error (i.e. $\varepsilon \leq$ 6.9%) compared to Stacks 1, 4 and 6 (i.e. $\varepsilon \leq$ 4.3%) the accuracy is considerably improved over *Method A*.

iv. *Method C* continues this trend, showing a further improvement in accuracy with Stacks 2 and 5 continuing to have the higher trap location error (i.e. $\varepsilon \leq$ 4.6%) compared with Stacks 1, 4 and 6 (i.e. $\varepsilon \leq$ 2.0%).

These results have demonstrated that the reflected wave technique can be applied for the detection and location of depleted trap seals in multi-single-stack systems, allowing the status of all connected traps (in this case 112 traps) to be determined from one system test using only a single transient entry point and distributed measurement points (i.e. one pressure transducer located at the base of each additional stack.

The *junction effect* was responsible for large trap location errors observed for *Method A* (i.e. $\varepsilon < 33\%$), however, both *Methods B* and *C* were capable of locating the depleted traps with good accuracy ($\varepsilon \leq 6.9\%$ and 4.6%, respectively). These correspond to a maximum trap location estimation error of 2.4 m and 1.6 m, respectively, which would, at the very least, allow the depleted trap to be detected and located to the correct floor on the correct stack. The majority of the results for *Methods B* and *C*, however, show a far better trap location estimation error, with some in the region of 0.1 m.

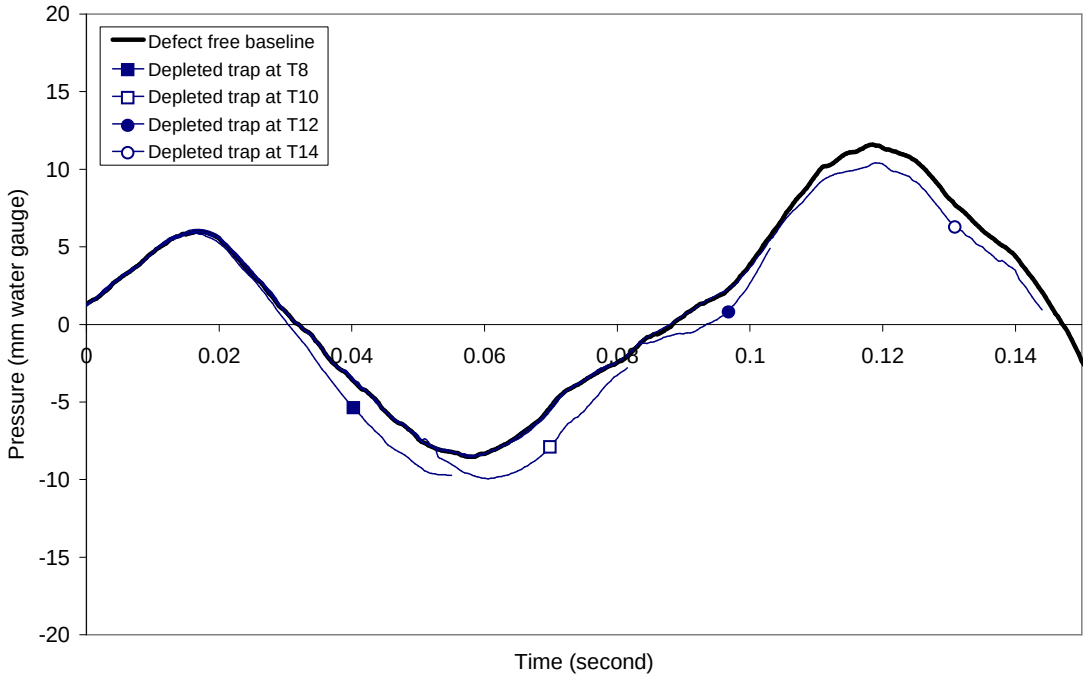

Figure 6.33 Measured system response at VPT2 on Stack 1 showing effect of depleted trap distance for *Configuration VIII* (Transient generated at Stack 3). Note: for clarity each pressure trace has been discontinued shortly after its deviation from the defect free baseline.

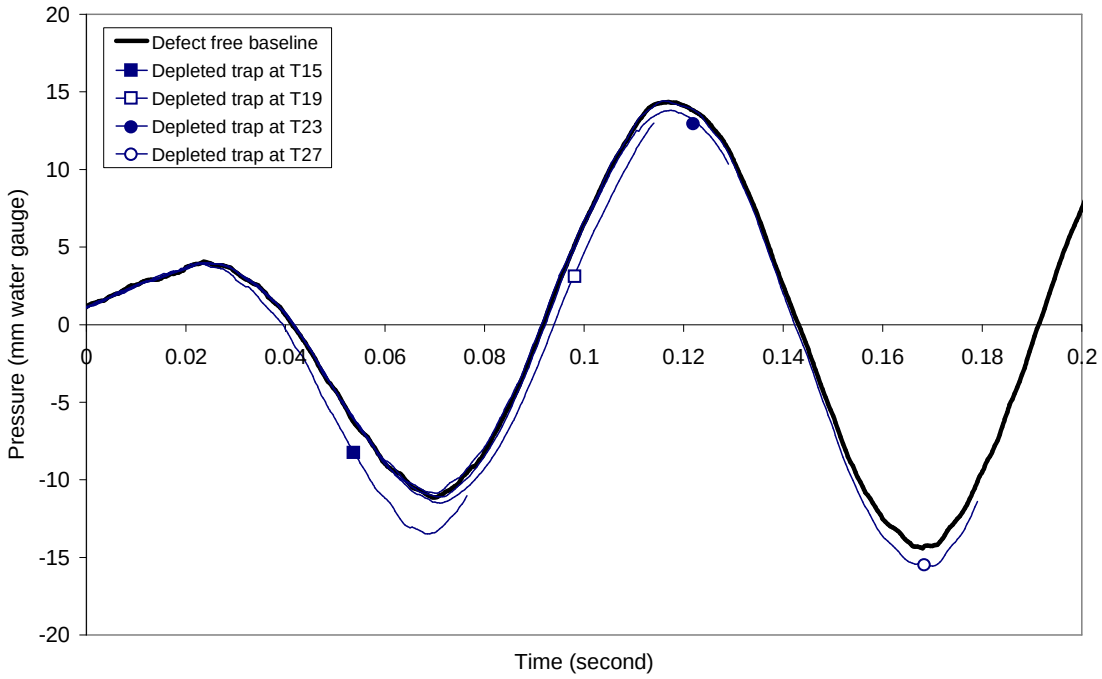

Figure 6.34 Measured system response at VPT2 on Stack 2 showing effect of depleted trap distance for *Configuration VIII* (Transient generated at Stack 3). Note: for clarity each pressure trace has been discontinued shortly after its deviation from the defect free baseline.

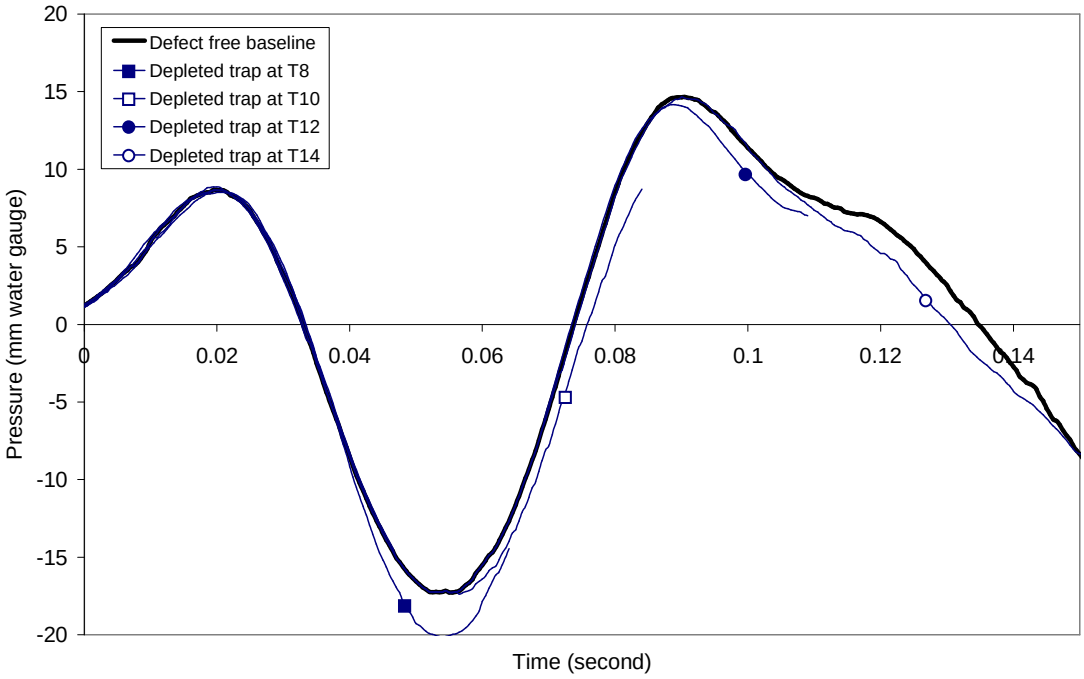

Figure 6.35 Measured system response at VPT2 on Stack 4 showing effect of depleted trap distance for *Configuration VIII* (Transient generated at Stack 3). Note: for clarity each pressure trace has been discontinued shortly after its deviation from the defect free baseline.

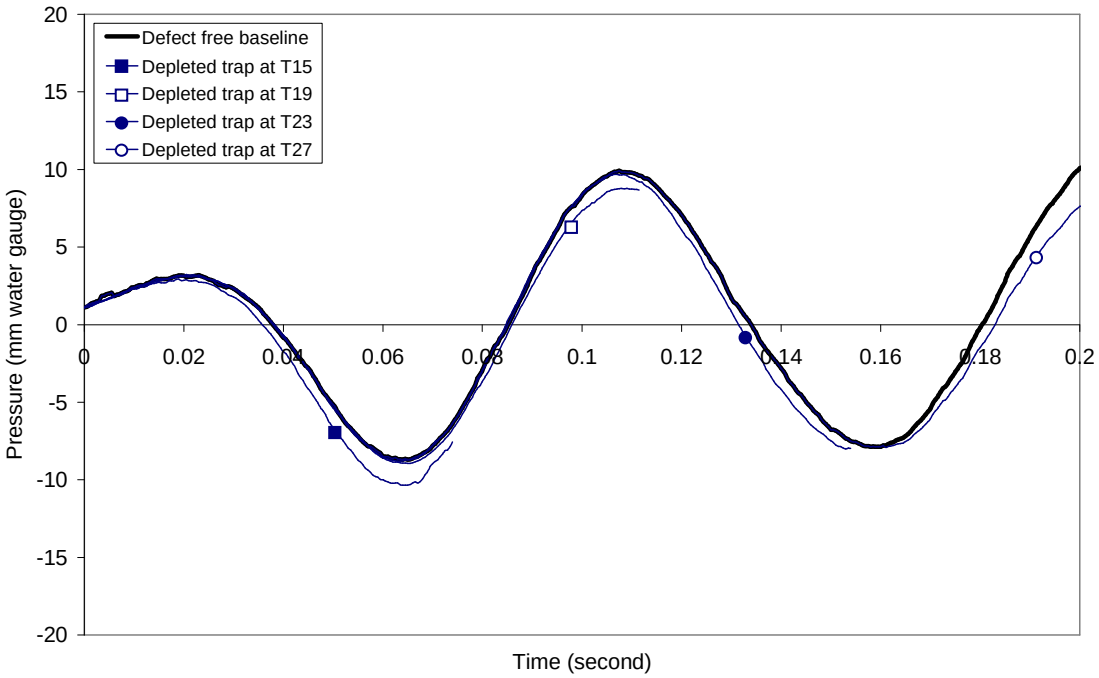

Figure 6.36 Measured system response at VPT2 on Stack 5 showing effect of depleted trap distance for *Configuration VIII* (Transient generated at Stack 3). Note: for clarity each pressure trace has been discontinued shortly after its deviation from the defect free baseline.

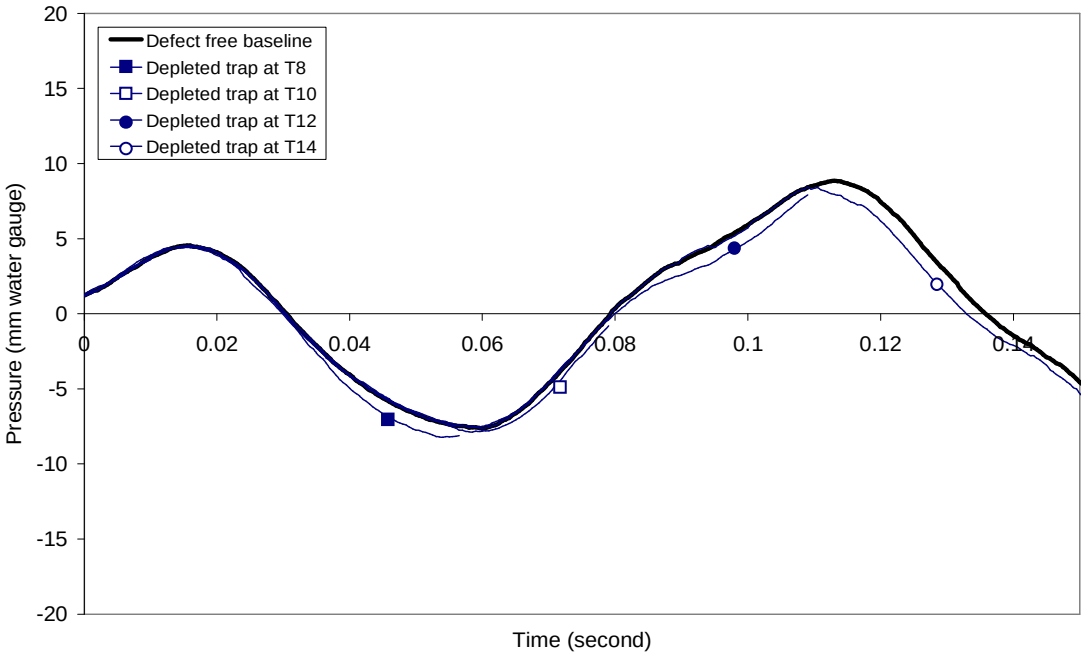

Figure 6.37 Measured system response at VPT2 on Stack 6 showing effect of depleted trap distance for *Configuration VIII* (Transient generated at Stack 3). Note: for clarity each pressure trace has been discontinued shortly after its deviation from the defect free baseline.

Table 6.14 Assessment of the depleted trap location by the reflected wave technique for *Configuration VIII* using data measured at VPT2 (Transient generated at Stack 3)

Measured trap characteristics from system response			**True trap location and pipe period**			**AIRNET simulated trap location and pipe period**			**Probed trap location and pipe period**		
			Method A			***Method B***			***Method C***		
No	$t_D^{measured}$ (s)	$X_D^{measured}$ (m)	t_D^{true} (s)	X_D^{true} (m)	ε_A	t_D^{AIRNET} (s)	X_D^{AIRNET} (m)	ε_B	t_D^{probe} (s)	X_D^{probe} (m)	ε_C
S1/T8	0.0332	**5.7**	0.0245	**4.2**	4.3%	0.0315	5.4	0.9%	0.0327	5.6	0.3%
S1/T10	0.0577	**9.9**	0.0478	**8.2**	4.9%	0.0618	10.6	2.0%	0.0571	9.8	0.3%
S1/T12	0.0898	**15.4**	0.0711	**12.2**	9.1%	0.0915	15.7	0.9%	0.0892	15.3	0.3%
S1/T14	0.1143	**19.6**	0.0945	**16.2**	9.7%	0.1213	20.8	3.4%	0.1137	19.5	0.3%
S2/T15	0.0350	**6.0**	0.0227	**3.9**	6.0%	0.0367	6.3	0.9%	0.0332	5.7	0.9%
S2/T19	0.0764	**13.1**	0.0461	**7.9**	14.9%	0.0805	13.8	2.0%	0.0758	13.0	0.3%
S2/T23	0.1108	**19.0**	0.0694	**11.9**	20.3%	0.1143	19.6	1.7%	0.1137	19.5	1.4%
S2/T27	0.1598	**27.4**	0.0927	**15.9**	32.9%	0.1458	25.0	6.9%	0.1545	26.5	2.6%
S4/T8	0.0303	**5.2**	0.0245	**4.2**	2.9%	0.0315	5.4	0.6%	0.0338	5.8	1.7%
S4/T10	0.0618	**10.6**	0.0478	**8.2**	6.9%	0.0618	10.6	0.0%	0.0577	9.9	2.0%
S4/T12	0.0863	**14.8**	0.0711	**12.2**	7.4%	0.0915	15.7	2.6%	0.0886	15.2	1.1%
S4/T14	0.1125	**19.3**	0.0945	**16.2**	8.9%	0.1213	20.8	4.3%	0.1108	19.0	0.9%
S5/T15	0.0426	**7.3**	0.0227	**3.9**	9.7%	0.0367	6.3	2.9%	0.0332	5.7	4.6%
S5/T19	0.0799	**13.7**	0.0461	**7.9**	16.6%	0.0805	13.8	0.3%	0.0770	13.2	1.4%
S5/T23	0.1201	**20.6**	0.0694	**11.9**	24.9%	0.1143	19.6	2.9%	0.1178	20.2	1.1%
S5/T27	0.1598	**27.4**	0.0927	**15.9**	32.9%	0.1458	25.0	6.9%	0.1551	26.6	2.3%
S6/T8	0.0362	**6.2**	0.0245	**4.2**	5.7%	0.0315	5.4	2.3%	0.0321	5.5	2.0%
S6/T10	0.0641	**11.0**	0.0478	**8.2**	8.0%	0.0618	10.6	1.1%	0.0647	11.1	0.3%
S6/T12	0.0880	**15.1**	0.0711	**12.2**	8.3%	0.0915	15.7	1.7%	0.0857	14.7	1.1%
S6/T14	0.1149	**19.7**	0.0945	**16.2**	10.0%	0.1213	20.8	3.1%	0.1120	19.2	1.4%

When L = 35.0 m (the total stack height)

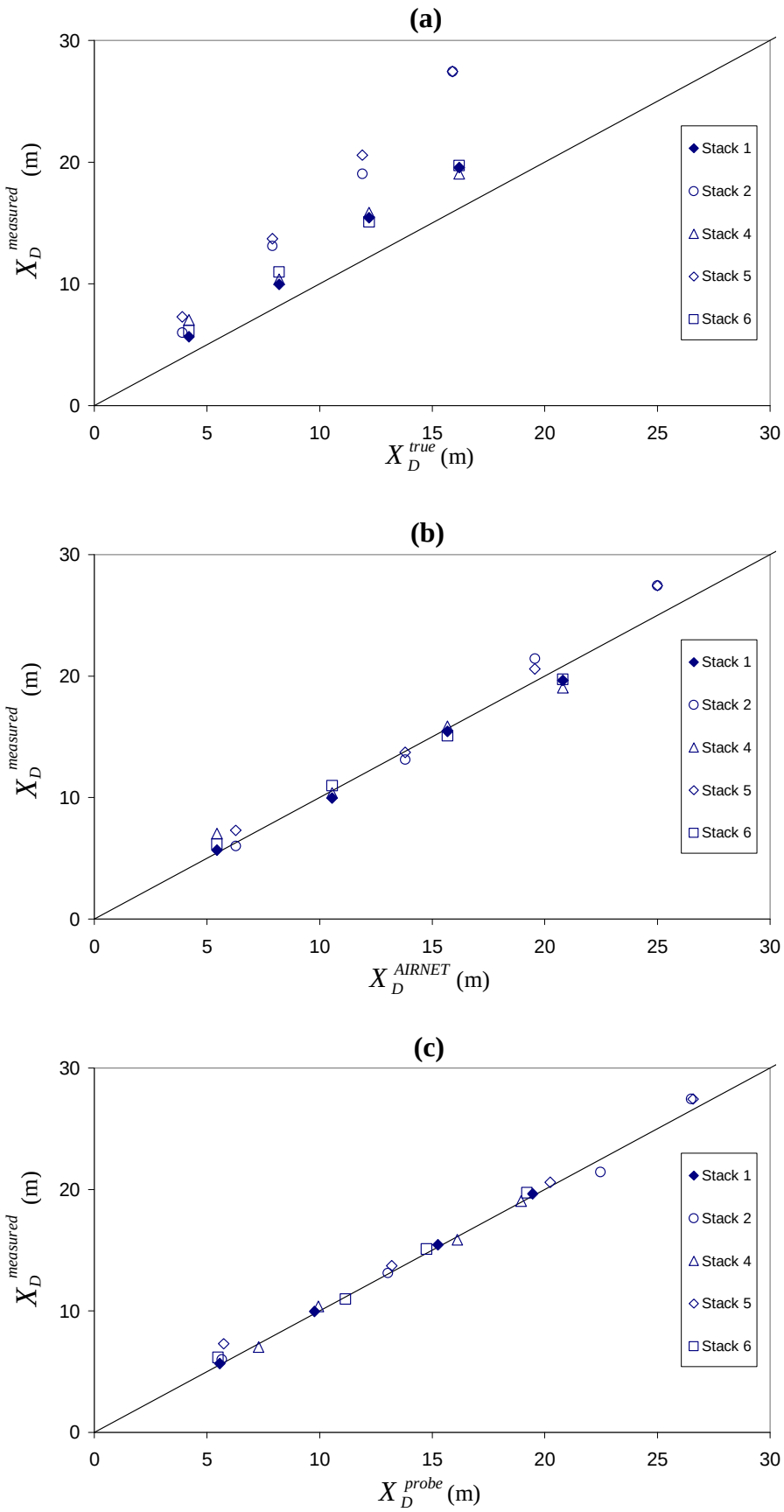

Figure 6.38 Comparison of the measured and predicted depleted trap locations for *Configuration VIII* using data measured at VPT2 on Stack 1, 2, 4, 5 & 6 while the transient was generated at Stack 3 (a) *Method A*; (b) *Method B* and (c) *Method C*

6.8.4 Glasgow multi-stack (field) system – blind test

The tests undertaken prior to the Glasgow installation had concentrated on assessing the accuracy of the reflected wave technique (and the ability of the TRACER program) to detect and locate a depleted trap of known position within the system. In the field, however, the trap position will not previously be known and the reflected wave technique would be relied upon to determine its location.

As a challenge for the reflected wave technique a series of *blind tests* were carried out where, having obtained the defect free baseline and having previously used *Method C* to determine each trap reflection return time, a trap seal was depleted by the project technician at a location within the system which was unknown to the author. The test was then run and the system response measured and analysed by the TRACER program. **Figure 6.39** shows an example of the system response recorded during one of these blind tests.

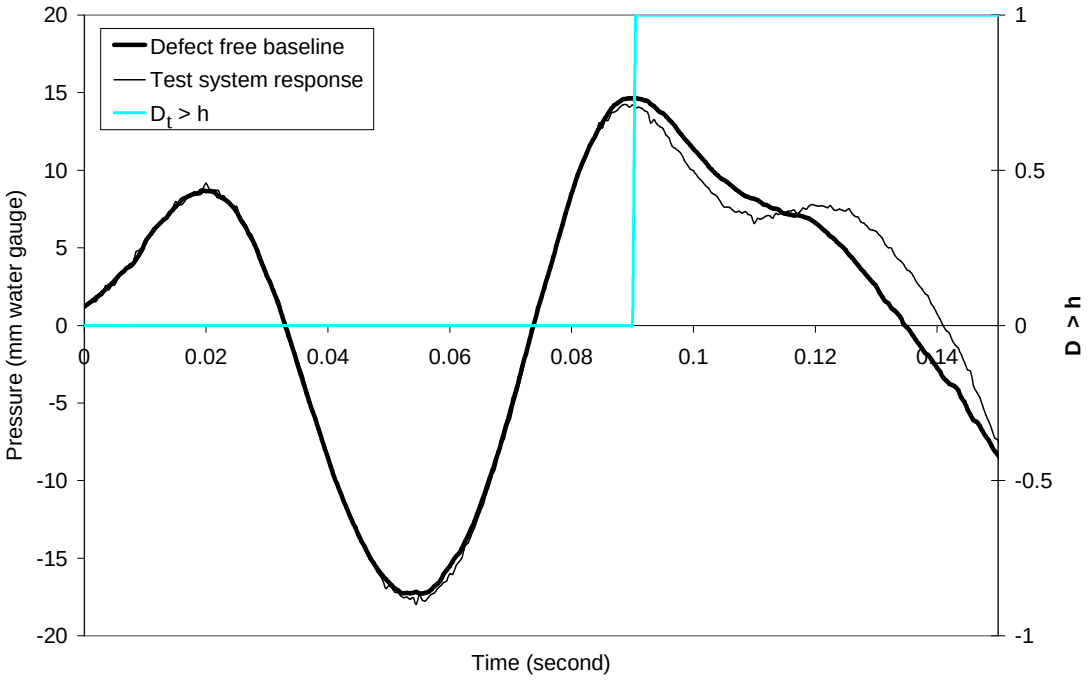

Is $D_t > h$ over calibration period? NO, trace is reliable.
Is $D_t > h$ over test period? YES, t_D = 0.09 seconds.
Depleted trap location? T12 (Stack 4).

Figure 6.39 Result of blind test carried out in the Glasgow multi-stack (*field*) system showing the detection and location of the depleted trap T12 on Stack 4

It can be seen that in this case the TRACER program has identified a change from the defect free baseline which occurs at 0.09 seconds. Automatic cross-reference with the trap reflection return times obtained using *Method C* identify the true trap location of T12 on Stack 4. During a separate series of blind tests, the project technician was again asked to deplete a trap seal at a location unknown to the author. The test was run and the system response measured and analysed by the TRACER program. The first test detected no depleted trap within the system, see **Figure 6.40**. The test was then re-run for a second time and then a third time with no depleted trap being detected during any of the tests. About to concede that this blind test had failed, the project technician announced that he had in fact decided, as an extra challenge, not to deplete any trap seal during this test. Despite the best efforts of the author to detect a depleted trap which he had mistakenly believed to be present within the system, the reflected wave technique continually confirmed that the system was defect free. This result gave further confidence in the reliability of this technique.

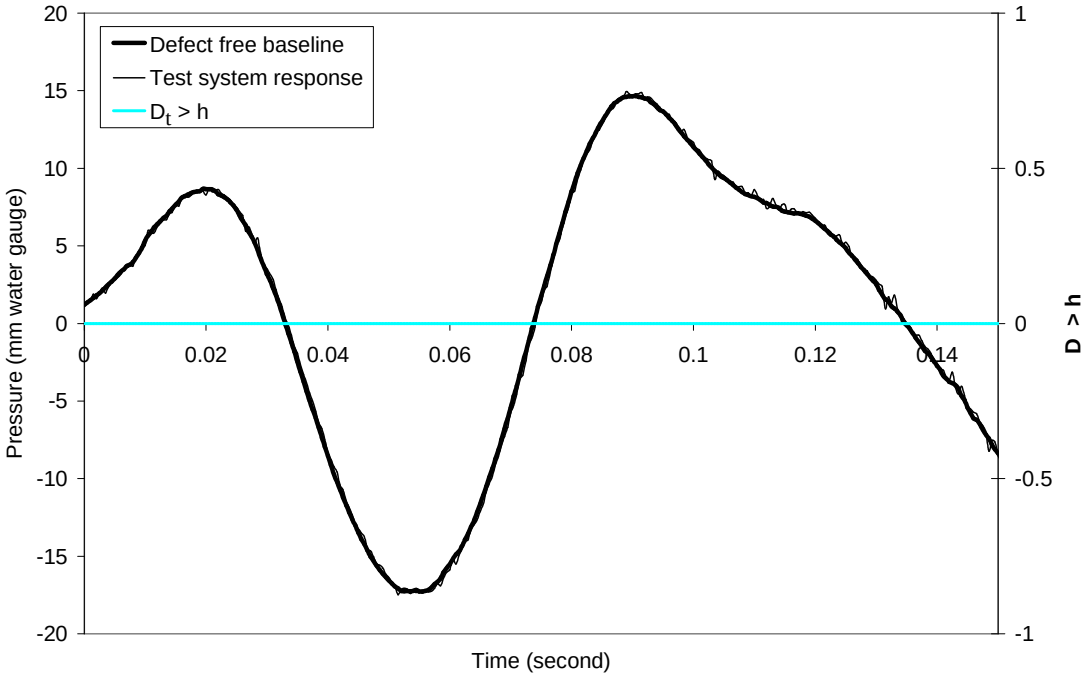

Is $D_t > h$ over calibration period? NO, trace is reliable.
Is $D_t > h$ over test period? NO, system is defect free.

Figure 6.40 Result of blind test carried out in the Glasgow multi-stack (*field*) system showing the system to be defect free

6.8.5 Summary

The data collected during the Glasgow (*field*) system trials have not only allowed the reflected wave technique to be trialled and tested within a fully operational building which was not under the direct control of the investigators, but also allowed the performance of the technique to be investigated for systems consisting of differing junction configurations, and allowed the operating range of the technique to be tested.

Analysis of the measured system response data, using Method *A*, has shown that the resultant trap location error is considerably higher in the data collected from the wc stacks (Stacks 2 and 5) than that collected from the wash-hand-basin stacks (Stacks 1, 3, 4 and 6). This difference has been attributed to the different branch to stack area ratios present in each of the two stacks and the different dampening effect that each junction type has on the waveform of the transient leading edge which, in turn, is dependant upon their respective reflection and transmission coefficients.

As the largest system tested during these investigations, the Glasgow (*field*) system has demonstrated that the reflected wave technique is effective in detecting and locating depleted trap seals in large multi-stack systems. A total of 6 single-stacks (including a total of 112 connected appliances) have been successfully monitored using the reflected wave technique giving scope for its application in large complex buildings.

A series of blind tests have shown that the reflected wave technique successfully identifies the correct location of a depleted trap of an unknown location within the system. It has been demonstrated that the reflected wave technique can be relied upon to confirm the correct system condition, even if the system is defect free.

6.9 System boundary effects on the measured system response

This section evaluates the influence that different system boundaries have on the propagation of the incident transient wave and, in turn, on the measured system response. Successful application of the reflected wave technique requires a clear understanding of the effect of system boundaries to enable an accurate interpretation of the important information contained within the system response. This will become particularly important when system modifications are performed (which may include the addition or removal of appliances, or the inclusion of pressure control devices) which will alter the defect free baseline.

Experimental and numerical studies were carried out to identify the effects of three system boundaries which are common to building drainage systems: branch/trap diameter, air admittance valves (AAVs), and positive air pressure attenuators (PAPAs). Attention is given to how these boundaries alter the defect free baseline and whether they can affect the successful application of the reflected wave technique. To aid analysis the system configurations details previously in Chapter 5 have been repeated here in **Figure 6.41**.

6.9.1 The effect of branch/trap diameter

Using the HWU 2 (*laboratory*) system, *Configuration IX(a-f)* (**Figure 6.41**), data was collected to evaluate the effect that the addition of a single side branch would have on the measured system response. The inclusion of a side branch creates a 3-pipe junction within the stack. Different branch diameters, common to the building drainage system (i.e. 32 mm, 40 mm, 50 mm, 75 mm and 100 mm), were tested. Each branch was terminated with a trap of the same diameter. Tests were carried out first using a fully primed trap (so that the effect of the junction geometry could be analysed) and then by using a depleted trap (so that the effect of the depleted trap diameter could be analysed).

6.9.1.1 Side branch terminated with a fully primed trap

Figure 6.42 shows the effect that the new junction has on the measured pressure response when compared with the pressure response without any side branch (stack only). It can be seen that a reflection is generated by the junction, in response to the applied pressure transient. The magnitude of the reflection increases as the diameter of the side branch increases (relative to the branch to the stack area ratio, A_{branch}/A_{stack}). A similar relationship can be seen in **Figure 6.43** which shows the simulated pressure response modelled using AIRNET.

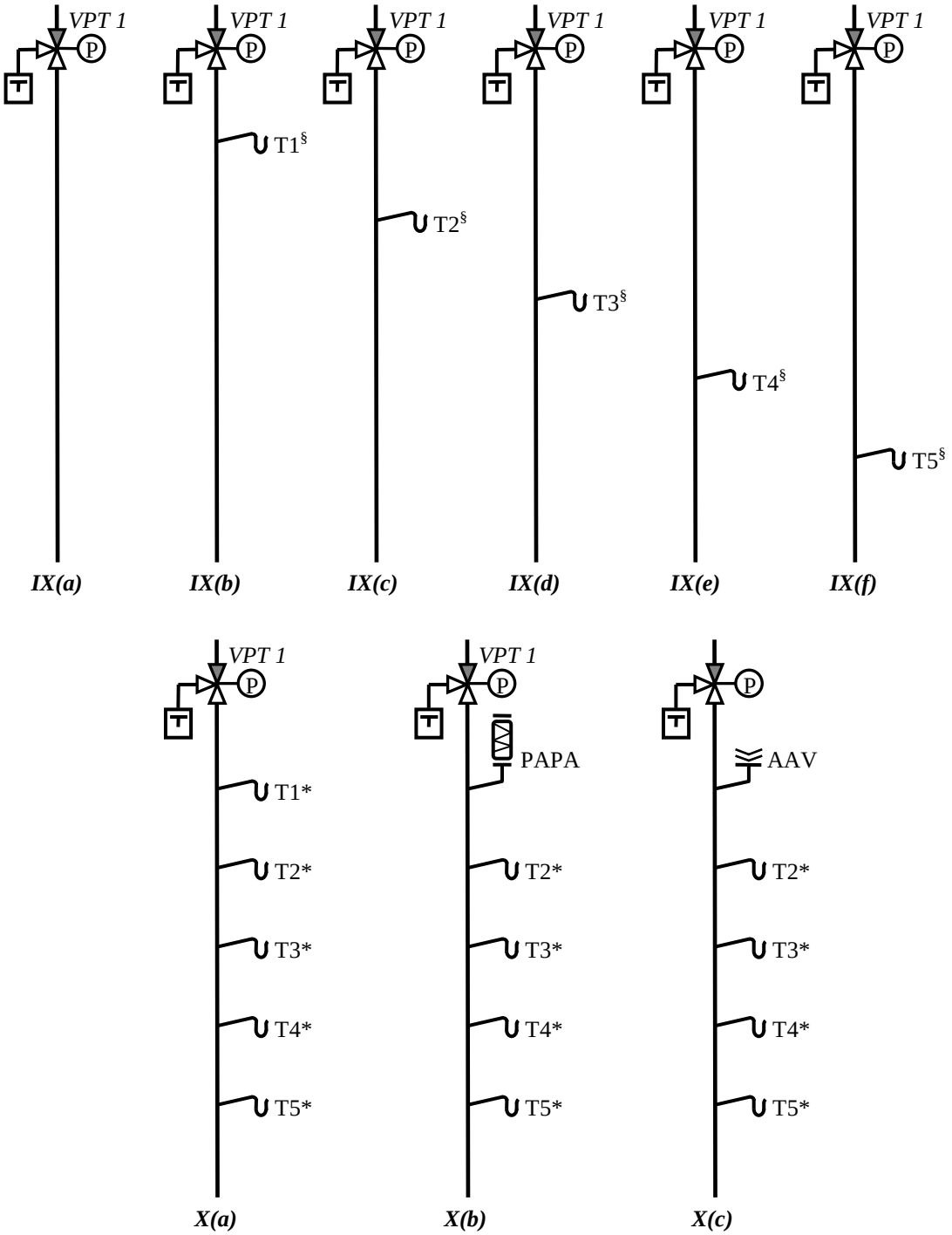

Notes
1. All pipes are uPVC.
2. The stacks are 100 mm diameter.
3. All branches are 1.2 m long and are spaced at 3.2 m centers
4. § branch/trap diameters of 32 mm, 40 mm, 50 mm, 75 mm and 100 mm investigated at each location.
5. * branch/trap diameter of 100 mm.

Figure 6.41 The HWU 2 (*laboratory*) system showing each configuration tested. Shown previously in Figure 5.40 but repeated here for convenience.

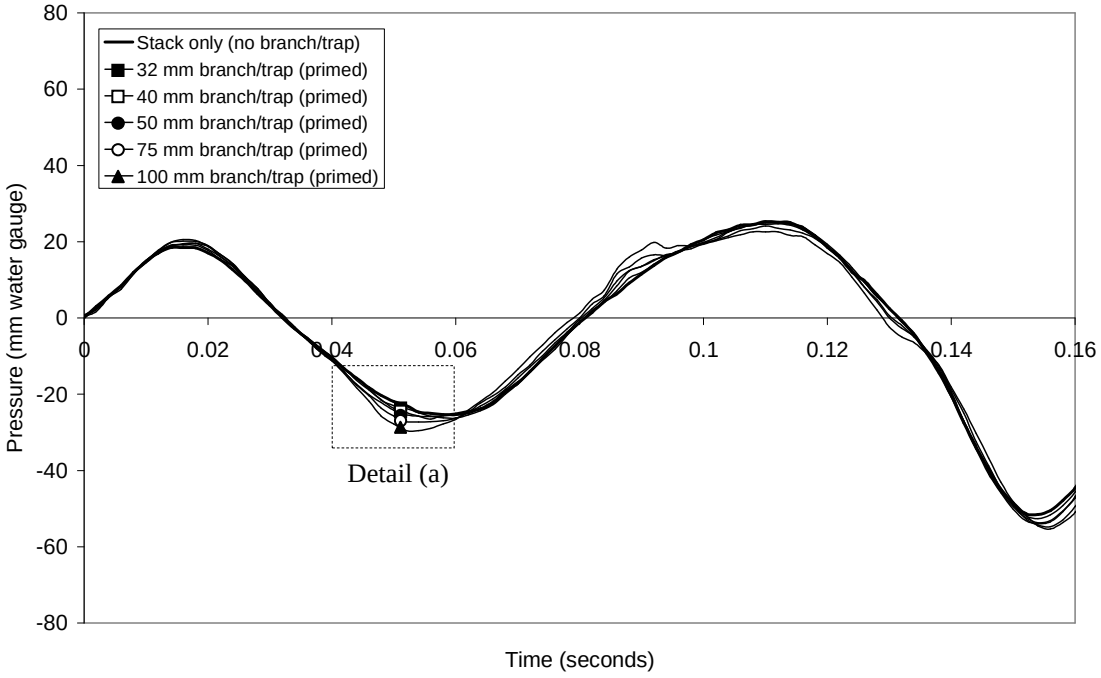

Detail (a)

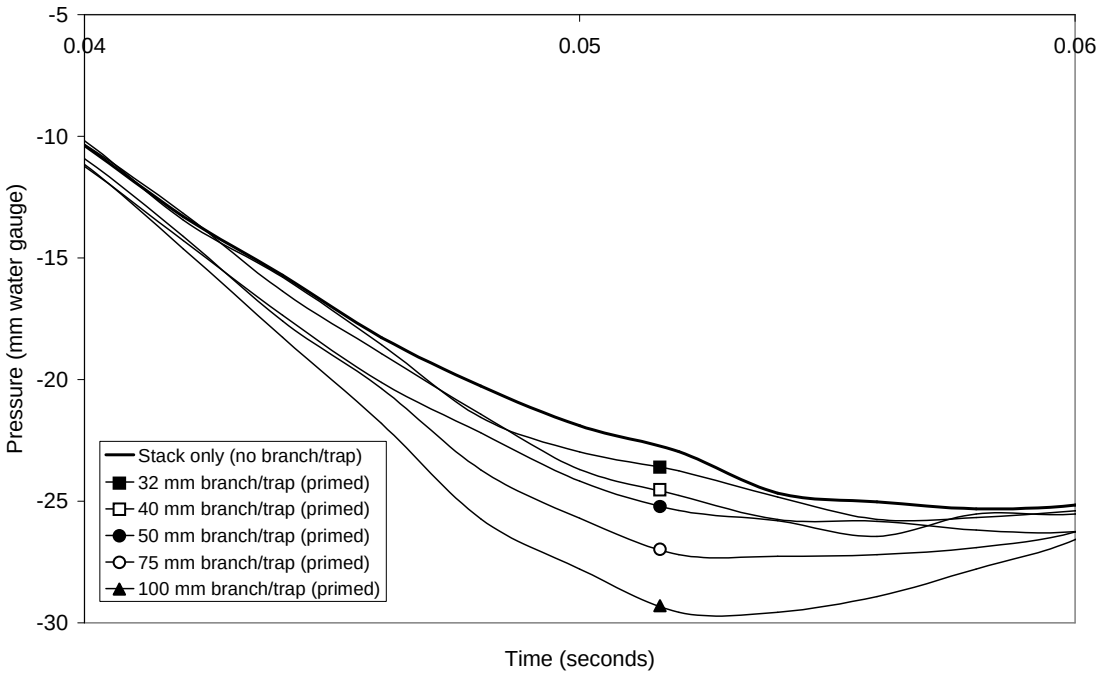

Figure 6.42 Comparison of the measured system response at VPT1 on *Configuration IX(a-f)* for a new junction at T1 showing the effect of side branch diameter

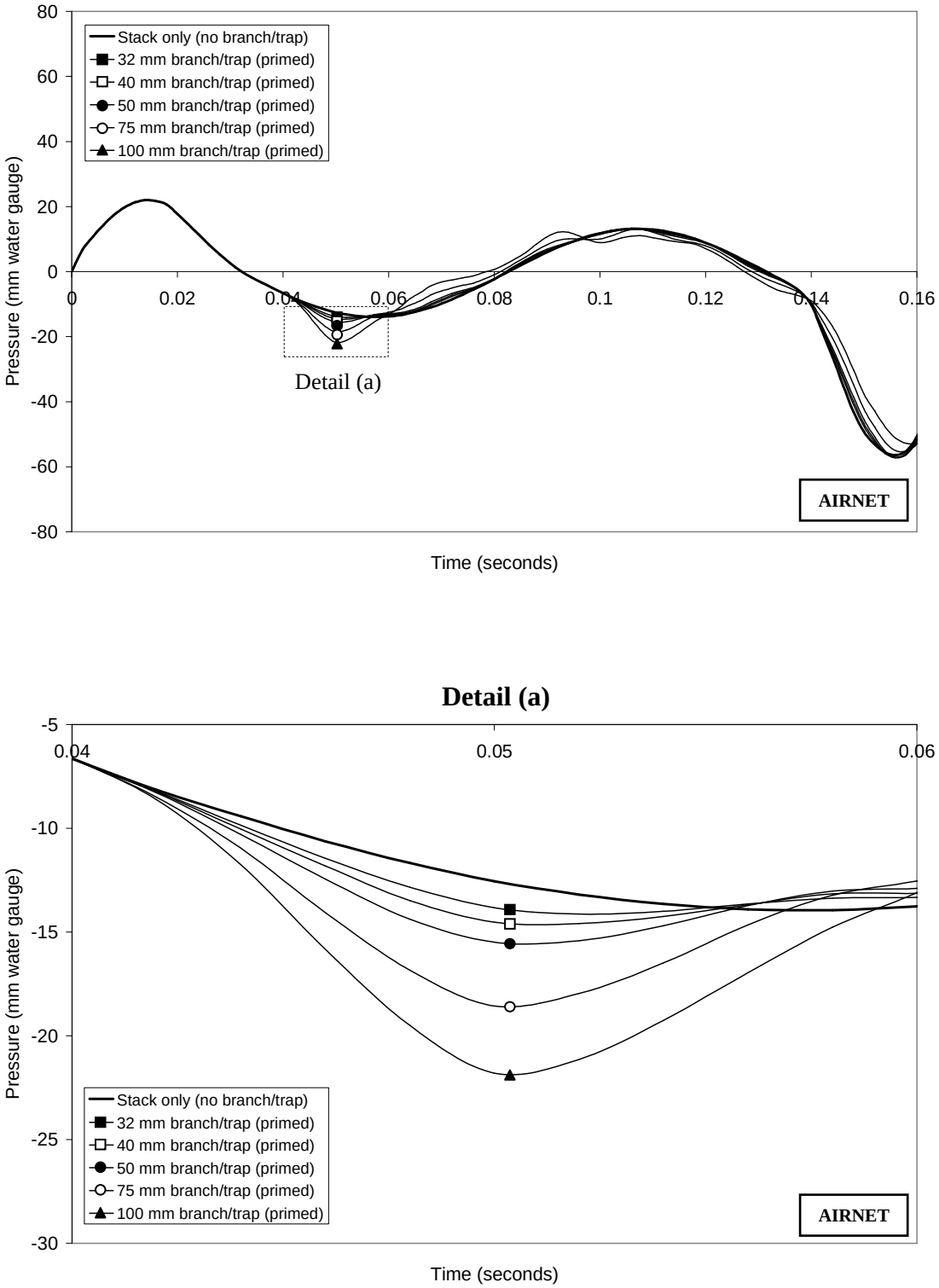

Figure 6.43 Comparison of the system response of *Configuration IX(a-f)* simulated using AIRNET for a new junction at T1 showing the effect of side branch diameter

Equations (2.12) and (2.13) define the reflection $C_R^{junction}$ and transmission $C_T^{junction}$ coefficients, respectively, for a junction, allowing the magnitude of both the reflected wave, Δp_R, and transmitted wave, Δp_T, to be determined for any number and diameter of connecting pipes, when the magnitude of the incident wave, Δp_I, is known.

The reflection coefficient can also be defined as the ratio of the reflected wave, Δp_R, to the incident wave, Δp_I:

$$C_R^{junction} = \frac{\Delta p_R}{\Delta p_I} \tag{6.2}$$

and as $|\Delta p_I| = |\Delta p_T| + |\Delta p_R|$ this yields:

$$\left|C_T^{junction}\right| = 1 - \left|C_R^{junction}\right| \tag{6.3}$$

Table 6.15 and **Figure 6.44** compare the reflection and transmission coefficients calculated theoretically from Equations (2.12) and (2.13) with those calculated from the experimental data (i.e. $C_{R(EXP)}^{junction}$ and $C_{T(EXP)}^{junction}$, respectively) and the simulated data (i.e. $C_{R(AIRNET)}^{junction}$ and $C_{T(AIRNET)}^{junction}$, respectively) using Equations (6.2) and (6.3).

As branch to stack area ratio increases (i.e. as the branch diameter increases in relation to the stack diameter) $C_R^{junction}$ can be seen to increase with a corresponding decrease of $C_T^{junction}$. This is observed in both the experimental and simulated data, both of which correspond well with the theoretical values.

As confirmed by Wood and Chao (1971), the commonly used relationships for transmission and reflection characteristics of pressure waves at pipe junctions (Equations (2.12) and (2.13)) which neglect pipe orientation and concentrated losses at the junction and which are primarily based on area ratios of the connected pipes are adequate for describing air pressure propagation at system junctions.

Table 6.15 Validation of Equations (2.12) and (2.13) using experimental and simulated data

Ø	$C_R^{junction}$	$C_T^{junction}$	Δp_I^{EXP}	Δp_R^{EXP}	$C_{R(EXP)}^{junction}$	$C_{T(EXP)}^{junction}$	Δp_I^{AIRNET}	Δp_R^{AIRNET}	$C_{R(AIRNET)}^{junction}$	$C_{T(AIRNET)}^{junction}$
(mm)	Eqn. (2.12)	Eqn. (2.13)	(mm wg)	(mm wg)	Eqn. (6.2)	Eqn. (6.3)	(mm wg)	(mm wg)	Eqn. (6.2)	Eqn. (6.3)
32	**0.05**	**0.95**	19.978	1.292	**0.06**	**0.94**	23.980	1.280	**0.05**	**0.95**
40	**0.07**	**0.93**	19.978	1.786	**0.09**	**0.91**	23.980	1.970	**0.08**	**0.92**
50	**0.11**	**0.89**	19.978	2.418	**0.12**	**0.88**	23.980	2.940	**0.12**	**0.88**
75	**0.22**	**0.78**	19.978	4.230	**0.21**	**0.79**	23.980	5.567	**0.23**	**0.77**
100	**0.33**	**0.67**	19.978	6.595	**0.33**	**0.67**	23.980	8.345	**0.35**	**0.65**

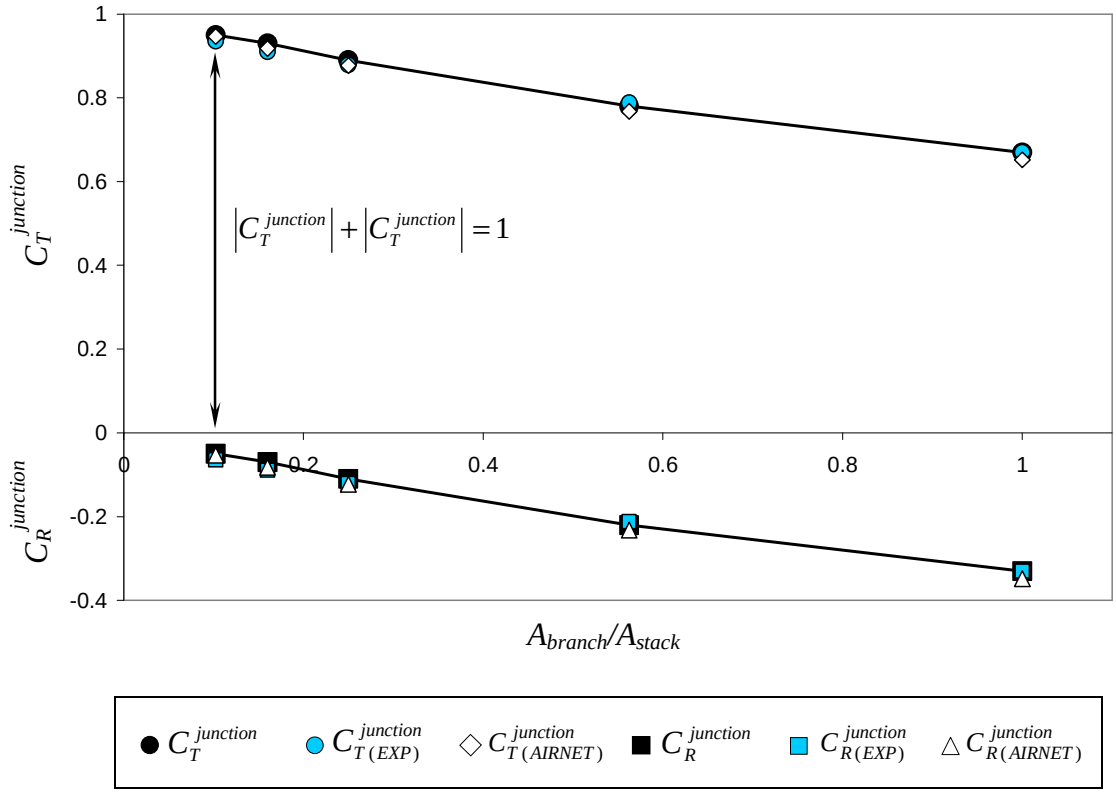

Figure 6.44 Validation of Equations (2.12) and (2.13) using experimental and simulated data showing influence of branch to stack area ratio on the transmission and reflection coefficients at a three-pipe junction

6.9.1.2 Side branch terminated with a depleted trap

System junctions alter the propagating pressure transient and, therefore, the consequent measured system response due to the transmission and reflection process which takes place. When preceded by a junction, the reflection returned by a depleted trap is dependant upon the reflection and transmission coefficients at that junction, as these decide not only what proportion of the incident wave arrives at that trap, but also what proportion is consequently returned back to the measurement point.

Figure 6.45 compares the measured system response for *Configuration IX(a & b)* (**Figure 6.41**) with a depleted trap at T1 for each side branch diameter. The trap induced reflection shows a very clear decrease with decreasing side branch diameter (i.e. the smallest trap induced reflection is generated by the 32 mm trap, while the largest is generated by the 100 mm trap).

A similar relationship can be seen in **Figure 6.46** which shows the simulated pressure response modelled using AIRNET. The reason the smallest diameter trap generates the smallest reflection, despite receiving the largest proportion of the transmitted incident wave at the junction (Equations (2.12) and (2.13)), can be explained by the following example.

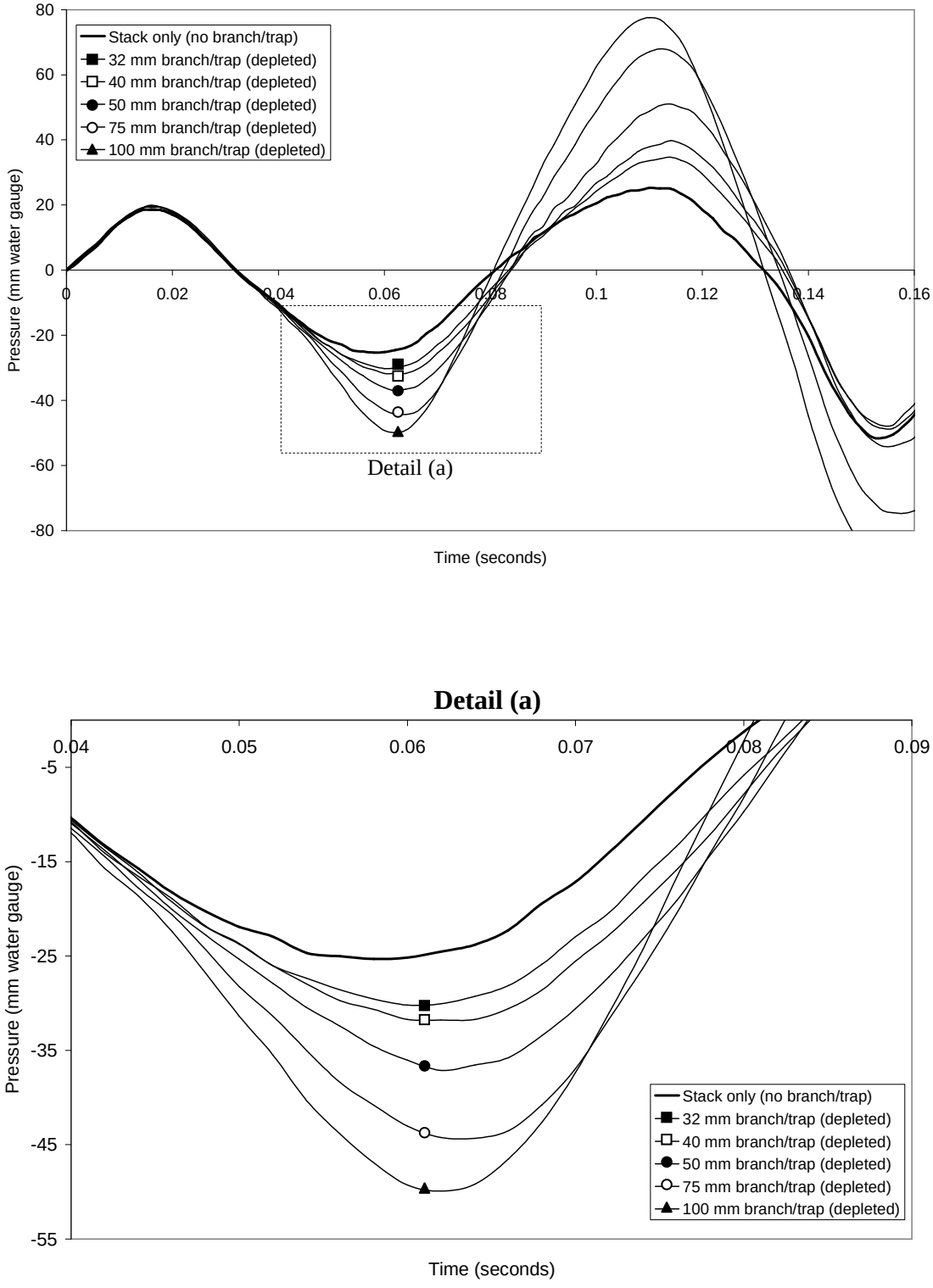

Figure 6.45 Comparison of the measured system response at VPT1 on *Configuration IX(a-f)* for a depleted trap at T1 showing the effect of trap diameter

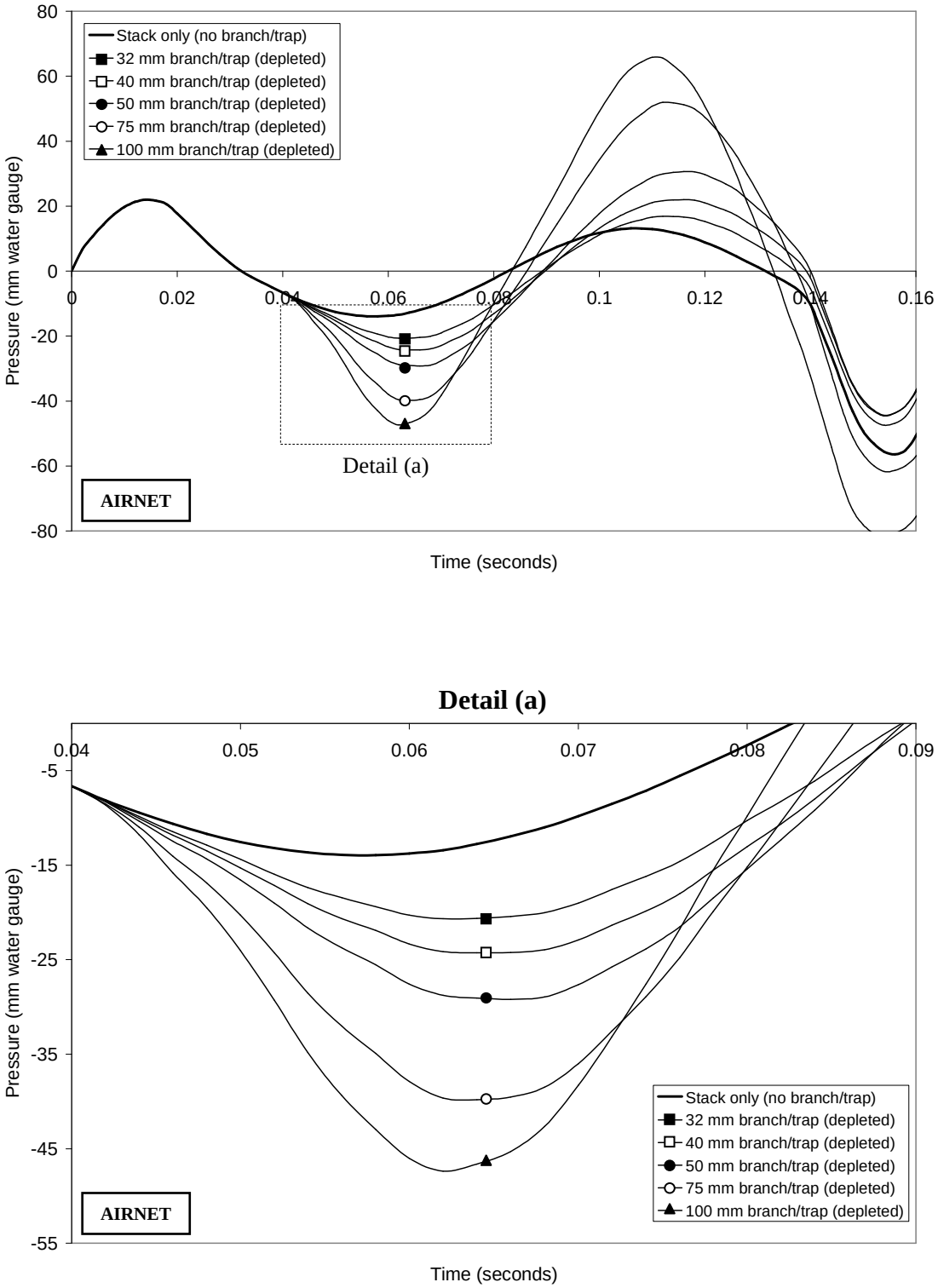

Figure 6.46 Comparison of the system response of *Configuration IX(a-f)* simulated using AIRNET for a depleted trap at T1 showing the effect of trap diameter

Consider a junction created by a 100 mm stack and a 32 mm side branch. If the propagation of the transient towards the trap is described as *Stage A*, and the return of the reflected transient away from the trap is *Stage B*, **Figure 6.47**, and by using Equations (2.12) and (2.13) to predict the reflection and transmission coefficients respectively, it is apparent that, during *Stage A*, on approaching the junction from pipe 1 (the index pipe), 95% of the incident transient is transmitted into pipes 2 and 3 (the receiving pipes), while only 5% is reflected back along pipe 1 ($C_{R(A)}^{junction}$ = -0.05 and $C_{T(A)}^{junction}$ = +0.95). During *Stage B*, however, pipe 3 becomes the index pipe and pipes 1 and 2 the receiving pipes. Therefore, only 10% of the trap induced reflection (now only 95% of the incident wave) is transmitted into pipes 1 and 2, while the remaining 90% is reflected back along pipe 3 ($C_{R(B)}^{junction}$ = -0.9 and $C_{T(B)}^{junction}$ = +0.1). The re-reflected transient (now only 95% x 90% = 86% of the original incident wave) travels back towards the depleted trap for a second time where it is again reflected. This process continues, with the transient propagating back and forth within pipe 3 (each time reducing by 10% as part is transmitted into pipes 1 and 2), having been *trapped* within the branch, until it completely dissipates. Conversely, a junction created by identical pipes (i.e. all 100 mm diameter) permits, during *Stage A*, 67% of the incident transient wave to be transmitted into pipes 2 and 3, while 33% is reflected back along pipe 1 ($C_{R(A)}^{junction}$ = -0.33 and $C_{T(A)}^{junction}$ = +0.67). During Stage B 67% of the trap induced reflection (now only 67% of the incident wave) is transmitted into pipes 1 and 2, while the remaining 33% is reflected back along pipe 3. The transient again propagates back and forth within pipe 3, each time reducing by 33% as part is transmitted into pipes 1 and 2, until it completely dissipates.

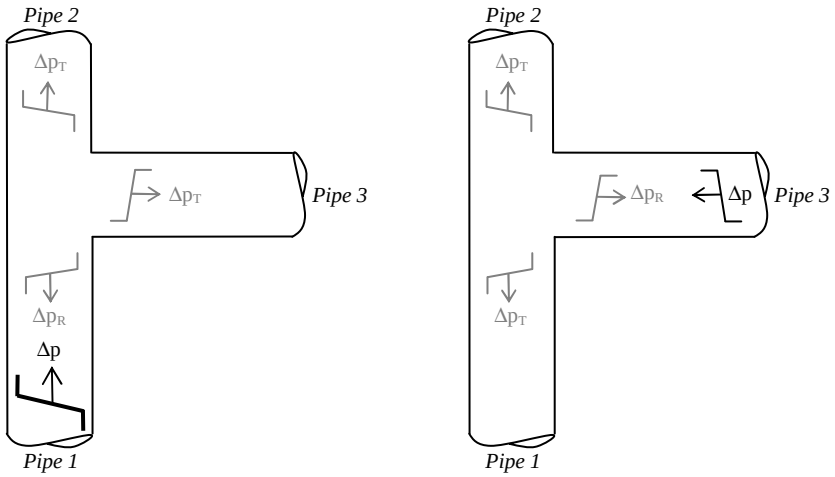

Figure 6.47 Stage A and Stage B of the transient reflection at a junction

So, even though the 32 mm trap receives a larger proportion of the incident wave than any other trap (i.e. $C_{T(A)}^{junction}$ = 95%) this does not lead to a correspondingly large trap induced measured reflection as only a small proportion of this reflected wave is initially transmitted back through the junction towards the measurement point (i.e. $C_{T(B)}^{junction}$ = 10%). On the other hand, the 100 mm trap, which receives the smallest proportion of the incident wave (i.e. $C_{T(A)}^{junction}$ = 66%) generates the largest trap induced reflection as a larger proportion is initially transmitted back through the junction towards the measurement point (i.e. $C_{T(B)}^{junction}$ = 66%). The magnitude of the trap induced reflection initially transmitted back towards the measurement point can be determined by combining $C_{T(A)}^{junction}$ and $C_{T(B)}^{junction}$ such that:

$$C_{T(A+B)}^{junction} = C_{T(A)}^{junction} \times C_{T(B)}^{junction}$$

when $C_{T(A+B)}^{junction}$ is the combined transmission coefficient. **Table 6.16** presents the combined transmission coefficients for each side branch diameter combination.

Table 6.16 The resultant combined transmission coefficient for a pressure transient propagating a junction during both *Stage A* and *Stage B*

$Ø_{Stack}$ (mm)	$Ø_{Branch}$ (mm)	A_{branch}/A_{stack}	$C_{T(A)}^{junction}$	$C_{T(B)}^{junction}$	$C_{T(A+B)}^{junction}$
100	32	0.10	**0.95**	**0.10**	**0.095**
100	40	0.16	**0.93**	**0.15**	**0.140**
100	50	0.25	**0.89**	**0.22**	**0.196**
100	75	0.56	**0.78**	**0.44**	**0.343**
100	100	1.00	**0.67**	**0.67**	**0.449**

6.9.1.3 Effect of branch/trap diameter on reflected wave technique accuracy

To assess if the diameter of the side branch/trap had an effect on the accuracy of the reflected wave technique the data gathered during the HWU 2 (*laboratory*) system tests, *Configuration IX(a-f)* (**Figure 6.41**) were analysed using the TRACER program to determine the return time of the trap induced reflection. A comparison of the true and measured trap locations was conducted using *Method A* as this allowed the effect of side branch/trap diameter to be easily identified. **Table 6.17** compares the results of the selected side branch diameters (i.e. 32 mm, 40 mm, 50 mm, 75 mm and 100 mm) for five branch locations (i.e. trap T1 to T5).

Table 6.17 Assessment of the side branch/trap diameter on the accuracy of the reflected wave technique using *Configuration IX(a-f)*

Measured trap characteristics from system response				**True trap location and pipe period** Method A		
Trap No. /diameter	A_{branch}/A_{stack}	$t_D^{measured}$ (s)	$X_D^{measured}$ (m)	t_D^{true} (s)	X_D^{true} (m)	ε_A
T1/32	0.1	0.0520	**8.92**	0.0468	**8.03**	3.8%
T1/40	0.2	0.0500	**8.58**			2.3%
T1/50	0.3	0.0500	**8.58**			2.3%
T1/75	0.6	0.0480	**8.23**			0.8%
T1/100	1.0	0.0480	**8.23**			0.8%
T2/32	0.1	0.0720	**12.35**	0.0657	**11.26**	4.6%
T2/40	0.2	0.0720	**12.35**			4.6%
T2/50	0.3	0.0700	**12.01**			3.2%
T2/75	0.6	0.0680	**11.66**			1.7%
T2/100	1.0	0.0680	**11.66**			1.7%
T3/32	0.1	0.0900	**15.44**	0.0845	**14.49**	4.0%
T3/40	0.2	0.0900	**15.44**			4.0%
T3/50	0.3	0.0880	**15.09**			2.5%
T3/75	0.6	0.0880	**15.09**			2.5%
T3/100	1.0	0.0880	**15.09**			2.5%
T4/32	0.1	0.1100	**18.87**	0.1033	**17.72**	4.9%
T4/40	0.2	0.1080	**18.52**			3.4%
T4/50	0.3	0.1080	**18.52**			3.4%
T4/75	0.6	0.1060	**18.18**			1.9%
T4/100	1.0	0.1060	**18.18**			1.9%
T5/32	0.1	0.1280	**21.95**	0.1222	**20.95**	4.2%
T5/40	0.2	0.1280	**21.95**			4.2%
T5/50	0.3	0.1280	**21.95**			4.2%
T5/75	0.6	0.1260	**21.61**			2.8%
T5/100	1.0	0.1260	**21.61**			2.8%

$$\varepsilon_A = \frac{\left| X_D^{measured} - X_D^{true} \right|}{L}$$

When L = 23.6 m (the total stack height)

The trap can be seen to be more easily detected when it has a larger diameter. In each case, the trap location error for the 32 mm diameter trap (i.e. ε = 3.8% to 4.9%) is higher than that measured for the 100 mm diameter trap (i.e. ε = 0.8% to 2.8%) which equates, in some instances, to a difference of 3% (or a trap location estimation error of 0.69 m). This is consistent with the earlier observation in Section 6.9.1.2 which showed that the larger the branch to stack area ratio (i.e. the larger the branch diameter in relation to the stack diameter) the larger the returned trap induced reflection. Thus, the larger the returned reflection, the easier its time of arrival can be determined as the reflection is shaper and clearer, therefore, improving the trap location error.

6.9.2 The effect of a PAPA installed within the system

Using the HWU 2 (*laboratory*) system, *Configurations X(a)* and *X(b)* (**Figure 6.41**), data was collected to evaluate the effect that the installation of a PAPA would have on the measured system response and whether the inclusion of such a device would have any impact on the accuracy of the reflected wave technique. Designed to alleviate positive air pressure transients, the PAPA provides pressure transient control by providing an extra control volume to which the transient airflow can be diverted under positive pressure conditions. The diverted airflow is absorbed by the flexible bag within the PAPA which reduces the rate of change of the flow velocity (one of the fundamental objectives of transient control) while allowing the flow to be maintained, thereby providing flow deceleration and avoiding propagation of large pressure transients. Until the accumulated air inflow reaches the capacity of the flexible bag, the transient is discharged to a constant pressure zone.

First, to provide a point of comparison, the system response was measured for each depleted trap (i.e. trap T1 to T5) for the system with no PAPA installed (*Configuration X(a)* in **Figure 6.41**). As expected, the measured system response, **Figure 6.48(a)**, confirms the presence of each depleted trap by the induced reflection which alters the system response from the defect free baseline at a time specific to the location of each trap within the system. A PAPA was then installed at T1, replacing the trap at this location (*Configuration X(b)* in **Figure 6.41**). The PAPA can be seen to induce a reflection similar to that generated by the depleted trap at T1 when no PAPA was installed, **Figure 6.46(b)**. The reflection return time can be seen to be identical for both the PAPA and the depleted trap. The only difference is that the reflection generated by the PAPA is of slightly lower magnitude than that generated by the depleted trap.

Depleted traps were then introduced at traps T2 to T5 while the PAPA was installed at T1, **Figure 6.48(c)**. The defect free baseline was replaced by the pressure response of the defect free system with the PAPA at T1 from **Figure 6.48(b)**. This ensures that the effect of the boundary condition created by the PAPA is incorporated into the defect free baseline which, as the reflected wave technique detects and locates depleted traps by searching for a change to the system boundary condition, prevents the PAPA being mistaken for a depleted trap. In each case, the magnitude of the induced reflection is now considerably smaller than that observed when no PAPA was installed, compare **Figure 6.48(a)** and **Figure 6.48(c)**.

The reducing effect that the PAPA has on the magnitude of the reflection induced by the depleted traps - although problematic in regard to the success of the reflected wave technique - is testimony to the effective operation of this pressure control device. Displaying similar reflective characteristics as an open ended pipe, the PAPA effectively allows the airflow to leave the stack under positive pressure conditions (only returning to the stack once a negative pressure regime is established), thus attenuating this portion of the diverted transient and removing it from the final system response. The magnitude of the returning reflection is, therefore, reduced by the proportion of the transient which is *lost* to the PAPA during both the outward and returning propagation. As the junction to the PAPA consists of three identical pipes, from Equation (2.13), two thirds of the transient is lost in this way (i.e. $C_T^{junction} = +0.67$).

The tests were simulated using the AIRNET program. Again, for comparison, the system was first simulated without the PAPA installed, **Figure 6.49(a)**. The simulated data matches closely with that derived from the real system, **Figure 6.48(a). Figure 6.49(b)** compares the simulated defect free baseline for both the system with and without the PAPA installed together with the system response for a depleted trap at T1 without the PAPA installed. As observed from the real system data, **Figure 6.48 (b)**, the PAPA induces a negative reflection in the defect free baseline. However, the simulation shows this reflection to match exactly that generated by the depleted trap at T1 when no PAPA was installed. This discrepancy between the real system data and the simulated data suggests the assumption that the pressure within the PAPA matches atmospheric pressure (Swaffield *et al.* 2005) which effectively provides similar conditions at the PAPA as at a depleted trap (or open end), as discussed in Section 3.6.6.2, was overly simplistic and that, in fact, the pressure within the PAPA is slightly higher than atmospheric pressure. It is outwith the scope of this work to establish a more accurate description of the boundary condition of the PAPA. In any case, for the purposes of this investigation, the assumption that the pressure within the flexible bag matches atmospheric pressure is a good approximation.

Figure 6.49(c) shows the simulated pressure response for depleted traps at T2 to T5 while the PAPA was installed at T1. Again, the defect free baseline was replaced by the pressure response of the defect free system with the PAPA at T1 from **Figure 6.49(b)**. Comparing **Figure 6.49(c)** with **Figure 6.48(c)** it can be seen that the simulated data correlates well with the real system data, showing the same reduction in the magnitude of the depleted trap induced reflection due to the PAPA installed at T1.

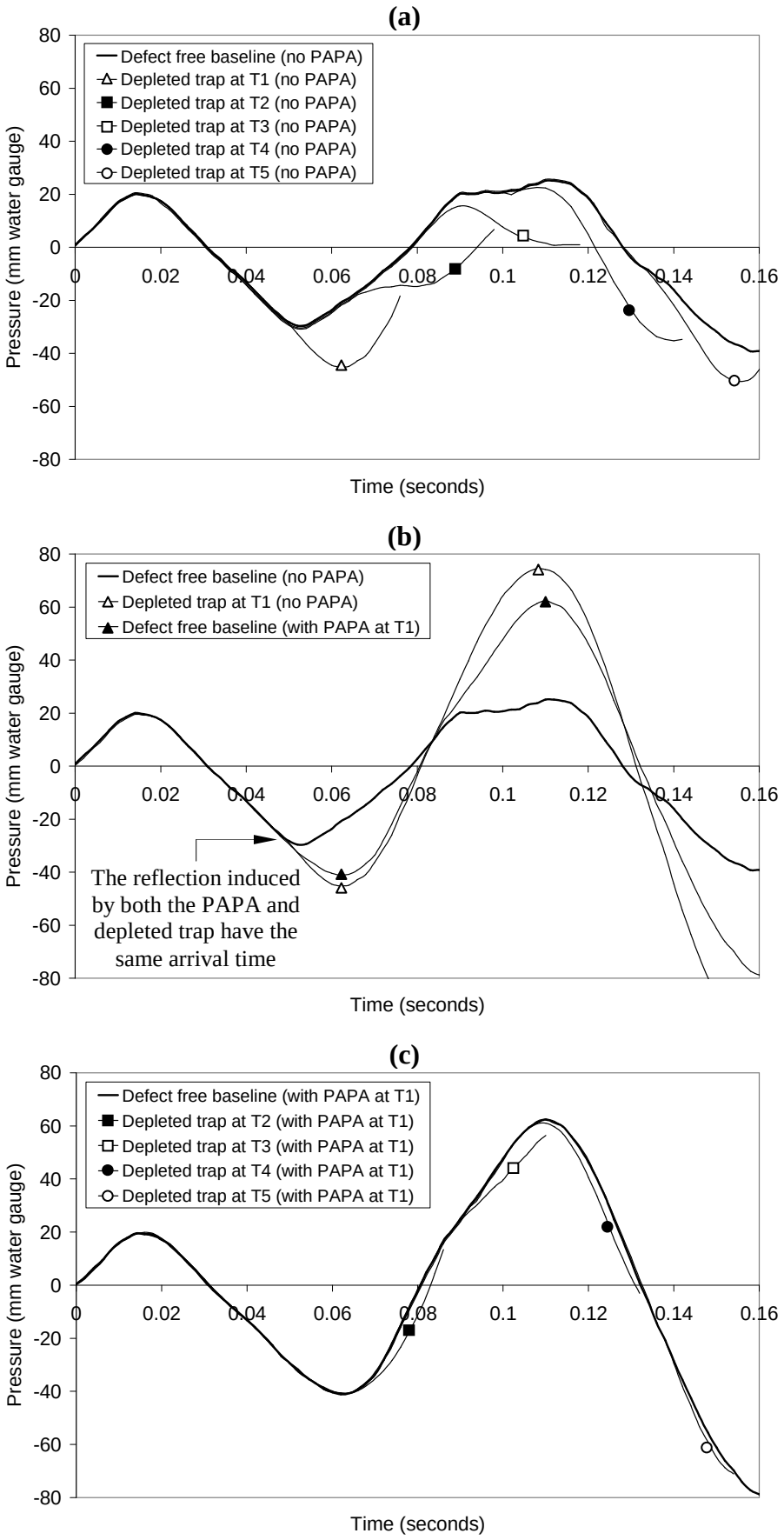

Figure 6.48 The impact of a PAPA: (a) system response for depleted traps T1 to T5 with no PAPA; (b) impact of installing a PAPA at T1; (c) system response for depleted traps T2 to T5 with PAPA installed at T1. Note: for clarity each pressure trace has been discontinued shortly after its deviation from the defect free baseline.

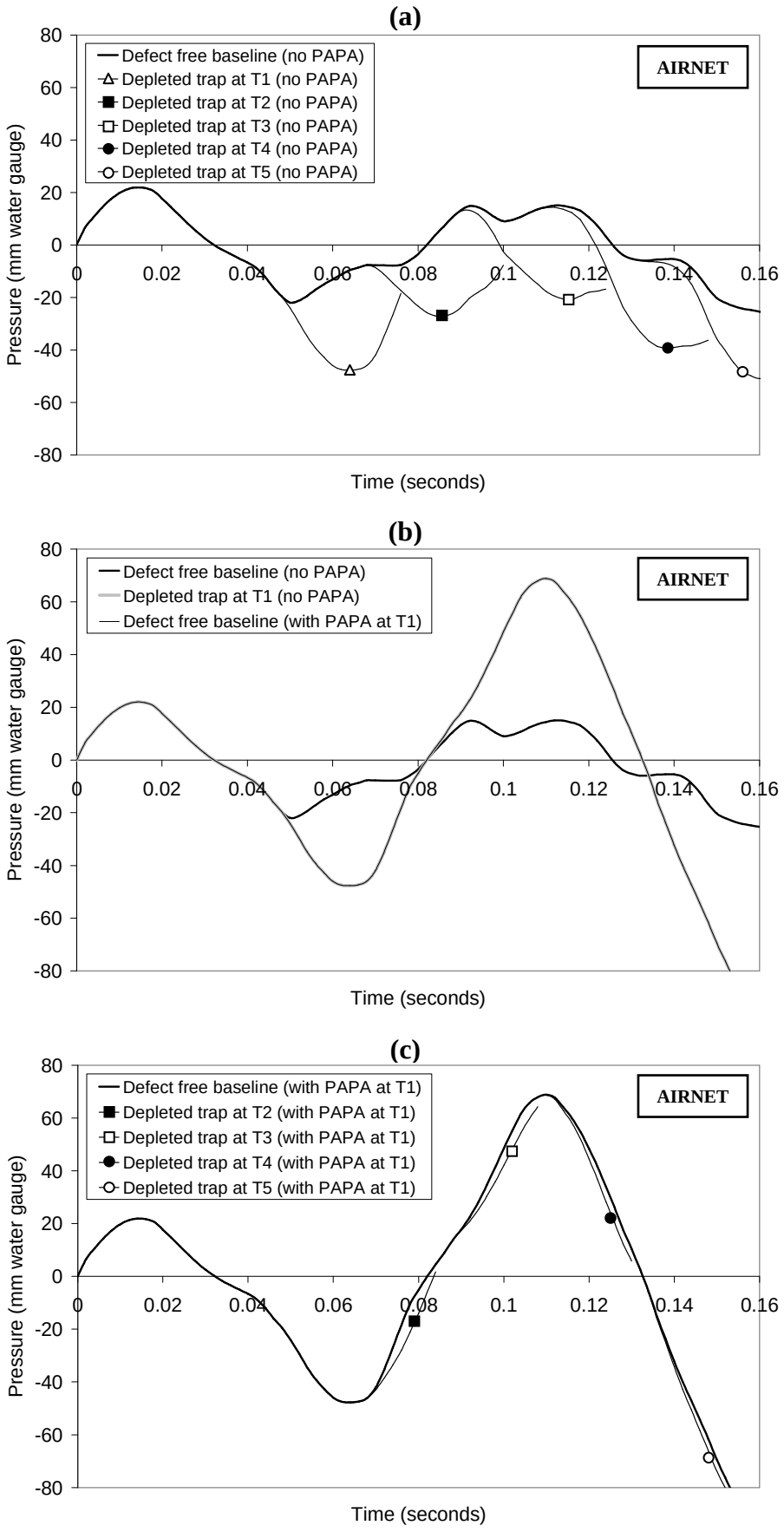

Figure 6.49 The impact of a PAPA using AIRNET: (a) the system response for depleted traps T1 to T5 with no PAPA; (b) impact of installing a PAPA at T1; (c) the system response for depleted traps T2 to T5 with PAPA installed at T1. Note: for clarity each pressure trace has been discontinued shortly after its deviation from the defect free baseline.

6.9.2.1 Effect of a PAPA on the accuracy of the reflected wave technique

To assess if the inclusion of a PAPA has an effect on the accuracy of the reflected wave technique the data gathered during the HWU 2 (*laboratory*) system tests, *Configurations X(b)* (**Figure 6.41**) were analysed using the TRACER program to determine the return time of the trap induced reflection. **Table 6.18** compares the measured depleted trap location $X_D^{measured}$, determined using *Method A*, for the system with and without the PAPA installed. The inclusion of the PAPA does in fact reduce the accuracy of the reflected wave technique. For example, when no PAPA was installed the trap location error ranges from 1.9% to 4.4%, respectively, for traps T2 to T5 (increasing with trap distance). However, when the PAPA was installed at T1, the trap location error ranges from 3.1% to 11.7% (again increasing with trap distance). Inclusion of the PAPA substantially increases the trap location error as it reduces the magnitude of the trap induced reflection, which in turn reduces both the sharpness of the returned reflection and the accuracy to which it's time of arrival can be determined.

This will not be so great a problem when the PAPA is installed downstream of all connected traps (i.e. when the PAPA is installed at the bottom of the drainage stack, which is the most likely position as positive transients are generated by stack base surcharge) and the transient entry device is located at the top of the stack, however, in certain circumstances when a PAPA may be located up the height of the stack to alleviate major transient problems, the effectiveness of the reflected wave technique may be compromised.

Table 6.18 Investigating the impact of a PAPA on the accuracy of the reflected wave technique by comparing the measured trap location for the system with and without a PAPA installed at T1 using laboratory data

True trap location and pipe period			**Measured system response with no PAPA installed**			**Measured system response with PAPA installed at T1**		
			Method A			**Method A**		
No	t_D^{true} (s)	X_D^{true} (m)	$t_D^{measured}$ (s)	$X_D^{measured}$ (m)	ε_A	$t_D^{measured}$ (s)	$X_D^{measured}$ (m)	ε_A
T1	0.0468	**8.03**	0.0478	**8.2**	0.7%	*PAPA installed at T1*		
T2	0.0657	**11.26**	0.0682	**11.7**	1.9%	0.0700	**12.0**	3.1%
T3	0.0845	**14.49**	0.0880	**15.1**	2.6%	0.0921	**15.8**	5.6%
T4	0.1033	**17.72**	0.1079	**18.5**	3.3%	0.1120	**19.2**	6.3%
T5	0.1222	**20.95**	0.1283	**22.0**	4.4%	0.1382	**23.7**	11.7%

$$\varepsilon_A = \frac{\left| X_D^{measured} - X_D^{true} \right|}{L}$$

When L = 23.6 m (the total stack height)

6.9.3 The effect of an air admittance valve installed within the system

Using the HWU 2 (*laboratory*) system, *Configurations X(a) and X(c)* (**Figure 6.41**), data was collected to evaluate the effect that the installation of an AAV would have on the measured system response and whether the inclusion of such a device would have any impact on the accuracy of the reflected wave technique. First, the system response was measured for each depleted trap (i.e. trap T1 to T5) with no AAV installed (*Configuration X(a)* in **Figure 6.41**). This is, of course, identical to the tests undertaken in Section 6.9.2 for the system with no PAPA installed, but is reproduced in **Figure 6.50(a)** for ease of comparison.

An AAV was then installed at T1, replacing the trap at this location (*Configuration X(c)* in **Figure 6.41**). **Figure 6.50(b)** shows the pressure response of the system with and without the AAV installed at T1. A positive reflection can be seen to occur at 0.084 seconds by the inclusion of the AAV, however, this does not coincide with the pipe period of the AAV which, at a distance of 8.03 m, is 0.047 seconds (i.e. (2 x 8.03)/343). An explanation of the effect of the AAV can be derived by considering the known reflection coefficients representing the system boundaries and the AAV operation.

Assuming quiescent conditions within the system prior to testing, the diaphragm within the AAV would have been initially closed. As the sinusoidal transient arrives at the AAV, the diaphragm remains closed as the leading edge of the transient has a positive pressure, due to the initial forwards movement of the piston exciter. As the diaphragm remains closed it displays similar reflection characteristics to a fully primed trap – having a +1 reflection coefficient and thus generating a positive reflection – which explains why the system remains unchanged at the pipe period of the AAV. Only when the pressure at the AAV reaches its opening threshold does the diaphragm open to allow airflow into the system. The opening threshold for the AAV used in these tests is unknown, however, previous investigations by Swaffield and Campbell (1992) have shown that the opening threshold can range from between -5 to -10 mm water gauge for various types of AAV. Taking the mean of these as an approximation, an opening threshold of -7.5 mm water gauge will be assumed. The time that the pressure reaches this opening threshold is 0.037 seconds and so allowing for the time taken for this opening threshold pressure to arrive at the AAV, be reflected by this partially open end with a reflection coefficient > -1, and for the reflection to be returned, gives a reflection return time of 0.084 seconds (0.047 seconds + 0.037 seconds) which corresponds with

the observed reflection return time in **Figure 6.50(b)**. The reflection appears as a positive reflection as it represents a negative reflection of a negative pressure wave.

Depleted traps were then introduced at traps T2 to T5 while the AAV was installed at T1. **Figure 6.50(c)** shows the resultant measured system responses. The defect free baseline was replaced by the system response of the defect free system with the AAV installed at T1, from **Figure 6.50(b)**, to ensure that the effect of the AAV boundary condition was incorporated into the defect free baseline and that it would not be mistaken for a defect. It can be seen from **Figure 6.50(c)** that, with the AAV installed at T1, the magnitude of the depleted trap induced reflection is considerably smaller than when there was no AAV installed. This can be explained by the principle of pressure wave superposition. The positive reflection induced by the AAV combines with the negative reflection induced by the depleted traps providing a net decrease in the measured reflection from the open trap.

The tests were then simulated using the AIRNET program. First, for comparison, the system was simulated without the AAV installed, **Figure 6.51(a)**. An AAV was then installed at T1 and **Figure 6.51(b)** compares the simulated pressure response of the system with and without the AAV. As was observed during the laboratory experiments, a positive reflection occurs due to the inclusion of the AAV. It should be noted, however, that the arrival time and magnitude of this reflection differs from the system response measured in the laboratory. A likely explanation for this discrepancy is that the opening threshold and the loss coefficient K used in the AAV boundary condition descriptions, Equations (3.34) and (3.35), within the AIRNET program do not match that of the AAV used during the laboratory tests. AIRNET contains the characteristic boundary condition equations for three types of AAV (derived by Swaffield and Campbell, 1992) and **Figure 6.51(b)** shows the response to the AAV that most closely matches the laboratory tests.

Figure 6.51(c) shows the simulated pressure response for depleted traps at T2 to T5 with the AAV installed at T1. As was the procedure with the previous tests, the defect free baseline was replaced by the pressure response of the defect free system with the AAV installed at T1. As observed during the laboratory investigation, the presence of the AAV has the effect of reducing the magnitude of the depleted trap induced reflection, however, the extent of the reduction is less due to the smaller positive reflection induced by the AAV in the simulation which combines with the reflection.

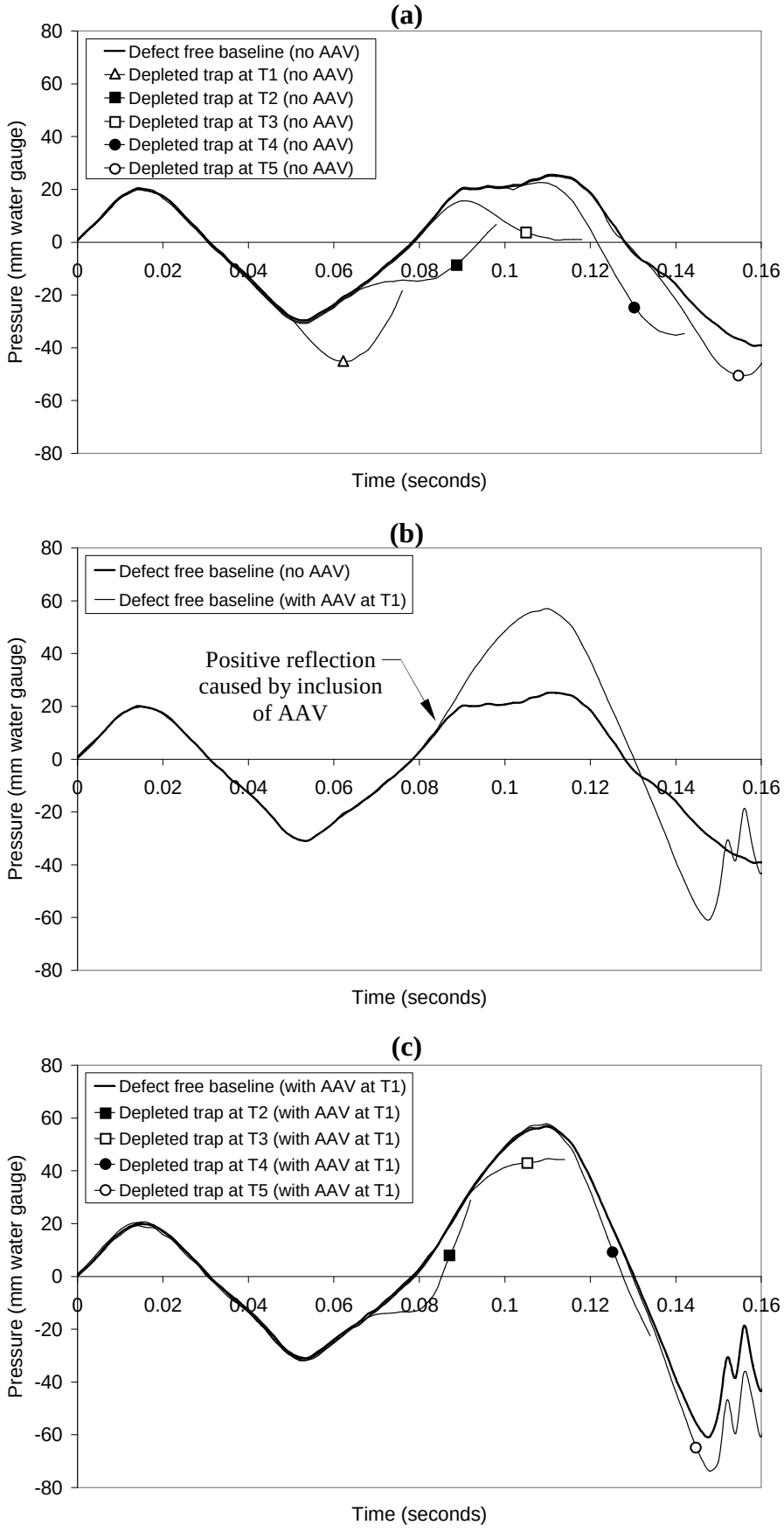

Figure 6.50 The impact of an AAV: (a) system response for depleted traps T1 to T5 with no AAV; (b) impact of installing an AAV at T1; (c) system response for depleted traps T2 to T5 with AAV installed at T1. Note: for clarity each pressure trace has been discontinued shortly after its deviation from the defect free baseline.

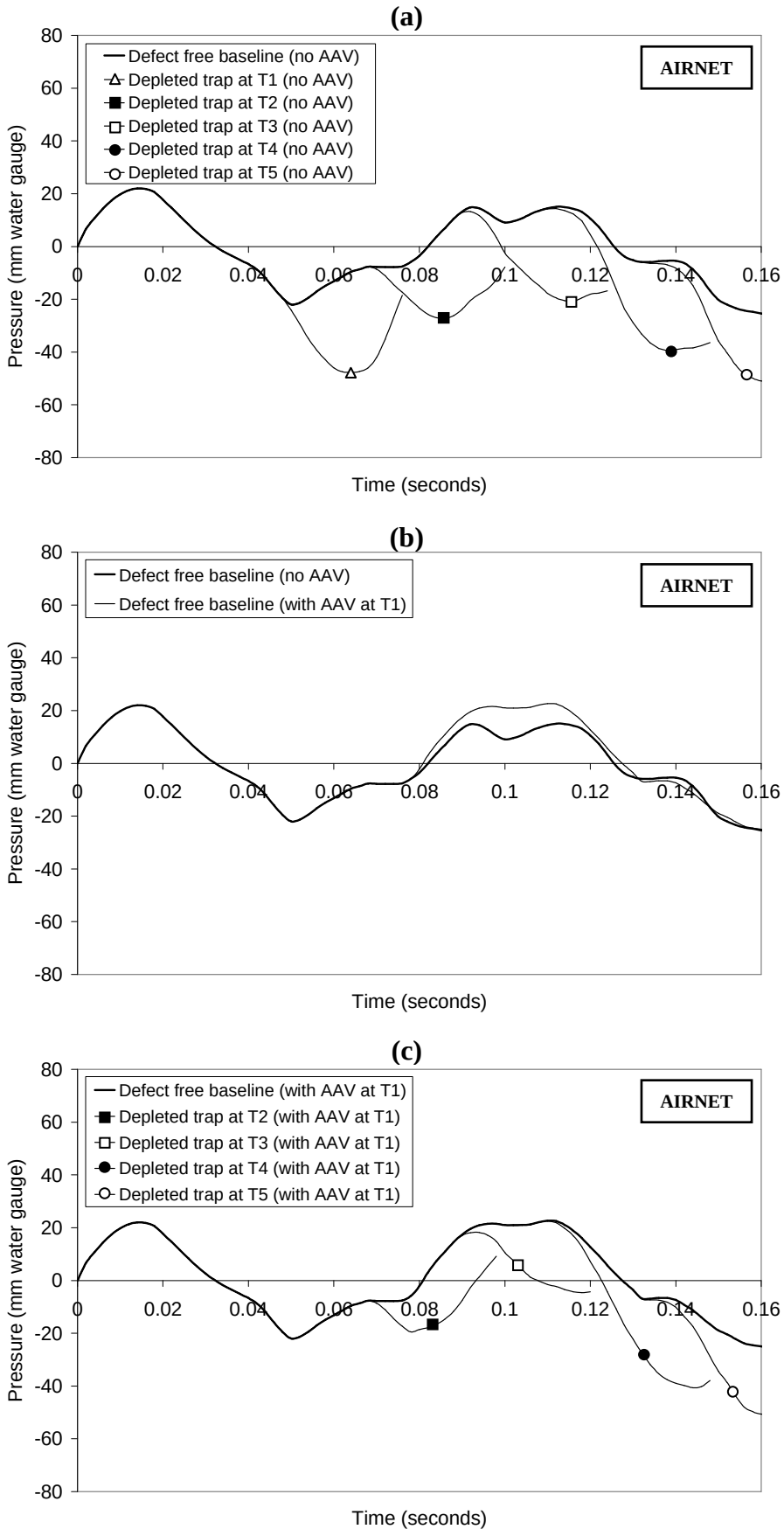

Figure 6.51 The impact of an AAV using AIRNET: (a) the system response for depleted traps T1 to T5 with no AAV; (b) impact of installing an AAV at T1; (c) the system response for depleted traps T2 to T5 with an AAV installed at T1. Note: for clarity each pressure trace has been discontinued shortly after its deviation from the defect free baseline.

6.9.3.1 Effect of AAV on the accuracy of the reflected wave technique

To investigate if the inclusion of an AAV would have any impact on the accuracy of the reflected wave technique the data gathered during the HWU 2 (*laboratory*) system tests, *Configuration X(c),* were analysed using the TRACER program. **Table 6.19** compares the measured depleted trap location $X_D^{measured}$, determined using *Method A*, for the system with and without an AAV installed at T1 together with the trap location error ε. The trap location error for trap T2 for the system with the AAV matches exactly that for the system without the AAV (i.e. ε = 1.9%). For traps T3, T4 and T5, however, the trap location error is considerably greater when the AAV is installed (i.e. increasing from ε = 2.6% to 6.8% for T3; from ε = 3.3% to 8.0% for T4; and from ε = 4.4% to 8.7% for T5). The reason that T2 is not affected by the installation of the AAV is that the AAV induced reflection does not affect the system response until after the pipe period of this trap and, therefore, the trap induced reflection remains unchanged. The pipe periods of traps T3, T4 and T5, however, all occur after the AAV induced reflection is returned.

The inclusion of an AAV within the system may, therefore, affect the accuracy of the reflected wave technique by effectively reducing the magnitude of the depleted trap induced reflection which consequently affects the accurate identification of the reflection return time. However, there would be no effect when the AAV is used as a stack termination as, in the case of a single stack system, the termination will be closed off during the test, and for a multi-stack system, each AAV will be downstream of any connected trap. Problems may only arise if AAVs are located at various locations throughout the system itself.

Table 6.19 Investigating the impact of an AAV on the accuracy of the reflected wave technique by comparing the measured trap location for the system with and without an AAV installed at T1 using laboratory data

True trap location and pipe period			Measured system response with no AAV installed			Measured system response with AAV installed at T1		
			Method A			Method A		
No	t_D^{true} (s)	X_D^{true} (m)	$t_D^{measured}$ (s)	$X_D^{measured}$ (m)	ε_A	$t_D^{measured}$ (s)	$X_D^{measured}$ (m)	ε_A
T1	0.0468	**8.0**	0.0478	**8.2**	0.7%	*AAV installed at T1*		
T2	0.0657	**11.3**	0.0682	**11.7**	1.9%	0.0682	**11.7**	1.9%
T3	0.0845	**14.5**	0.0880	**15.1**	2.6%	0.0939	**16.1**	6.8%
T4	0.1033	**17.7**	0.1079	**18.5**	3.3%	0.1143	**19.6**	8.0%
T5	0.1222	**21.0**	0.1283	**22.0**	4.4%	0.1341	**23.0**	8.7%

$$\varepsilon_A = \frac{\left| X_D^{measured} - X_D^{true} \right|}{L}$$

When L = 23.6 m (the total stack height)

6.10 Quantifying the junction effect

Throughout this chapter the *junction effect* has been shown to have a significant influence over the trap location error. The *junction effect* introduces a perceived delay in the arrival time of the depleted trap induced reflection which generates a corresponding overestimation of the depleted trap location. The results have shown that the extent of this overestimation is a function of both the number, *n*, and branch to stack area ratio, A_{branch}/A_{stack}, of each of the individual junctions passed as the transient travels to and returns from the trap. This section aims to quantify the influence of these parameters allowing the overestimation of the depleted trap location to be predicted.

Having already demonstrated excellent correlation with real system data collected during both the laboratory experiments and the field trials, the AIRNET model was used to help quantify the *junction effect* in this investigation. The simple system shown previously in **Figure 6.6(a)** was used again here. Starting with all pipes set to 100 mm diameter (A_{branch}/A_{stack} = 1.0) the system response was simulated first to determine the defect free baseline and then to determine the response for each of the fourteen depleted traps in turn. The branches were then reduced to 75 mm diameter (A_{branch}/A_{stack} = 0.56), 50 mm diameter (A_{branch}/A_{stack} = 0.25), 40 mm diameter (A_{branch}/A_{stack} = 0.16) and 32 mm diameter (A_{branch}/A_{stack} = 0.1) in turn. **Table 6.20** compares the trap location error, ε, for each branch to stack area ratio tested and for every number of junctions traversed by the incident transient.

Table 6.20 Comparison of the effect of branch to stack area ratio and junction number on the trap location error as simulated using AIRNET

No. of junctions traversed, *n*	A_{branch}/A_{stack} = 1.0		A_{branch}/A_{stack} = 0.56		A_{branch}/A_{stack} = 0.25		A_{branch}/A_{stack} = 0.16		A_{branch}/A_{stack} = 0.1	
	ε (%)	ε_j (%)	ε (%)	ε_j (%)	ε (%)	ε_j (%)	ε (%)	ε_j (%)	ε (%)	ε_j (%)
1	0.000	**0.000**	0.000	**0.000**	0.000	**0.000**	0.000	**0.000**	0.000	**0.000**
2	0.103	**0.052**	0.103	**0.052**	0.103	**0.052**	0.213	**0.106**	0.213	**0.106**
3	0.316	**0.105**	0.316	**0.105**	0.316	**0.105**	0.316	**0.105**	0.316	**0.105**
4	0.748	**0.187**	0.529	**0.132**	0.529	**0.132**	0.529	**0.132**	0.529	**0.132**
5	4.142	**0.828**	0.852	**0.170**	0.742	**0.148**	0.742	**0.148**	0.852	**0.170**
6	4.903	**0.817**	1.284	**0.214**	0.955	**0.159**	0.955	**0.159**	0.955	**0.159**
7	5.445	**0.778**	4.458	**0.637**	1.277	**0.182**	1.168	**0.167**	1.168	**0.167**
8	8.839	**1.105**	5.000	**0.625**	1.600	**0.200**	1.490	**0.186**	1.490	**0.186**
9	9.490	**1.054**	5.432	**0.604**	1.923	**0.214**	1.703	**0.189**	1.594	**0.177**
10	10.581	**1.058**	5.865	**0.586**	2.465	**0.246**	2.026	**0.203**	1.916	**0.192**
11	13.535	**1.230**	6.626	**0.602**	4.871	**0.443**	2.239	**0.204**	2.129	**0.194**
12	14.297	**1.191**	9.361	**0.780**	5.303	**0.442**	2.452	**0.204**	2.452	**0.204**
13	16.813	**1.293**	10.013	**0.770**	5.845	**0.450**	3.432	**0.264**	2.665	**0.205**
14	18.232	**1.302**	10.555	**0.754**	6.168	**0.441**	4.194	**0.300**	3.206	**0.229**

As expected, the results show that ε increases as the number of junctions traversed by the incident transient increases. This has been a common finding throughout all of the laboratory investigations and field trials.

Additionally, as observed during the field trials discussed in Section 6.8.3, ε is larger for higher values of A_{branch}/A_{stack}. Taking the case when n = 14 as an example, then if A_{branch}/A_{stack} = 1.0 the trap location error ε = 18.232%, however, when A_{branch}/A_{stack} = 0.56 the trap location error drops to ε = 10.555% and when A_{branch}/A_{stack} = 0.25 the trap location error drops again to ε = 6.168%, and so on. Despite having demonstrated in Section 6.9.1, when considering the effect of a single junction, that lower values of A_{branch}/A_{stack} returned smaller magnitude reflections and were thus responsible for a small increase in values of ε, when a system contains many junctions with a low value of A_{branch}/A_{stack} the overall significance of the *junction effect* is reduced. This is due to the fact that when A_{branch}/A_{stack} is low a larger proportion of the transient is transmitted forwards throughout the system. The *junction effect* is therefore most significant in systems with junctions of equal diameter (i.e. A_{branch}/A_{stack} = 1.0) as this type of junction transmits a smaller proportion of the transient. Note that in current drainage design the possibility that the branch would have a greater diameter than the main stack may be discounted.

Furthermore, by calculating the individual junction error, ε_j, ($\varepsilon_j = \varepsilon/n$) it can be seen that as the number of junctions increases, ε_j increases progressively. For example, when A_{branch}/A_{stack} = 1.0 and n = 3, ε = 0.316% and ε_j = 0.105%. However, when A_{branch}/A_{stack} = 1.0 and n = 14, ε = 18.232% and ε_j = 1.293%. It is, therefore, shown that as the number of junctions traversed by the incident transient becomes larger, the effect of each junction on the overestimation of the depleted trap location becomes more significant, with each junction encountered being attributed a higher contributory error value. When the number of junctions within the system is increased by one, the number of reflections and re-reflections generated as a result of this new junction is increased by a factor many times higher – dependant upon the number of reflective boundary conditions present within the system – which together contribute to a higher increase in the dampening effect of the waveform and thus increases the perceived reflection arrival time and results in an increased trap location error per trap.

Figure 6.52, which provides a graphical representation of the results, can be used in conjunction with **Table 6.20** to estimate the influence of the *junction effect* on the trap

location error for the range of branch to stack area ratios tested. As there are a number of possible pipe configurations and types of junctions used in the building drainage system it is not practical to attempt to generalise these results. It is possible that in more complex systems, where pipe lengths are greater and the number of connected appliances is larger, that the junction effect would differ from that shown here.

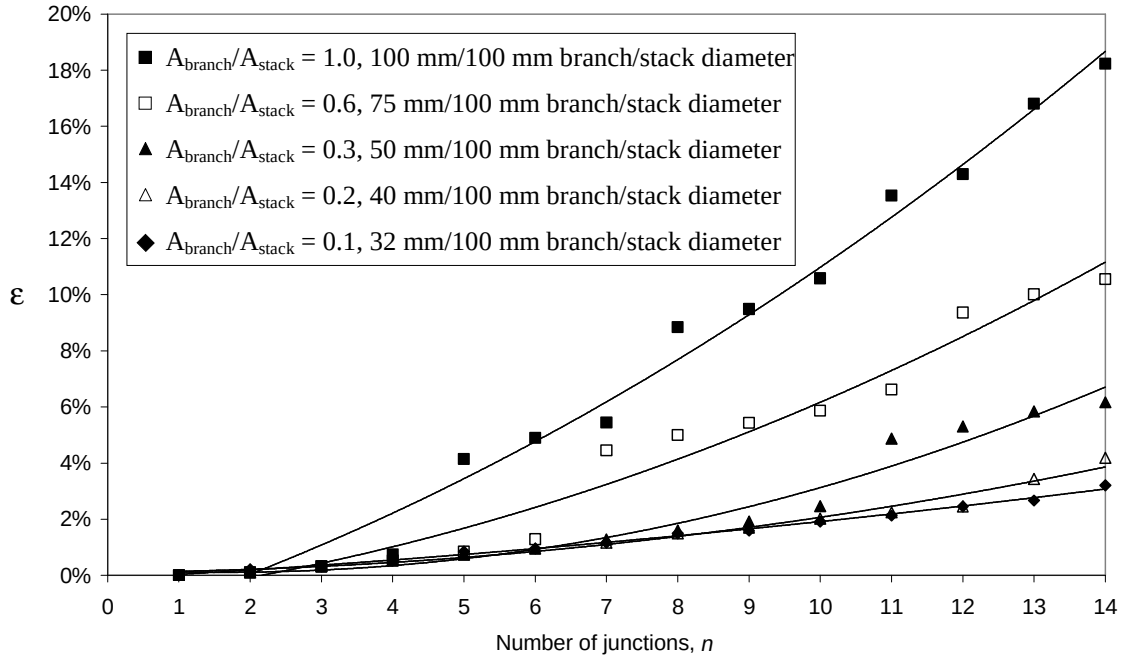

Figure 6.52 Relation between branch to stack area ratio and junction number on the trap location error as simulated using AIRNET

6.11 Chapter summary

This chapter has demonstrated the successful application of the reflected wave technique for the detection and location of depleted trap seals from extensive experimental and site installation investigations. The AIRNET simulation has been shown to be a valuable tool in the identification of depleted trap seals by providing an accurate prediction of the system response (which has been shown to correlate well with real system data) and by providing an accurate prediction of the observed arrival time of a depleted trap induced reflection.

The *junction effect* was shown to have a detrimental effect on the trap location error when relying solely on Equation (4.2), *Method A*. However, both *Methods B* and *C* show excellent correlation between the predicted and measured depleted trap locations, in both single and multi-stack systems, thus offering confidence in this novel application of the reflected wave technique.

Assessment of the impact of various system boundaries has shown that trap diameter and the inclusion of pressure control devices such as AAVs and PAPAs can have an effect on the trap location error.

Chapter 7
Conclusions and recommendations for further work

7.1 Overview

This research set out to establish a systematic method of monitoring the building drainage system against the threat of cross-contamination of disease by remotely monitoring trap seal status. This was approached through the development of the reflected wave technique as a tool for detecting and locating depleted trap seals and by the collection of transient data sets for the testing and validation of the technique.

An extensive review was carried out that included (i) the health risks attributable to the foul air within the building drainage system, (ii) the potential threat of trap depletion by propagating pressure transients and other such factors, (iii) methods used for defect detection on other piped systems, and (iv) classic transient theory. This review was important in order to understand the potential consequences of trap seal depletion, and to realise the urgent requirement for a novel approach to building drainage maintenance. The review also highlighted that although the reflected wave technique had been previously applied to the detection and location of leaks and blockages in other piped systems it had not been properly tested using real system data.

The method of characteristics approach to modelling low amplitude air pressure transient propagation as experienced within the building drainage system was introduced. The boundary and internal conditions employed by the method of characteristics based numerical model, AIRNET, were presented together with a new boundary condition implemented to represent the transient generator.

A ***tra**p **c**ondition **e**valuato**r*** (TRACER) program was developed and implemented into the data collection package to carry out automatic detection and location of depleted trap seals. The TRACER program used a time series change detection algorithm to estimate the arrival of a depleted trap induced reflection by computing the absolute difference between the observed test data and a previously obtained defect free baseline.

A numerical example using perfect data was used to establish and test the TRACER program.

A series of experimental investigations were carried out with the aim of collecting data sets of system responses – with and without the presence of depleted trap seals – under both laboratory and field conditions. The influence of some common system boundaries on the measured system response were analysed. Several problems were encountered during the data collection which, when overcome, gave a better understanding of the difficulties of applying this technique as a continual monitoring system in the field.

The reflected wave technique and the TRACER program were tested and validated using physical data collected from the laboratory and field investigations. The major problem was the influence of the *junction effect* on the perceived arrival time of the returned trap induced reflection. Three approaches were used to predict the reflection return time. Numerical results obtained from the AIRNET model agreed well with the collected data.

This research was the first major experimental validation and testing of the reflected wave technique for the detection and location of depleted trap seals in the building drainage system. Furthermore, this research was the first known to systematically investigate and quantify the junction delay effect in terms of the junction geometry expressed in terms of area ratios.

7.2 Main findings

The main findings of this work are summarised as follows:

Experimental programs

(i) A total of five extensive experimental programmes were carried out (Chapter 5). The first set of tests was carried out under controlled laboratory conditions using a specially designed test-rig at Heriot-Watt University, HWU 1 (*laboratory*) system. The second was carried out under field conditions at a 17-storey unoccupied residential building in Dundee, Dundee (*field*) system. The third also under field conditions within an academic building at Heriot-Watt

University, HWU Arrol (*field*) system. The fourth were again under field conditions at an office building in Glasgow, Glasgow (*field*) system. And the final set of tests was conducted under controlled laboratory conditions using a second test-rig at Heriot-Watt University, HWU 2 (*laboratory*) system.

Numerous transient tests were carried out by collecting pressure data of each system, with and without depleted traps, in response to an applied incident transient. Each set of tests were undertaken to allow further development of the technique, each time building confidence on both its effectiveness and applicability as a system monitoring tool.

(ii) Several problems arising from the Dundee (*field*) system tests were resolved following the development of the transient entry device to control the flow and the generation of the incident transient. The significant and sudden pressure drop generated as the incident transient encountered the three pipe junction created between the stack and the inlet branch was removed by the use of a 3-port valve. The valve removed the reflection generated by the junction allowing 100% through flow of the incident transient. Additionally, the adoption of a sinusoidal piston exciter ensured the test was completely non-destructive and did not pose a threat to the integrity of the connected trap seals (Section 5.2.4).

(iii) During data collection at the HWU Arrol (*field*) system the reliability of the technique was enhanced by increasing the data scan rate which improved the successful alignment of the test system response with the defect free baseline (Section 5.2.5.5.2). Furthermore, the repeatability of the test, which was observed to be dependant upon the susceptibility of the piston exciter to changes in temperature, was improved by operating the piston exciter at a constant and stable temperature. This ensured that the incident transient was the same for all tests (Section 5.2.5.5.2).

Transient data analysis

(i) A depleted trap generates a sudden pressure drop in response to a positive pressure wave by inducing a negative reflection of the wave. The reflection is then reduced by frictional and mechanical losses until it dissipates.

Additionally, the depleted trap increases the natural damping of transient pressures by behaving like a relief valve.

(ii) The identification of the depleted trap reflected wave can very precisely pinpoint a depleted trap, as long as the wave propagation speed is known, the arrival time of the trap reflected wave is identified and the *junction effect* is taken into account.

(iii) The *junction effect* has been quantified for a number of different branch to stack area ratios, constituting the most common junction types found in the building drainage system, using data derived from the AIRNET numerical model. The *junction effect*, and its effect of increasing the trap location error, becomes more significant as the branch to stack area ratio increases and as the number of junctions within the system is increased.

(iv) The *junction effect* dampens the returning trap induced reflection, delaying its observed arrival time. The consequence is that the trap location may be overestimated when compared with the predicted trap location calculated from the theoretical trap pipe period. Realistic and reliable results were obtained when the AIRNET numerical model was used to estimate the trap pipe period and when the reflected wave technique was used as a probe to determine the observed trap pipe period as both of these methods include the *junction effect*.

(v) The inclusion of pressure control devices such as AAVs and PAPAs were observed to increase the trap location error as these devices introduce additional transient dampening effects. However, the good correlation demonstrated by the AIRNET numerical model with real system data gives confidence in its use to again take account of these dampening effects and provide an accurate prediction of the trap pipe period.

(vi) The reflected wave technique together with the TRACER program automatically detected and located every depleted trap in all of the analysed test cases, although with different uncertainties. In addition, the technique has been shown to be applicable to multi-stack systems, consisting of many pipes and containing many different boundary conditions, requiring only one transient entry point and distributed pressure measurement points.

(vii) Although the reflected wave technique appears relatively simple to apply to building drainage systems, accurate trap location depends on: the accuracy of the pressure measurement equipment; data uncertainty; system noise; the change detection algorithm; size and location of the depleted trap seal; system geometry; and the estimation accuracy of the trap pipe period.

(viii) The successful field application of the reflected wave technique has provided confidence that the technique has potential to provide a holistic approach to building drainage maintenance. This research has demonstrated both the practical and operational merits of the technique in this novel application.

7.3 Recommendations for future work

The current research has identified areas that require further work. These are as follows:

(i) The technique has thus far been applied only to single stack systems. Further research is required to investigate its application to other system designs such as, for example, the modified one pipe system which incorporates additional ventilation pipework. It is recognised that such systems may increase the transient dampening and so may have a detrimental effect on the accuracy of the technique.

(ii) In this study, the depleted trap was simulated by completely removing the water seal. Further research is needed to analyse the response of a partially depleted trap seal – which would still potentially provide a threat of cross-contamination – and to determine whether or not this would induce a reflection of sufficient magnitude to allow its detection and location.

(iii) As detailed in Chapter 4, to provide the required level of protection against cross-contamination the technique must offer systematic system monitoring. To achieve this, the technique must provide automated test scheduling and data analysis. The TRACER program allows automatic data analysis, however, further work is required to provide a control strategy whereby the test can be fully integrated as an automated maintenance regime. Further funding has been secured to ensure this research continues.

Appendix A

Variability of wave propagation speed in the AIRNET simulation

As shown in Section 3.4 the value of the wave propagation speed is dependant upon air pressure. Equation (A.1), previously shown as Equation (3.12) but repeated here for convenience, shows the expression used for calculating the local air pressure within the AIRNET numerical model and demonstrates the dependence of the wave propagation speed on both local air pressure and density:

$$p = \left[\left(\frac{p_o}{\rho_o{}^{\gamma}} \right) \left(\frac{\gamma}{c^2} \right)^{\gamma} \right]^{\frac{1}{(1-\gamma)}} \tag{A.1}$$

However, as discussed in Section 1.2, the successful application of the reflected wave technique for the detection and location of depleted trap seals within the building drainage system requires the wave propagation speed to be known in order that the depleted trap may be identified by the return time of the first trap reflected wave.

It is therefore important to determine, within the limits of the conditions typical to the reflected wave technique, the extent to which the wave propagation speed varies with air pressure. To do so, the simple system used in Section 4.6 (repeated for convenience in **Figure A.1**) will be simulated here by AIRNET to determine the variability of the wave propagation speed in response to the imposed air pressure transients applied during the reflected wave technique. The effect of both the single positive pressure pulse and the 10 Hz sinusoidal transient wave will be analysed.

The stack diameter was set to D = 100 mm while both the branch and trap diameters were set to D = 50 mm. The time step and space step were set to Δt = 0.002 s and Δx = 0.1 m, respectively. The base value for the wave propagation speed was set to

c_{base} = 343.14 m/s assuming atmospheric pressure and density at a typical temperature of 20 ^{o}C (or 0 mm water gauge).

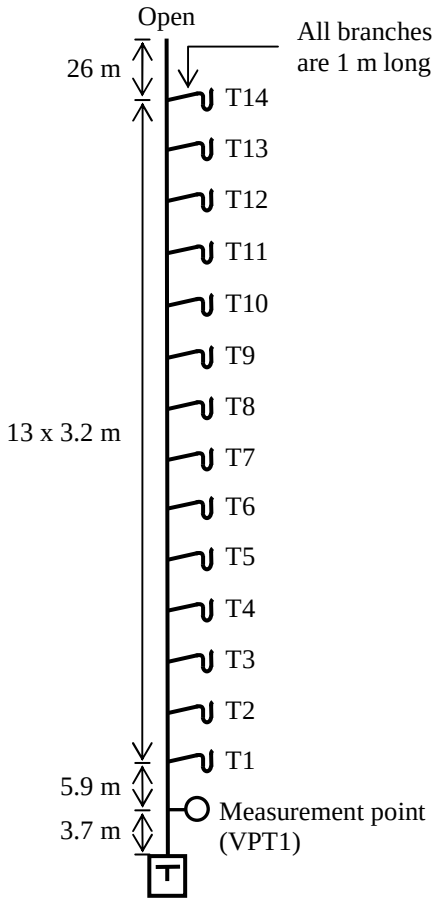

Figure A.1 Simple system used to assess the variability of wave speed with air pressure in the AIRNET numerical model

Figure A.2 and **Figure A.3** show the variation of the wave propagation speed with air pressure in response to the applied single positive pressure pulse and the 10 Hz sinusoidal transient wave respectively.

In the case of the single positive pressure pulse (**Figure A.2**) the wave propagation speed can be seen to attain a minimum value of 342.28 m/s (when the air pressure is -180.65 mm water gauge) and a maximum value of 343.96 m/s (when the air pressure is 173.43 mm water gauge) which constitutes a variation from the base value (c_{base} = 343.14 m/s at 0 mm water gauge atmospheric pressure) of 0.86 m/s (i.e. a 0.25% decrease) and 0.82 m/s (i.e. a 0.24% increase) respectively, giving a total wave propagation variation of 0.49%.

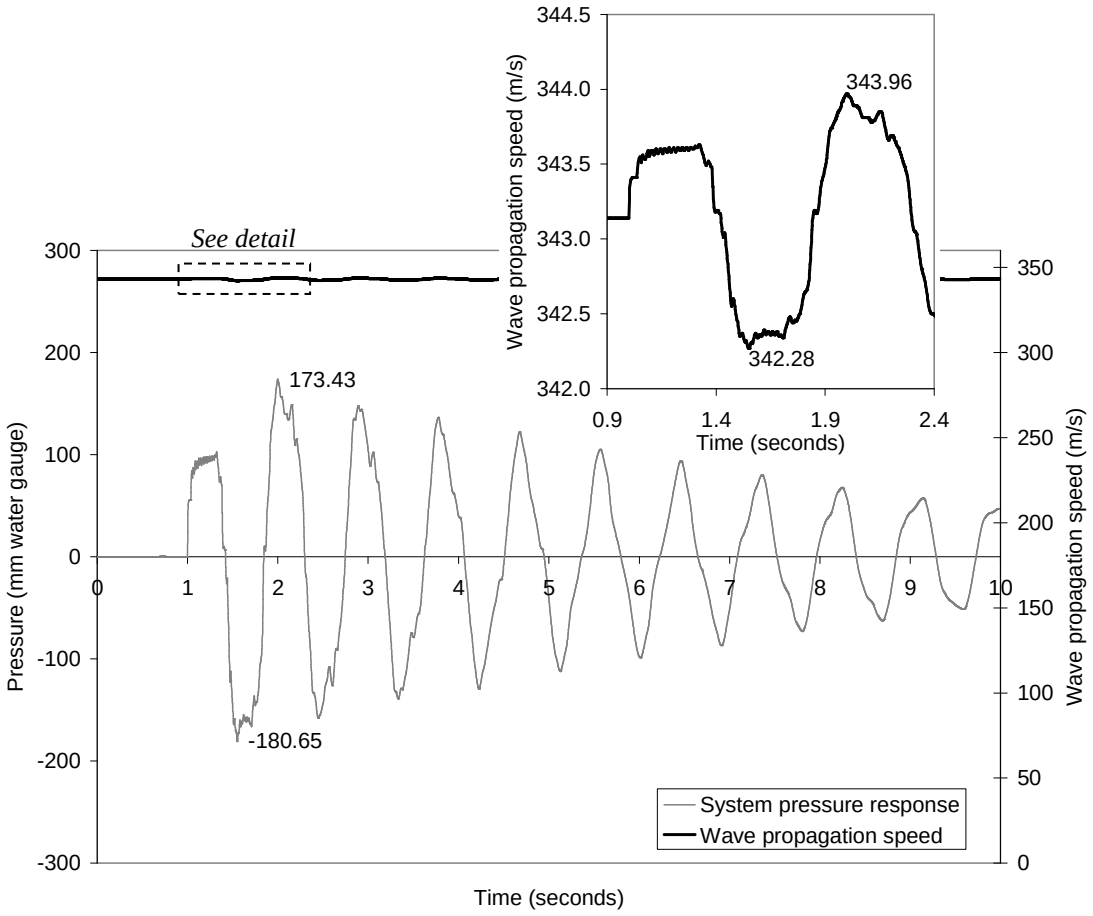

Figure A.2 The variation of wave propagation speed with air pressure in response to an applied single positive pressure pulse

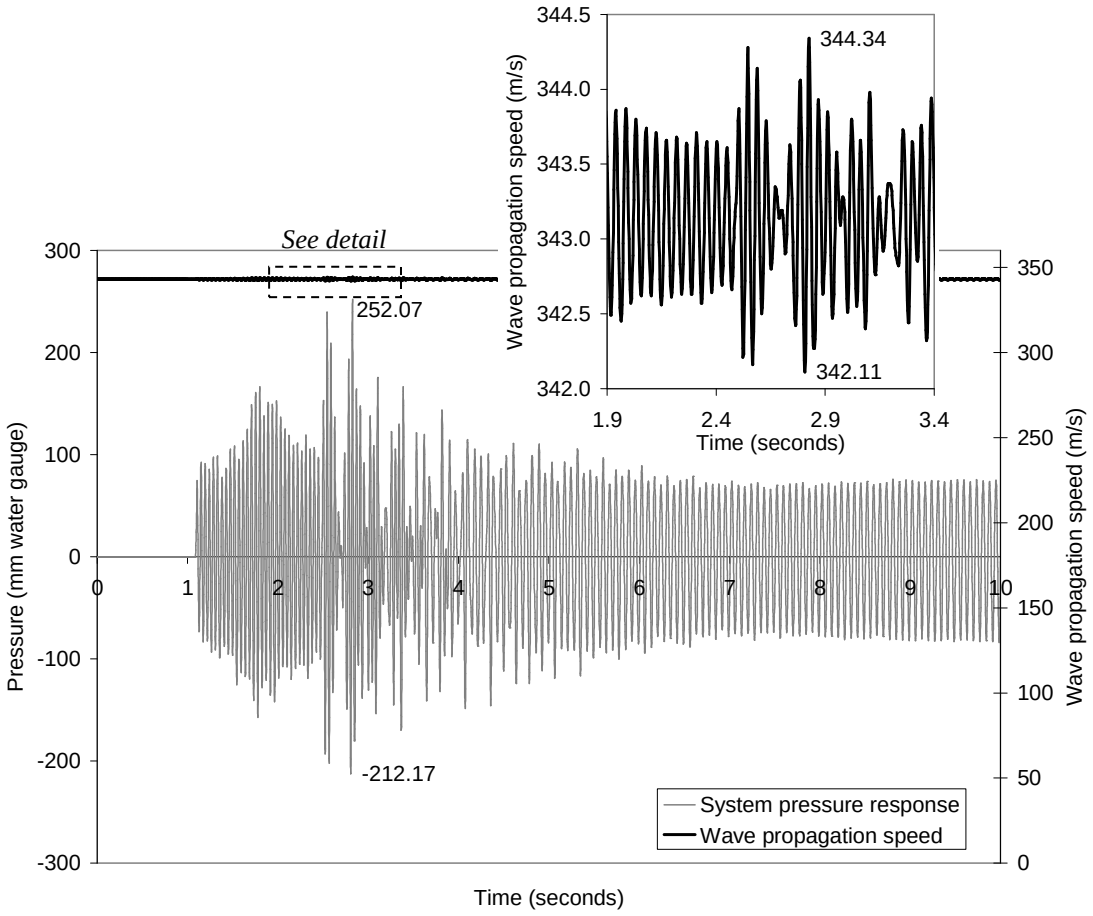

Figure A.3 The variation of wave propagation speed with air pressure in response to an applied 10 Hz sinusoidal transient wave

When the 10 Hz sinusoidal transient wave is applied (Figure A.3) the wave propagation speed can be seen to attain a minimum value of 342.11 m/s (when the air pressure is -212.17 mm water gauge) and a maximum value of 344.34 m/s (when the air pressure is 252.07 mm water gauge) which constitutes a variation from the base value of 1.03 m/s (i.e. a 0.3% decrease) and 1.2 m/s (i.e. a 0.35% increase) respectively, giving a total wave propagation variation of 0.65%.

As the ambient air pressure within the building drainage system is atmospheric pressure and the transient pressure excursions are small (i.e. measured in mm water gauge) the variability of the wave propagation speed is negligible. In fact, as the variation in wave propagation speed within the building drainage system is so small, it can be considered to be sensibly constant[2] under normal conditions and therefore pipe period, or reflected wave travel times, based on a constant *c* value are acceptable within the methodology proposed.

[2] Perceived as unchanged

REFERENCES

Adewumi, M.A., Eltohami, E.S., Ahmed, W. H., (2000). "Pressure transients across constrictions." *Journal of Energy Resources Technology: Petroleum Division*, ASME, **122**, 34-41.

Adewumi, M.A., Eltohami, E.S., Solaja, A., (2003). "Possible detection of multiple blockages using transients." *Journal of Energy Resources Technology: Petroleum Division*, ASME, **125**, 154-159.

Allen, M. (2002). "From cesspool to sewer: Sanitary reform and the rhetoric of resistance, 1848-1880." *Victorian Literature and Culture*, **30**, 383-402.

Allievi, L. (1903). "Notes I-IV" translated as Theory of Waterhammer by E.E. Holmes, Ricardo Garoni, Rome, 1925.

American Public Health Association (1951). Committee on the hygiene of housing: Construction and equipment of the home. Chicago, Public Administration Service.

An, P.G. (2005). "Constructing and dismantling frameworks of disease etiology: The rise and fall of sewer gas in America, 1870-1910." *Yale Journal of Biology and Medicine*, **77**, 75-100.

Antonopoulous-Domis, M. (1980). "Frequency dependence of acoustic resonances on blockage position in a fast reactor subassembly wrapper." *Journal of Sound and Vibration*, **72**(4), 443-450.

Arbon, N.S., Stephens, M., Lambert, M.F., Simpson, A. R. and Lucas, B. (2008). " Field validation of transient analysis for in-line valve condition assessment." *Proceedings of 10th International Conference on Pressure Surges*, BHR Group Ltd, Edinburgh, UK.

Baylor, E.R., Baylor, M.B., Blanchard, D.C., Syzdek, L.D. and Appel, C. (1977). "Virus transfer from surf to wind." *Science*, **198**, 575-580.

Baylor, E.R., Peters, V. and Baylor, M.B. (1977). "Water-to-air transfer of virus." *Science*, **197**, 763-764.

Beck, S.B.M, Williamson, N.J., Sims, N.D. and Stanway, R. (2002). "Pipeline system identification through cross-correlation analysis". *Proceedings of the Institution of Mechanical Engineers*, Part E, **216**, 133-142.

Bergeron, L. (1935). “Etudes des variations de regime dans les conduits d’eau”. *Rev. Gen, Hydraulique,* No. 1 and 2.

Billington, N.S. and Roberts, B.M. (1982). “Building services engineering, a review of its development”, Pergamon Press: Oxford.

Bird, P.H. (1877). "Hints on drains, traps, closets, sewer gas, and sewage disposal". "Gazette" Printing Works: Blackpool.

Boldy, A.P. (1976). "Waterhammer analysis in hydroelectric pumped storage installations", *Proc. 2nd Int. Pressure Surge Conference*, BHRA, Cranfield, England.

Booth, G.R. “The London sewerage question. Some serious observations and suggestions upon the defective plan of sewerage proposed by the Metropolitan Board of Works, Together with a method for remedying the evil”. London, 1853.

Brunone, B. (1999). "Transient test-based technique for leak detection in outfall pipes." *Journal of Water Resources Planning and Management*, ASCE, **125**(5), 302-306.

Brunone, B. and Ferrante, M. (2001). "Detecting leaks in pressurised pipes by means of transients." *Journal of Hydraulic Research*, IAHR, **39**(5), 539-547.

Brunone, B. and Ferrante, M. (2004). "Pressure waves as a tool for leak detection in closed conduits." *Urban Water Journal*, **1**(2), 145-155.

BS EN 12056 : 2000 "Gravity drainage systems inside buildings", European Committee for Standardisation, Brussels.

Butler, N.C. (1982). "Pipeline leak detection techniques." *Pipes and Pipelines Int.*, 24-29.

Campbell, D.P.C. (1992). "Mathematical modelling of air pressure transients in building drainage and vent systems." PhD thesis, Department of Building Engineering and Surveying, Heriot-Watt University.

Campbell, D.P.C. and MacLeod, K.D. (1999). “Investigation of the causative factors of air flow entrainment in building drainage-waste-ventilation systems”, *Building Services Engineering Research and Technology*, **20**(3), 99-104.

Carstens, M.R. and Roller, J.E. (1959). "Boundary-shear stress in unsteady turbulent pipe flow", *Journal of the Hydraulic Division*, ASCE, **65**(HY2), 67-81.

Chadwick, E. (1842). Report on the sanitary conditions of the labouring population of Great Britain Edinburgh University Press Edition, 1965.

Chaudhry, M. H. (1987). Applied Hydraulic Transients, Van Nostrand Reinhold Co., New York, USA.

Cheng, P. K.C., Wong, D.A., Tong, L.K.L., Sin-Ming Ip, Lo, A.C.T., Chin-Shan Lau, Yeung, E.Y.H., Lim, W.W.L. (2004). "Viral shedding patterns of coronavirus in patients with probably severe acute respiratory syndrome." *The Lancet*, **363**, 1699-1700.

Cook, G.C. (2001). "Construction of London's Victorian sewers: the vital role of Joseph Bazalgatte." *Postgraduate Medical Journal*, **77**, 802-804.

Couch, R.B., Cate, T.R., Douglas, R.G., Gerone, P.J and Knight, V. (1966). "Effect of route of inoculation on experimental respiratory viral disease in volunteers and evidence for airborne transmission." *Bacteriol Rev*, **30**, 517-529.

Courant, R. and Fredrichs, K.O. (1948). Supersonic flow and shock waves. Interscience publishers, New York.

Covas, D. (2003). "Inverse transient analysis for leak detection and calibration of water pipe systems modelling special dynamic effects." PhD Thesis, Imperial College of Science, Technology and Medicine, London.

Covas, D. and Ramos, H. (1999). "Leakage detection in single pipeleines using pressure wave behaviour." *Proceedings of Water Industry Systems: Modelling and Optimisation Applications*, CCWI'99, CWS, Exeter, UK, 287-299.

Covas, D. and Ramos, H. (2001). "Hydraulic transients used for leakage detection in water distribution systems." *Proceedings 4th International Conference on Water Pipeline Systems*, Lowdown, A., BHR Group Ltd., York, UK, 227-241.

Covas, D., Almeida, A.B., Ramos, H. (1998). "Leaks detection and control for a better environment." *Proceedings of 1st International Conference on Protecting the Environment and Controlling Leakage*, BHR Group Ltd., Rome, Italy.

Covas, D., Almeida, A.B., Ramos, H. (1999). "Leakage monitoring control and management of water distribution systems: a challenge for the XXI." *Proceedings of XXVIII IAHR Congress, Pub*. IAHR, Graz, Austria.

Covas, D., Graham, N., Maksimovic, C., Ramos, H., Kapelan, Z., Savic, D., and Walters, G. (2003). "An assessment of the application of inverse transient analysis for leak detection. II: Collection and application of experimental data." *Advances in water supply management*, CCWI'03, London, 79-87.

Covas, D., Ramos, H. and Almeida, A.B. (2005). "Standing wave difference method for leak detection in pipeline systems." *Journal of Hydraulic Engineering*, ASCE, **131**(12), 1106-1116.

Covas, D., Ramos, H., Brunone, B., and Young, A. (2004). "Leakage detection in water trunk mains using transient system responses: Field tests in Scottish Water." 9th *International Conference on Pressure Surges*, BHR Group, Chester, UK, 185-198.

Cronholm, L.S. (1980). “Potential health hazards from microbial aerosols in densely populated urban regions”. *Applied and Environmental Microbiology*, **39**, 6-12.

Darlow, H.M. and Bale, W. R. (1959). "Infective hazards of water closets." *Lancet ii*, 1196-1200.

De Salis, M.H.F. and Oldham, D.J. (1999). "Determination of the blockage area function of a finite duct from a single system response measurement." *Journal of Sound and Vibration*, **221**(1), 180-186.

De Salis, M.H.F. and Oldham, D.J. (2001). "The development of a rapid single spectrum method for detecting the blockage characteristics of a finite length duct." *Journal of Sound and Vibration*, **243**(4), 625-640.

Doyle, T.J. and Swaffield, J.A. (1972). "Evaluation of the method of characteristics applied to a pressure transient analysis of the B.A.C./S.N.A.I.S. Concorde refuelling system", *Proceedings of the Institution of Mechanical Engineers*. **186**, 40/70, 509-518.

Druet, H.A., Henderson, D.W. and Peacock, S. (1956). "Studies on respiratory infection III. Experiments with Brucella Suis." *Journal of Hygiene*, **54**, 49-57.

Druet, H.A., Henderson, D.W., Packman, L.P., Peacock, S. (1953). "Studies on respiratory infection. The influence of particle size on respiratory infection with anthrax spores. *Journal of Hygiene*, **51**, 359-371.

Emara-Shabaik, H.E., Khulief, Y.A. and Hussaini, I. (2002). "A non-linear multiple-model state estimation scheme for pipeline leak detection and isolation." *Proceedings of the Institution of Mechanical Engineers: Systems and Control Engineering*, **216**(1), 497-512.

Evangelisti, G. (1969). "Waterhammer analysis by the method of characteristics", *L'Energia Ellectrica*, **10**, 10-12.

Feachem, R.G., Bradley, D.G., Garelick, H. and Mara, D.D. (1983). "Sanitation and disease: Health aspects of excreta and wastewater management," Wiley and Sons.

Ferrante, M. and Brunone, B. (2003). "Pipe system diagnosis and leak detection by unsteady-state tests. 1. Harmonic analysis." *Advances in Water Resources*, **26**, 95-105.

Ferrante, M., Brunone, B. and Rossetti, A. G. (2001). "Harmonic analysis of system response during transient for leak detection in pressurized pipes." *Proceedings of the 4th International Conference on Water Pipeline System Managing Pipeline Assets in an Evolving Market*, BHR Group, York, U.K., 28-30.

Fox, J.A. (1968). "The use of the digital computer in the solution of waterhammer problems", *Proc. I.C.E.* 39.

Fox, J.A. (1977). "Hydraulic analysis of unsteady flow in pipe networks." Macmillan Press, London.

Fukushima, K., Maeshima, R., Kinoshita, A., Shiraishi, H. and Koshijima, I. (2000). "Gas pipeline leak detection system using the online simulation method." *Computers and Chemical Engrg*, **24**, 453-456.

Gebra, C.P., Wallis, C. and Melnick, J.L. (1975). "Microbiological hazards of household toilets: droplet production and the fate of residual organisms." *Applied Environmental Microbiology*, **30**, 229-237.

Gokhale, S. and Graham, J.A. (2003). "A new development in locating leaks in sanitary sewers." *Tunnelling and underground space technology*, **19**, 85-96.

Gray, C.A.M. (1953). "The analysis of the dissipation of energy in waterhammer", *Australian Journal of Applied Science*, **5**(2), 125-131.

Halliday, S. (1999). The great stink of London: Sir Joseph Bazalgatte and the cleansing of the Victorian metropolis. Sutton Publishing Limited: Gloucestershire.

Han, F., Yu, X., Wang, Y. and Al-Dabbagh, M. (2004). "Sinusoidal steady-state analysis for fault location in power distribution systems." *The 30th Annual Conference of the IEEE Industrial Electronics Society*, November 2-6, 2004, Busan, Korea.

Hendley, J.O. Wenzel, R.P. and Gwaltney, J.M. (1973). "Transmission of rhinovirus colds by self-inoculation." *New Eng.l J Med.*, **288**, 1361-1364.

Henson, D.D. and Fox, J.A. (1977). "Transient flows in tunnel complexes of the type proposed for the Channel Tunnel", *Proc. I.Mech.E*., **188**, 153-167.

Hong Kong Department of Health. (2003). "Outbreak of severe acute respiratory syndrome (SARS) at Amoy Gardens, Kowloon Bay, Hong Kong, Main Findings of the Investigation." April 2003.

Hong Kong SAR Government - SARS Expert Committee. SARS in Hong Kong: From Experience to Action, 2003.

Hough, J.E. (1988). "Leak testing of pipelines uses pressure and acoustic velocity". *Oil & Gas Journal, Technology*, 35-41.

Hunaidi, O. and Chu, W.T. (1999). "Acoustical characteristics of leak signals in plastic water distribution pipes." *Applied Acoustics*, **58**, 235-254.

Hunaidi, O. and Wang, A. (2006). "A new system for locating leaks in urban water distribution pipes." *Management of Environmental Quality: An International Journal*, **17**(4), 450-466.

Hung, H.C.K., Chan, D.W.T., Law, L.K.C., Chan, E.H.W. and Wong E.S.W. (2006). "Industrial experience and research into the causes of SARS virus transmission in a high-rise residential housing estate in Hong Kong," *Building Services Engineering Research and Technology*, **27**(2): 91-102.

Hutchinson, R.I. (1956). "Some observations on the method of spread of Sonne dysentery." *Mon Bull Minist Health Public Health Lab Serv*, **15**, 110-118.

Jack, L.B. (2006) "Drainage design: factors contributing to SARS transmission," *Proceedings of the Institution of Civil Engineers*, **159**, 43-48.

Jack, L.B. (1997). "An investigation and analysis of the air pressure regime within building drainage and vent systems." PhD Thesis, Heriot-Watt University, Edinburgh.

Jack, L.B. (2000). "Developments in the definition of fluid traction forces within building drainage vent systems", *Building Services Engineering Research and Technology*., **21**, 266-273.

Jacobi, A. (1894). "The production of diseases by sewer air". *Trans. Congress Am. Phys. Surg*., **3**, 86.

Johnson, P. (1978). The National Trust book of British castles, Book Club Associates.

Jonsson, L. (1995). "Leak detection in pipelines using hydraulic transients - laboratory measurements." University of Lund, Sweden, Lund.

Joukowsky N. Uber den hydraulisher Stoss in Wasserlietungsrohen, Memoirs de l'Academie Imperiale des Sciences de St Petersburg, 1900, translated by Miss O Simin, *Proceedings American Water Works Associations*, **24**. 1904. p. 341-424.

Jung, B.S. and Karney, B.W., (2008). "Systematic exploration of pipeline network calibration using transients." *Journal of Hydraulic Research*, **46**(1), 129-137.

Karney, B., Brunone, B., and Tang, K. (2000). "Role and characterisation of leaks under transient conditions." *Proc. of Joint Water Resources Eng. And Planning Management Conference*, 30th July to 2nd August, Minneapolis, USA.

Kelly D.A., Identification of depleted appliance trap seals within the building drainage and ventilation system - A transient based technique: *Proceedings from the CIBW62 Water Supply and Drainage for Buildings*, Brno, Czech Republic, September, 2007.

Kelly D.A., Swaffield J.A., Jack L.B., Campbell D.P. and Gormley M. (2008). "Pressure transient identification of depleted appliance trap seals: A sinusoidal wave technique." *Building Services Engineering Research & Technology*, **29** (3), 219-232.

Kiuchi, T. (1993). "A leak localisation method of pipeline by means of fluid transient model." *Journal of Energy Resources Technology*, Trans. ASME, **15**(5), 378-383.

Kranenberg, C. (1974). "Gas release during transient cavitation in pipes", *J. Hyd. Div*, ASCE, **100**(HY10), 1383-1398.

Lamoen, J. (1947). "Le coup de belier d'Allievi, compte tenu des pertes de charge continues", Bull. Centre de Etudes, de Recherches et d'Essais Scientifiques des Constructions de Gerrie Civil et Hydraulique Fluviale, Tome II, Doseor, Liege.

Lee, P.J., Vitkovsky, J.P., Lambert, M.F., Simpson, A.R. and Ligget, J.A. (2005). "Frequency domain analysis for detecting pipeline leaks." *Journal of Hydraulic Engineering*, ASCE, **131**(7), 596-604.

Leung, G.M., Hedley, A.J., Ho, L.M., Chau, P., Wong, I.O.L., Thach, T.Q., Ghani, A.C., Donnelly, C.A., Fraser, C., Riley, S., Ferguson, N.M., Anderson, R.M., Tsang, T., Leung, P.Y., Wong, V., Chan, J.C.K., Tsui, E., Lo, S.V., Lam, T.H. (2004). "The epidemiology of severe acute respiratory syndrome in the 2003 Hong Kong epidemic: An analysis of all 1755 patients." *Ann. Intern. Med.*, **141**, 662-673.

Liggett, J.A., and Chen, L.C. (1994). "Inverse transient analysis in pipe networks." *Journal of Hydraulic Engineering*, **120**(8), 934-955.

Liou, C.P. and Tian, J. (1995). "Leak detection - Transient flow simulation approaches." *Journal of Energy Resources Technology*, Trans. ASME, **117**(3), 243-248.

Liou, C.P. (1993). "Pipeline variable uncertainties and their effect on leak detectability". API publications 1149, American Petroleum Institute, Washington D.C.

Liou, C.P. (1998). "Physical basis of software-based leak detection methods." *Proceedings of the 1998 International Pipeline Conference*, Pub. ASME, Calgary, Alberta, Canada, 851-857.

Lister, M. (1960). "Numerical solution of hyperbolic partial differential equations by the method of characteristics", Numerical methods for digital computers, John Wiley and Sons, New York.

Liu, W.C. and Lu, M.H., (2003). "Locating faults on cables by applying the principle of the transmission line oscillator." *International Journal of Electronics*, **90**(5), 355-359.

MacLeod, K.D. (2000). "Numerical modelling of air pressure transients resulting from detergent dosed annular flows within building drainage systems", PhD thesis, Department of Building Engineering and Surveying, Heriot-Watt University.

Maloney, C.A. (1973). "Locating cable faults." IEEE Transactions on Industry Applications. **1A-9**(4), 380-394.

Massau, J. (1900). "Memoirs sur l'integration graphique des equations aux derives partialles", Ann. Ass. Ingrs. Sortis des Ecoles Speciales de Gand, 23, 95-214. Translated as Unsteady Flow, H.J. Putman, Rocky Mountain Hydraulic Lab., Colorado, 1948.

Massey, B. and Ward-Smith, J. (2006). Mechanics of fluids. 8th Edition. Taylor & Francis Routledge (Publishers) Ltd, London, New York.

May, K.R. and Druett, H.A. (1953). *Brit J industry Med*, **10**, 142.

Misiunas, D., Lambert, M., Simpson, A. and Olsson, G. (2005). "Burst detection and location in water distribution networks". *Water Science and Technology: Water Supply*. **5**(3-4), 71-80.

Nash, G.A. and Karney, B. (1999). "Efficient inverse transient analysis in series pipe systems." *Journal of Hydraulic Engineering*, ASCE, **125**(7), 761-764.

Nicholas, R.E. (1987). "Leak detection by model compensated volume balance." *ASME Pipeline Engineering Symposium*, ETCE, 13-20.

Nightingale, Florence (1860). Notes on Nursing: What it is and what it is not. Harrison, London.

Parker, D.T., Spendlove, J.C., Bondurant, J.A. and Smith, J.H. (1977). “Microbial aerosols from food processing waste spray fields.” *Journal of the Water Pollution Control Federation*, **49**, 2359-2365.

Parliamentary Papers (1854-5), **21**, pp. 155-161: Appendix 4: Report on Golden Square).

Parliamentary Papers (1846), **10**, p. 651.

Price, R.K. (1974). "Comparison of four numerical methods for flood routing", *Journal ASCE*.

Qunli, W. and Fricke, F. (1989). "Estimation of blockage dimensions in a duct using measured eigenfrequency shifts." *Journal of Sound and Vibration*, **133**(2), 289-301.

Qunli, W. and Fricke, F. (1991). "Determination of blockage locations and cross-sectional area in a duct by eigenfrequency shifts." *Journal of the Acoustic Society of America*, **87**(1), 67-75.

Reynolds, O. (1872). "Sewer gas, and how to keep it out of houses." Second Edition. London.

Sattar, A.M. and Chaudhry M.H. (2008). "Leak detection in pipelines by frequency response method." *Journal of Hydraulic Research*, **46**(1), 138-151.

Schnyder, O. (1929). “Druckstosse Pumpensteigleitengungen”. *Schweitz Bauztg.* 94, No. 22 and 23.

Song, C.C.S. (1976). "Two-phase flow hydraulic transient model for storm sewer systems", *Proc. 2nd Int. Pressure Surge Conference*, BHRA, Cranfield, England.

St Venant, A.J.C.B. (1870). "Elementary demonstration of the propagation formula for a wave in a prismatic channel…", Comptes renus des séances de l'Academie des Sciences, **71**, 186-195.

Stephens, M., Simpson, A.R., Lambert, M.F. and Vitkovsky, J.P. (2005). "Field measurments of unsteady friction effects in a trunk transmission pipeline." *7th Annual Symposium on Water Distribution Systems Analysis*, ASCE, Anchorage, Alaska.

Stephens, M., Vitkovsky, J., Lambert, M.F., Simpson, A.R., Karney, B. and Nixon, J. (2004). " Transient analysis to assess valve status and topology in pipe networks." *Proceedings of 9th International Conference on Pressure Surges*, BHR Group Ltd, Edinburgh, UK.

Stoke-on-Trent Council, Sir John Harington - the first flushing loo? http://www.stoke.gov.uk (last accessed: 01/08/2008).

Streeter, V.L. (1969). "Waterhammer analysis", *J. Hyd. Div*, ASCE, **88**(HY3), 79-113.

Streeter, V.L. and Lai, C. (1962). "Waterhammer analysis including friction", *J. Hyd. Div*., ASCE, **88**(HY3), 79-112.

Streeter, V.L. and Wylie, E.B. (1967). Hydraulic Transients, McGraw-Hill, New York.

Swaffield J.A. and Jack, L.B. (2004). "Simulation and analysis of airborne cross-contamination routes due to the operation of building drainage and vent systems," *Bldg Research and Inform*, **32**(6), 451-467.

Swaffield J.A. and Boldy A.P. (1993). Pressure surge in pipe and duct systems. England: Avebury Technical Press.

Swaffield J.A. and Campbell D.P. Air pressure transient propagation in building drainage vent systems, an application of unsteady flow analysis. *Building and Environment*, 1992; **27**(3): 357-365.

Swaffield J.A. and Campbell D.P. Numerical modelling of air pressure transient propagation in building drainage systems, including the influence of mechanical boundary conditions. *Building and Environment*, 1992; **27**(4): 455-467.

Swaffield J.A. and Galowin L.S. (1992). The engineered design of building drainage systems. England: Ashgate Publishing Limited.

Swaffield, J.A, Campbell, D.P. and Gormley, M. (2005a). "Pressure transient control: Part I - criteria for transient analysis and control." *Building Services Engineering Research and Technology*, **26**(2), 99-114.

Swaffield, J.A, Campbell, D.P. and Gormley, M. (2005b). "Pressure transient control: Part II - simulation and design of a positive surge protection device for building drainage networks." *Building Services Engineering Research and Technology*, **26**(3), 195-212.

Swaffield, J.A. (1972). "Column separation in an aircraft fuel system", *Proc. 1st Int. Pressure Surge Conference*, Canterbury, England, Paper C2, BHRA, pp13-28.

Swaffield, J.A. (2005). "Transient identification of defective trap seals," *Building Research and Information*, **33**(3), 245-256.

Swaffield, J.A. and Boldy, A.P. (1993). Pressure surge in pie and duct systems. Ashgate Publishing Limited, England.

Swaffield, J.A. and Galowin, L.S. (1992). The engineered design of building drainage systems. Ashgate Publishing Limited, England.

Swaffield, J.A. and Jack, L.B. (1998). "Drainage vent systems: investigation and analysis of air pressure regime," *Building Services Engineering Research and Technology*, **19**, 141-148.

Swaffield, J.A., Jack, L.B. and Campbell, D. P. (2004). "Control and suppression of air pressure transients in building drainage and vent systems," *Building and Environment*, **39**, 783-794.

Swaffield, J.A. (1970). "A study of column separation following valve closure in a pipeline carrying aviation kerosene", Thermodynamics and Fluid Mechanics Convention, Steady and Unsteady flows, *Proc, I.Mech.E*., **57**, 184.

Swaffield, J.A. (2007). "Influence of unsteady friction on trap seal depletion", *Proc. 33rd Int. Water Supply & Drainage for Bldgs Symposium*, Brno, Czech Republic, 407-419.

Teale, T.P. (1881). Dangers to health: A pictorial guide to domestic sanitary defects. Third Edition. J & A Churchill, London.

Tenth Annual Report of the Registrar-General, 1847, p. xvii.

Thompson, W.C. and Skogman, K.D. (1983). "The application of real time flow modelling to pipeline leak detection." *ASME Pipeline Engineering Symposium*, ETCE, 39-45.

Vardy, A.E. (1976). "On the use of the method of characteristics for the solution of unsteady flows in networks", *Proc. 2nd Int. Pressure Surge Conference*, BHRA, Cranfield, England, 15-30.

Vitkovsky, J.P., Lambert, M.F., Simpson, A.R. and Liggett, J.A. (2007). "Experimental observation and analysis of inverse transients for pipeline leak detection." *Journal of Water Resources Planning and Management*, ASCE, **133**(6), 519-530.

Vitkovsky, J.P., Simpson, A.R., and Lambert, M.F. (2000). "Leak detection and calibration issues using transient and genetic algorithms." *Journal of Water Resources Planning and Management*, ASCE, **126**(4), 262-265.

Wade, W.R. and Rachford, H.H. (1987). "Detecting leaks in pipelines using SCADA information, Part 1" *Pipeline Industry*, December, 16-22.

Winslow, C.-E.A (1909). "The conveyance of bacteria in sewer air." *American Journal of Public Hygiene*, **19**(3), 641.

Wise A.F.E. (1979). "Water, sanitary and waste services for buildings". Mitchell: London.

Wise, A.F.E. (1973). "Drainage services in buildings," UK Building Research Establishment, Current Paper CP35/73.

Wise, A.F.E. (1957). Drainage pipework in dwellings: hydraulic design and performance. Department of Scientific and Industrial Research: Building Research Station. Her Majesty's Stationary Office, London.

Wise, A.F.E. and Swaffield, J.A. (1995). Water, sanitary and waste services for buildings, 4th Edition, Longman Scientific and Technical.

Wise, A.F.E. and Swaffield, J.A. Water, sanitary and waste services for buildings. Butterworth-Heinemann, 2002.

Wood, D.J. and Chao, S.P. (1971). "Effect of pipeline junctions on water hammer surges." *Proceedings of the ASCE: Transportation Engineering Journal*, 441-457.

Woodhead, C.A., Fox, J.A. and Vardy, A.E. (1976). "Analysis of water curtains in transient gas flows in ducts", *Proc. 2nd Int. Pressure Surge Conference*, BHRA, Cranfield, England.

World Health Organisation. (2003a). Final Report: Amoy Gardens, WHO Environmental Investigation.

World Health Organisation. (2003b). Consensus document of the epidemiology of severe acute respiratory syndrome (SARS). Geneva: Department of Communicable Diseases Surveillance and Response, World Health Organisation.

World Health Organisation. Environmental Health Team Report on Amoy Gardens, 2003.

Wylie, E.B. and Steeter, V.L. (1978). "*Fluid Transients*". McGraw-Hill, New York.

Wyly, R.S. and Eaton, H.N. (1961). "Capacity of stacks in sanitary drainage systems for buildings," US Department of Commerce. National Bureau of Standards, Monograph 2, July.

Yalamanchili, C. and Smith, M.D. (2008) "Acute hydrogen sulphide toxicity due to sewer gas exposure." *The American Journal of Emergency Medicine*, **26**, 518.e5 - 518.e7.

Yu, I.T.S., Yuguo, M.P.H., Wong, T.W., Tam, W., Chan, A.T., Lee, J.H.W., Leung, D.Y.C. and Ho, T. (2004). "Evidence of airborne transmission of the severe acute respiratory syndrome virus." *New England J Med*, **350**(17), 1731-1739.

Zilke, W. (1968). "Frequency dependant friction in transient pipe flow", *Journal of Basic Engineering, Trans*. ASME, **90**(1), 109-115.